LEABHARLANN CHOLÁISTE NA TRÍONÓIDE, BAILE ÁTHA CLIATH | TRINITY COLLEGE LIBRARY DUBLIN
Ollscoil Átha Cliath | The University of Dublin

Terms and Conditions of Use of Digitised Theses from Trinity College Library Dublin

Copyright statement

All material supplied by Trinity College Library is protected by copyright (under the Copyright and Related Rights Act, 2000 as amended) and other relevant Intellectual Property Rights. By accessing and using a Digitised Thesis from Trinity College Library you acknowledge that all Intellectual Property Rights in any Works supplied are the sole and exclusive property of the copyright and/or other IPR holder. Specific copyright holders may not be explicitly identified. Use of materials from other sources within a thesis should not be construed as a claim over them.

A non-exclusive, non-transferable licence is hereby granted to those using or reproducing, in whole or in part, the material for valid purposes, providing the copyright owners are acknowledged using the normal conventions. Where specific permission to use material is required, this is identified and such permission must be sought from the copyright holder or agency cited.

Liability statement

By using a Digitised Thesis, I accept that Trinity College Dublin bears no legal responsibility for the accuracy, legality or comprehensiveness of materials contained within the thesis, and that Trinity College Dublin accepts no liability for indirect, consequential, or incidental, damages or losses arising from use of the thesis for whatever reason. Information located in a thesis may be subject to specific use constraints, details of which may not be explicitly described. It is the responsibility of potential and actual users to be aware of such constraints and to abide by them. By making use of material from a digitised thesis, you accept these copyright and disclaimer provisions. Where it is brought to the attention of Trinity College Library that there may be a breach of copyright or other restraint, it is the policy to withdraw or take down access to a thesis while the issue is being resolved.

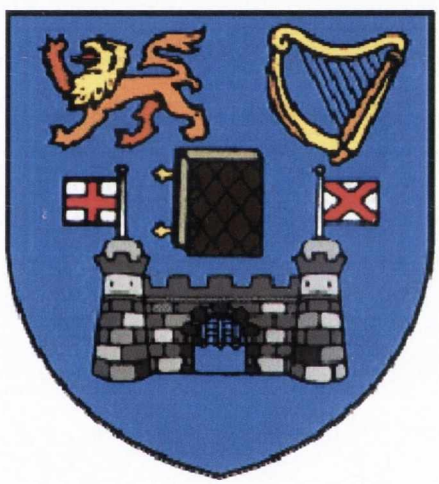
Access Agreement

By using a Digitised Thesis from Trinity College Library you are bound by the following Terms & Conditions. Please read them carefully.

I have read and I understand the following statement: All material supplied via a Digitised Thesis from Trinity College Library is protected by copyright and other intellectual property rights, and duplication or sale of all or part of any of a thesis is not permitted, except that material may be duplicated by you for your research use or for educational purposes in electronic or print form providing the copyright owners are acknowledged using the normal conventions. You must obtain permission for any other use. Electronic or print copies may not be offered, whether for sale or otherwise to anyone. This copy has been supplied on the understanding that it is copyright material and that no quotation from the thesis may be published without proper acknowledgement.

A Synthetic Development of Tetrazines as Ligands in Group 8 Coordination Complexes

Gareth Cooke



A Thesis Submitted to the University of Dublin for the Degree of Doctor of Philosophy

School of Chemistry
Trinity College Dublin
October 2008

TRINITY COLLEGE
10 AUG 2009
LIBRARY DUBLIN
THES
8780

Declaration

This thesis has not been submitted as an exercise for a degree at this or any other university. Except where acknowledgement is given, all work is original and was carried out by the author alone. I agree that the library may lend or copy this thesis upon request.

Summary

Chapter 1 describes the synthesis and characterization of a number of novel pyridazine-centred ligands prepared from substituted tetrazines. The use of these compounds as precursors for planar nitrogen containing graphite-type molecules is then discussed; specifically via cyclodehydrogenation.

Chapter 2 describes the synthesis of a number of the ruthenium(II) bis bpy complexes of these ligands and their characterization by NMR and UV-Vis spectroscopy and single crystal X-Ray diffraction. The synthesis of both the homoleptic iron(II) and ruthenium(II) *tris* complexes of these ligands and their subsequent separation into meridional and facial isomers is described. The spectroscopic properties of geometric isomers of each complex are then characterized and compared.

Chapter 3 discusses the attempted synthesis of a novel diterpyridyl-graphene molecule. A number of novel phenyl-centred compounds were isolated during this work such as fluorenes, fluorenones and fluorenols as well as a number of small novel chromophores. Subsequent attempts at terpyridine synthesis *via* coupling reactions of suitable precursors are also described.

Chapter 4 describes the experimental work undertaken during the course of this project.

Acknowledgements

Firstly I would like to thank my supervisor Prof. Sylvia Draper for all her help, support and encouragement during my time as her student; in particular for remaining positive at all times and showing great faith in me. I would also like to thank Dr. Emma Schofield and Prof. David Grayson for their helpful input at various points during the course of my work. A big thank you to Dr. John O' Brien for all the hours spent running various complicated NMR experiments with your unique relentless enthusiasm and patience. Thanks to Dr. Manuel Reuther for the NMR analysis, Martin Feeney for the mass spectrometry and Dr. Tom McCabe, Dr. Chris Fitchett and Dr. Sunil Varghese for the X-Ray crystallography.

A big thank you is due to all the Draper group members past and present – Ania, Amy, Angie, Belen, Buddhie, Carlos, Cecile, Colin, Dan, Deanne, Dilwyn, Fran, Gearóid, Guillaume, Lorraine, Pablo, Philip, Robbie, Sarath, Sunil and Tash. I have to give a special thanks to Cecile, Dan, Pablo and Robbie for all their help and patience at various points when it was needed and very much appreciated. A big thank you to Fran as well for being such a deadly mate and generally providing the kind of friendship, support and laughs which made working here a pleasure – most of the time! Thanks go to Mike and all the lads in the department I met through football; despite the fact I came from another college I felt very welcome from the outset.

Many thanks are due to my brothers and sister, Aoife, Barry and Ronan – thanks guys for putting up with the grumps and generally being great friends as well as siblings. None of this work would have been possible without the love and support of my parents Anne and Terry – thanks for being there for me and encouraging me always to work hard, give it my best shot and keep the chin up. Finally a big thank you goes to Patricia for all her support and love and for showing enormous character despite life's twists and turns. Thanks for always being there for me and for being one person I can always say I'm proud to know, let alone love.

Table of Contents

List of Abbreviations ..... **I**

List of Figures ..... **V**

List of Schemes ..... **IX**

List of Tables ..... **XI**

Chapter 1 ..... **1**

1.1 Introduction **1**

1.1.1 The Properties of PAHs *1*

1.1.2 Synthesis of Polyaromatic Hydrocarbons *2*

1.1.2.1 The Synthesis of Oligopolyphenylenes 3

1.1.2.2 Cyclodehydrogenation 5

1.1.3 Incorporating Heteroatoms into PAH Systems *7*

1.1.4 Increasing the Quantity of Heteroatoms in the PAH system *9*

1.1.4.1 Tetrazines 9

1.1.4.2 Diels-Alder Reactions of Tetrazines 11

1.1.4.3 Pyridazines 14

1.1.4.4 Substituted Pyridazines as Ligands 16

1.1.4.5 Pyridazine-Centred Ligands as Precursors to N-HSBs 17

1.2 Results and Discussion **19**

1.2.1 Synthesis of 3,6-di(2-pyridyl)-1,2,4,5-tetrazine *19*

1.2.2 The Attempted Synthesis of tetrasubstituted pyridazine ligands *19*

1.2.3 The synthesis of tri-substituted pyridazine ligands *20*

1.2.4 The synthesis of 3,4,5,6-tetrasubstituted pyridazine ligands *22*

1.2.5 Pyridazines from other substituted tetrazines *23*

1.2.6 Diels-Alder Reaction Yields *25*

1.2.7 Cyclodehydrogenation – The Final Step Towards Novel N-HSB Compounds *26*

1.2.8 Modification of pyridazine-centred ligands for cyclodehydrogenation *27*

1.2.8.1 Preparation of 3,3,5,5-tetramethoxy stilbene 29

1.2.8.2 Synthesis of a novel methoxy-substituted pyridazine –centred compound 30
1.2.8.3 Cyclodehydrogenation of 19 31

1.3 Characterization of Pyridazine–Centred Compounds 33

1.3.1 Characterization by NMR Spectroscopy 33

1.3.1.1 Pyridyl-substituted pyridazines 33
1.3.1.2 Pyrazine substituted pyridazine ligands 42
1.3.1.3 Compound 18 and comparison of pyridazine 19 with diaza-triphenylene 20 47

1.3.2 Characterization of Compounds 3, 4 and 6 by Single Crystal X-Ray Diffraction 50

1.3.3 Characterization of 20 and 21 by UV-Vis and Fluorescence Spectroscopy .. 54

1.3.4 Characterization by IR Spectroscopy and Mass Spectrometry 57

1.4 Conclusions and Future Work 57

1.5 References 58

Chapter 2 61

2.1 Introduction 61

2.1.1 Introduction to Ruthenium Chemistry 62

2.1.1.1 Luminescence of Ruthenium (II) Complexes 70
2.1.1.2 Electrochemistry 72

2.1.2 The Coordination Chemistry of Iron 74

2.1.2.1 The Spectroscopic Properties of Iron (II) Complexes 75

2.1.3 Isomerism in Coordination Chemistry 77

2.2 Results and Discussion 83

2.2.1 Synthesis of Ru(II) bis bpy Complexes of Ligands 3, 4, 6, 8 and 11 83

2.2.1.1 Synthetic Procedure 83
2.2.1.2 Characterisation of 22 and 23 85
2.2.1.3 Characterisation of Compounds 24, 25 and 26 90
2.2.1.4 X-Ray Crystallographic Determination of 22 and 23 97
2.2.1.5 UV-Vis and Fluorescent Spectroscopy of 22-26 101
2.2.1.6 Electrochemistry of 22-26 106

2.2.2 Synthesis of Ruthenium (II) Tris Complexes of 27, 28 and 29 112

2.2.2.1 Synthetic Procedure 112
2.2.2.2 Characterisation of Compounds 27, 28 and 29 by Mass Spectrometry and NMR Spectroscopy 115
2.2.2.3 Chemical Exchange in NMR 118
2.2.2.4 Application to the Characterisation of the facial Isomer of 27 120
2.2.2.5 X-Ray Crystallographic Determination of the facial Isomer of 27 123
2.2.2.6 Characterization of 28 and 29 by NMR Spectroscopy 127
2.2.2.7 UV-Vis Absorption Spectra of Ru (II) tris Isomers 134
2.2.2.8 The UV-Vis Absorption Spectra of fac and mer isomers of 27, 28 and 29 135
2.2.2.9 Emission Spectra of the fac and mer isomers of 27, 28 and 29 138
2.2.3 The Synthesis of Iron (II) Complexes 30, 31 and 32 139
2.2.3.1 Synthetic Procedure 139
2.2.3.2 Characterisation of 30, 31 and 32 by NMR Spectroscopy 140
2.2.3.3 UV-Vis Absorption Spectra of the facial and meridional Isomers of 30, 31 and 32 147
2.3 Conclusion 149
2.4 References 149
Chapter 3 153
3.1 Introduction 154
3.1.1 Introduction to Terpyridines 156
3.1.2 Synthetic Routes Towards Terpyridines 157
3.1.2.1 Coupling Methods 157
3.1.2.2 Ring Formation 158
3.1.2.3 Functionalised Terpyridines 159
3.1.2.4 Diads and "back-to-back" tpy ligands 162
3.1.3 Precursors to Phenyl-centred Terpyridyl Compounds 163
3.1.4 Diels-Alder Reactions (Normal-Electron Demand) 164
3.1.5 Synthetic Routes Towards Aldehydes 167
3.2 Results and Discussion 169
3.2.1 Diels-Alder Reactions of 2,4-dimethyl-3,5-diphenyl cyclopentadienone 169
3.2.2 Attempted Oxidation of 33 171

3.2.3 Incorporating other Functionalities onto the Phenyl centre *174*

3.2.4 Reduction of Esters to Aldehydes *175*

3.2.5 Attempted Reduction of Carboxylic Acid to Aldehyde *176*

3.2.6 Attempted Cyclodehydrogenation of Phenyl-Centred Compounds *178*

3.3 Characterisation of Phenyl-Centred Compounds **180**

3.3.1 NMR Spectroscopy *180*

3.3.2 Characterisation of 36 and 43 by X-Ray Crystallography *188*

3.3.3 Characterisation of Fluorenyl/Fluorenonyl Compounds by UV-Vis Spectroscopy *193*

3.3.4 Characterisation of Compounds 33-44 by I.R. Spectroscopy and Mass Spectrometry *195*

3.4 Introduction to Part II **197**

3.5 Results and Discussion of Part II **198**

3.6 Characterisation of Anthracene and Tpy Compounds **204**

3.7 Conclusion **207**

3.8 References **208**

Chapter 4 ..... **211**

4.0 Experimental **212**

General Methods *212*

Synthesis of ligands *213*

Synthesis of Ruthenium(II) bisbipyridine Complexes *212*

Synthesis of Ruthenium (II) tris homoleptic Complexes *234*

Attempted Cyclodehydrogenation 238

Formation of Iron Complexes using $Fe(BF_4)_2$ *239*

Annex **259**

List of Abbreviations

δ	chemical shift
μm	micromolar
1-D	one-dimensional
2-D	two-dimensional
9-BBN	9-borabicyclo[3.3.1]nonane
Å	Angstrom
abs	absorption
Anal	elemental analysis
aq.	Aqueous
bpdz	3,3'-bipyridazine
bpm	4,4'-bipyrimidine
bppn	3,6-di(2-pyridyl) pyridazine
bptz	3,6-di(2-pyridyl)-1,2,4,5-tetrazine
bpy	2,2'-bipyridine
bpym	2,2'-bipyrimidine
bpz	2,2'-bipyrazine
bpztz	3,6-di(2-pyrazinyl)-1,2,4,5-tetrazine
br	broad
cm	centimetre
COD	Cyclooctadiene
COSY	Correlation Spectroscopy
CV	Cyclic Voltammogram
d	doublet
dcb	4,4'-dicarboxylate-2,2'-bipyridine
DCM	dichloromethane
DDQ	Dichloro Dicyano Quinone
DEPT	Distortionless Enhancement by Polarization Transfer
dhb	4,4'-bis(hydroxymethyl)-2,2'-bipyridine
DibAl	Diisobutyl Aluminium hydride
dmb	4,4'-dimethyl-2,2'-bipyridine
DMF	dimethylformamide
DMSO	dimethylsulfoxide

DSC	Differential Scanning Calorimetry
DSSC	Dye-Sensitized Solar Cell
em	emission
ES	Electrospray
ESR	Electron Spin Resonance
Et	ethyl
EtOH	ethanol
fac	facial
FID	Free Induction Decay
FVP	Flash Vaccuum Pyrolysis
g	gram
h	hour
HBC	hexa-peri-benzocoronene
HOMO	Highest Occupied Molecular Orbital
HPLC	High Performance Liquid Chromatography
Hz	Hertz
IC	Intersystem Crossing
IR	infrared
J	coupling constant
LC	Ligand Centred
LMCT	Ligand to Metal Charge Transfer
LTBA	tri-*tert*-butoylaluminiumhydride
LUMO	Lowest Unoccupied Molecular Orbital
m	multiplet
m.p.	melting point
m/z	mass to charge ratio
max	maximum
mbpm	3,3',4,4',5,5'-hexamethoxy-4,4'-bipyrmidine
MC	Metal Centred
mer	meridional
mg	milligram
MHz	Megahertz
min	minutes
mL	millilitre

MLCT	Metal to Ligand Charge Transfer
mmol	millimole
MS	mass spectrometry
nbpm	2-naphtyl-4,4'-bipyrimidine
NEt_3	triethylamine
N-HSB	Nitrogen containing heterosuperbenzenes
nm	nanometer
NMR	Nuclear Magnetic Resonance
NMR	nuclear magnetic resonance
NOe	nuclear Overhauser effect
ns	nanosecond
PAH	Polyaromatic Hydrocarbon
Ph	phenyl
phen	phenanthroline
pmpy	2-(2-pyridyl) pyrimidine
ppm	parts per million
pppz	3,6-bis[2-(6-phenylpyridine)pyridazine]
prpm	4-(2-pyridyl) pyrimidine
RedAl	sodium bis(2-methoxyethoxy) aluminium hydride
R_f	Retention Factor
ROESY	Rotational nuclear Overhauser Effect Spectroscopy
RT	Room Temperature
s	second
sat.	saturated
SCE	Saturated Calomel Electrode
SCE	Standard Calomel Electrode
SEM	Scanning Electron Microscope
SLUMO	Second Lowest Unoccupied Molecular Orbital
STM	Scanning Tunnelling Microscopy
t	triplet
T_c	Coalescence Temperature
terpyridine	2,2':6',2''-terpyridine
THF	Thin Layer Chromatography
TMS	trimethylsilyl-

TOCSY	Total Correlation Spectroscopy
tpy	2,2':6',2"-terpyridine
UV-Vis	Ultraviolet-Visible
vs.	versus
λ	wavelength
ν	stretching frequency

List of Figures

Figure 1: Two pictorial descriptions of phenanthrene 1
Figure 2: Two tautomers of anthracene showing the π-electron set 1
Figure 3: Triphenylene and two of its many geometric isomers, benz[a]anthracene and [4]helicene 2
Figure 4:Hexa-*peri*-hexabezocoronene 2
Figure 5: 1,2,4,5-tetrazine 10
Figure 6: 3,6-di(2-pyridyl)-1,2,4,5-tetrazine (bptz) 10
Figure 7: The Ru(II) bpdz complex of Kaim which adopts the transoid conformation (left) and the cisoid Ag(I) bptz complex of Constable (right) 11
Figure 8: Diagram showing the frontier orbital interactions in normal demand and inverse demand Diels-Alder reactions 12
Figure 9: Some metal complexes prepared from bppn 16
Figure 10: The greater electron-withdrawing effect of the pyridyl ring 26
Figure 11: NOe showing an interaction between H^6 and H^8 33
Figure 12: The ^1H-^1H COSY of 3 showing the two 2-pyridyl ring systems in $CDCl_3$. The most downfield pyrimidyl signal due to H^{10} is not included 34
Figure 13: The ^{13}C-NMR spectrum of 3 in $CDCl_3$ 35
Figure 14: The ^1H-NMR spectrum of 4 in $CDCl_3$ 36
Figure 15: The long-range 2-dimensional ^{13}C-^1H-COSY experiment of 5 in $CDCl_3$. The carbon spectrum is shown from δ 100ppm and hence does not include the most upfield carbon signal, C^{12}. 38
Figure 16: The ^1H-NMR spectrum of hydropyridazine 5 in $CDCl_3$ 39
Figure 17: The ^1H-NMR spectrum of 6 in $CDCl_3$ 40
Figure 18: The ^{13}C-NMR spectrum of 6 in $CDCl_3$ 40
Figure 19: The ^1H-NMR spectrum of 7 in $CDCl_3$ 41
Figure 20: The ^1H-NMR spectrum of 8 in $CDCl_3$ 42
Figure 21: The ^1H-NMR of 11 in $CDCl_3$ 43
Figure 22: The ^{13}C-NMR spectrum of 11 in $CDCl_3$ 43
Figure 23: The ^1H-NMR of ligand 12 in $CDCl_3$ 44
Figure 24: The ^1H-NMR of 13 in $CDCl_3$ 45
Figure 25: The ^1H-NMR of pyridazine 14 in $CDCl_3$ 45
Figure 26: The ^1H-NMR spectrum of 16 in $CDCl_3$ 46
Figure 27: The ^1H-NMR spectrum of 18 in $CDCl_3$ 47
Figure 28: Comparison of the ^1H-NMR spectra of 19 and 20 in $CDCl_3$ 48
Figure 29: Comparison of the ^{13}C-NMR spectra of 19 and 20 in $CDCl_3$ 49
Figure 30: The asymmetric unit of the crystal of 3 50
Figure 31: The packing in the crystal lattice of 3 50
Figure 32: The two-dimensional layering arrangement of the crystals of 3 (left) and the resulting three-dimensional architecture (right) 51
Figure 33: The asymmetric unit of 4 51
Figure 34: The molecular assembly formed in the crystal lattice of 4 52
Figure 35: The herring-bone arrangement formed in the crystal lattice of 4 (left) with the three-dimensional representation on the right 52
Figure 36: the asymmetric unit of crystals of 6, which contains two molecules 53
Figure 37: The molecular interactions in the crystal lattice of 6 53
Figure 38: A schematic of the interactions present in the crystal lattice of 6 54
Figure 39: The UV-Vis Absorption Spectra of 19, 20 and 21 in CH_3CN 55
Figure 40: The Emission Spectrum of 20 56
Figure 41:The fluorescence emission spectra of 20 and 21 in CH_3CN 56

Figure 42: Compound 22 on the left, with the similarly fused diphenanthro[9,10,1def;1',10',9'hij]phthalazine on the right and their emission maxima. 57
Figure 43: Molecular orbital diagram showing the orbitals for an octahedral complex. The four types of transitions are indicated with arrows..... 63
Figure 44: Molecular Orbital diagram showing the orbitals involved in an MLCT transition for Ru(II) polypyridyl complexes..... 63
Figure 45: The asymmetric ligands of the Ait-Haddou and Rilemna group (above) and the four symmetrical members of the diazine family studied by Ernst and Kaim (lower)..... 66
Figure 46: The three ligands prepared by Campagna comparing substituents effects on the absorption spectra. 69
Figure 47: 3, 6- bis(2'-pyridyl)pyridazine (bppn)..... 69
Figure 48: Energy level diagram showing the various pathways of excited state decay..... 71
Figure 49: The three closely spaced excited states involved in the luminescence of Ru *tris* bpy.[23] 71
Figure 50:The excited state decay mechanism for iron (II) polypyridyl complexes[31]..... 75
Figure 51: The two enantiomers of the $[Ru(bpy)_3]^{2+}$ cation..... 78
Figure 52: Facial and Meridional Isomers of a Ruthenium Complex 79
Figure 53: The templated ligand of Weizman[49]..... 80
Figure 54: Two of the bulky ligands prepared by Fletcher. The Ru(II) *tris* complex of the ligand on the left favours the *fac* conformation, whilst that on the right was synthesised exclusively in the *mer* configuration 81
Figure 55: Figure showing the numbering system used for complex 22..... 86
Figure 56: The ^{1}H-NMR spectra of the non-deuterated bpy complex 22 in green in CD_3CN, with the free ligand 3 (red) and the deuterated bpy Ru(II) Complex $22d_8$ in blue. 86
Figure 57: ROESY experiment showing the through - space interaction between H3' and H13 in 22 d8..... 87
Figure 58:NOe experiment showing the same interaction between the H3' and H13 of 22d8..... 88
Figure 59: The non-deuterated *bis* bpy Ru(II) complex in green with the free ligand 4 shown in red, and the deuterated Ru(II) *bis* bpy complex $23d_8$ in blue. 89
Figure 60: The ^{1}H-NMR spectrum in CD_3CN of the Ru(II) *bis* bpy complex 24 in green, ligand 6 in red, with the deuterated *bis* bpy Ru(II) complex $24d_8$ in blue 90
Figure 61: Graphic showing the shielding effect prevalent in 24, 25 and 26..... 91
Figure 62: The ^{1}H-NMR spectrum in CD_3CN of the regular Ru (II) bis bpy complex 25 in green, ligand 8 in red, with the deuterated bis bpy Ru(II) complex $25d_8$ in blue. 93
Figure 63: ^{1}H-^{1}H COSY experiment showing the two 2-pyridyl rings on 26..... 94
Figure 64: The ^{1}H-NMR spectra on CD_3CN of 11 in red with the related Ru(II) bis bpy complex 26 in blue..... 95
Figure 65: The aromatic regions of the ^{1}H-NMR spectra of 11 and 26 in CD_3CN..... 96
Figure 66: Perspective view of the crystal structure of 22 97
Figure 67: The host framework formed in the crystal lattice of 22 showing the C-H···N hydrogen bonds. 98
Figure 68: The host-guest complex of 22..... 98

Figure 69: Perspective view of 23 99
Figure 70: The host framework assembly formed in the crystal lattice of 23 100
Figure 71: The host-guest complex observed in the crystal lattice of 23 100
Figure 72:UV-Vis Absorption Spectra of 22, 23 and Ru tris bpy in CH_3CN..... 101
Figure 73: The MLCT Region of the UV-Vis Spectra of 22, 23 and $[Ru(bpy)_3]^{2+}$ in MeCN 102
Figure 74: The normalised luminescence Emission Spectra of 22 and 23 in MeCN excited at λ 464 nm. 103
Figure 75: The UV-Vis Absorption Spectra of 24, 25 and 26 in MeCN..... 103
Figure 76: The Low Energy Region of the UV-Vis Spectra of 24, 25 and 26 in MeCN 104
Figure 77: The normalised Emission Spectra of 24, 25 and 26 in MeCN excited at λ 464 nm 106
Figure 78: Cyclic Voltammogram of 23 showing the Ru(II/III) redox peak (1 mmol in MeCN *vs.* SCE)..... 108
Figure 79: The Cyclic Voltamogram of 26 showing the Ru(II/III) redox peak (1 mmol in MeCN *vs.* SCE)..... 108
Figure 80: The Cyclic Voltamagram of 23 showing the ligand-based reduction peaks (1 mmol in MeCN *vs.* SCE) 109
Figure 81: Cyclic Voltammogram of 24 showing the ligand-based reduction peaks (1 mmol in MeCN *vs.* SCE) 110
Figure 82: Schematic showing some of the isomers which would result from the synthesis of metal *tris* complexes using compound 3 as the coordinating ligand. 112
Figure 83: Schematic showing the symmetry present in the meridional and facial isomers 113
Figure 84: The ^{1}H-NMR spectrum of the mer isomer of 27 in CD_3CN 116
Figure 85: ^{1}H-^{1}H COSY showing the two pyridyl and two phenyl systems of the *fac* isomer of 27 118
Figure 86: ^{1}H-NMR spectrum of the *fac* isomer of 27 in CD_3CN 121
Figure 87: A 60°C ^{1}H-NMR spectrum of the *fac* isomer of 27 (blue) superimposed on the room temperature spectrum (green). 121
Figure 88:^{13}C-NMR spectrum of the *fac* isomer of 27 in CD_3CN 122
Figure 89: The region between 127 and 130 ppm in the ^{13}C-NMR spectrum of the *fac* isomer of 27 123
Figure 90: Perspective view of the asymmetric unit of the fac isomer of 27. The PF_6^- anions and the methanol molecule have been removed for clarity..... 124
Figure 91: The coordination sphere of the *fac* isomer of 27 124
Figure 92: The porous assembly formed by the self-assembly process in the *fac* isomer of 27 125
Figure 93: The intermolecular interactions between the PF_6^- anions and the complexes. The schematic on the left depicts the C-H···π and π··· π interactions which stabilise the host framework. On the right is the PF_6^- anion which occupies the one-dimensional channel. 125
Figure 94: The hexagonal host framework of the *fac* isomer of 27 in space filling mode..... 126
Figure 95: The ^{1}H-NMR spectrum of the mer isomer of 28 in CD_3CN..... 127
Figure 96: The ^{1}H-NMR spectrum of the *fac* isomer of 28 in CD_3CN 128
Figure 97: The ^{13}C-NMR DEPT of the *fac* isomer of 28 in CD_3CN..... 129
Figure 98: The ^{1}H-NMR spectrum of the *mer* isomer of 29 in CD_3CN..... 130

Figure 99: ^{1}H-^{1}H COSY showing the two 2-pyridyl systems and the two phenyl systems of the *fac* isomer of 29 in CD_3CN 131
Figure 100:The methoxy peak shifts of the *fac* isomer of 29 run at room temperature (green) and at 60°C (blue) in CD_3CN 133
Figure 101: The aromatic region of the ^{1}H-NMR spectra of the *fac* isomer of 29 run at room temperature (green) and at 60°C (blue) in CD_3CN 133
Figure 102: The ^{13}C-NMR of the *fac* isomer of 29 in CD_3CN 134
Figure 103: The UV-Vis absorption spectra of the meridional and facial isomers of 27, 28 and 29 in MeCN 136
Figure 104: The Low Energy Region of the UV-Vis spectra of 27, 28 and 29 137
Figure 105: Emission Spectra of both Isomers of 27 28 and 29 in MeCN 138
Figure 106: ^{1}H-NMR spectrum of the mer isomer of 30 in CD_3CN 141
Figure 107: The ^{1}H-NMR spectrum of the *fac* isomer of 30 in CD_3CN 142
Figure 108: The ^{1}H-NMR spectrum of the mer isomer of 31 143
Figure 109: The ^{1}H-NMR spectrum of the facial isomer of 31 in CD_3CN 144
Figure 110: The ^{1}H-NMR spectrum of the *mer* Isomer of 32 in CD_3CN 145
Figure 111: The ^{1}H-NMR spectrum of the *fac i*somer of 32 in CD_3CN 146
Figure 112: UV-Vis Absorption Spectra of both isomers of 30, 31 and 32 in MeCN147
Figure 113: The Low Energy Region of the UV-Vis Spectra of *fac* and *mer* isomers of 30, 31 and 32 in MeCN 148
Figure 114: The relative reactivities of various cyclic dienes 165
Figure 115: The ^{1}H-NMR spectrum of 33 in $CDCl_3$ 180
Figure 116: The aromatic region of the ^{1}H-NMR Spectrum of 34 in $CDCl_3$ 181
Figure 117: The aromatic region of the ^{13}C-NMR spectrum of 34 in $CDCl_3$ 181
Figure 118: The aromatic region of the ^{1}H-NMR spectrum of 36 in $CDCl_3$ 182
Figure 119: The aromatic region of the ^{13}C-NMR spectrum of 37 in $CDCl_3$ 183
Figure 120: The ^{1}H-NMR Spectrum of 38 in $CDCl_3$ 184
Figure 121: The ^{13}C-NMR Spectrum of 41 in $CDCl_3$ 185
Figure 122: The ^{1}H-NMR spectrum of 42 in $CDCl_3$ 185
Figure 123: The ^{1}H-NMR spectrum of 43 in $CDCl_3$ 186
Figure 124: The ^{1}H-NMR spectrum of 44 in $CDCl_3$ 187
Figure 125: The asymmetric unit in the crystal structure of 36 with selected labelling. 188
Figure 126: A row of the crystals of 36 showing the interaction between the oxygen atom and one of the hydrogen atoms of the neighbouring molecule... 189
Figure 127: Diagram showing the inter-columnar CH-π interactions between two molecules of 36 189
Figure 128: The packing arrangement of the molecules of 36 190
Figure 129: The asymmetric unit of 43 with selected labelling 191
Figure 130: The intra-layer interactions of 43 with the hydroxyl hydrogens removed for clarity 191
Figure 131: Diagram showing the CH-π intermolecular bonds which results in staggered columnar stacking in 43 192
Figure 132: The packing of 43 viewed along the y axis 192
Figure 133: The layered packing viewed along the z axis of 43 193
Figure 134: The UV-Vis Absorption Spectra of Compounds 34, 36, 37, 43 and 44 in cyclohexane 194
Figure 135: The ^{1}H-NMR spectrum of 49 in $CDCl_3$ 205
Figure 136: The aromatic region of the ^{13}C-NMR spectrum of 49 in $CDCl_3$ 205
Figure 137: The ^{1}H-NMR spectrum of 52 in $CDCl_3$ 207

List of Schemes

Scheme 1:The cyclotrimerization of a diphenyl substituted ethyne 3
Scheme 2: An example of the Diels-Alder reaction between a substituted cyclopentadienone and a substituted ethyne 4
Scheme 3: The synthesis of a giant polyphenylene by a combination of Diels-Alder and cyclotrimerization reaction 5
Scheme 4: The fundamental reaction of oxidative cyclodehydrogenation 5
Scheme 5: The mechanism proposed by Kovacic for the oxidative cyclodehydrogenation reaction 6
Scheme 6: The cyclodehydrogenation of large polyphenylenes using Lewis acid catalysts 7
Scheme 7: The synthesis of N-HSB 8
Scheme 8: The synthesis of Ru (II) (N-HSB)$(bpy)_2$ 9
Scheme 9: The mechanism of inverse-electron demand Diels-Alder reactions involving tetrazines 12
Scheme 10: The oxidation of hydropyridazines to pyridazines (higher) with the direct one-step preparation of pyridazines from tetrazines using acetylenes (lower) 13
Scheme 11: Some of the ditetrazine products obtained from the double Diels-Alder reaction of bptz with a variety of dienophiles. Yields are also shown. 14
Scheme 12: The condensation of hydrazine and a diketone to form pyridazines 15
Scheme 13: Diels-Alder reactions involving pyridazines 15
Scheme 14: The intramolecular Diels-Alder reaction which occurs in the synthesis of a phosphodiesterase inhibitor 16
Scheme 15: The synthesis of a novel pyridazine-centred dimetallic ruthenium complex as a catalyst for water oxidation 17
Scheme 16: The route towards novel pyridazine-centred N-HSB Compounds 18
Scheme 17: The synthesis of 1 and 2 19
Scheme 18: The attempted synthesis of a number of novel tetrasubstituted pyridazines 20
Scheme 19: The synthesis of substituted pyridazine 3 21
Scheme 20: The preparation of a novel tri-substituted pyridazine-centred ligand, 3 .. 21
Scheme 21: The synthesis of 5 and 6 22
Scheme 22: The synthesis of 7 and 8 23
Scheme 23: The synthesis of 9 and 10 24
Scheme 24: The preparation of pyrazinyl substituted pyridazines 11 and 12 24
Scheme 25: The synthesis of 14 and 16 from 10 25
Scheme 26: The unsuccessful attempts at cyclodehydrogenation of pyridazine-centred polyaromatic compounds 27
Scheme 27: The incorporation of methoxy groups on the peripheral rings of polyphenylenes 27
Scheme 28: The methoxy-directed cyclodehydrogenation resulting in spirocyclic compounds prepared by Müllen (upper) and Draper (lower) 28
Scheme 29: The resonance canonical forms available with para substituted methoxy (upper) and meta substituted methoxy functional groups (lower) 29

Scheme 30: The synthesis of 3,3,5,5-tetramethoxystilbene, 17 30
Scheme 31: The synthesis of methoxy-substituted pyridazine centred ligand 19 30
Scheme 32: The cyclodehydrogenation of 19 giving 20 and 21 32
Scheme 33: General scheme for the synthesis of Ru(II) bis bpy complexes of pyridazyl ligands 84
Scheme 34: Synthesis of 27, 28 and 29 114
Scheme 35: Schematic showing the two methods (1) and (2) of the synthesis of the iron (II) tris complexes of ligands 6, 8 and 11 139
Scheme 36: The proposed synthesis of a novel nitrogen containing phenyl centred aromatic hydrocarbon 154
Scheme 37: The synthesis of 1,4-dibromo-2,3,5,6-tetraphenyl benzene 155
Scheme 38: The synthetic route towards 1,4-di-4'-(2,2':6',2"-terpyridyl)-2,3,5,6-(tetraphenyl) benzene 155
Scheme 39: 2,2':6'2" terpyridine 156
Scheme 40: The coupling of 6-bromo 2,2' bipyridine with pyridine[19] 157
Scheme 41: The Stille coupling of substituted terpyridines 158
Scheme 42: The Hantzsch Synthesis of pyridines 158
Scheme 43: The Tschitschibabin terpyridine synthesis 158
Scheme 44: The Kröhnke use of pyridinium salts in tpy synthesis 159
Scheme 45: The Potts Method of tpy Synthesis 159
Scheme 46: The synthesis of 4'-chloro-2,2':6',2" terpyridine 160
Scheme 47: The Potts method applied to asymmetricly substituted tpy compounds[27] 161
Scheme 48: Two alternative syntheses of 6-bromo-2,2':6':2" terpyridine 161
Scheme 49: The principle of electron transfer from ruthenium to osmium in terpyridine species 162
Scheme 50: The coordination of Zn to a $[Ru(tpy)_2]^{2+}$ system 163
Scheme 51: Synthetic route towards 1,4-dicarboxy tetraphenyl benzene 164
Scheme 52: Schematic showing the overlap of p orbitals and the subsequent movement of electrons to form the new ring 164
Scheme 53: The dimerization of cyclopentadiene at room temperature 165
Scheme 54: The synthesis of a tetra substituted cyclopentadienone 165
Scheme 55: The relative reactivitites of three substituted cyclopentadienones towards Diels-Alder reactions with an acetylenic dienophile[47, 48] 166
Scheme 56: Various literature methods of converting alkyl groups to aldehydes and ketones. 168
Scheme 57: The synthesis of 33 169
Scheme 58: The synthesis of 34 170
Scheme 59: The synthetic method of Wang towards substituted indenofluorenes ... 171
Scheme 60: The synthesis of 35 via oxidation of 33 172
Scheme 61: Synthesis of 36 and 37 from 33 172
Scheme 62: Proposed mechanism for the oxidative ring cleavage of 33 with benzene seleninic anhydride 173
Scheme 63: The Diels-Alder reaction resulting in the formation of 38 174
Scheme 64: The synthetic route towards di-ester substituted cyclopentadienone 175
Scheme 65: The Synthetic routes towards 41 and 42 175
Scheme 66: The reduction of 35 to give fluorenol 43 176
Scheme 67: The proposed reaction mechanism for the formation of 43 177
Scheme 68: The proposed route for the formation of fluorenols by reduction with 9-BBN 178

Scheme 69: The synthetic preparation of 44 178
Scheme 70: Proposed mechanism for the formation of 44 179
Scheme 71: The synthetic route towards 2,3,6,7-tetraphenyl substituted anthracene 197
Scheme 72: The route towards novel anthracene-centred di-terpyridyl compounds 199
Scheme 73: The synthesis of a number of substituted anthracenes 200
Scheme 74: The synthesis of 51 200
Scheme 75: The synthesis of 52 201
Scheme 76: The synthetic route towards 53 and 54 202
Scheme 77: The unsuccessful Negishi-coupling of 45 and 54 202
Scheme 78: The Synthesis of 55 203

List of Tables

Table 1: Comparison of the yields obtained in the Diels-Alder reactions of 2 and 10 with the four dienophiles 25
Table 2: The pKa's of the ligands discussed here, along with the pKa's of their conjugate acids as compared with those of bpy. 66
Table 3: Absorption Maxima of Ru(II) *bis* bpy L heteroleptic complexes in CH_3CN 68
Table 4: The low energy absorption maxima of a selection of substituted heteroleptic complexes 70
Table 5: The oxidation and reduction potentials of the Ru(II) heteroleptic bpy complexes 74
Table 6: The low energy absorption maxima of the tris iron(II) complexes of a number of ligands 77
Table 7: Yields obtained for both forms of Ru (II) *bis*-bpy Complexes 22-26 85
Table 8: The ^{1}H-NMR shift of the two 2-pyridyl ring systems in compounds 24, 25 and 26 and their respective ligands 96
Table 9: The Absorbance Maxima of 22, 23, 24, 25, 26 and Ru(II) tris bpy 105
Table 10: Electrochemistry results for compounds 22-26 in CH_3CN 107
Table 11: Reduction Potentials of the five ligands *vs.* SCE 111
Table 12: Yields obtained of each isomer for compounds 27, 28 and 29 115
Table 13: The Dihedral Angles Associated with the *fac* isomer of 27 124
Table 14: ^{1}H-NMR data of the two 2-pyridyl rings of the *fac* isomers of 27, 28 and 29 132
Table 15: Summary of the absorption bands of $[Ru(bpy)_3]^{2+}$ and both isomers of 27, 28, 29 and in MeCN 137
Table 16: Isolated yields of each isomer of the Fe(II) tris complexes 30, 31 and 32 140
Table 17: NMR data for the 2-pyridyl systems in the facial isomers of 30, 31 and 32 in CD_3CN 146
Table 18: The UV-Vis Absorption maxima associated with the Fe (II) *tris* Iron Complexes 30, 31 and 32 148
Table 19: Some of the assigned absorptions observed in the I.R. spectra of compounds 33-44 195
Table 20: The ^{1}H-NMR chemical shifts associated with disubstituted anthracenes 45-50 in $CDCl_3$ 206
Table 21: The ^{13}C-NMR chemical shifts associated with these compounds in $CDCl_3$ 206

Chapter 1

Pyridazine-Centred Ligands

1.1 Introduction

1.1.1 The Properties of PAHs

Polyaromatic hydrocarbons are different from other aromatic hydrocarbons due to their benzene-like character. This concept was first described by Clar who assigned the π-electrons that participate in the aromatic sextet to individual rings so as to obtain the maximum number of π-electron sextets, and thus the lowest energetic state.[1] This concept is described pictorially in Figure 1 for the case of phenanthrene. There are two possible arrangements, one with an aromatic sextet in the inner ring, and one with two aromatic sextets in the outer rings. The structure shown on the left in Figure 1 contains two sets of sextets and is thus the most appropriate pictorial description of phenanthrene according to Clars' theory.

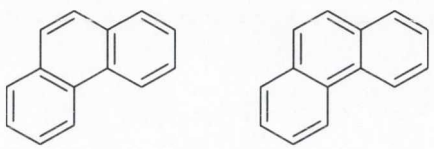


Figure 1: Two pictorial descriptions of phenanthrene

This also explains the fact that the larger more fused compounds are less stable because they have a lower quantity of π-electron sextets relative to the overall quantity of rings. Furthermore, when rings are fused angularly as in phenanthrene rather than linearly as in anthracene (Figure 2), the resulting compounds are more stable; anthracene can only contain one π-electron sextet, unlike the two in phenanthrene.



Figure 2: Two tautomers of anthracene showing the π-electron set

Figure 3 shows four different annelated 6-membered rings. Triphenylene which is shown on the left, is the only one of the three containing three π-electron sextets, and this gives rise to its different chemical properties, specifically lower reactivity and higher thermodynamic stability.[1] Triphenylene has the highest first ionization energy, largest resonance energy and is insoluble in sulfuric acid. The effect of this all-benzenoid character therefore is to suppress the olefinic behaviour of the molecule and increase its aromatic character.

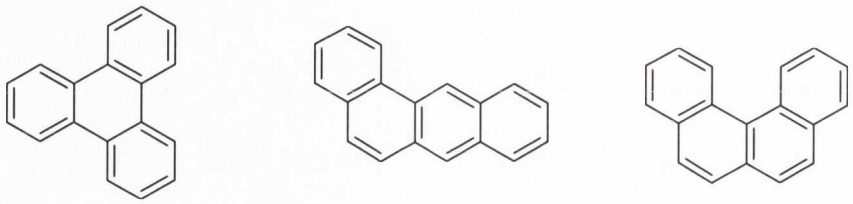


Figure 3: Triphenylene and two of its many geometric isomers, benz[a]anthracene and [4]helicene

Similar behaviour has been observed for larger PAHs which are essentially groups of fused benzene rings that have good thermal stability, low reactivity and poor solubility. In addition, these larger molecules have interesting two-dimensional and three dimensional properties; e.g. the PAH, hexa-*peri*-hexabenzocoronene shown in Figure 4 possesses diode-like electronic conduction properties according to molecular tunnelling microscopy.[2]

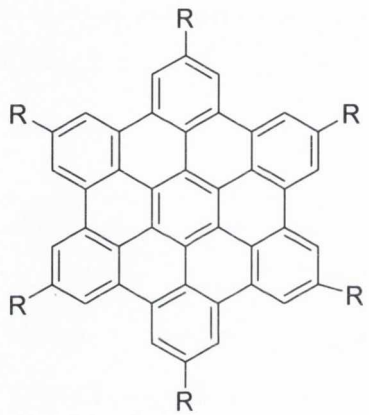


Figure 4: Hexa-*peri*-hexabezocoronene

As a result of their extended planarity, these molecules are also known to stack in solution and can form nematic or columnar liquid crystalline phases. These columns can stack side-to-side in individual non-interacting rows, which, coupled with their intrinsic ability to conduct electrons gives rise to a range of novel applications e.g. as 1-dimensional conducting nanowires. Much work has been carried out on the generation of three dimensional networks of these materials. Highly pure novel PAHs with high fluorescence quantum yields and electroluminescence properties have attracted much interest.

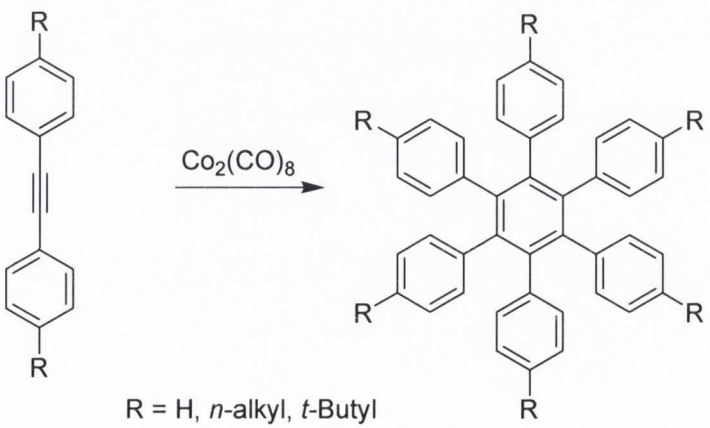
1.1.2 Synthesis of Polyaromatic Hydrocarbons

Although there are a number of methods that can be applied to the synthesis of large PAHs, a few dominate the literature. In the early days of aromatic chemistry, the standard method for the preparation of these compounds involved reaction conditions of extreme

temperature and pressure and a lengthy process of separation of the many products. The ability to produce specific target molecules was poor and better control of synthetic outcomes was necessary. Conceptually, a number of methods are possible, such as the dimerization of smaller PAHs and the addition of small carbon units to pre-formed PAH compounds.[1] In practice however, the inherent stability and unreactivity of PAHs discussed earlier precludes dimerization and hampers the addition of small aliphatic units. The popular modern route towards PAHs involves a controlled two-step procedure, the first of which is the formation of pre-organised oligophenylenes consisting of a central benzene ring with a number of aromatic substituents, each consisting of a π-electron sextet. The second step involves the oxidative cyclodehydrogenation of these systems, which in effect involves fusing the aromatic substituents to form one large planar graphite-type sheet.

1.1.2.1 The Synthesis of Oligopolyphenylenes

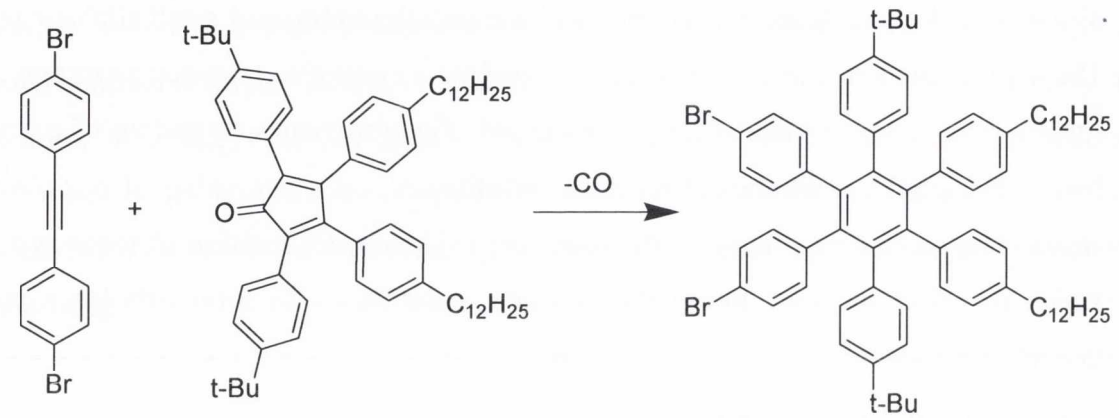
There are two routes used regularly in the synthesis of large polyphenylenes as precursors to PAHs. One of those involves the catalytic trimerization of a diphenyl substituted ethyne (Scheme 1) using cobalt octacarbonyl or more rarely nickel, palladium and ruthenium catalysts.[3-5] The substituted ethynyl compounds are prepared from standard coupling reactions such as those of Heck and Sonogashira. The diversity of these well-established reactions allows for the incorporation of a wide variety of substituents on the phenyl group such as long alkyl chains, halides or other functional groups. This is particularly relevant in overcoming the insolubility of the unsubstituted larger PAH compounds.



Scheme 1:The cyclotrimerization of a diphenyl substituted ethyne

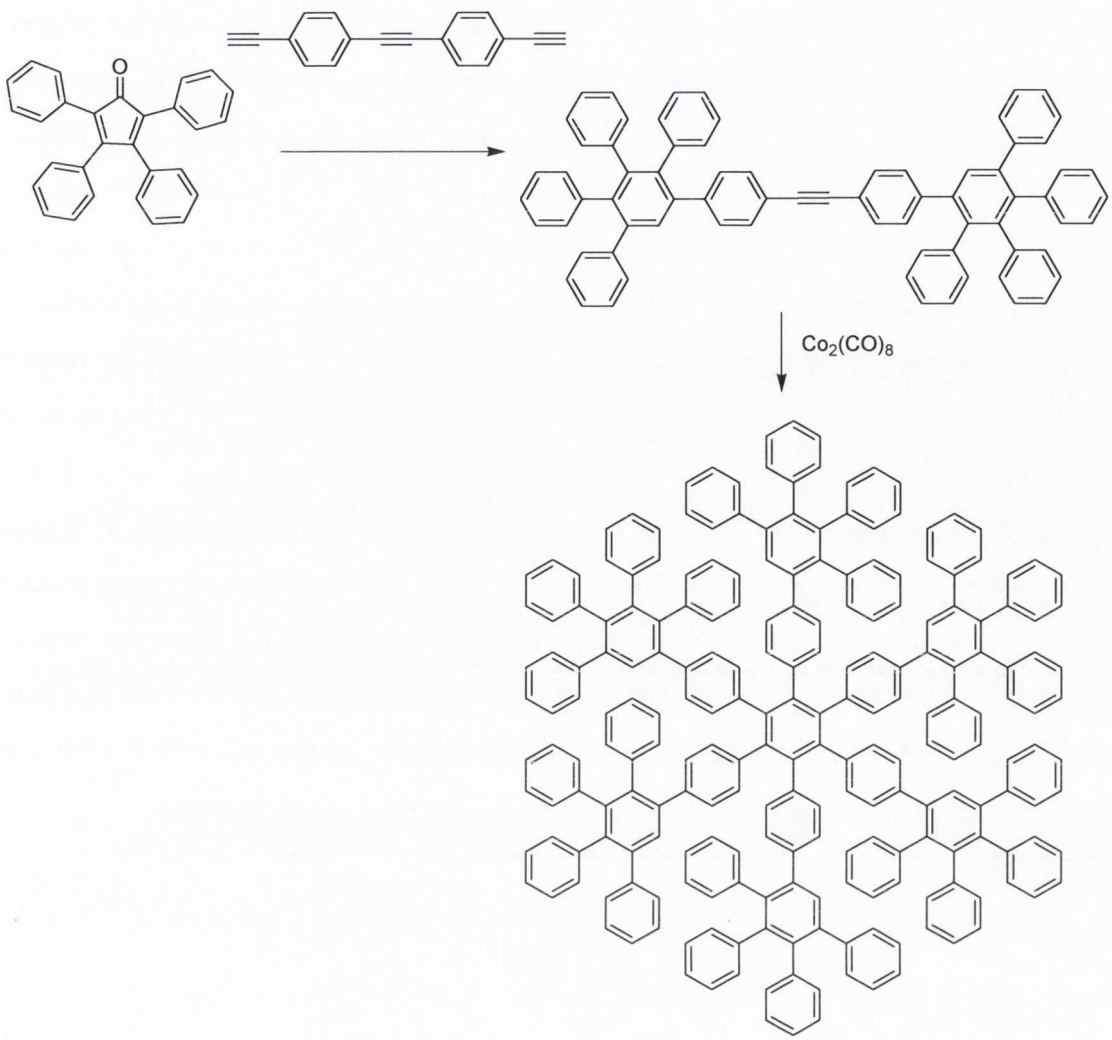
The limitation of the trimerization reaction is that it precludes asymmetrical polyphenylene compounds, e.g. with different R groups on the various aromatic rings.

Clearly the lack of selectivity in the trimerization reaction renders this method of little use for the preparation of multiply substituted compounds. The more versatile route is the well-established [4+2] Diels-Alder cycloaddition reaction between tetraphenyl substituted cyclopentadienones and diphenyl substituted ethynes at 230°C with the extrusion of carbon monoxide gas (Scheme 2).[6]



Scheme 2: An example of the Diels-Alder reaction between a substituted cyclopentadienone and a substituted ethyne

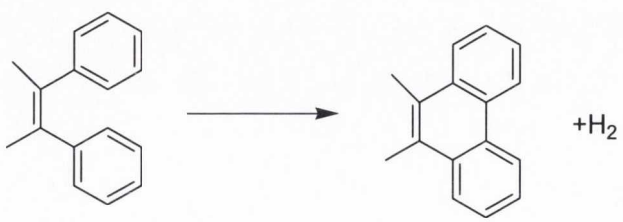
Extended multiple Diels-Alder reactions using multi-ethynyl containing compounds can be performed. Both methods have been used very effectively in successive formations to give a giant PAH. Scheme 3 illustrates one example where the first step uses a double Diels-Alder reaction between a tri-ethyne and a substituted cyclopentadienone leading to a phenyl-substituted tolane product. The central ethynyl functionality is less reactive towards Diels-Alder due to the surrounding steric bulk. The tolane can then undergo cyclotrimerization to give the large oligophenylene shown in Scheme 3.[1]



Scheme 3: The synthesis of a giant polyphenylene by a combination of Diels-Alder and cyclotrimerization reaction

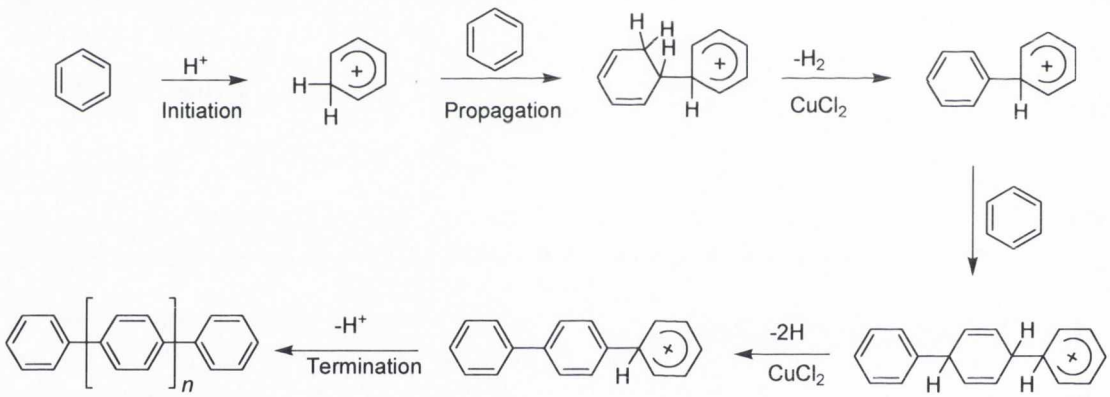
1.1.2.2 Cyclodehydrogenation

The polyphenylenes described so far consist of conjoined phenyl rings, each with the desired π-electron sextet. However, most of these rings are free to rotate and therefore these structures are three dimensional entities. In order to convert them to planar PAHs, it is necessary to fuse neighbouring phenyl rings by the removal of hydrogen atoms on each ring in an oxidative cyclodehydrogenation step (Scheme 4).



Scheme 4: The fundamental reaction of oxidative cyclodehydrogenation

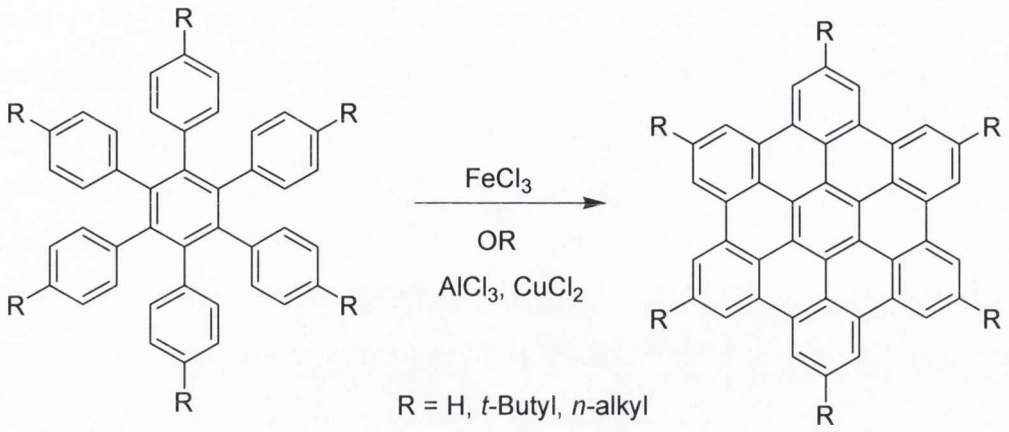
This reaction is usually carried out in the presence of a Lewis acid, capable of removing the protons. Metal salts of vanadium, thallium and even palladium-platinum charcoal have been used.[7-9] The most popular however are aluminium or iron salts. Historically these reactions were carried out at high temperature in an aluminium or iron "melt" often with the use of a co-catalyst such as sodium chloride.[10] However due to the work of Kovacic in the 1960's a combination of aluminium chloride and copper chloride is now the most popular method.[11] The reaction is carried out by the addition of the reagent to a benzene solution of aluminium chloride and copper chloride at 35°-37°C. The mixture is washed with acid and water and the cyclodehydrogenation product isolated. Kovacic proposes a cationic polymerization mechanism (Scheme 5). The addition of a proton to the phenyl system results in the formation of an arenium cation. Nucleophilic attack by an electron pair from the neighbouring ring results in coupling of the two rings. The copper co-catalyst then removes two protons and the process begins again with the addition of an acidic proton to the next phenyl ring. The reaction is quenched by the removal of the arenium proton with methanol or a weak base.



Scheme 5: The mechanism proposed by Kovacic for the oxidative cyclodehydrogenation reaction

A second possible reaction mechanism via radical formation was proposed by Pummerer and co-workers.[12] This involves the single-electron oxidation of the starting material and subsequent electrophilic C-C bond formation. Deprotonation and loss of a H atom then follow. Recent computational and experimental results have since suggested that the arenium ion method is favoured, in particular for the cyclodehydrogenation of larger systems.[13]

Kovacic also developed the synthesis by using ferric chloride ($FeCl_3$) as the Lewis acid catalyst.[14] This has the added advantage of being a strong enough oxidising agent to remove the protons without the need for a co-catalyst. Both these methods were later adopted by Müllen in the cyclodehydrogenation of large polyphenylenes (Scheme 6).[1]



Scheme 6: The cyclodehydrogenation of large polyphenylenes using Lewis acid catalysts

Both catalysts appear to work well for most of the polyphenylene precursors, although only partial cyclisation has been reported for some of the compounds containing halide substituents.[2] In addition to this, due to the effectiveness of $AlCl_3$ as a Friedel-Crafts catalyst, polyphenylenes containing aliphatic substituents may be rearranged or acylated in preference to cyclodehydrogenation. There have also been reports of chlorinated side-products in the case of the larger polyphenylene compounds.[2] Nonetheless, the success of the cyclodehydrogenation step has yielded a series of novel planar polyaromatic compounds which have provided an exciting platform for the investigation of nanowire technology and novel electron transport mechanisms.

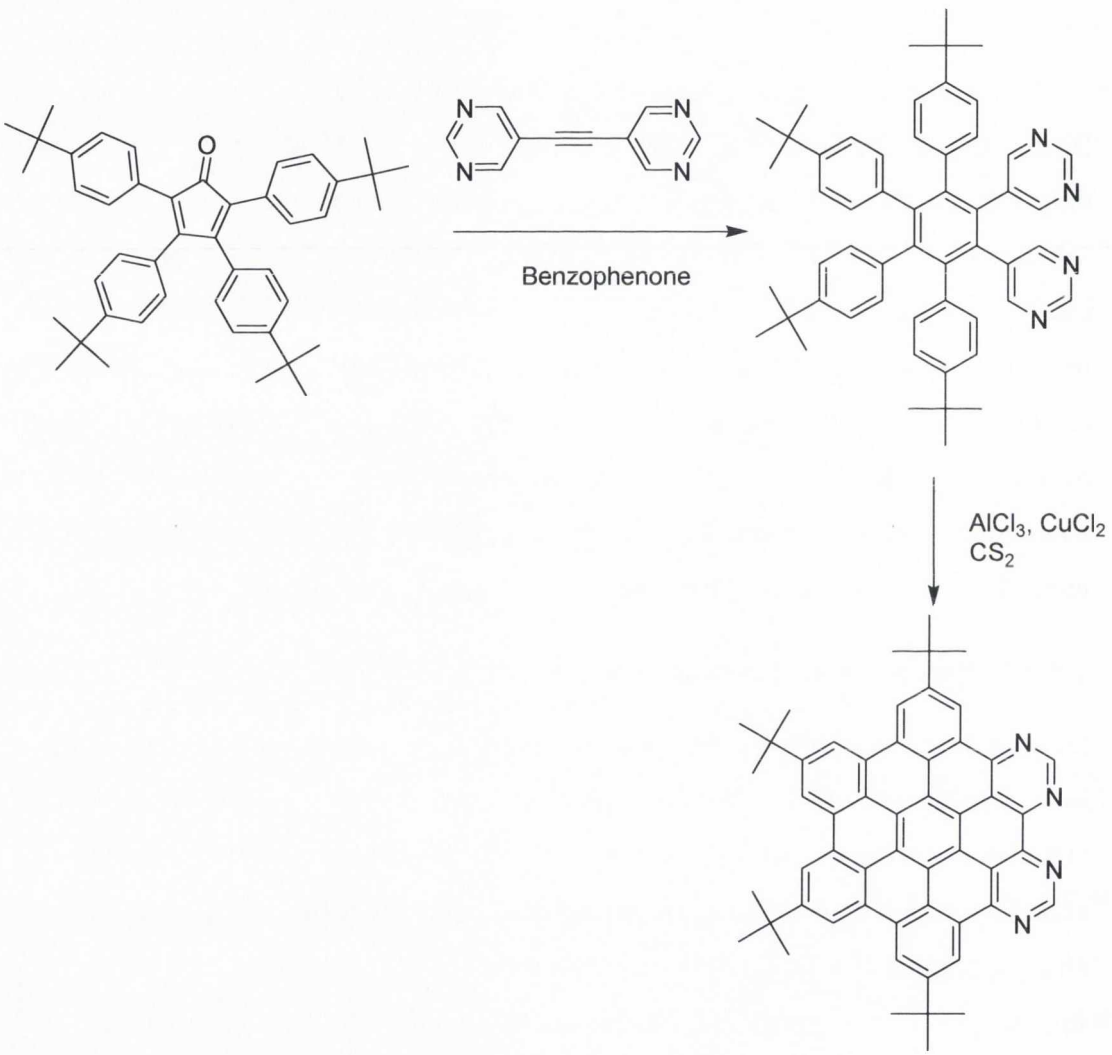
1.1.3 Incorporating Heteroatoms into PAH Systems

Despite the successful synthesis of a number of giant polyaromatic hydrocarbons as well as promising preliminary results regarding their electronic applications, a number of significant problems with these compounds have been encountered such as poor solubility which can preclude proper spectral characterisation. Such compounds rely on analysis using STM, DSC and X-ray crystallography.[1]

In 2002, our group published results which included the first heteroatomic containing HBC compound.[15] This nitrogen-functionalised "heterosuperbenzene" (N-HSB) was prepared by modifying the Diels-Alder polyphenylene synthesis of Müllen discussed earlier and adding a nitrogen-containing acetylene (Scheme 7). The incorporation of heteroatoms into the PAH framework improved solubility substantially and increased the potential applications of these compounds.

This new compound exhibited several interesting novel properties. In particular, the increased solubility in laboratory solvents such as chloroform and methanol allowed for

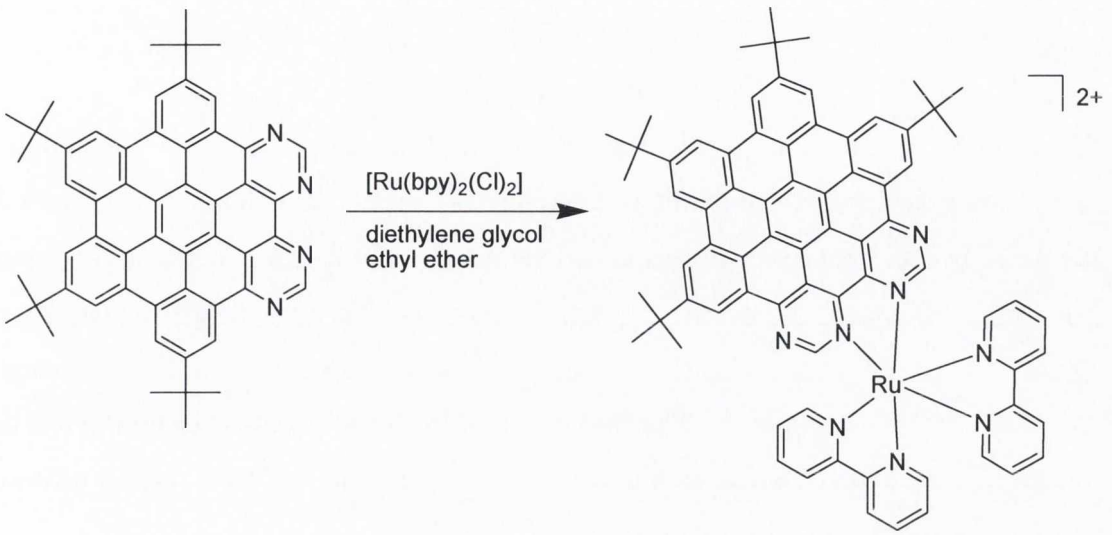
characterisation by NMR spectroscopy. The increased solubility was a result of the inherent dipole moment within the molecule due to the opposing positions of electron withdrawing nitrogen atoms and electron-donating *t*-butyl groups. The presence of the electron-rich nitrogen atoms within the planar sheet strongly influences the spectroscopic properties of the molecule. It was found to fluoresce strongly (λ 545 nm) and to have a green emission under visible and UV light. Thermogravimetric analysis indicated that the heteroatoms did not alter thermal stability which was up to 800°C.



Scheme 7: The synthesis of N-HSB

The presence of heteroatoms also gives N-HSB one obvious advantage over the all-carbon analogue – the potential for coordination chemistry with transition metals. This ligand property has also been investigated by our group and both the ruthenium *bis* bpy and ruthenium *tris* complexes of N-HSB have been prepared and characterised.[16] The spectroscopic properties of these complexes have been investigated. They possess MLCT absorptions at long wavelengths (λ 600 nm) indicative of the low-lying π*-acceptor

orbitals of the N-HSB molecule. The Ru(II) complexes are both near IR emitters and black MLCT absorbers.



Scheme 8: The synthesis of Ru (II) (N-HSB)(bpy)$_2$

Additional work on the important cyclisation step in the formation of N-HSB resulted in the synthesis of a "half-cyclised" analogue which also has interesting spectroscopic properties.[17] Unusually, the ruthenium *bis* bpy complex of this ligand maintains many of the photochemical properties of the fully cyclised analogue despite the reduced planarity of the molecule. It avoids some of the aggregation issues which are inherent in the original N-HSB molecule. Work continues on other variations of this interesting novel family of compounds, and investigations in to more and less cyclised products and their spectroscopic properties are in progress.

1.1.4 Increasing the Quantity of Heteroatoms in the PAH system

Clearly the incorporation of heteroatoms into the polyaromatic systems has led to a novel class of compound with unique and interesting chemical and photochemical properties. There are many possible positions for the inclusion of nitrogen atoms and opportunities to extend the number of nitrogen atoms in the framework. A simple method toward heteroatom -containing polyphenylenes could be through the Diels-Alder reaction of substituted tetrazines with suitably substituted dienophiles. This was one of the motivations behind the work presented in this chapter.

1.1.4.1 Tetrazines

Tetrazines consist of six-membered rings with four nitrogens in the ring. The most stable form of this compound is the 1,2,4,5-tetrazine isomer shown in Figure 5.

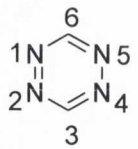


Figure 5: 1,2,4,5-tetrazine

This compound was first prepared in 1907 by Hantzsch and Lehmann.[18] Although some examples have appeared in the literature involving the coordination chemistry of 1,2,4,5-tetrazine it is the 3,6-disubstituted tetrazines which have become increasingly popular in the field of coordination and supramolecular chemistry.[19] In particular 3,6-di-(2-pyridyl)-1,2,4,5-tetrazine (bptz) has been extensively used in coordination chemistry (Figure 6).[20] This compound was first prepared in 1959 by Dallacker by the reaction of cyanopyridine hydrochloride with hydrazine in the presence of Raney nickel followed by subsequent oxidation of the hydrotetrazine.[21]

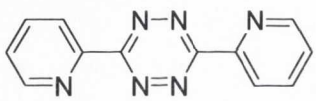


Figure 6: 3,6-di(2-pyridyl)-1,2,4,5-tetrazine (bptz)

Much of the recent supramolecular work involving bptz has arisen due to the ease of reduction of tetrazines which results in highly conductive coordination polymers and strongly coupled mixed-valent bimetallic systems.[20] This high conductivity and overall electron affinity is due to the unusually low-lying π^* unoccupied a_u orbital which arises from the presence of the four electronegative nitrogen atoms on the central ring. This low-lying LUMO greatly facilitates the transmission of charge by forming a radical anion as an intermediate. Furthermore, due to the presence of a nodal plane along the axis of the two carbons of the a_u orbital, substitution at the 3- and 6- position has very little effect on the electron delocalization, and therefore the LUMO of bptz and other substituted tetrazines remains a largely tetrazine-centred a_u orbital. The highest occupied molecular orbitals (HOMO) of tetrazine systems are combinations of the lone pairs from the nitrogen atoms. The presence of four electronegative nitrogen atoms in a conjugated system, and the inherent electron-acceptance of the tetrazine result in a very low basicity of the individual nitrogen atoms on the tetrazine ring. This results in different metal binding properties between the tetrazine nitrogen and the 2-pyridyl nitrogen of bptz. The tetrazine donor atoms have poor σ-donor character but are excellent π-acceptor ligands, whereas the 2-pyridyl ring has poor back donor ability but good σ-donation properties. The metal-N bond lengths of these compounds vary therefore from metal to metal.

Kaim and co-workers have prepared a number of ruthenium complexes using bptz as a bridge between two $[Ru(bpy)_2]^{2+}$ or $[Ru(NH_3)_4]^{2+}$ units and investigated the electrochemical properties of these compounds.[22] The same group published an ESR (electron spin resonance) study of several metal carbonyl complexes where bptz was used as a bridging ligand between tungsten, molybdenum and chromium carbonyl moieties.[23] Other investigations have included the study of a paramagnetic nickel centred bpdz complex which was obtained in high yield from the simple addition of a nickel salt to bpdz in methanol at room temperature.[24] Constable and co-workers have prepared di-metallic silver and copper complexes of bptz in a similar manner.[25] Interestingly, the two silver units coordinated in a cisoid conformation to the bptz ligand as opposed to the more common transoid conformation obtained by Kaim and others (Figure 7).

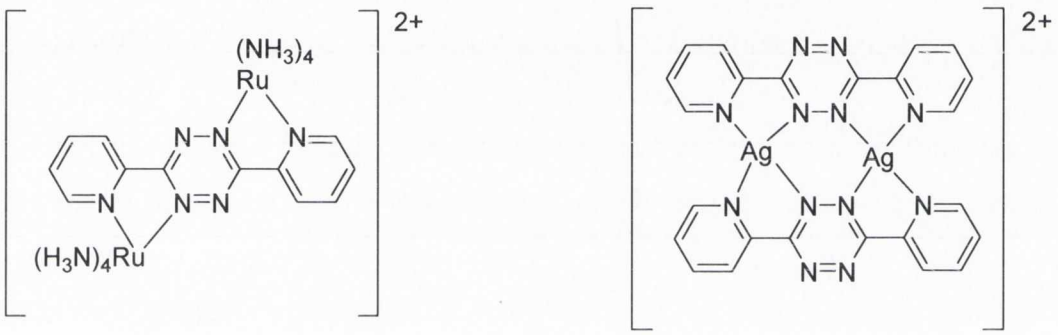


Figure 7: The Ru(II) bpdz complex of Kaim which adopts the transoid conformation (left) and the cisoid Ag(I) bptz complex of Constable (right)

1.1.4.2 Diels-Alder Reactions of Tetrazines

Apart from the novel coordination and supramolecular properties of tetrazines, their ability to undergo inverse electron demand Diels-Alder reactions with suitably electron rich dienophiles has led to other avenues of research. Carboni and Lindsey reported the first of these types of reactions using phenyl and fluoro-substituted tetrazines and substituted dienophiles.[26] They noted the improved reactivity of the tetrazine when electron-withdrawing groups are present.

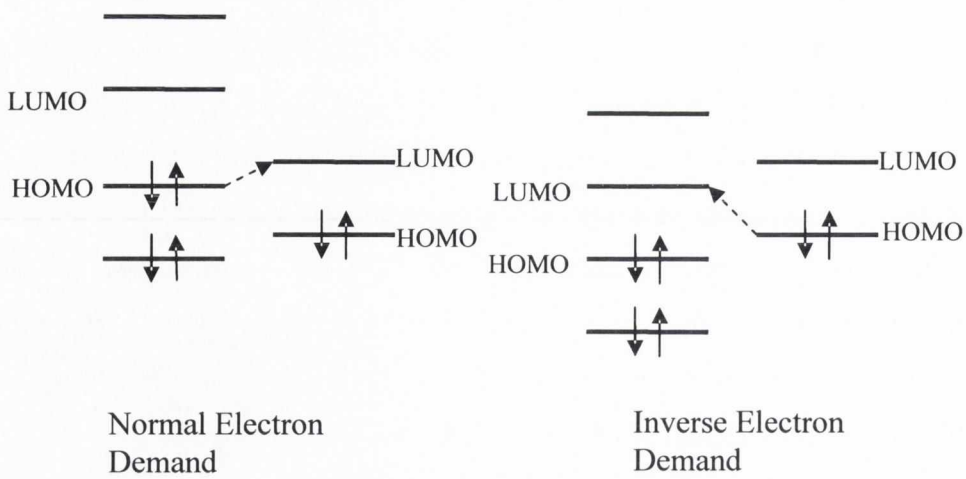
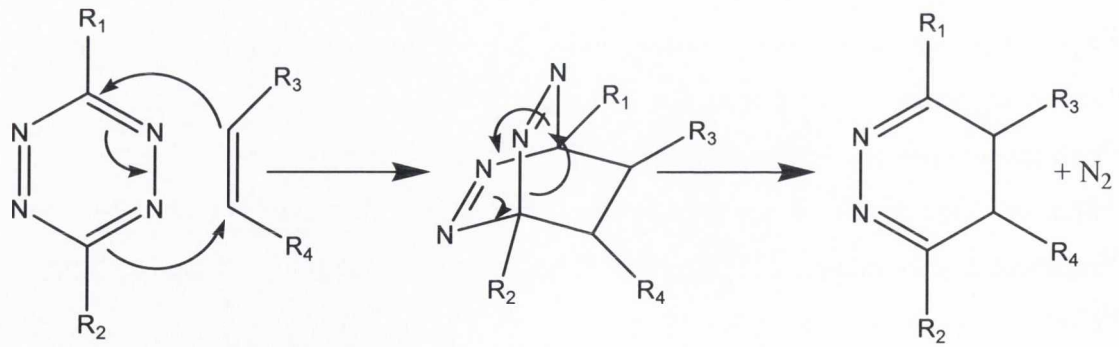


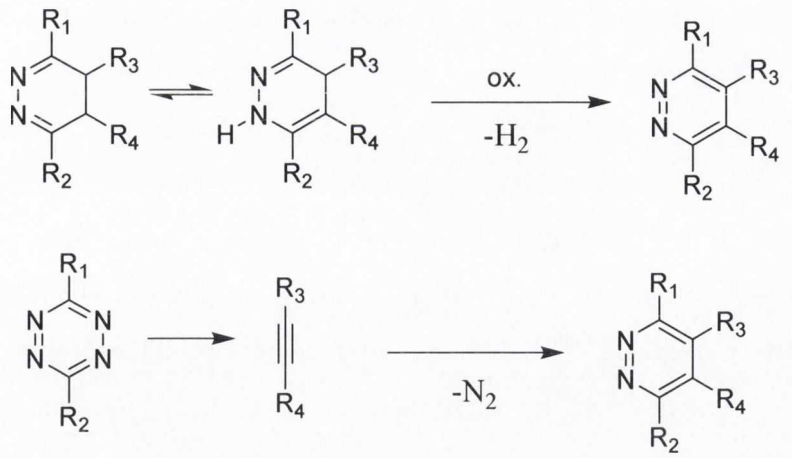
Figure 8: Diagram showing the frontier orbital interactions in normal demand and inverse demand Diels-Alder reactions

In Diels-Alder reactions, two new bonds are formed *via* a 4n+2 cycloaddition reaction. In normal demand Diels-Alder electrons move from the HOMO of the diene to the LUMO of the dienophile (Figure 8). However, in the case of tetrazines, the unusually low LUMO allows for the electrons to flow between the HOMO of the dienophile and the LUMO of the diene. It is for this reason that electron-withdrawing groups on the tetrazine and electron-donating groups on the dienophile encourage this reaction. The Diels-Alder reaction is believed to occur in a one step concerted mechanism which involves the extrusion of nitrogen when tetrazines are used as the diene (Scheme 9). The resulting heterocyclic compound is a dihydro-pyridazine-centred moiety with two nitrogens in the 1- and 2- positions.



Scheme 9: The mechanism of inverse-electron demand Diels-Alder reactions involving tetrazines

These compounds often undergo sigmatropic rearrangement to give 1,4-dihydropyridazines, which can then be oxidised with common oxidising agents to pyridazines (Scheme 10, higher). Alternatively, the use of acetylenes as dienophiles results directly in pyridazine products, due to their higher oxidation state (Scheme 10, lower).



Scheme 10: The oxidation of hydropyridazines to pyridazines (higher) with the direct one-step preparation of pyridazines from tetrazines using acetylenes (lower)

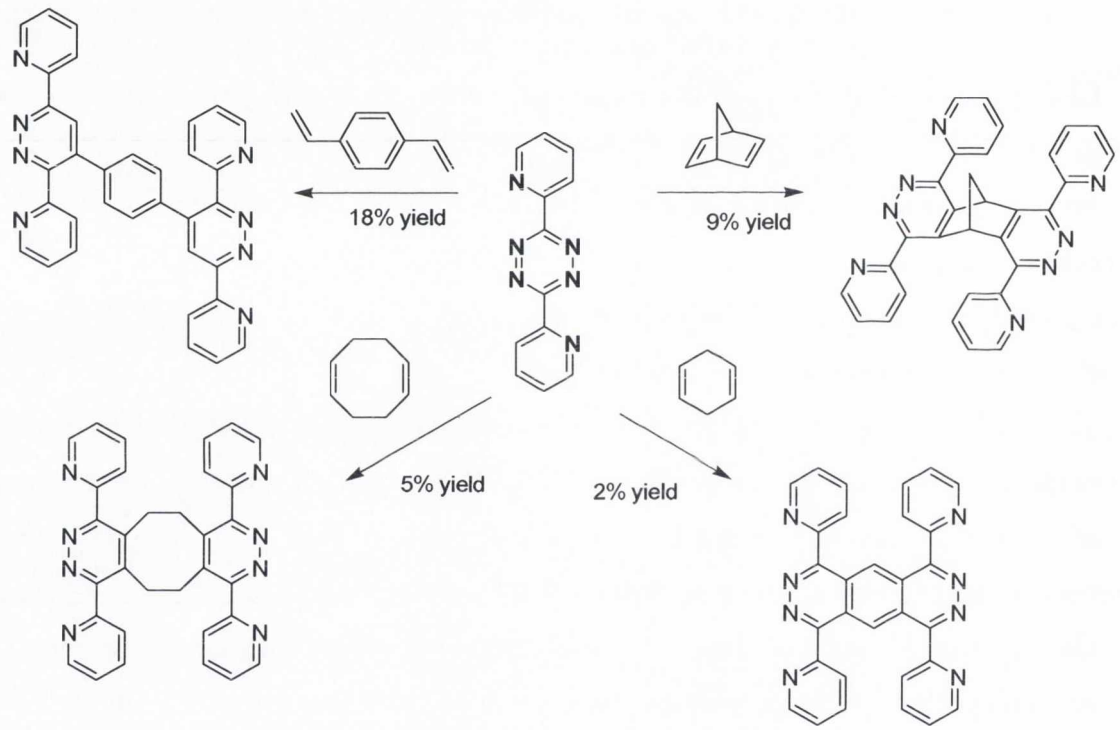
Clearly the two 2-pyridyl substituents of bptz cannot be considered as electron-donating groups. The majority of the literature regarding Diels-Alder reactions of tetrazines involves greater electron donating substituents at the 3- and 6- positions such as methoxy esters and perfluoronate chains.[27] The first use of bptz as a diene in Diels-Alder reactions was reported by Butte and Case using alkenes substituted with cyano and phenyl substituents as dienophiles.[28]

The mild electron-withdrawing effect of the 2-pyridyl substituents on the bptz clearly renders this ligand less reactive towards Diels-Alder reactions, and carefully selected use of appropriate dienophiles is necessary. Substituted acetylenes, ketones or alkenes have been used extensively in this regard. Until recently, these difficulties appeared to discourage much research into the use of bptz as a diene. However, the advent of the supramolecular age has encouraged chemists to discover novel multi-dentate ligands and it appears that the pyridazyl products of bptz Diels-Alder reactions are excellent candidates for the building of novel metal-centred supramolecular frameworks.

Schubert and co-workers employed alkyl-substituted acetylenes to prepare substituted pyridazines which were used in the successful formation of silver-centred supramolecular assemblies.[29] The same group have also used substituted alkenes and ketones successfully as dienophiles and synthesised a series of novel pyridazines *via* microwave irradiation in DMF.[30] Other groups have used bptz in Diels-Alder reactions with large bulky dienophiles such as fullerene.[31] Schröder, Champness and co-workers have reported the synthesis of a number of di- and tripyridazyl ligands by the selective double and triple Diels-Alder reactions between bptz and a number of alkenes .[32] However

yields were generally poor and varied from 0.2 % to 43%. Some of the products obtained are shown in Scheme 11.

As discussed above, one of the advantages of using acetylenes in preference to alkenes as dienophiles is that due to the higher oxidation state of acetylenes, the pyridazine product will be obtained directly. Unless the alkene substituents on the dienophile are excellent leaving groups, such as methoxy or hydroxyl groups, a further oxidation step is necessary to obtain the pyridazine.[30] Schröder and Champness address this by oxidising the hydropyridazine *in situ* with the use of [bis(trifluoroacetoxy)iodo]benzene as an oxidising agent.



Scheme 11: Some of the ditetrazine products obtained from the double Diels-Alder reaction of bptz with a variety of dienophiles. Yields are also shown.

Recent publications suggest that Diels-Alder reactions involving bptz may be further encouraged by catalysis. Wang and co-workers reported high yields using substituted 2-butanone as a dienophile and L-proline as a a catalyst to give the substituted pyridazine product.[33] A variety of both acyclic and cyclic ketones gave similar substituted pyridazines in excellent yields.

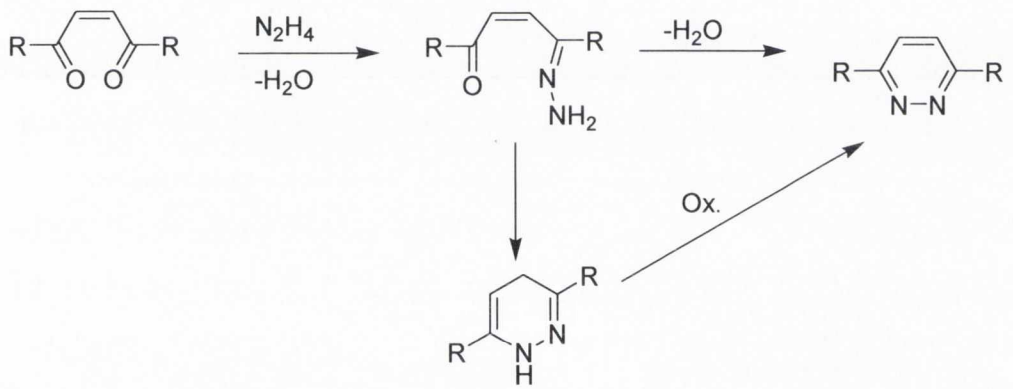
1.1.4.3 Pyridazines

Pyridazines are six-membered rings with four carbons and two adjacent nitrogens. They are one of the lesser-studied heterocyclic ring systems due to their rare occurrence in

nature, although their application as growth-inhibitors, herbicides and calcium sensitizers applied for treatment of heart failure ensures that there is an ongoing field of pyridazine synthetic research.[34, 35]

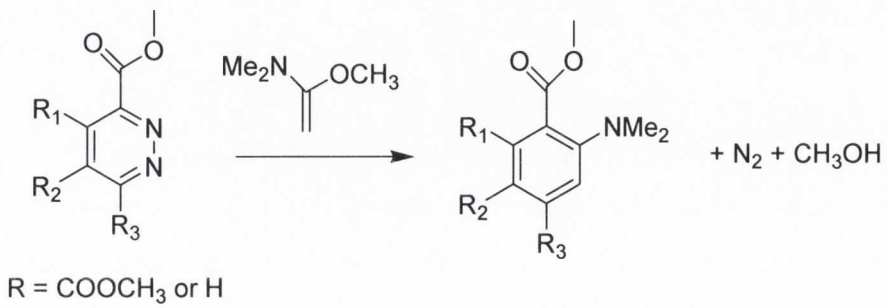
The pyridazine ring is a very stable heteroatomic ring system, and most of the chemistry relating to these compounds involves the chemistry of the substituents – the central ring generally remains intact, although the nitrogen atoms, being more basic than the other diazines (pK_a = 2.3) willingly accept protons to form dihydropyridazines. They are also susceptible to electrophilic attack from metal halides or Grignard reagents.

An alternative synthesis of pyridazines from the Diels-Alder reaction of tetrazines involves the condensation of diketones and hydrazine (Scheme 12).[34] Depending on the reaction conditions, a pyridazine may be directly obtained with the loss of two equivalents of water, or a further oxidation step may be necessary to oxidise the hydropyridazine. Bromine in glacial acetic acid or common oxidising agents such as potassium dichromate are excellent for this purpose.



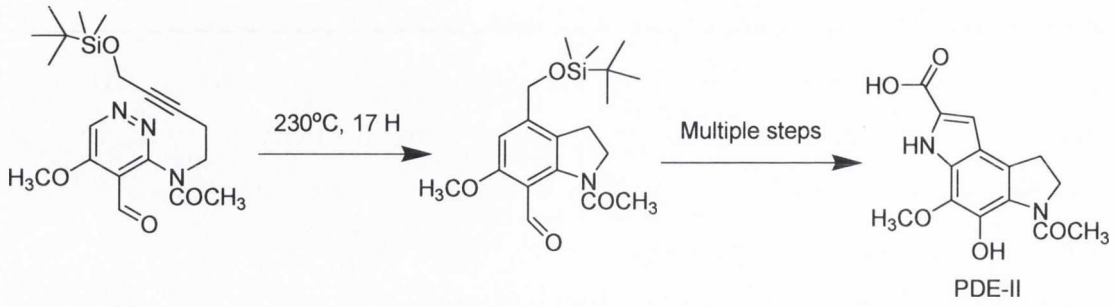
Scheme 12: The condensation of hydrazine and a diketone to form pyridazines

Diels-Alder reactions involving pyridazines are uncommon and feature pyridazines with electron-donating methyl-ester groups and strongly electron-donating dienophiles (Scheme 13).[36]



Scheme 13: Diels-Alder reactions involving pyridazines

Another example of a Diels-Alder reaction involving pyridazines is the intramolecular reaction of an alkynyl substituted pyridazine during the synthesis of phosphodiesterase inhibitor, PDE-II.[27] Once again the presence of electron-donating methoxy groups as well as harsh reaction conditions are necessary for this reaction to occur.



Scheme 14: The intramolecular Diels-Alder reaction which occurs in the synthesis of a phosphodiesterase inhibitor

1.1.4.4 Substituted Pyridazines as Ligands

2-pyridyl substituents at the 3- and 6- positions of the pyridazine ring enable the molecule to chelate to metal centres, just as in the bptz molecule. Indeed, 3,6-di(2-pyridyl) pyridazine (bppn) has become almost as popular as bptz in the field of supramolecular chemistry. One reason for this is the increased control that this ligand can bring to supramolecular frameworks as it can chelate only in a cisoid conformation.

Dunbar and co-workers have investigated the self-assembly properties of the bppn ligand with a silver salt and carried out a number of crystallographic studies on the resultant silver grids.[37] Other groups have used palladium to form dinuclear complexes with two palladium atoms in close proximity.[38] Other metals which have been coordinated to bppn include copper and iridium (Figure 9).[39, 40]

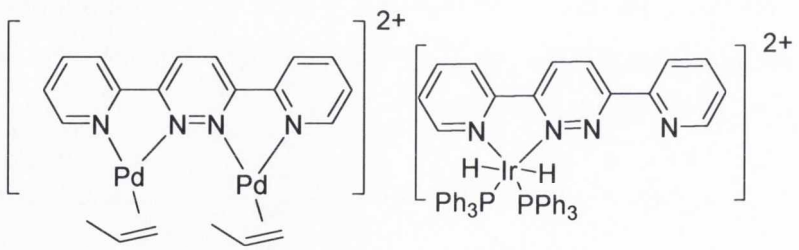
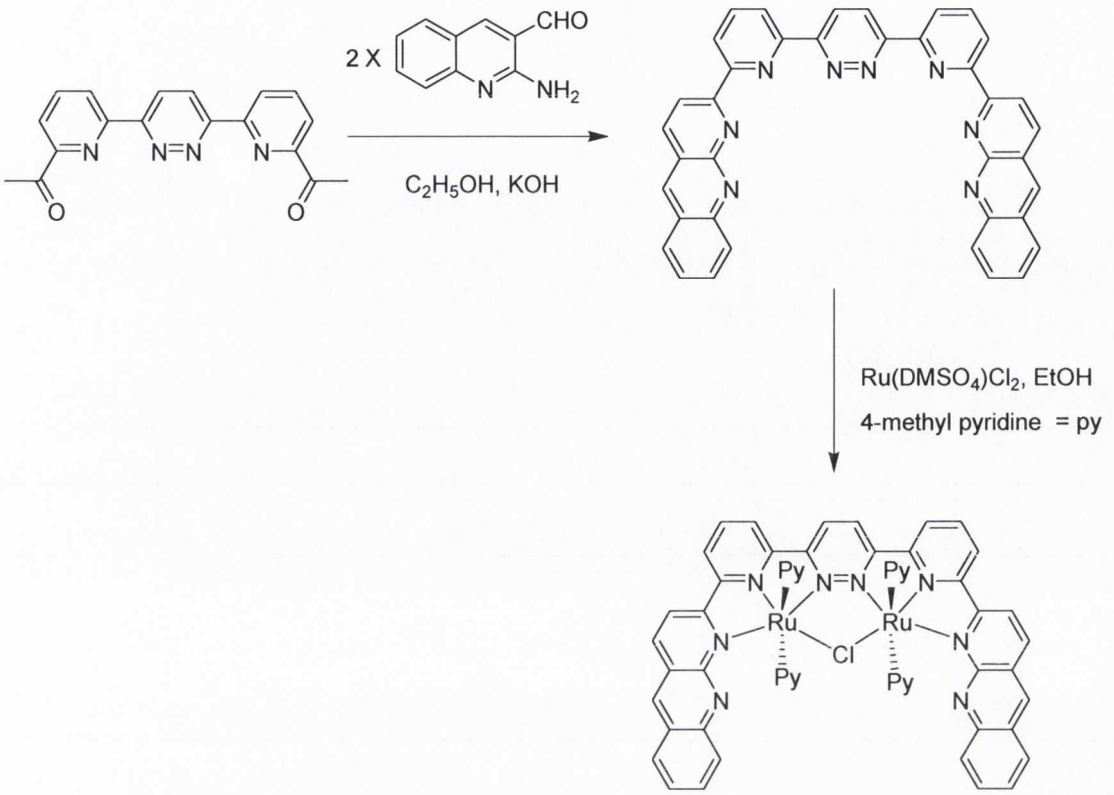


Figure 9: Some metal complexes prepared from bppn

Other groups have extended the substituents on the 3- and 6- positions to investigate the effect of the metal on the ligands. Lehn and co-workers investigated the supramolecular chemistry of 3,6-bis[2-(6-phenylpyridine)]pyridazine (pppz) by applying the free ligand in chloroform to solutions of silver triflate and characterising the resulting complex by SEM and X-ray diffraction.[41] A more elaborate substitution of the 3- and 6- position was

carried out by Thummel and co-workers in the synthesis of their ruthenium-centred metal complexes for the catalysis of water oxidation (Scheme 15).[42]



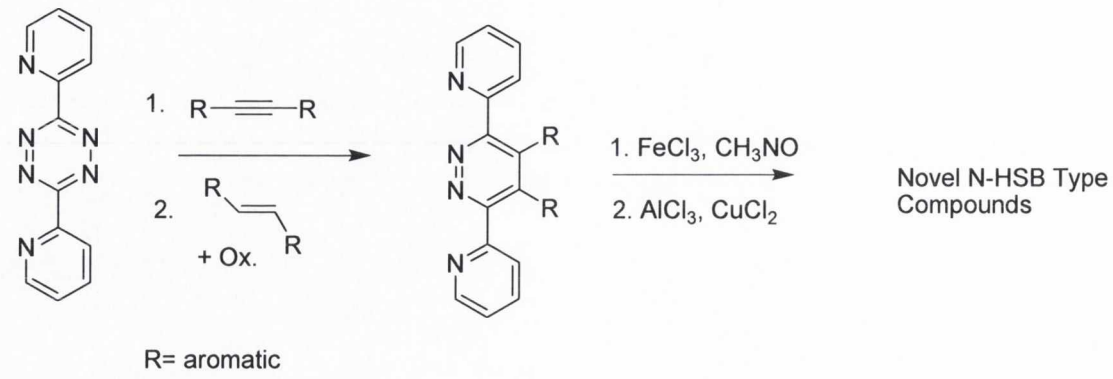
Scheme 15: The synthesis of a novel pyridazine-centred dimetallic ruthenium complex as a catalyst for water oxidation

By reacting 3,6-di(6'-acetylpyrid-2'-yl)-pyridazine with two equivalents of aminoquinoline-3-carbaldehyde, a novel multidentate ligand was formed. This ligand was then reacted with two equivalents of a ruthenium salt in pyridine to give the di-nuclear complex shown in Scheme 15. The catalytic activity of these complexes continues to be investigated.

1.1.4.5 Pyridazine-Centred Ligands as Precursors to N-HSBs

The ability to control the substituents on the 4- and 5- positions of 3,6-di(2-pyridyl) pyridazines depends on the nature of the dienophile, and it was hoped that by reacting bptz with suitably substituted acetylenes or alkenes, potential precursors for novel N-HSBs could be prepared. These N-HSB type compounds would be sterically smaller, consisting of fewer fused rings, and thus hopefully more soluble, in addition to containing more heteroatoms than the original N-HSB compound. Furthermore, the simple one-step Diels-Alder reactions involving bptz allows for the introduction of a wide variety of substituents at the 4- and 5- positions of these compounds by appropriate selection of the

dienophile, and could lead to interesting multidentate ligands for supramolecular chemistry.



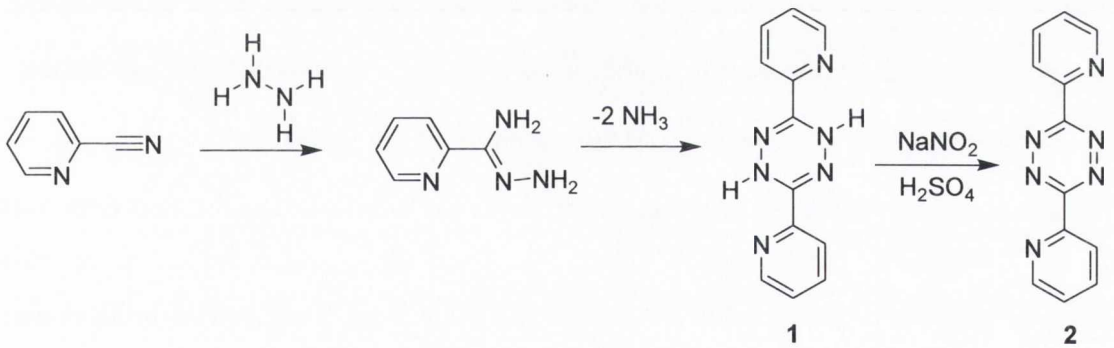
Scheme 16: The route towards novel pyridazine-centred N-HSB Compounds

The following work describes the attempts to prepare and characterise these novel ligands and discusses some of the challenges and difficulties encountered along the way.

1.2 Results and Discussion

1.2.1 Synthesis of 3,6-di(2-pyridyl)-1,2,4,5-tetrazine

The first step in the preparation of novel N-HSB type compounds involved the synthesis of the tetrazine starting material, 3,6-di(2-pyridyl)-1,2,4,5-tetrazine. This compound was prepared according to the synthesis described by Geldard and Lions in the 1960's which involves the heating of 2-cyanopyridine with an excess of hydrazine hydrate at 90°C (Scheme 17). The resulting amide hydrazone condenses to form 3,6-di(2-pyridyl)-1,2,4,5-dihydrotetrazine (**1**) in 41% yield.[43] The oxidation step was modified slightly in accordance with Boger's description of the preparation of dimethyl-1,2,4,5-tetrazine-3,6-dicarboxylate by preparing the nitrous oxide gases in a separate vessel and blowing them through the hydrotetrazine solution.[44] This allows for a higher yield and easier product work-up. Thus, nitrous oxide gases were prepared from sulfuric acid and bubbled through a dichloromethane solution of **1**. The solvent was then removed and the mixture dissolved in water and neutralised. Subsequent recrystallisation from toluene gave 85% of bptz (**2**).



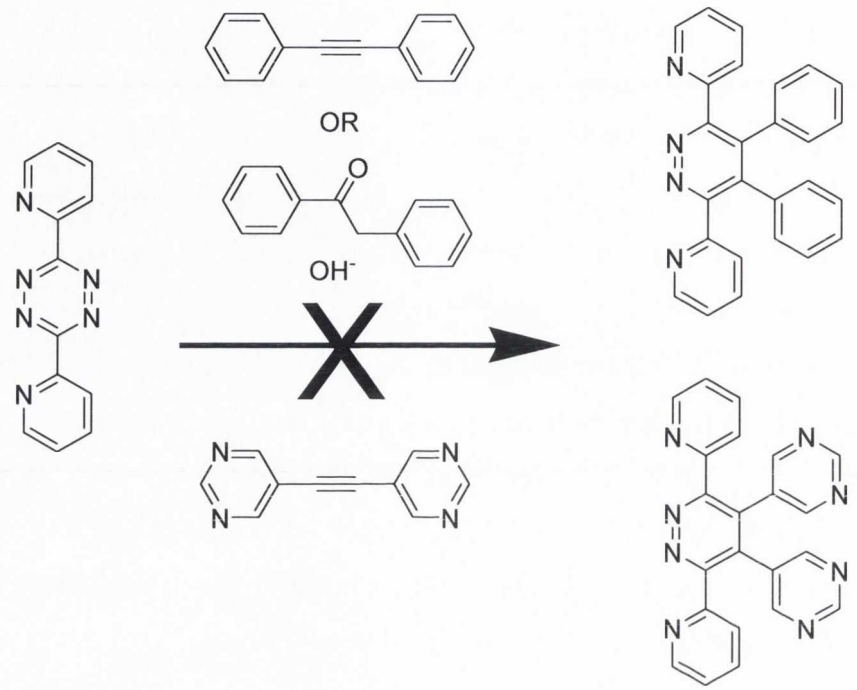
Scheme 17: The synthesis of 1 and 2

1.2.2 The Attempted Synthesis of tetrasubstituted pyridazine ligands

A number of compounds were highlighted as potentially good dienophiles for Diels-Alder reactions with **2**. Amongst these were diphenyl acetylene, and di-(pyrimidin-3,5-yl)ethyne. The former is commercially available, and the latter is prepared *via* a double Sonagashira coupling reaction from 2-bromo-pyrimidine and 2-methyl-3-butyn-2-ol.[15] Both of these reagents were refluxed separately with **2** in toluene for 48 hours. After this time no colour change was noticed and TLC confirmed that no reaction had occurred.

Following the method described by Haddadin and co-workers, it was decided to use a substituted ketone in basic media as a dienophile.[45] Deoxybenzoin or 1,2-diphenylethanone, was added to a stirring THF solution containing **2**. A small quantity of

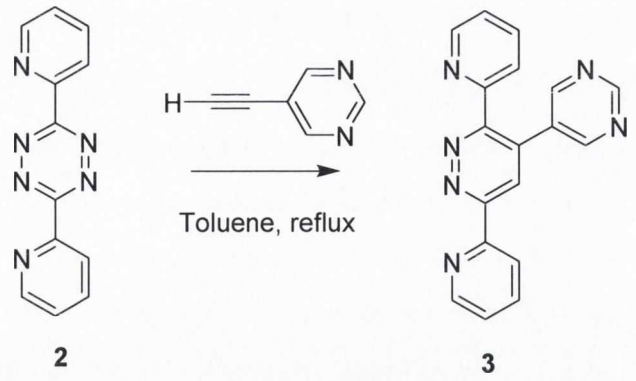
methanolic KOH was added to this, and the reaction was heated, but once again there was no change in the tetrazine colour and TLC confirmed no reaction had occurred. These results are summarised in Scheme 18.



Scheme 18: The attempted synthesis of a number of novel tetrasubstituted pyridazines

1.2.3 The synthesis of tri-substituted pyridazine ligands

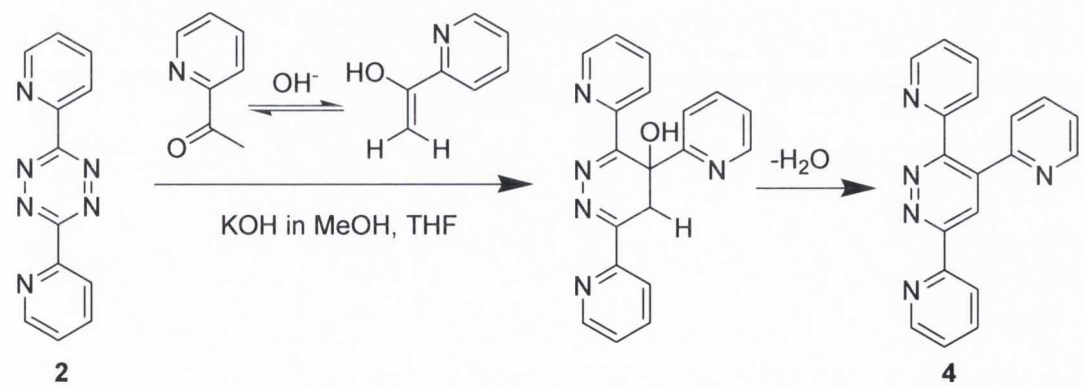
It was then thought that there may be steric considerations during the ring formation step when using these di-aromatically substituted dienophiles, and therefore the reaction was attempted with mono-substituted dienophiles. To this end, 5-ethynyl pyrimidine was used as a substituted acetylenic dienophile. This acetylene is prepared *via* a Sonogashira coupling reaction and is an intermediate in the preparation of di-(pyrimidin-3,5-yl)ethyne. This was refluxed in toluene with **2** overnight, during which time the reaction mixture turned light brown. After removal of the solvent and purification by column chromatography, 3,6-di-(2-pyridyl)-4-pyrimidyn-pyridazine (**3**) was isolated in 65% yield (Scheme 19). This clearly indicates that both acetylenic and alkenyl dienophiles can be successfully used with **2** in Diels-Alder reactions.



2 3

Scheme 19: The synthesis of substituted pyridazine 3

Following on from this success, the Haddadin method was again attempted; this time using a mono-substituted ketone, 2-acetyl pyridine. A THF solution containing **2** and 2-acetyl pyridine was stirred and warmed to 40°C. A 10% solution of methanolic KOH was added dropwise to the mixture. Immediately bubbles formed in the reaction indicating the evolution of nitrogen, and the pink colour was replaced by a dark brown. After five minutes the reaction was quenched and extracted into dichloromethane. Purification by column chromatography followed by recrystallisation yielded 3,4,6-tri(2-pyridyl) pyridazine (**4**) in 80% yield. The reaction scheme is shown in Scheme 20. The addition of a base to the substituted ketone allows for the enol tautomer to add in a 4n + 2 cycloaddition to form the substituted hydropyridazine. However, the OH at position 4- is such a good leaving group that this compound is not isolated and the pyridazine **4** is formed in one-step with the loss of water.



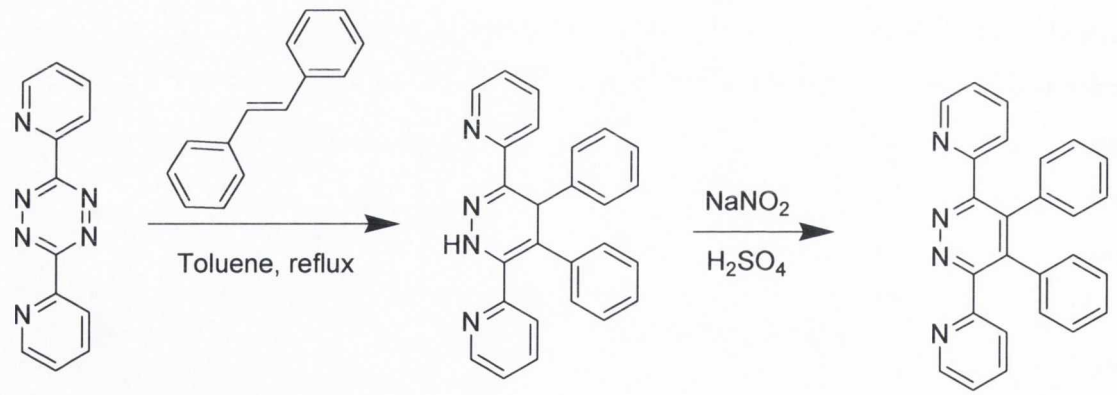
2 4

Scheme 20: The preparation of a novel tri-substituted pyridazine-centred ligand, 3

This success indicated that aromatic substituents could be added to pyridazines at the 4-position via Diels-Alder reactions with **2** using ketones in basic media.

1.2.4 The synthesis of 3,4,5,6-tetrasubstituted pyridazine ligands

Despite the initial setback using di-substituted acetylenes and ketones, it was hoped that by choosing more reactive dienophiles, steric issues could be overcome and four aromatic substituents could be added to a pyridazine centre, providing excellent precursors for N-HSB compounds. With this in mind it was hoped that the alkenyl analogue of diphenyl acetylene, stilbene, would be more reactive with **2**, and consequently, *trans*-stilbene was reacted with bptz in toluene by refluxing overnight. The gradual replacement of the pink tetrazine colour with a bright yellow indicated that some reaction was taking place, and this was confirmed by TLC. After the pink colour had completely disappeared, the solvent was removed and the reaction purified by column chromatography to give 3,6-di(2-pyridyl)-4,5-diphenyl hydropyridazine (**5**) in 92% yield. This bright yellow compound was then oxidised. Nitrous gases were produced by the dropwise addition of sulfuric acid to an aqueous solution of sodium nitrite, and these gases were then blown through a dichloromethane solution of **5** at 0°C. This mixture was then stirred and allowed to return to room temperature before removing the solvent. The remaining solid was dissolved in water, neutralised with ammonia and extracted into the organic phase. 3,6-di(2-pyridyl)-4,5-diphenylpyridazine (**6**) was isolated by column chromatography in 74% yield (Scheme 21).



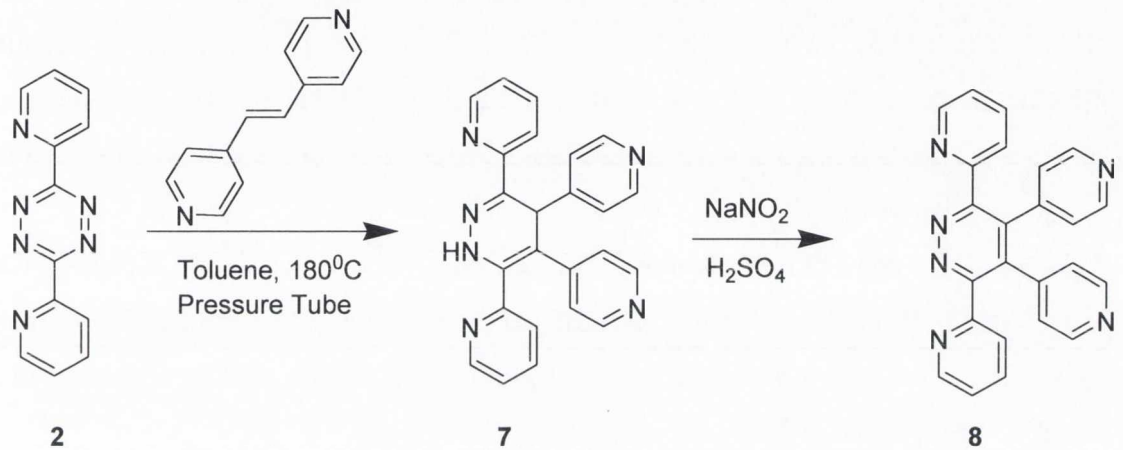
2 **5** **6**

Scheme 21: The synthesis of 5 and 6

Concurrent with the writing of this thesis, Constable and co-workers reported the synthesis of compound **6** by heating diphenyl acetylene and bptz at 170°C without solvent.[46] This work also includes a number of novel substituted pyridazines suitable for coordination and supramolecular chemistry.

Following the success of using trans-stibene as a dienophile with **2**, a similar reaction was then attempted with 1,4-di(4-pyridyl) phenylene by refluxing this compound with **2** in

toluene overnight. The reaction only proceeded to a very small degree. The alkene and **2** were thus added to a sealed tube with 5 mL of toluene and heated at 180°C overnight. After this time the pink tetrazine colour had completely disappeared and was replaced by bright yellow. A similar work-up as before yielded 3,6-di(2-pyridyl) 4,5-di(4-pyridyl) hydropyridazine (**7**) in 75% yield. Oxidation was again carried out using nitrous oxide gases to give the pyridazine analogue, 3,6-di(2-pyridyl) 4,5-di(4-pyridyl) pyridazine (**8**) in 50% yield. The lower yield associated with this reaction may be due to the more electron-withdrawing 4-pyridyl substituents on the hydropyridazine ring, which render the ring more difficult to oxidise. Scheme 22 shows the synthetic route towards **8**.



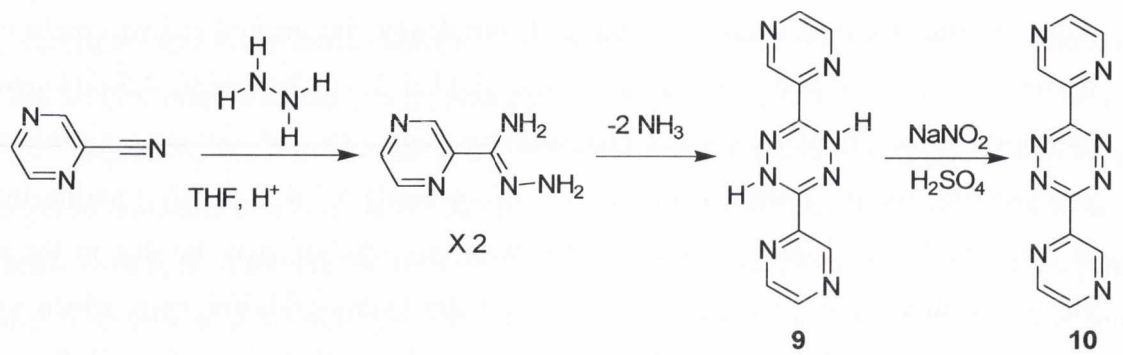
Scheme 22: The synthesis of 7 and 8

1.2.5 Pyridazines from other substituted tetrazines

One of the key aspects of this project was to incorporate more heteroatoms into the polyaromatic N-HSB precursors. The success of the Diels-Alder reaction of 1,4-di(4-pyridyl) phenylene with bptz had clearly indicated the ability to introduce heteroatoms on the 4- and 5- positions of pyridazines by suitable choice of dienophile. However, incorporating more heteroatoms at the 3- and 6- positions is dependent on the appropriate choice of diene. With this mind, we began to look at the possibility of using other substituted tetrazines, in particular those that contained more nitrogen containing substituents at the 3- and 6- positions. One quite recent example of this is the synthesis of 3,6-di(2-pyrazinyl)-1,2,4,5-tetrazine (bpztz) which was prepared by Kaim and co-workers from 2-cyano pyrazine and hydrazine hydrate.[47]

This tetrazine was prepared by refluxing the same two reagents in acidic THF. The orange product was filtered and recrystallised from DMF to give 72% of 3,6-di(2-pyrazinyl)-1,2,4,5-hydrotetrazine (**9**). This was then oxidised as before with nitrous oxide to give 3,6-di(2-pyrazinyl)-1,2,4,5-tetrazine (**10**) in 38% yield. The electronegativity of

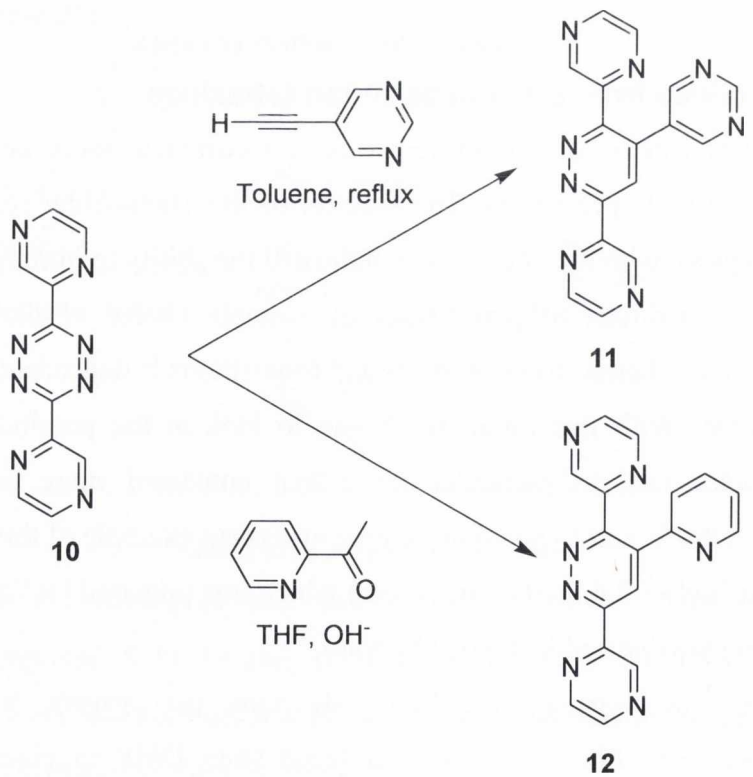
the pyrazinyl substituents may be responsible for the low yield of the oxidation step. This reaction is summarised in Scheme 23.



Scheme 23: The synthesis of 9 and 10

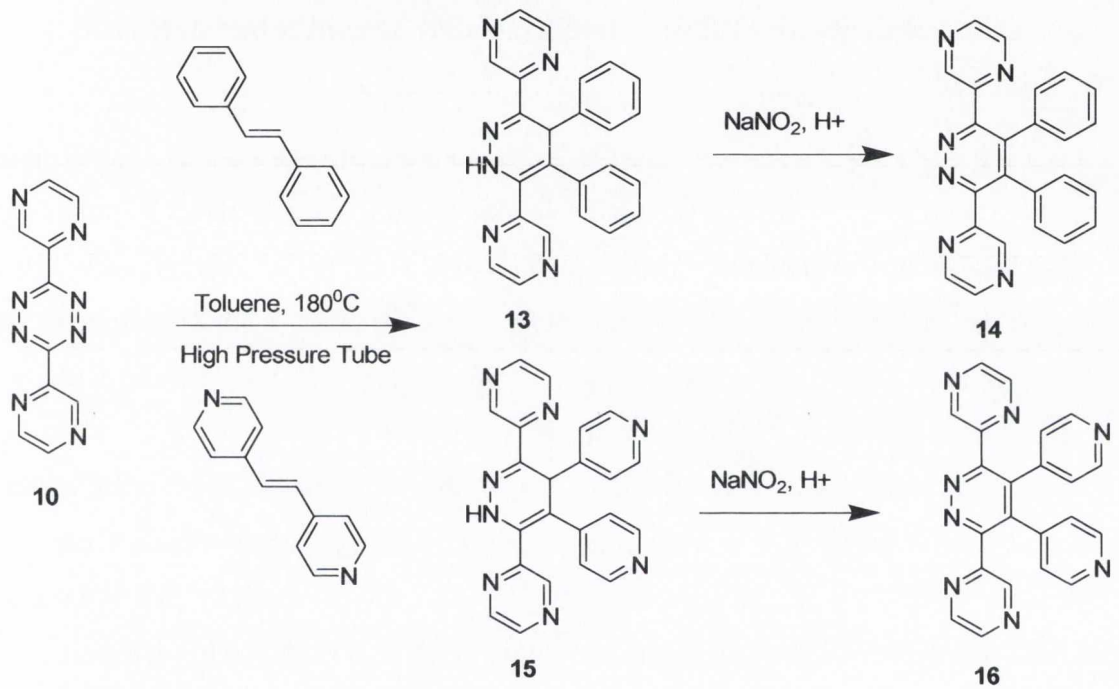
This tetrazine was then used as the diene to make the analogous pyridazyl-substituted ligands as those discussed earlier. **10** was added to a toluene solution containing 5-ethynyl pyrimidine and refluxed for 24 hours. After this time a 49% yield of 3,6-di-(2-pyrazinyl)-4-(pyrimidyl) pyridazine (**11**) was isolated by chromatography.

Following the same procedure as was used to prepare **4**, a methanolic solution of KOH was added to a THF solution of **10** and 2-acetyl pyridine. After purification by column chromatography, 3,6 di-(2-pyrazinyl)-4-(2-pyridyl)-pyridazine (**12**) was isolated in 25% yield. These results are summarised in Scheme 24.



Scheme 24: The preparation of pyrazinyl substituted pyridazines 11 and 12

Tetrazine **10** was also used in a Diels-Alder reaction with both phenyl and pyridyl substituted alkenes, *trans* stibene and 1,2-di(4-pyridyl) ethene. In these cases both reactions were carried out in a sealed tube at 180°C in toluene. 3,6-di-(2-pyrazinyl)-4,5-diphenyl hydropyridazine (**13**) was oxidised to 3,6-di-(2-pyrazinyl)-4,5-diphenylpyridazine (**14**) in 84% yield. The analogous 4-pyridyl substituted hydropyridazine, 3,6-di(2-pyrazinyl)-4,5-di(4-pyridyl) hydropyridazine (**15**) was isolated by column chromatography in 95% yield, but the oxidised pyridazine 3,6-di(2-pyrazinyl)-4,5-di(4-pyridyl) pyridazine (**16**) was obtained in only 40% yield. The synthesis of both of these ligands is summarised in Scheme 25.



Scheme 25: The synthesis of 14 and 16 from 10

1.2.6 Diels-Alder Reaction Yields

Table 1 compares the yields obtained from the Diels-Alder reaction of **2** and **10** with each dienophile.

Diene	% Yield obtained with each dienophile			
	2-acetyl pyridine	5-ethynyl pyrimidine	trans stilbene	1,2 di(4-pyridyl)ethene
2	80	65	92	75
10	26	49	75	60

Table 1: Comparison of the yields obtained in the Diels-Alder reactions of 2 and 10 with the four dienophiles

Clearly, tetrazine **10** is less reactive towards inverse electron demand Diels-Alder reactions generally. Pyridine N atoms are more electron withdrawing than their pyrazine

counter parts (pKa pyrazine = 0.51, pyridine = 4.51) making pyridyl substituted tetrazines more effective dienophiles.

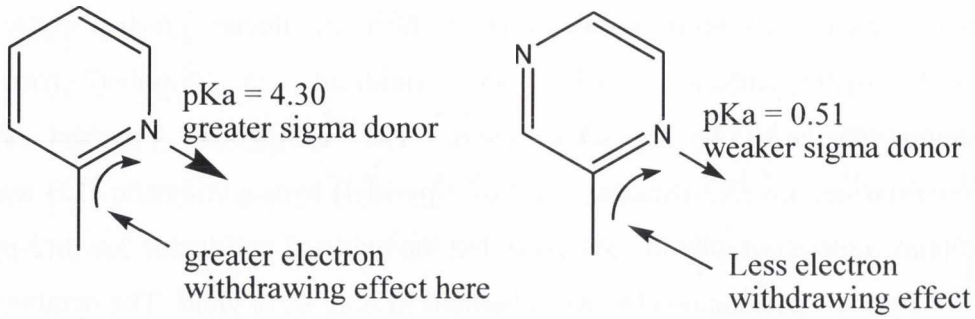


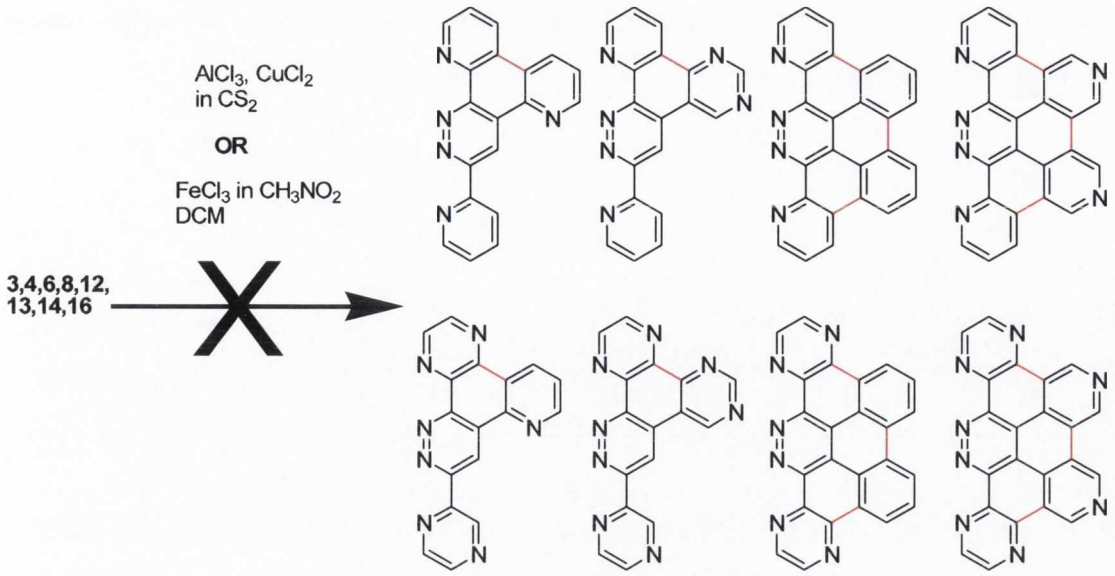
Figure 10: The greater electron-withdrawing effect of the pyridyl ring

1.2.7 Cyclodehydrogenation – The Final Step Towards Novel N-HSB Compounds

The successful Diels-Alder reactions involving both tetrazines produced a novel series of ligands which were potentially promising candidates for coordination and supramolecular chemistry, as well as suitable precursors for novel N-HSB type compounds. The final step in the preparation of N-HSB molecules is an oxidative cyclodehydrogenation, or ring-closing step. Two common procedures involve the use of Lewis acids – iron trichloride or aluminium trichloride with copper chloride.

When $AlCl_3$ and $CuCl_2$ were stirred in CS_2 with **6** for several days under argon, the solvent was evaporated and the product washed with aqueous ammonia. Only starting material was recovered. This process was repeated for each of the pyridazine-centred compounds described above but only starting material was retrieved in each case.

The second method was then carried out by adding a $FeCl_3$ solution in nitromethane to a dichloromethane solution containing **6**. This was stirred overnight and the reaction was quenched with methanol. After washing with water and purification by column chromatography, no cyclodehydrogenated product was obtained. However, the aqueous layer revealed the presence of iron complexes of the ligand, which are discussed in the next chapter. When the reaction was carried out with the other pyridazine – centred compounds again only the iron-complexes were obtained.

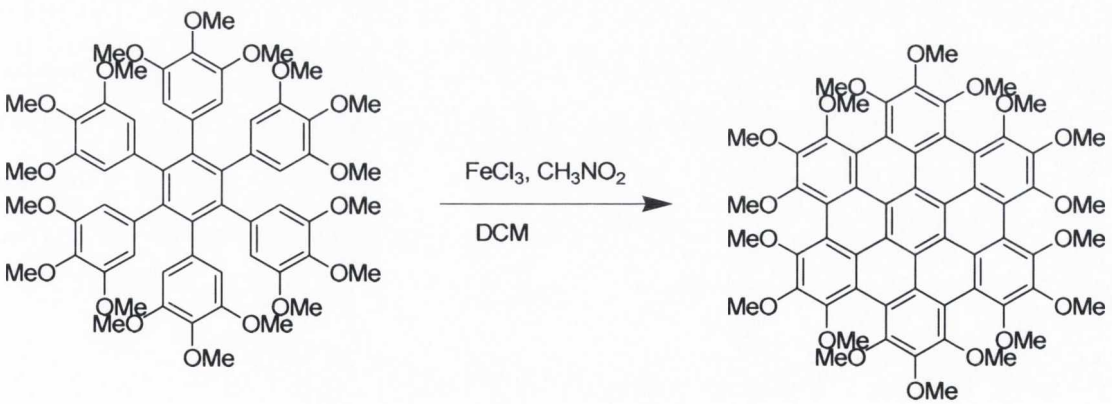


Scheme 26: The unsuccessful attempts at cyclodehydrogenation of pyridazine-centred polyaromatic compounds

1.2.8 Modification of pyridazine-centred ligands for cyclodehydrogenation

Clearly the pyridazine–centred ligands prepared here are not reactive towards cyclodehydrogenation, and in order to prepare novel N-HSB type compounds further avenues needed to be investigated.

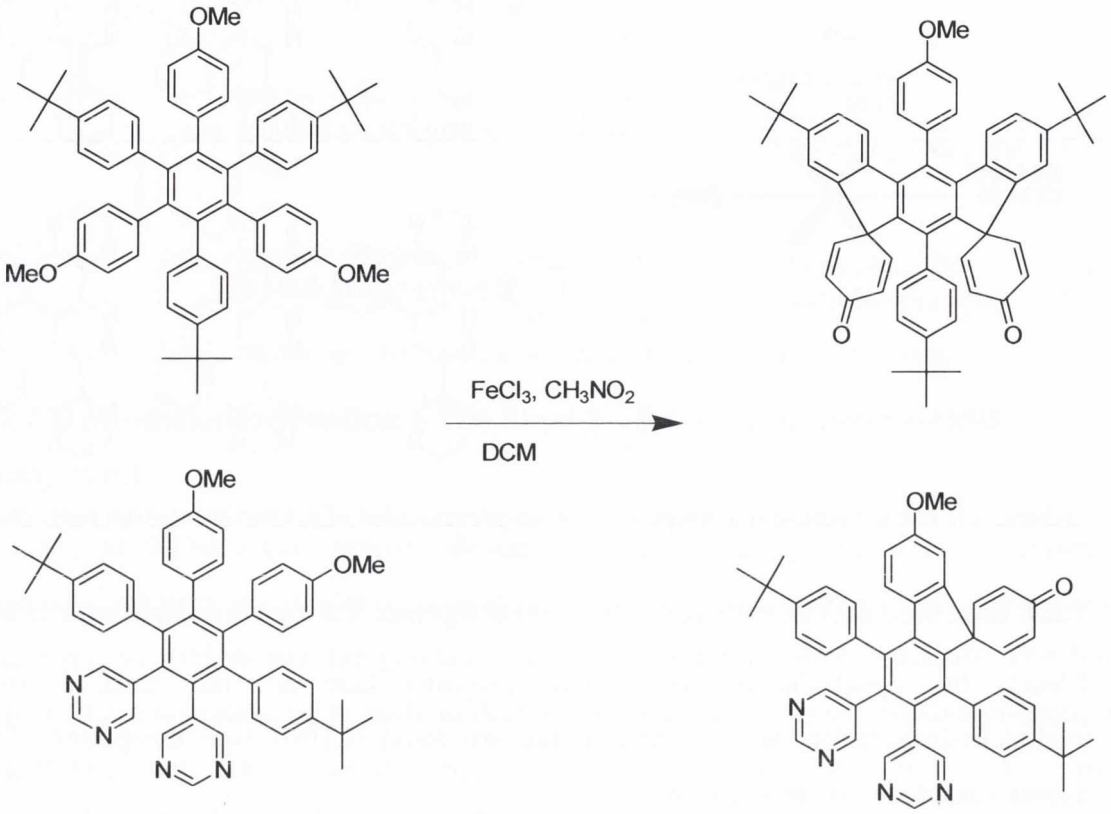
One possibility was the incorporation of functionalities onto the ring systems such as methoxy groups to encourage cyclodehydrogenation e.g. Müllen reports an improved reaction time for the cyclodehydrogenation of polyphenylenes when methoxy groups are located on the *ortho* and *meta* positions of the peripheral rings (Scheme 27).[48]



Scheme 27: The incorporation of methoxy groups on the peripheral rings of polyphenylenes

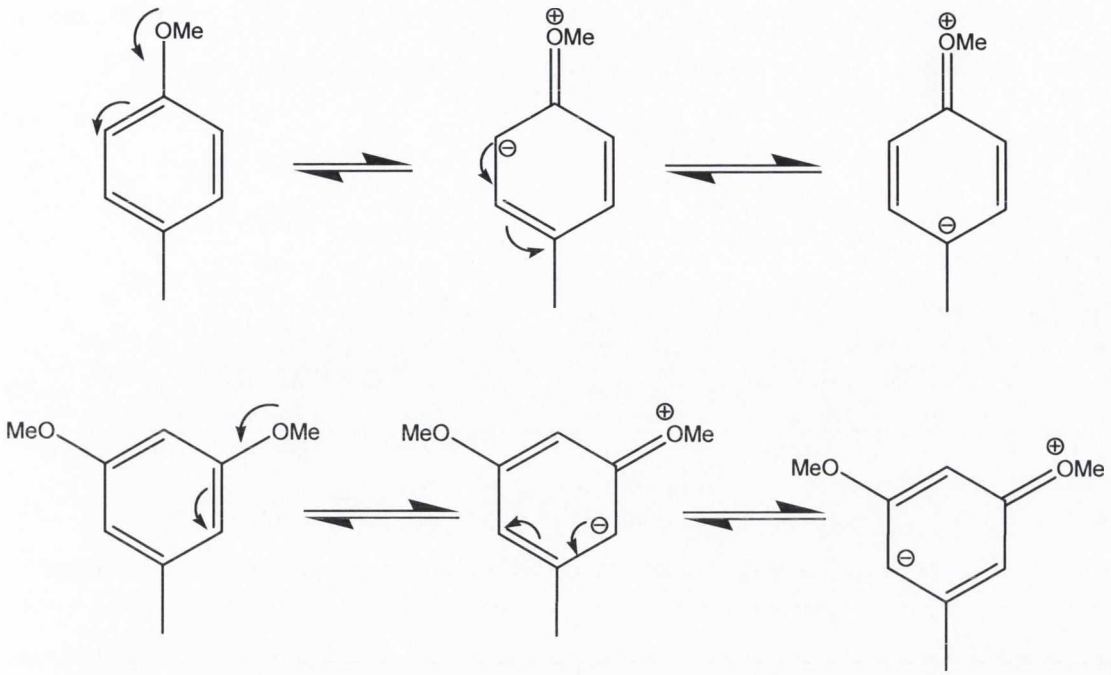
More unusual results however have been obtained by our own group and others when methoxy groups have been applied in the *para* position only.[49, 50] In this case methoxy groups in the *para* position appear to activate the carbon bonded to the central ring

towards cyclodehydrogenation, and results in formation of spirocyclic type compounds illustrated in Scheme 28.



Scheme 28: The methoxy-directed cyclodehydrogenation resulting in spirocyclic compounds prepared by Müllen (upper) and Draper (lower)

This directional control of the reaction can be explained by the resonance canonical forms available to the methoxy substituted phenyl species. Stabilization of the aromatic ring by an electron pair on the oxygen results in increased electronegativity at the *ortho* and *para* positions relative to the methoxy group as shown in Scheme 29. However, by introducing methoxy groups at the *meta* position on the phenyl ring, this will activate the phenyl ring at the two *ortho* positions relative to the methoxy group (Scheme 29). This is the desired site of cyclodehydrogenation for the pyridazine compounds discussed earlier and was a promising potential adaption to these compounds.



Scheme 29: The resonance canonical forms available with para substituted methoxy (upper) and meta substituted methoxy functional groups (lower)

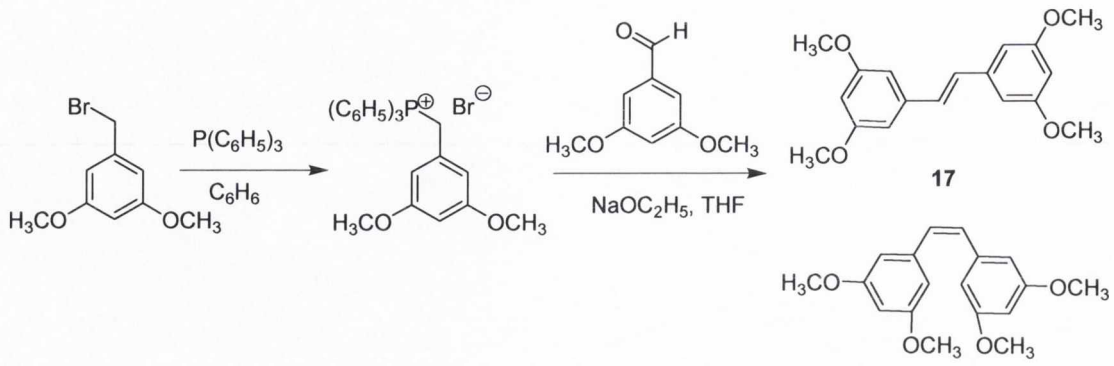
The easiest way to incorporate methoxy groups onto the phenyl rings of the pyridazine substituents is to introduce them on the dienophile at the pre-Diels-Alder stage. A number of methods exist in the literature for the preparation of functionalised alkenes, and this would appear to be the most desirable route towards methoxy substituted pyridazines, and ultimately, novel N-HSB compounds.

1.2.8.1 Preparation of 3,3,5,5-tetramethoxy stilbene

3,3,5,5-tetramethoxystilbene has been prepared using a number of techniques, but the Wittig reaction appears to be one of the most popular.[51] Pincock and Roberts prepared a number of methoxy-substituted alkenes as the methoxy substituents appear to prolong the excited state lifetimes of stilbene moieties.[52] Their synthetic method involved the initial preparation of the methoxy substituted phosphonium bromide salt and subsequent addition of the aldehyde in basic solution.

This initial salt formation was carried out by addition of 3,5-dimethoxy bromobenzene to triphenylphosphine. After stirring overnight, a white precipitiate was obtained and isolated by filtration. This was added to a THF solution containing sodium ethoxide which turned orange after several seconds. 3,5-dimethoxybenzaldehyde was added and the reaction refluxed overnight. After purification by column chromatography a mixture

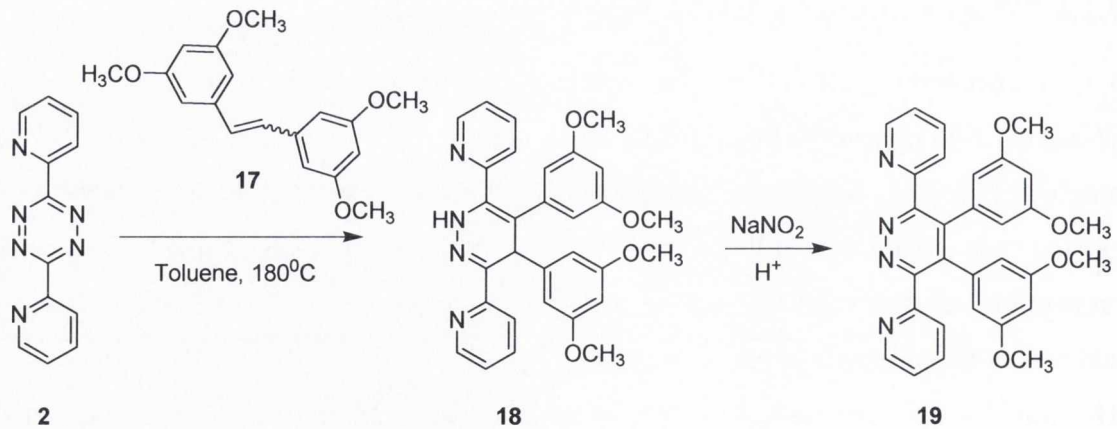
of the *cis* and *trans* isomers of 3,3,5,5-tetramethoxy stilbene (**17**) were isolated in 40% yield. These were later separated by recrystallisation from toluene.



Scheme 30: The synthesis of 3,3,5,5-tetramethoxystilbene, 17

1.2.8.2 Synthesis of a novel methoxy-substituted pyridazine –centred compound

17 was produced for a Diels-Alder reaction with bptz (**2**). This was carried out in a similar manner to the previous pyridazine-centred compounds by heating the dienophile **17** with tetrazine **2** in a pressure tube in toluene overnight at 180°C. After isolation by column chromatography, 3,6-di(2-pyridyl)-4,5-di-(3,5-dimethoxyphenyl) hydropyridazine (**18**) was obtained in 61% yield. This compound was then oxidised in the usual manner to 3,6-di(2-pyridyl)-4,5-di-(3,5-dimethoxyphenyl) pyridazine (**19**) with nitrous oxide gas (Scheme 31) in 75% yield. The synthesis of **19** resulted in a novel pyridazine-centred ligand which was also a suitable precursor for cyclodehydrogenation.

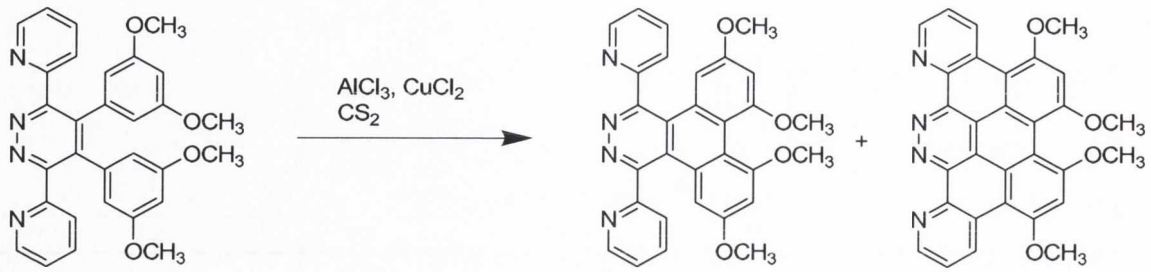


Scheme 31: The synthesis of methoxy-substituted pyridazine centred ligand 19

1.2.8.3 Cyclodehydrogenation of 19

The cyclodehydrogenation of **19** was carried out via the two methods discussed previously for pyridazine-centred ligands. The first method attempted involved the use of $FeCl_3$ in CH_3NO_2. This was added dropwise to a dichloromethane solution of **19** while nitrogen gas was bubbled through the solution to remove any hydrochloric acid. The reaction was left overnight and methanol was then added to quench it. After the usual work-up no product was obtained from the organic extract. However, the aqueous layer appeared to contain some complexed ligand which precipitated out upon the addition of KPF_6. TLC analysis of this precipitate revealed a complicated mixture of products which could not be separated by column chromatography and were very complicated in the ^{1}H-NMR spectrum. However, from the TLC it was clear that the colour of these complexes was considerably darker than the iron complexes obtained for the other pyridazine ligands, which was thought to indicate that some cyclodehydrogenation had occurred prior to complexation. An attempt was made to oxidise the iron by heating the precipitate in H_2O_2 and extracting the free ligand into dichloromethane. However, this was not successful.

A second attempt was made at cyclodehydrogenation using aluminium trichloride and copper dichloride. This was carried out by stirring a CS_2 solution of **19** with $AlCl_3$ and $CuCl_2$ at room temperature for four days. After this time the reaction was washed with aqueous ammonia and purified by column chromatography. A significant amount of starting material was recovered from the reaction. However, there was also a small quantity of two other products. These products were identified as 1,4-di(2-pyridyl)-6,8,9,11-tetramethoxy-2,3-diazatriphenylene (**20**) and 1,14,15,16-tetraazo-5,7,8,10-tetramethoxyphenanthro[f,g,h,i,j]picene (**21**) which were isolated in 8.3% and 4.5 % yields respectively. **20** was characterised by ^{13}C- and ^{1}H- NMR spectroscopy and mass spectrometry. However, difficulties arose with the characterization of **21** as a combination of low solubility in most solvents and an apparent stacking effect in solution made spectroscopic analysis difficult. This effect has been observed in other large graphene type molecules and often results in very broad signals in ^{1}H-NMR spectra.[1, 15] However **21** was successfully characterised by mass spectrometry and UV-Vis spectroscopy and this is discussed in greater detail in the next section.



19 **20** **21**

Scheme 32: The cyclodehydrogenation of 19 giving 20 and 21

1.3 Characterization of Pyridazine–Centred Compounds

1.3.1 Characterization by NMR Spectroscopy

1.3.1.1 Pyridyl-substituted pyridazines

Given the soluble nature of most of the compounds discussed above in most common laboratory solvents, characterization was possible by both ^{1}H- and ^{13}C- NMR spectroscopy. The spectroscopic data obtained for the tetrazine and hydrotetrazine precursors **1** and **2** compared well with the literature.[29] Compound **3** was also characterized by ^{1}H-NMR and ^{13}C-NMR spectroscopy. The greatest difficulty in assigning the signals in this spectrum was in differentiating between the two pyridyl rings. In order to achieve this, a number of NOe experiments were carried out, and a through-space interaction was observed between the H^6 proton at δ 8.4 ppm and the pyrimidyl proton H^8. This allowed for the assignation of this H^6 proton to the 3- position on the pyridazine ring, and from the ^{1}H-^{1}H COSY, all the other peaks could be fully assigned. This NOe interaction is shown in Figure 11.

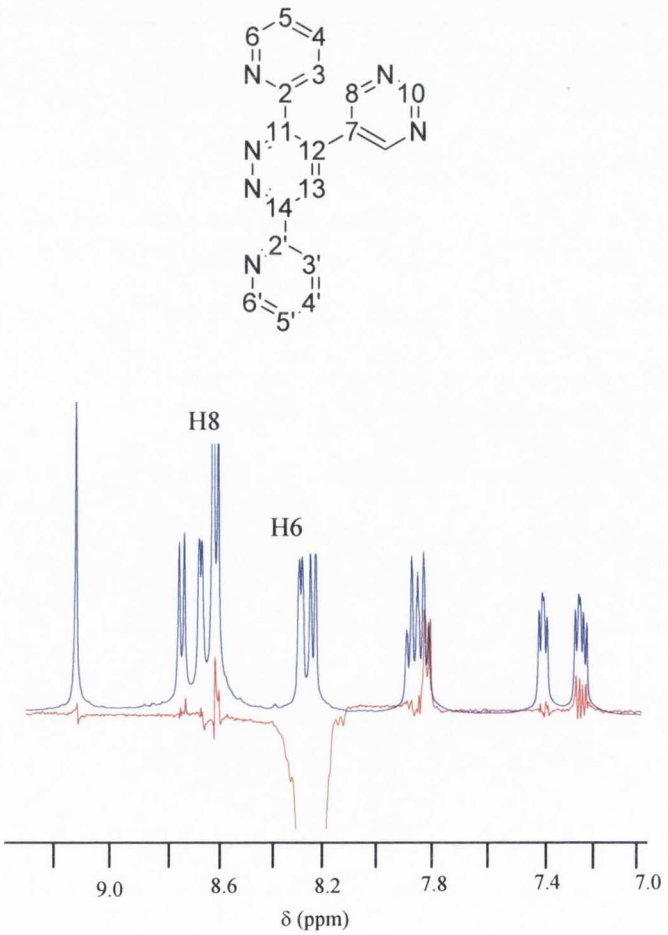


Figure 11: NOe showing an interaction between H^6 and H^8

The two-dimensional ^{1}H-^{1}H COSY NMR spectrum of **3** is shown in Figure 12. Assuming from the NOe in Figure 11 that the H^{6} proton at δ 8.4 ppm is that of the 2-pyridyl ring at the 3- position of the pyridazine ring, the neighbouring protons on this ring were assigned. The protons from the other 2-pyridyl ring were subsequently assigned. The two peaks in the spectrum which show no interaction with other systems are the H^{8} of the pyrimidine ring, and the H^{13} of the pyridazine ring system. These can be differentiated as the H^{8} proton integrates for two protons. The other pyrimidyl peak, which integrates for only one appears at δ 9.2 ppm and is not shown in the 2-dimensional COSY spectrum.

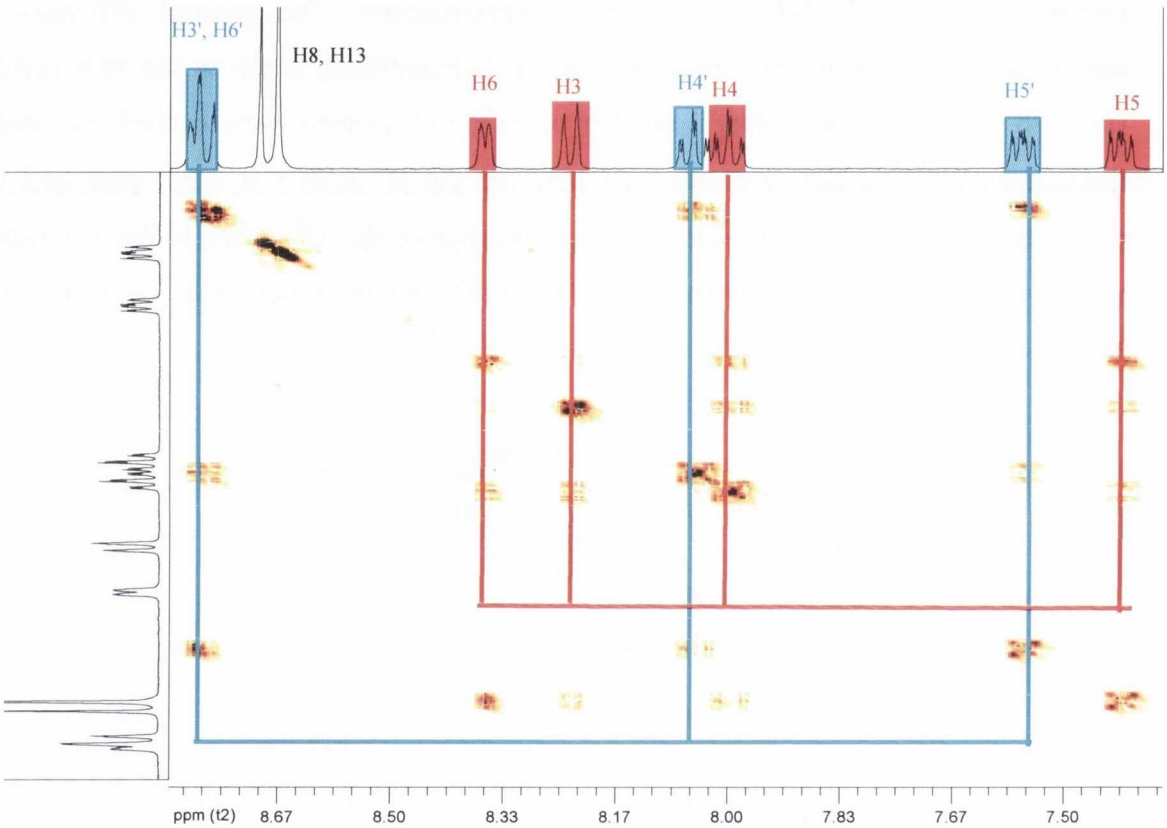


Figure 12: The ^{1}H-^{1}H COSY of 3 showing the two 2-pyridyl ring systems in $CDCl_3$. The most downfield pyrimidyl signal due to H^{10} is not included

The ^{13}C-NMR spectrum of **3** is shown in Figure 13. The spectrum was fully assigned with the help of a ^{13}C-^{1}H COSY NMR spectrum. The most downfield signals are those carbons which are the most deshielded by adjacent nitrogen atoms, such as C^{10} on the pyrimidyl ring and C^{11} and C^{14} on the pyridazine ring. These carbons are directly adjacent to two nitrogens and are thus more deshielded than the other signals. The other carbons which are less shielded by nitrogen atoms appear slightly more upfield in the spectrum e.g. C^{2} and C^{6} on the 2-pyridyl ring systems. The most upfield signals are those which are least influenced by the deshielding effect of the nitrogens, e.g. C^{3} and C^{5} peaks of the 2-pyridyl ring systems, and C^{13} of the pyridazine ring.

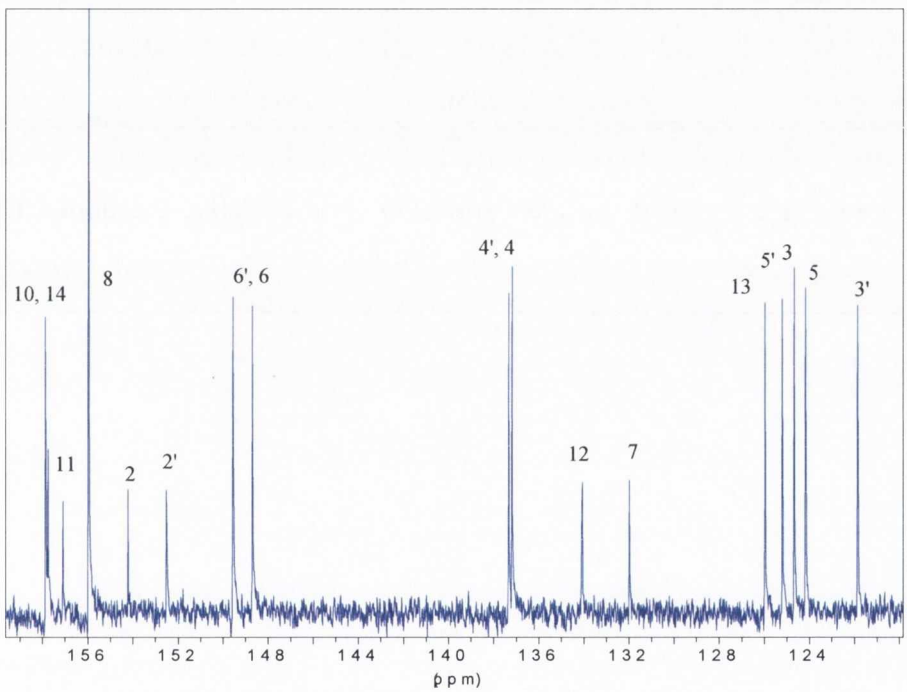


Figure 13: The ^{13}C-NMR spectrum of 3 in $CDCl_3$ (δ 120-158 ppm shown)

Despite a number of NOe experiments, no through space interactions were observed between the protons in the ^{1}H-NMR spectrum of **4**. As a result, the protons of the three 2-pyridyl ring systems have been arbitrarily assigned as A, B and C. From the ^{1}H-^{1}H COSY, each proton could be assigned to its neighbours on the same ring, but it was unclear which was which. The ^{1}H-NMR spectrum of **4** is shown in Figure 14. The most downfield signal is the singlet associated with H^{9} of the pyridazine ring system. The H^{6} and H^{3} protons of the 2-pyridyl ring systems appear between δ 8.1 and 8.8 ppm, with the exception of one H^{3} signal which appears at δ 7.3 ppm. This implies that this proton belongs to one of the 2-pyridyl rings at position 3- or 4- of the pyridazine, as this shielding may be due to the neighbouring pyridyl ring. However, this is not conclusive, and it is not feasible to say which position may influence which, i.e. whether the pyridyl ring at position 3- is shielding the H^{3} of the 2-pyridyl ring at position 4 – or *vice versa.* The 2-pyridyl ring signals were identified from their coupling constants. The H^{5} signals appear upfield between δ 7.2 and 7.4 ppm. The ^{13}C-NMR spectrum of **3** was also carried out and the details of this are given in the experimental.

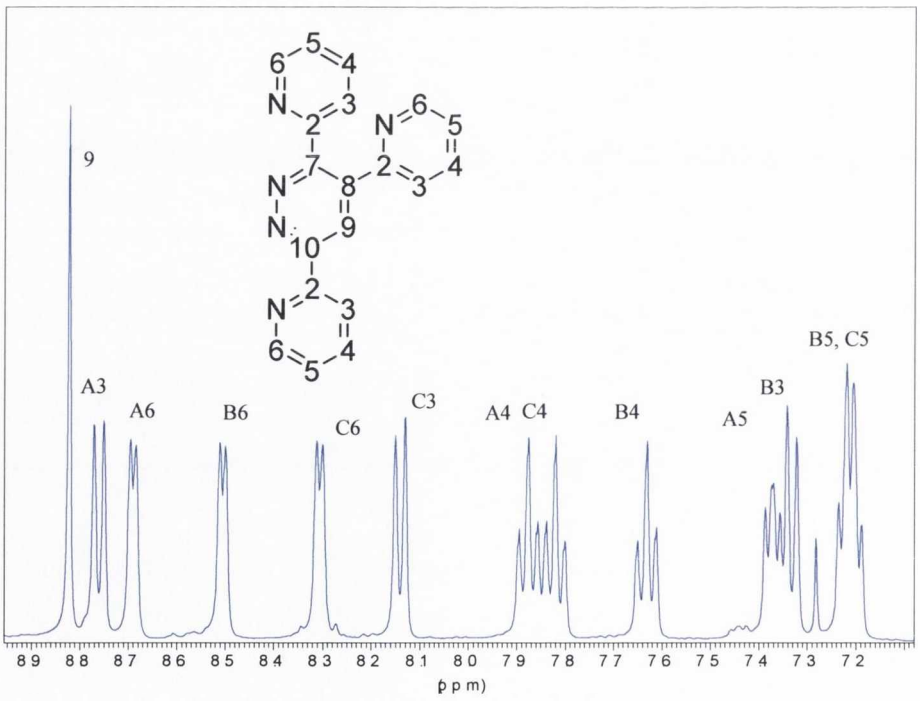
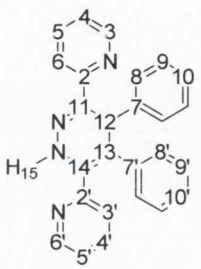


Figure 14: The ^{1}H-NMR spectrum of 4 in $CDCl_3$ (δ 7.1-8.9 ppm shown)

The ^{1}H-NMR spectrum of hydropyridazine **5** was complicated due to the lack of symmetry in the molecule arising due from the N-H bond present on one of the pyridazine nitrogens. This resulted in two separate sets of signals appearing for the two 2-pyridyl ring systems and the two phenyl ring systems. These could not be differentiated by through space interactions despite numerous attempts using NOe experiments. However, with the use of a long range ^{13}C-^{1}H COSY experiment, shown in Figure 15, the ring systems could be identified. The two most downfield signals in the ^{13}C-NMR spectrum were identified as the carbons C^{11} and C^{14}, and the N-H proton H^{15} can clearly be seen to shown an interaction with one of these carbons, which is most likely to be C^{11}. One of the H^{6} protons also clearly has an interaction with this carbon, so this must be the H^{6} from the adjacent 2-pyridyl ring. From the ^{1}H-^{1}H COSY, the other signals from this ring could be assigned, and hence the 2-pyridyl signals which remained were those of $H^{3'}$-$H^{6'}$.



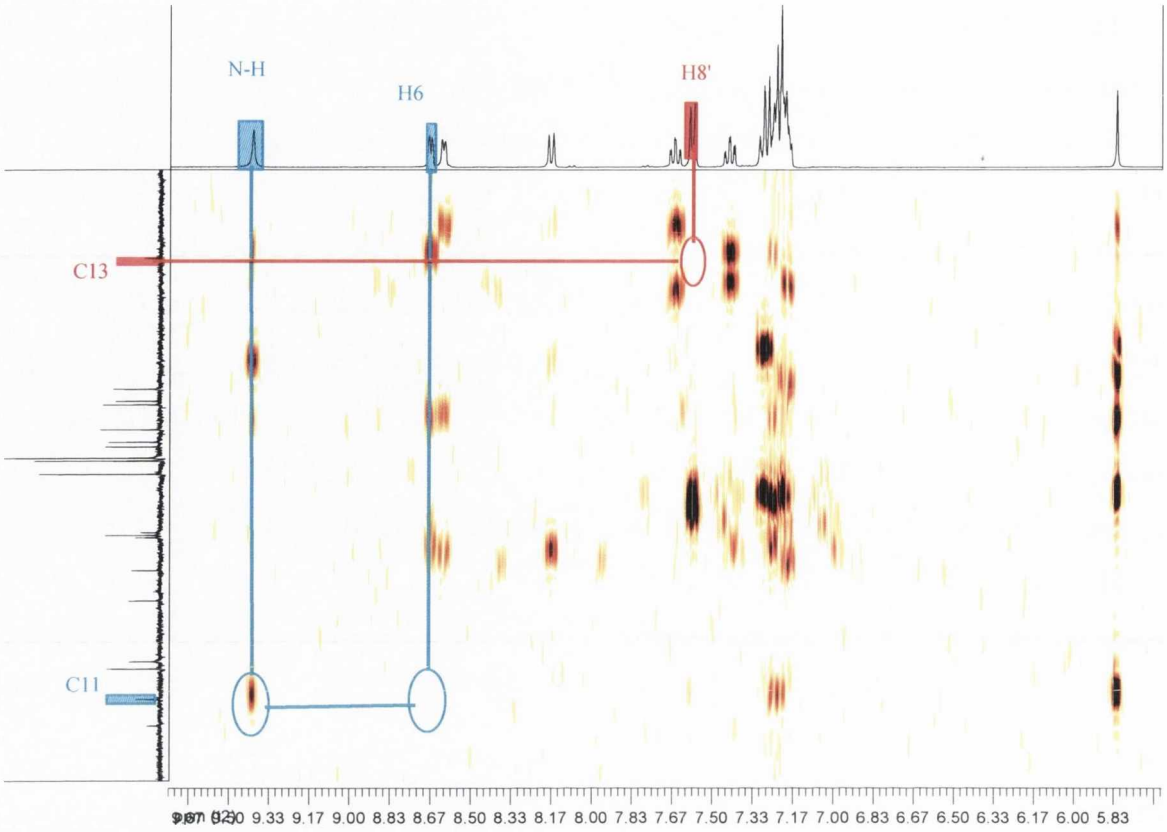


Figure 15: The long-range 2-dimensional ^{13}C-^{1}H-COSY experiment of 5 in $CDCl_3$. The carbon spectrum is shown from δ 100ppm and hence does not include the most upfield carbon signal, C^{12}.

The ^{1}H-NMR spectrum of **5** is shown in Figure 16. The most upfield signal is that of the proton H^{12} which appears as a singlet at δ 5.8 ppm. Most of the phenyl ring signals appear in the multiplet at δ 7.2 ppm with the exception of one signal, which appears as a doublet at δ 7.6 ppm and was assigned as the H8' signal due to the interaction between this signal and C^{13} in the two dimensional spectrum which is highlighted in Figure 15. The remaining 2-pyridyl signals were identified with the help of a ^{1}H-^{1}H COSY experiment.

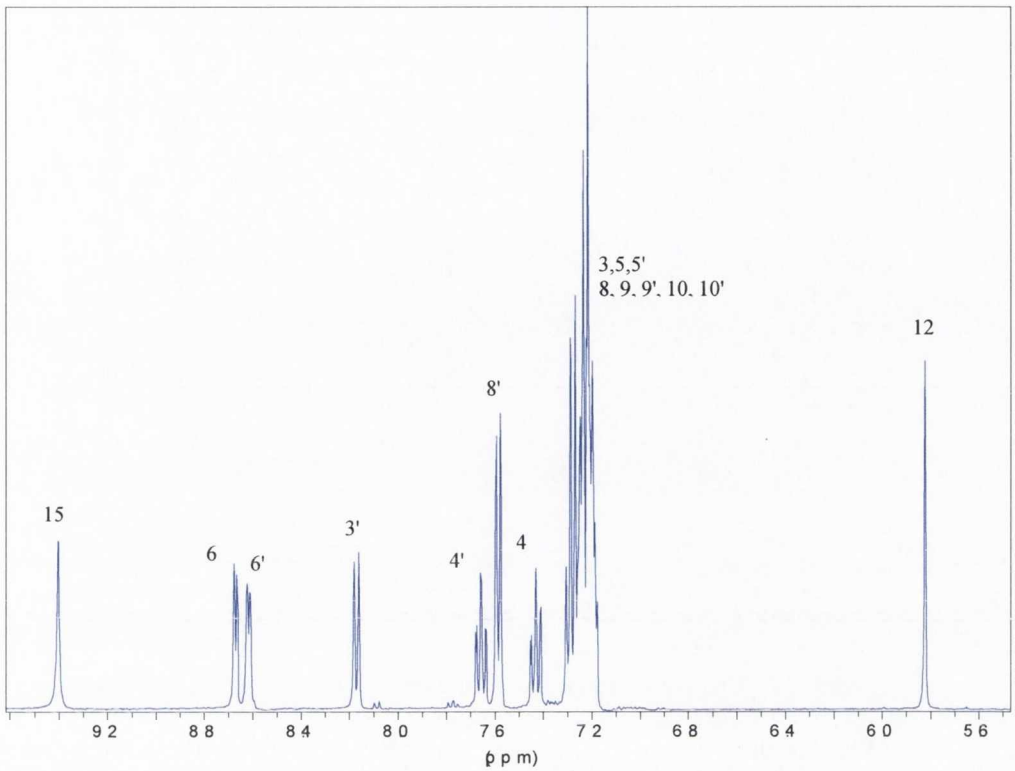


Figure 16: The ^{1}H-NMR spectrum of hydropyridazine 5 in $CDCl_3$ (δ 5.6-9.3 ppm shown)

The oxidation of **5** results in the disappearance of the N-H proton in the ^{1}H-NMR spectrum, and the simplification of the spectrum due to the presence of the C_{2v} symmetry which is now apparent in the molecule. The 2-pyridyl signals were identified by a combination of their coupling constants and the information obtained from the ^{1}H-^{1}H COSY experiment. The most downfield signal is the H^6 proton due to the shielding effect of the neighbouring nitrogen atom. The phenyl signals appear as two multiplets at δ 7.10 and δ 6.95 ppm. The most upfield pyridyl signal is the H^5 proton at δ 7.15 ppm.

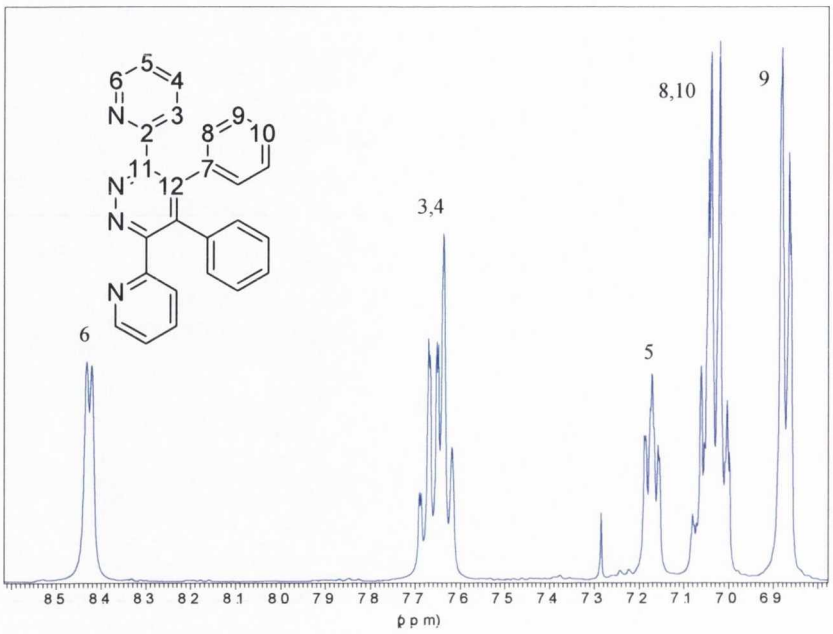


Figure 17: The ^{1}H-NMR spectrum of 6 in $CDCl_3$ (δ 6.9-8.5 ppm shown)

The ^{13}C-NMR spectrum of **6** was assigned with the help of a two-dimensional ^{13}C-^{1}H COSY and is shown in Figure 18. The most downfield signals were the two quaternary carbons, C^{11} and C^{2} which are deshielded by their proximity to the nitrogen atoms. The other quaternary carbons C^{12} and C^{7} appear at δ 138 and δ 133 ppm respectively. The carbon signal associated with the C^{6} of the 2-pyridyl ring systems are deshielded to δ 148 ppm. The three peaks associated with the phenyl ring system appear at δ 129 and 127.5 ppm. The most upfield carbon signal is the C^{5} which is shifted to δ 122.5 ppm.

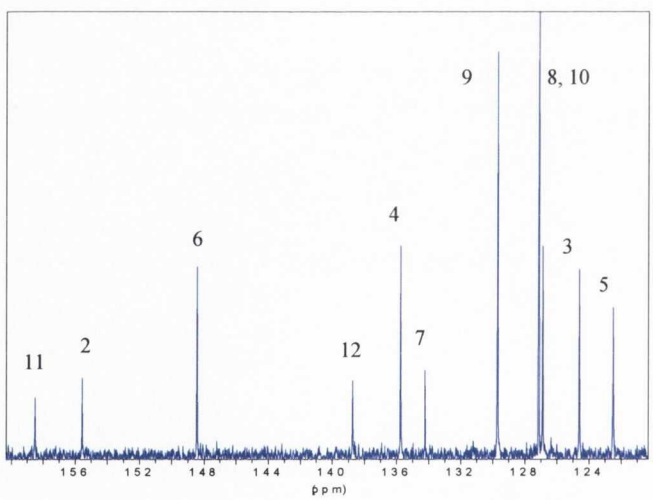


Figure 18: The ^{13}C-NMR spectrum of 6 in $CDCl_3$ (δ 123-160 ppm shown)

The ^{1}H-NMR spectrum of **7** is shown in Figure 19. The spectrum bears some similarities to hydropyridazine **5**, in that there are two sets of 2-pyridyl signals due to the lack of symmetry in the molecule. These two 2-pyridyl rings were distinguished by information obtained from the long-range ^{13}C-^{1}H COSY spectrum similar to that observed for **5**. Unfortunately the two 4-pyridyl ring systems could not be similarly distinguished. Once again, the most downfield signal is that of the N-H proton, followed by the protons directly adjacent to nitrogen atoms on the 2-pyridyl and 4-pyridyl ring systems. The most upfield signal is the H^{11} proton, which is shifted to δ 5.8 ppm. The most upfield pyridyl signals are the H^{8}, H^{5} and one of the H^{3} protons which are shifted between δ 7.0 and 7.5 ppm.

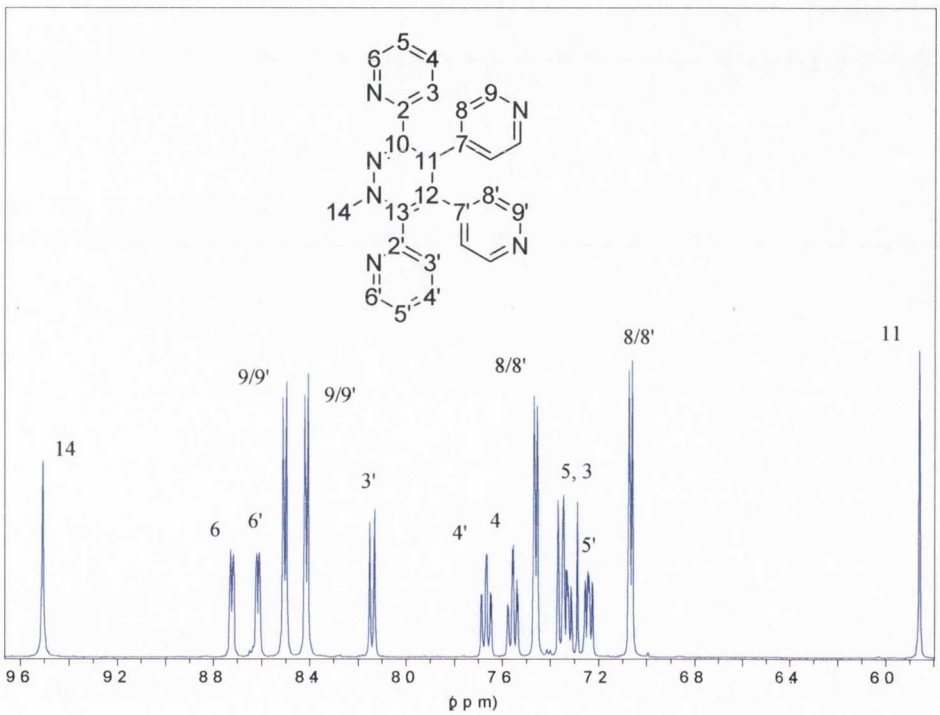


Figure 19: The ^{1}H-NMR spectrum of 7 in $CDCl_3$ (δ 5.9-9.6 ppm shown)

The ^{1}H-NMR spectrum of pyridazine **8** contains only one set of 2-pyridyl and one set of 4-pyridyl signals due to the symmetry of the molecule. The most deshielded signals are the H^9 and H^6 signals which are shifted to δ 8.4 and 8.3 ppm respectively. The other 2-pyridyl signals were identified from the ^{1}H-^{1}H COSY and their individual coupling constants. The most shielded signal is that for protons H^8 shifted to δ 6.85 ppm.

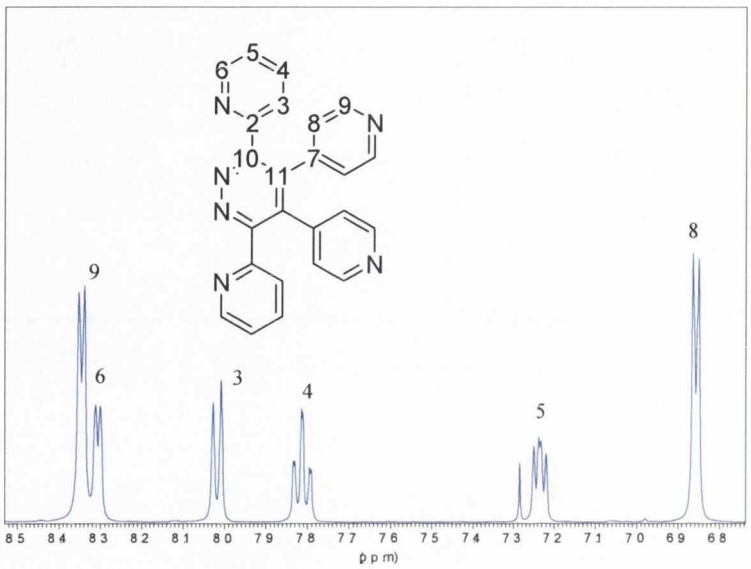


Figure 20: The ^{1}H-NMR spectrum of 8 in $CDCl_3$ (δ 6.8-8.5 ppm shown)

1.3.1.2 Pyrazine substituted pyridazine ligands

The hydrotetrazine and tetrazine **9** and **10** were characterized by proton and carbon NMR spectroscopy and the spectra compared favourably to literature reports.[47]

The ^{1}H-NMR of **11** is shown in Figure 21. The two 2-pyrazinyl substituents show the typical pattern associated with these compounds. The 3- position is the most deshielded and very often exhibits a small coupling constant with the H^5 of the ring. The H^5 and H^6 protons are more shielded and have larger coupling constants reflecting their proximity in the ring. In the case of **11** the two pyrazinyl rings were differentiated on the basis that the H^3 adjacent to the pyrimidyl ring is more likely to experience a shielding effect from the pyrimidyl ring current which would shift it upfield, whereas the shift of the $H^{3'}$ is similar to that of the parent tetrazine; i.e. unaffected by ring currents. From the ^{1}H-^{1}H COSY experiment the other peaks on these rings could be assigned, with the H^5 and H^6 peaks

appearing more upfield between δ 8.3 and 8.8 ppm. The two pyrimidyl signals H^{10} and H^{8} appear at δ 9.3 and 8.75 ppm respectively.

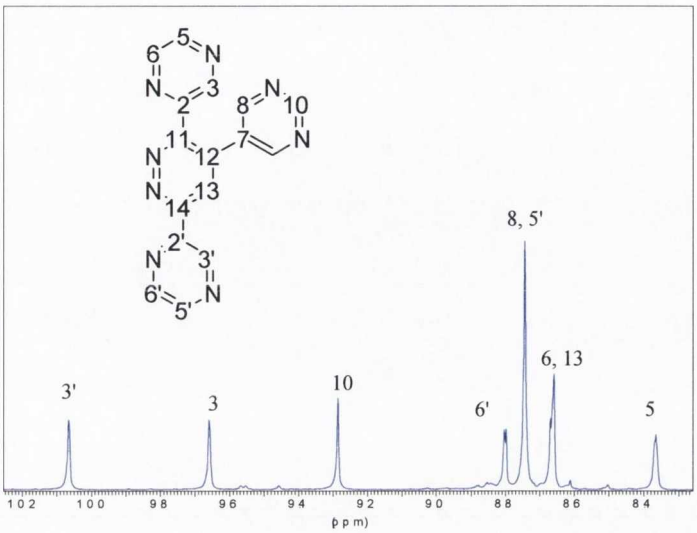


Figure 21: The ^{1}H-NMR of 11 in $CDCl_3$ (δ 8.3-10.2 ppm shown)

The ^{13}C-NMR spectrum of **11** was assigned with the help of two-dimensional experiments. The spectrum is shown in Figure 22. The most deshielded carbons are those in closest proximity to nitrogen atoms on the rings, such as the pyrimidyl C^{10} and C^{8} and the pyridazyl C^{11} and C^{14}. The pyrazinyl quaternary carbons C^{2} and $C^{2'}$ appear at δ 149.14 and 147.16 ppm respectively. The other carbons from the pyridazyl rings appear between δ 142 and 147 ppm, with the remaining signals appearing upfield between δ 126 and 134 ppm.

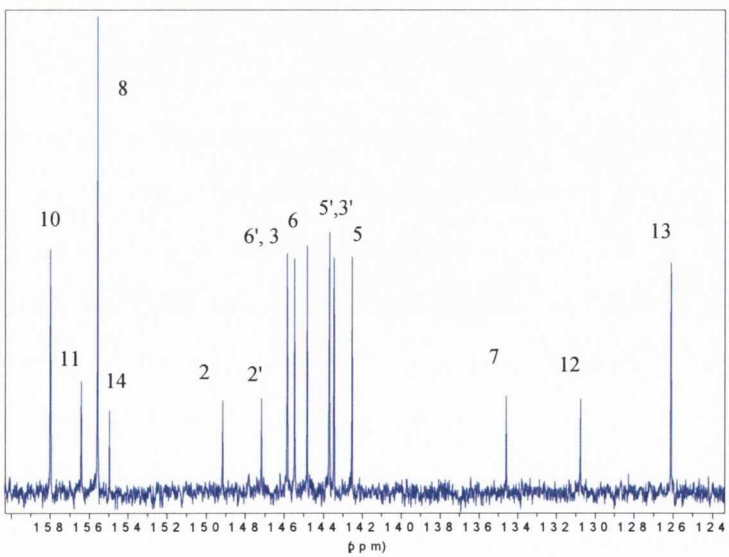


Figure 22: The ^{13}C-NMR spectrum of 11 in $CDCl_3$ (δ 124-159 ppm shown)

The ^{1}H-NMR spectrum of **12** is shown in Figure 23. The 2-pyridyl ring system was identified from the coupling constants associated with these peaks, and these signals are shifted between δ 7.3 and 7.8 ppm with the exception of H^{11} due to the deshielding effect of the neighbouring nitrogen atom, which shifts it downfield to δ 8.55 ppm. A similar logic was applied in this case to the two pyrazine ring systems as described for **11**, with the more shielded H^3 proton at δ 9.4 ppm assigned to the ring nearest the 2-pyridyl substituent. From the ^{1}H-^{1}H COSY experiment, the other peaks on the two rings could be assigned, leaving the pyridazine singlet, which is present at δ 8.8 ppm.

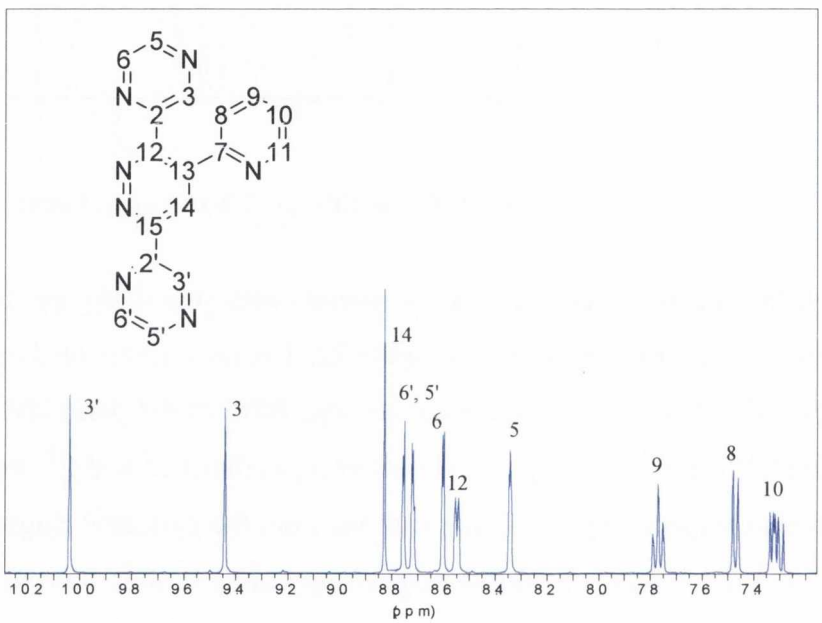


Figure 23: The ^{1}H-NMR spectrum of ligand 12 in $CDCl_3$ (δ 7.3-10.2 ppm shown)

The ^{1}H-NMR spectrum of hydropyridazine **13** is shown in Figure 24. As was the case for the pyridyl substituted hydropyridazines **5** and **7** there are four separate sets of signals for the four substituents. The two pyrazine and two phenyl ring systems could not be differentiated from each other in this case. The most downfield signal is that of the N-H hydropyridazine proton which appears at δ 9.5 ppm. This is followed by one of the H^3 protons from one of the pyrazine rings which is shifted to δ 9.3 ppm. The other pyrazinyl protons appear between δ 8.4 and 8.6 ppm. The phenyl signals appear together in a multiplet at δ 7.2 ppm, with the exception of one signal of a H^9 proton which is shifted slightly downfield to δ 7.55 ppm. The proton at H^{12} appears as a singlet at δ 5.6 ppm.

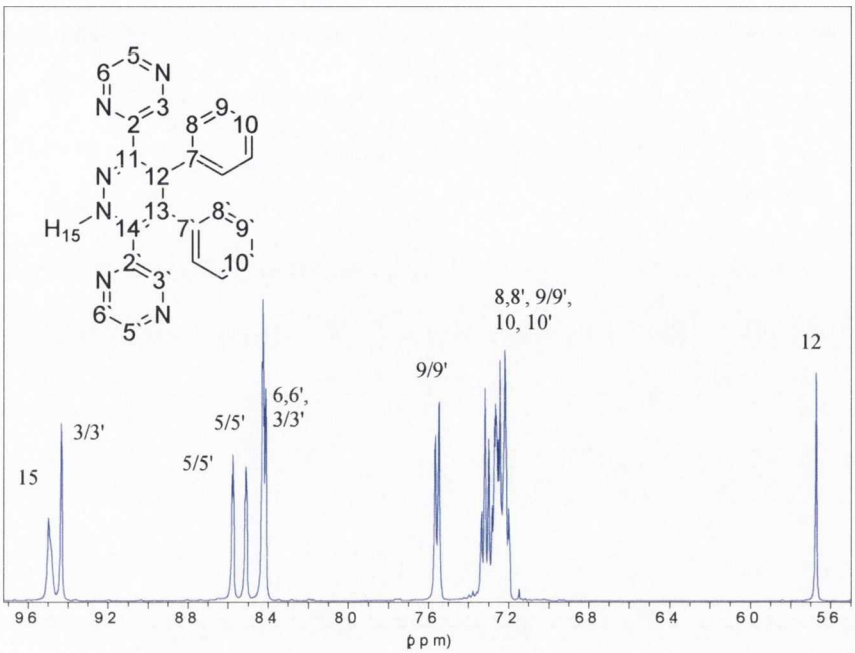


Figure 24: The ^{1}H-NMR spectrum of 13 in $CDCl_3$ (δ 5.6-9.6 ppm shown)

The oxidised pyridazine **14** has a much simpler characteristic ^{1}H-NMR spectrum which is shown in Figure 25. The symmetry present in the oxidised compound ensures that there is only one set of signals for the pyrazine rings, and one set of phenyl signals. The H^3 proton is the most deshielded appearing at δ 8.9 ppm, with the protons H^5 and H^6 appearing at δ 8.4 and 8.5 ppm respectively. The phenyl peaks appear as two peaks at δ 6.89 and 7.1 ppm, with the H^9 protons appearing more upfield.

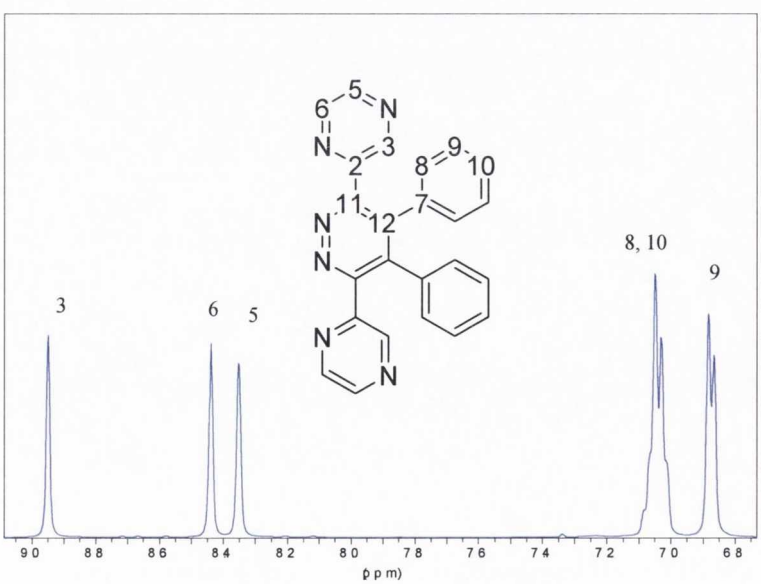


Figure 25: The ^{1}H-NMR spectrum of 14 in $CDCl_3$ (δ 6.8-9.0 ppm shown)

The hydropyridazine **15** was characterized by ^{1}H-NMR spectroscopy and details of this are given in the experimental section. The oxidised pyridazine **16** was fully characterized and the ^{1}H-NMR is shown in Figure 26. The H^{3} proton signal of the pyrazine rings is the most deshielded and appears at δ 9.36 ppm. The H^{9} signal of the 4-pyridyl substituents is shifted to δ 8.4 ppm due its proximity to the nitrogen atom. The most upfield signal is that of the H^{8} proton from the 4-pyridyl ring system which appears at δ 6.9 ppm. The H^{5} and H^{6} protons of the pyrazine appear at δ 8.6 and 8.3 ppm respectively.

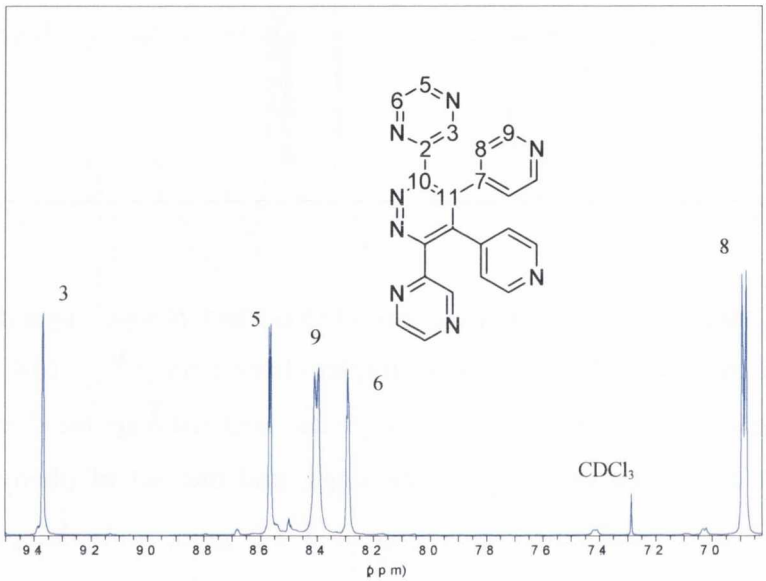


Figure 26: The ^{1}H-NMR spectrum of 16 in $CDCl_3$ (δ 6.9-9.4 ppm shown)

However the most significant difference appears in the region between δ 6.0 and 7.0 ppm in the spectra. The two phenyl signals H^8 and H^{10} in the spectrum of **19** which appear at δ 6.2 and 6.1 ppm and integrate for two and four protons respectively have been replaced by two signals which both integrate for two protons and are shifted to δ 6.7 and 6.4 ppm. These signals correspond to the loss of two protons at the H^8 position where the C-C bond has formed during the cyclodehydrogenation. This has also removed the symmetry of the phenyl rings resulting in two separate signals for the methoxy substituents in the spectrum of **20** which appear at δ 3.9 and 3.4 ppm.

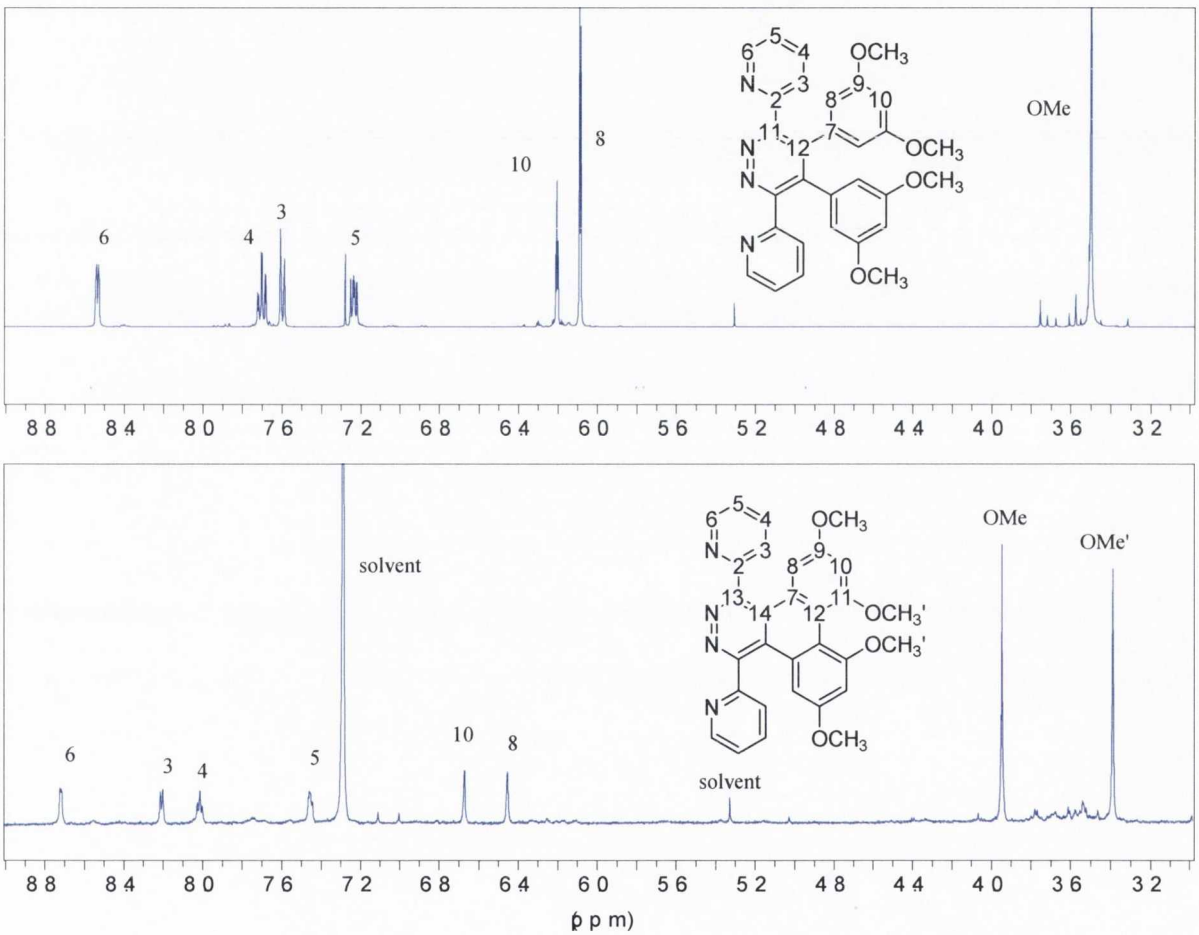


Figure 28: Comparison of the ^{1}H-NMR spectra of 19 and 20 in $CDCl_3$

The ^{13}C-NMR spectra of **19** and **20** are compared in Figure 29. Due to the low concentration of the NMR sample of **20** no long-range ^{13}C-^{1}H spectra could be obtained. As a result the four quaternary peaks between δ 155 and 160 ppm could not be specifically assigned, yet clearly there is an extra quaternary peak here due to the loss of symmetry in the phenyl ring where C^9 in **19** is now replaced by two non-identical carbons

C^9 and C^{13}. The 2-pyridyl ring carbons are shifted only slightly downfield, whereas the quaternary carbons C^7 and C^{12} are shifted slightly upfield. Clearly there is also a new quaternary peak present in the spectrum of **20** at δ 116 ppm which can be assigned to the new carbon-carbon bond formed in the cyclodehydrogenation step, C^{14}. The loss of symmetry in the phenyl ring system is further highlighted by the presence of two distinct methoxy carbon signals in the spectrum of **20**, replacing the single peak present in the spectrum of **19**.

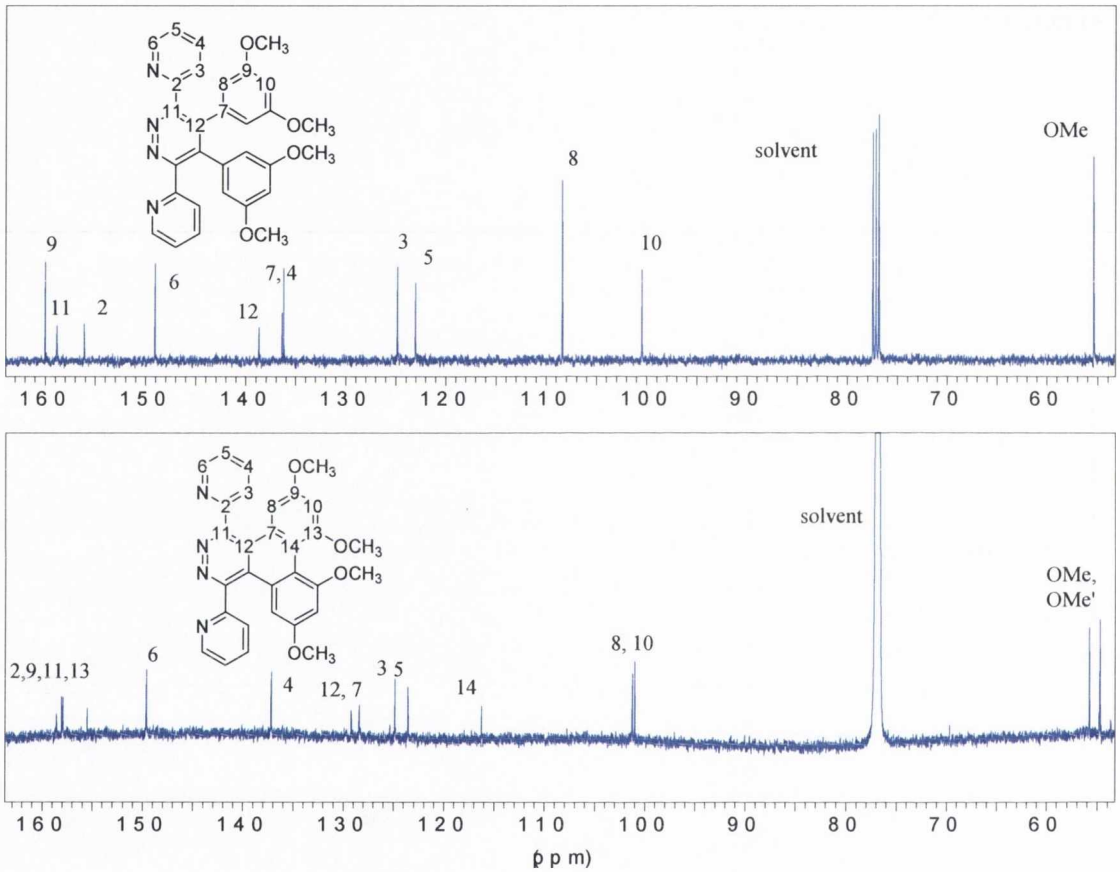


Figure 29: Comparison of the ^{13}C-NMR spectra of 19 and 20 in $CDCl_3$

1.3.2 Characterization of Compounds 3, 4 and 6 by Single Crystal X-Ray Diffraction

Colourless rod-like crystals of **3** were obtained from a dichloromethane-hexane solution of the compound. The single crystal x-ray analysis revealed that the ligand crystallized in an orthorhombic system with one molecule of **3** in the asymmetric unit. This unit is shown with atom labelling in Figure 30. There is a small dihedral angle between the rings labelled A and B of 5.02°. The angles between B and C, and C and D, are 31.47° and 48.18° respectively.

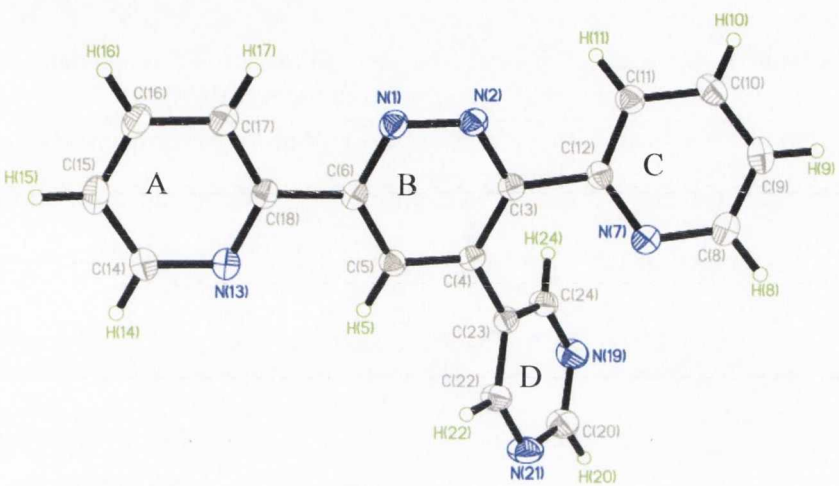


Figure 30: The asymmetric unit of the crystal of 3

In the crystal lattice, the molecules are stabilized by C-H···N hydrogen bonds involving both pyridyl units (H···N, 2.64Å) as well as the pyrimidyl ring (H···N, 2.68Å). This interaction leads to the formation of an undulated layer as shown in Figure 31.

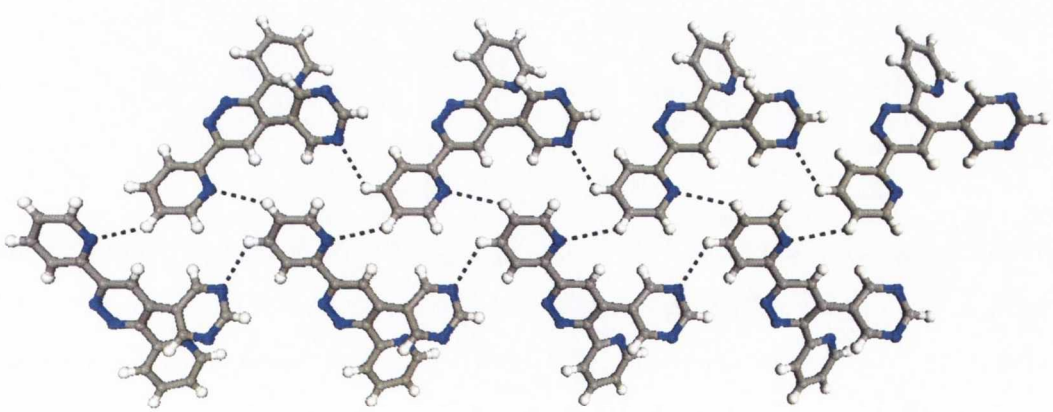


Figure 31: The packing in the crystal lattice of 3

These layers form an ABAB pattern and a zig-zag architecture is formed three-dimensionally. This is shown in Figure 32.

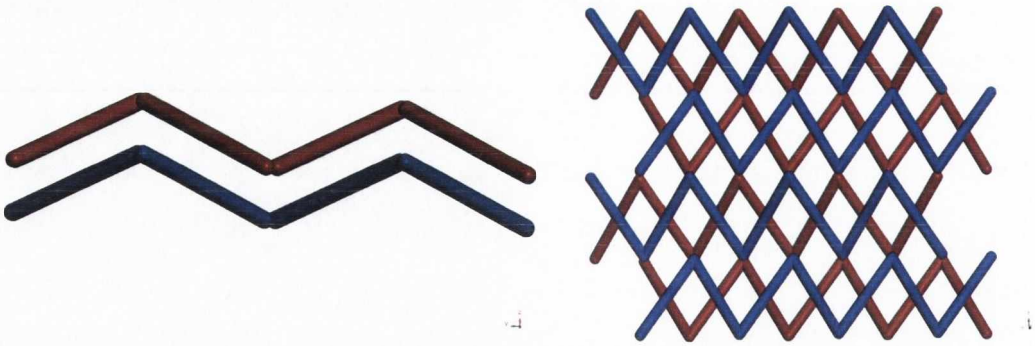


Figure 32: The two-dimensional layering arrangement of the crystals of 3 (left) and the resulting three-dimensional architecture (right)

Crystals of **4** were grown from a dichloromethane solution of the compound. The molecules crystallised in a $P2_1/n$ centrosymmetric space group with one molecule in the asymmetric unit which is shown in Figure 33. There is a dihedral angle of 7.13° between rings A and B. The angle between the central pyridazine ring (B) and ring C is 55.04°, with an angle of 29.05° between B and D.

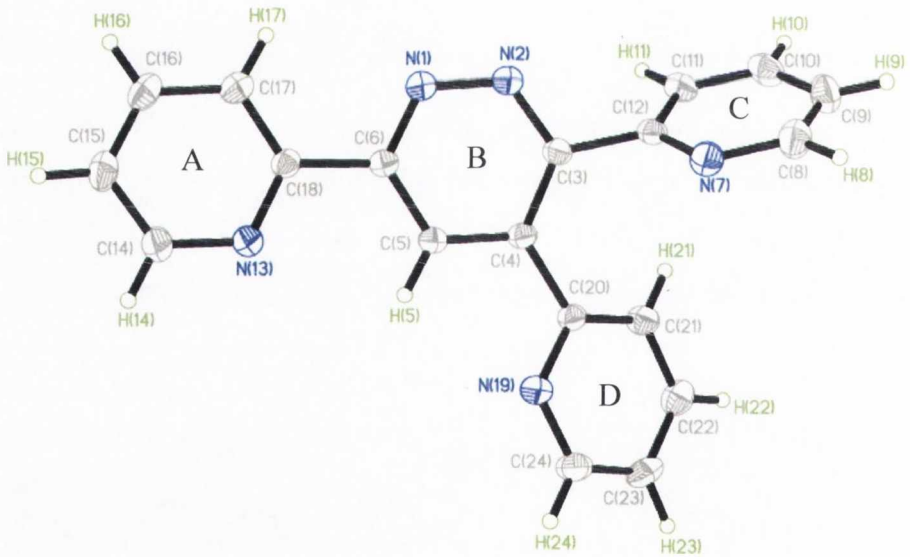


Figure 33: The asymmetric unit of 4

Unlike **3**, the pyridazine ring plays a major role in the hydrogen bond formation and stabilization of the molecular assembly. The collective interaction formed by the pyridazine as well as the 2-pyridyl units leads to the formation of infinite chains as shown in Figure 34.

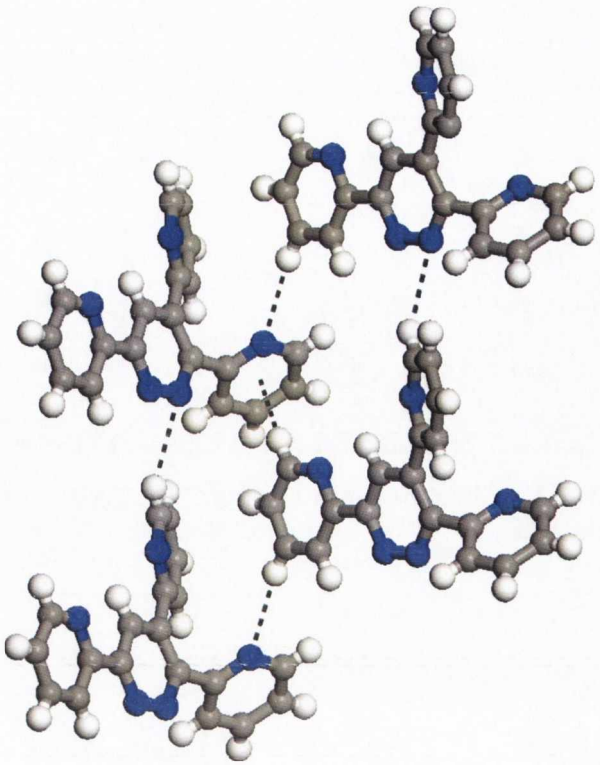


Figure 34: The molecular assembly formed in the crystal lattice of 4

The chains form a type of herringbone arrangement which is represented schematically in Figure 35. In the three-dimensional arrangement, these chains are held by C-H···π (H···π, 2.83Å) interactions. This is also shown schematically in Figure 35.

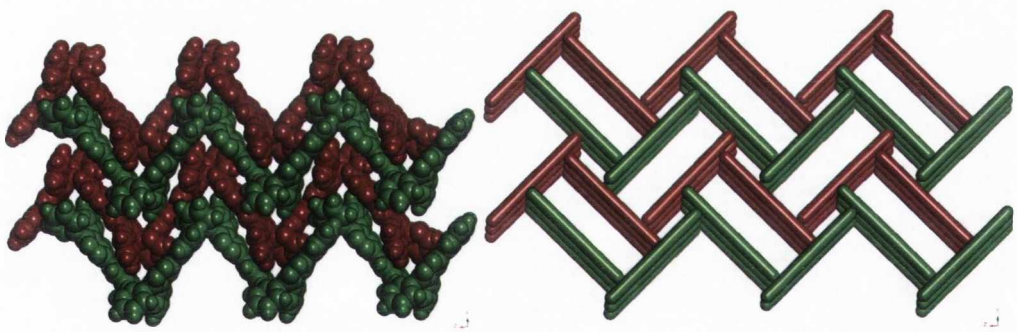


Figure 35: The herring-bone arrangement formed in the crystal lattice of 4 (left) with the three-dimensional representation on the right

Crystals of **6** were grown from a dichloromethane solution of the compound. The asymmetric unit of the crystal contains two molecules of **6** and is shown in Figure 36. The dihedral angle between the central ring (B) and the two 2-pyridyl rings (A and C) is 45.19° and 43.06° respectively. The torsion angles between ring B and the two phenyl rings D and E are 55.60° and 68.01°.

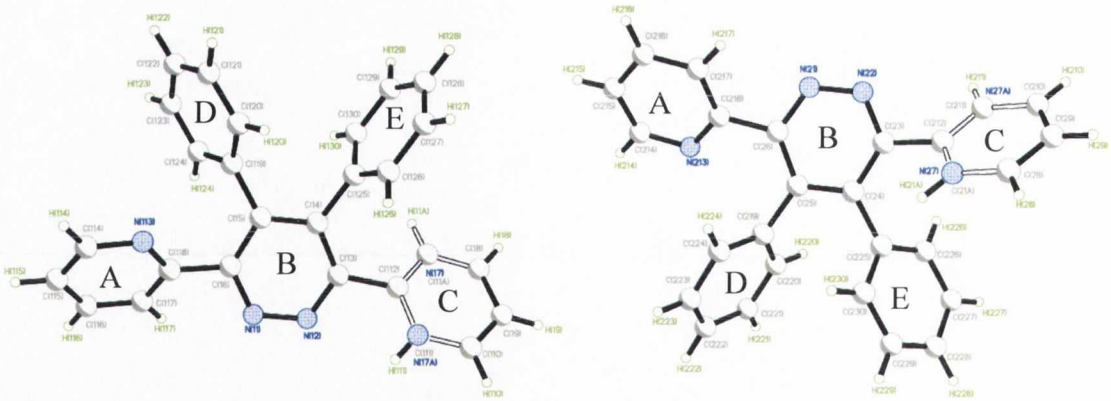


Figure 36: the asymmetric unit of crystals of 6, which contains two molecules

The molecules interact with each other through C-H···N interactions (2.5-2.6Å) and C-H···π (3.0-3.2Å) interactions to form linear chains with branches on one side. This is shown in Figure 37.

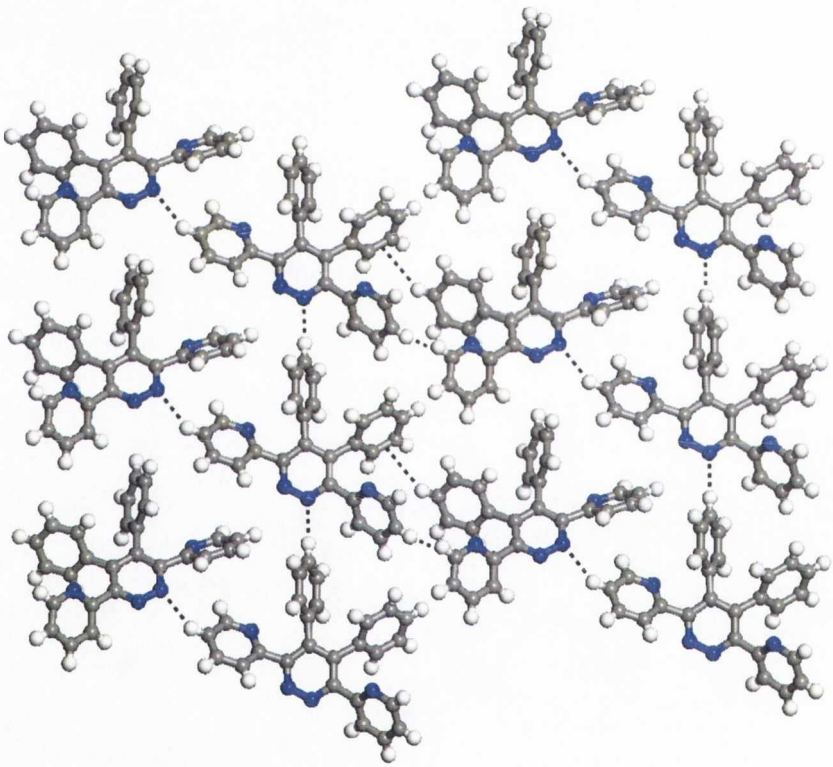


Figure 37: The molecular interactions in the crystal lattice of 6

This interaction can be viewed pictorially as two interlocking branched chains such as that represented in Figure 38.

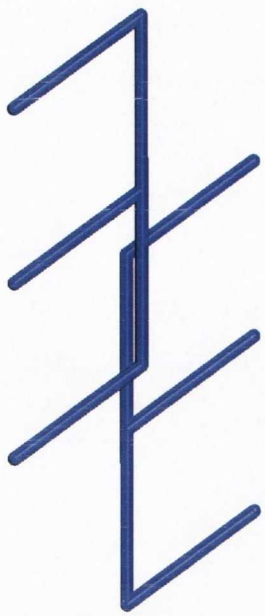


Figure 38: A schematic of the interactions present in the crystal lattice of 6

1.3.3 Characterization of 20 and 21 by UV-Vis and Fluorescence Spectroscopy

The UV-Vis spectra of **20** and **21** in acetonitrile are shown in Figure 39 and compared with that of **19**. Due to the low yields obtained for these compounds, the spectra shown are not independent of concentration and therefore the intensity of the absorptions are not directly comparable. Nonetheless, significant information can be derived from the differences between the three spectra. The spectra were carried out using a $1cm^3$ glass cuvette. Unusually, the spectrum of **20** appears almost featureless, with small shoulders at λ 264 and λ 334 nm. Clearly the absorption maximum at λ 264 nm present in the precursor **19** has disappeared, but there is no other major absorption present. This may be explained by the formation of excimers in the excited state which can interfere with the absorption of the parent molecule.

The spectrum of **21** shows much greater detail, with absorption maxima at λ 238, 313 and 345 nm. It has long been established that the fusion of neighbouring ring systems brings about a bathochromic shift in the absorption maxima of both all carbon and aza-hydrocarbon species.[55] Corbett and co-workers claim a bathochromic shift of between λ 15 and 25 nm for fusion of each bond, but this is only a rough guide and is dependent on the position of the fusion on the ring system. These shifting absorption maxima correspond to $\pi \rightarrow \pi^*$ transitions which are affected not only by the amount of ring fusion in the molecule, but also by the presence of heteroatoms in the system. The analogous all-carbon species usually have maxima which are at higher energy compared with similar

nitrogen containing compounds.[15] Therefore the presence of the maxima in the spectrum of **21** at λ 313 and 345 nm coupled with the disappearance of the maximum at λ 268 nm give strong evidence for the success of the cyclodehydrogenation reaction.

A further characteristic of these fused aza-hydrocarbon systems is the presence of n→π* transitions in the absorption spectra. Typically for pyridazines these occur at around λ 300 nm in polar solvents, and may account for the shoulder in the absorbance maximum at λ 345 nm.[56] The broadness of this maximum may be due to the presence of an n→π* transition in close proximity to a π→π* transition.

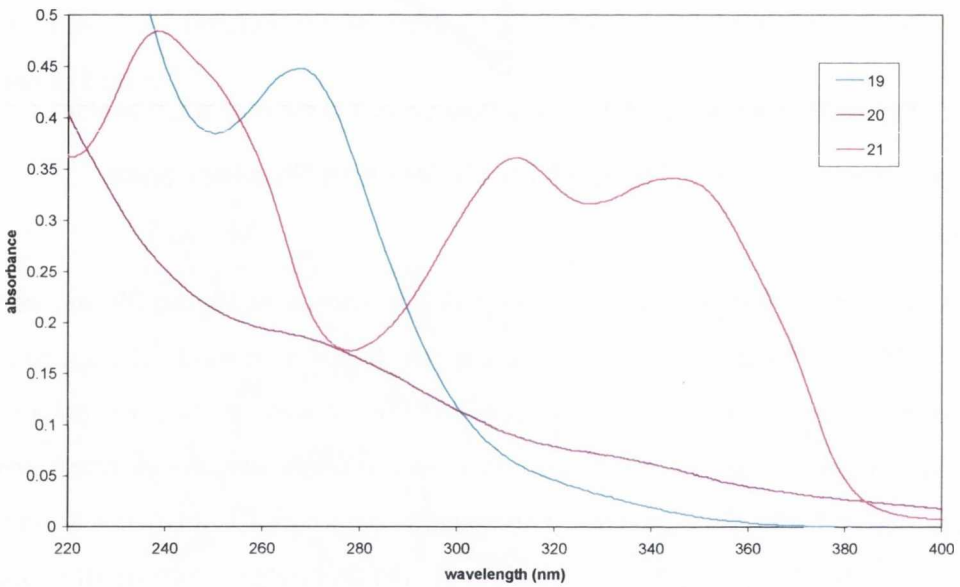


Figure 39: The UV-Vis Absorption Spectra of 19, 20 and 21 in CH_3CN

The fluorescence emission spectrum of **20** is shown in Figure 40 and indicates two weak emission maxima at λ 408 and 563 nm. The presence of this second emission gives further weight to the argument of excited state excimer formation, as similar emissions have been observed in the spectra of pyrene type compounds and can be assigned to excimer emissions.[57]

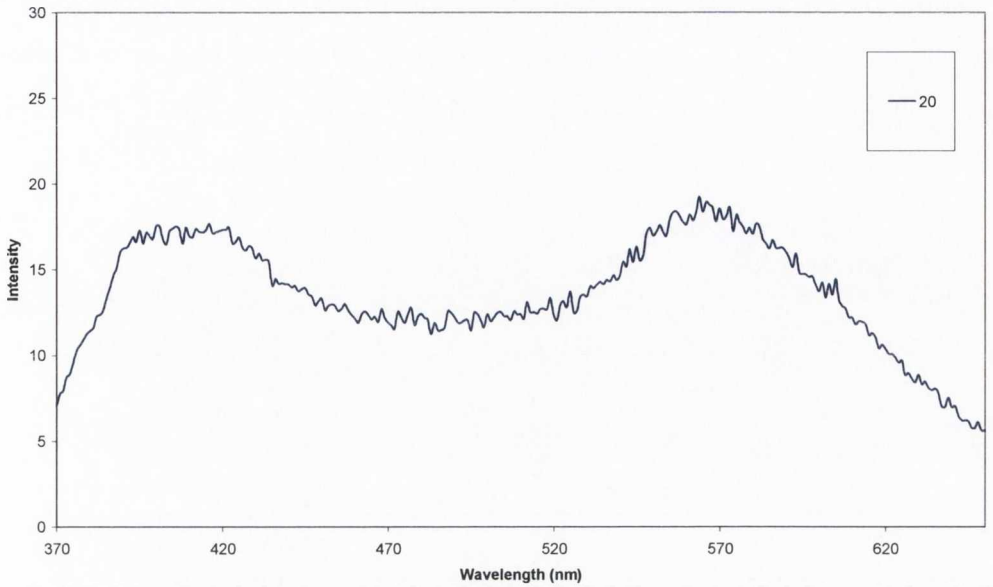


Figure 40: The Emission Spectrum of 20

Figure 41 shows the emission spectra of **20** and **21** and the increase in intensity upon full cyclisation is evident from a comparison of the intensity of the two curves. Both samples were excited at λ 350 nm and the emission of **21** is much more intense than that of **20**. However, it should be noted that the samples are not independent of concentration due to the low yields obtained and therefore this intensity difference is difficult to quantify.

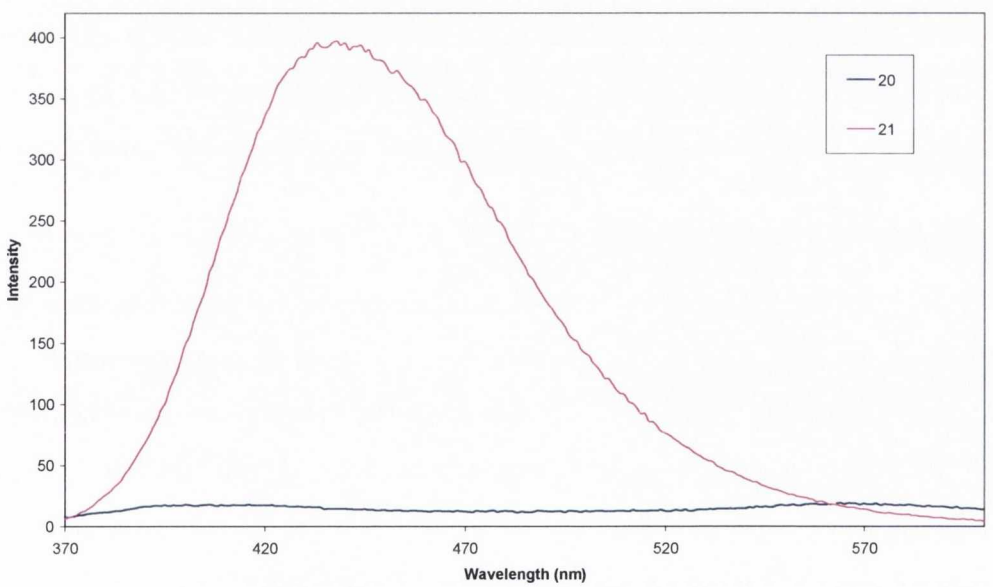
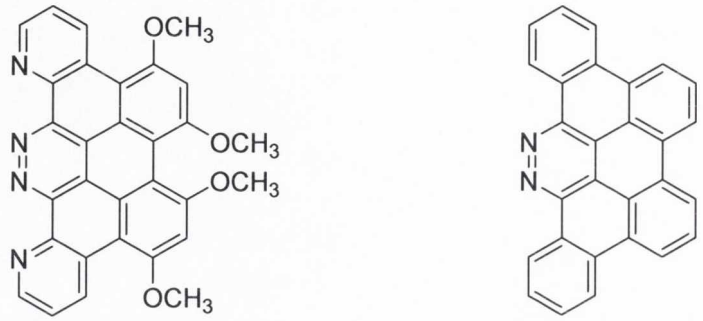


Figure 41: The fluorescence emission spectra of 20 and 21 in CH_3CN

The emission, at λ 438 nm is consistent with other examples in the literature such as diphenanthro[9,10,1def;1',10',9'hij]phthalazine, which has an emission maximum around λ 480 nm (Figure 42).[58] The presence of the methoxy groups on **21** may give rise to this shift in the emission wavelength, as the increased electron donating effect arising from these groups can cause the compound to emit at shorter wavelength.



λ em. = 438 nm λ em. = 480 nm

Figure 42: Compound 22 on the left, with the similarly fused diphenanthro[9,10,1def;1',10',9'hij]phthalazine on the right and their emission maxima.

1.3.4 Characterization by IR Spectroscopy and Mass Spectrometry

All the compounds discussed in this chapter were characterized by IR spectroscopy and details are given in the experimental section. The use of mass spectrometry was invaluable in particular for the characterization of compounds **20** and **21**. The peak obtained for the fully cyclised **21** equalled the mass of the compound plus a sodium cation with an accurate mass of m/z 523.1373. Given the inability to characterize this compound using NMR spectroscopy, this mass spectrum plus the additional UV-Vis and fluorescence spectra were invaluable. The other pyridazine –centred ligands were all characterized by mass spectrometry and details are given in the experimental section.

1.4 Conclusions and Future Work

The synthesis and characterization of a novel set of pyridazine-centred ligands has been carried out by reacting a variety of suitable dienophiles with two substituted tetrazine compounds. The resulting ligands are suitable candidates for coordination chemistry with a variety of metals including ruthenium and iron. Furthermore, the presence of two bidentate coordination sites in these ligands could lead to interesting mixed metal and di-nuclear complexes – a concept which is currently under investigation.

The cyclodehydrogenation of these ligands was largely unsuccessful; however the incorporation of methoxy functionalities onto the phenyl substituents appears to

encourage this reaction, and further work is being undertaken to introduce similar electron-donating groups onto the phenyl and pyridyl substituents of these pyridazines systems. With regard to this work, the cyclodehydrogenation of **19** was carried out to give two products in very low yield. The UV-Vis absorption and fluorescence spectra and the mass spectrum of **22** indicate that full cyclisation has occurred. However, for this reaction to become viable, the yields of both products must be improved and an investigation of their coordination chemistry carried out.

1.5 References

[1] M. Müller, C. Kübel, K. Müllen, *Chem. Eur. J.* **1998**, *4*, 2099.
[2] S. Ito, M. Wehmeier, J. D. Brand, C. Kübel, R. Epsch, J. P. Rabe, K. Müllen, *Chem. Eur. J.* **2000**, *6*, 4327.
[3] J. A. Teske, A. Deiters, *J. Org. Chem.* **2008**, *73*, 342.
[4] R. S. Senaiar, J. A. Teske, D. D. Young, A. Deiters, *J. Org. Chem.* **2007**, *72*, 7801.
[5] A. K. Jhingan, W. F. Maier, *J. Org. Chem.* **1987**, *52*, 1161.
[6] J. Wu, M. D. Watson, N. Tchebotareva, Z. Wang, K. Müllen, *J. Org. Chem.* **2004**, *69*, 8194.
[7] E. C. Taylor, J. G. Andrade, G. J. H. Rall, A. McKillop, *J. Am. Chem. Soc.* **1980**, *102*, 6513.
[8] A. J. Liepa, R. E. Summons, *J. Chem. Soc., Chem. Commun.* **1977**, 826.
[9] P. G. Copeland, R. E. Dean, D. McNeil, *J. Chem. Soc.* **1960**, 1687.
[10] G. M. Badger, B. J. Christie, J. M. Pryke, W. H. F. Sasse, *J. Chem. Soc.* **1957**, 4417.
[11] P. Kovacic, A. Kryiakis, *J. Am. Chem. Soc.* **1963**, *85*, 454.
[12] R. Pummerer, F. Luther, *Beriche der Deutschen Chemischen Gesellschaft* **1947**, *39*, 364.
[13] P. Rempala, J. Kroulik, B. T. King, *J. Org. Chem.* **2005**, *71*, 5067.
[14] P. Kovacic, F. W. Koch, *J. Org. Chem.* **1965**, *30*, 3176.
[15] S. M. Draper, D. J. Gregg, R. Madathil, *J. Am. Chem. Soc.* **2002**, *124*, 3486.
[16] S. M. Draper, D. J. Gregg, E. R. Schofield, W. R. Browne, M. Duati, J. G. Vos, P. Passaniti, *J. Am. Chem. Soc.* **2004**, *126*, 8694
[17] D. J. Gregg, E. Bothe, P. Höfer, P. Passaniti, S. M. Draper, *Inorg. Chem.* **2005**, *44*, 5654.
[18] A. Hantzsch, M. Lehmann, *Beriche der Deutschen Chemischen Gesellschaft* **1900**, *33*, 3668.
[19] O. Schneider, M. Hanack, *Angew. Chem. Int. Ed.* **1983**, *22*, 784.
[20] W. Kaim, *Coord. Chem. Rev.* **2002**, *230*, 127.
[21] F. Dallacker, *Monatsh. Chem.* **1960**, *91*, 302.
[22] J. Poppe, M. Moscherosch, W. Kaim, *Inorg. Chem.* **1993**, *32*, 2640.
[23] W. Kaim, S. Kohlmann, *Inorg. Chem.* **1986**, *25*, 3442.
[24] C. S. Campos-Fernandez, R. Clérac, K. R. Dunbar, *Angew. Chem. Int. Ed.* **1999**, *38*, 3477.
[25] E. C. Constable, C. E. Housecroft, B. M. Kariuki, N. Kelly, C. B. Smith, *Inorg. Chem. Commun.* **2002**, *5*, 199.
[26] R. A. Carboni, J. R. V. Lindsey, *J. Am. Chem. Soc.* **1959**, *81*, 4342.

[27] D. L. Boger, *Chem. Rev.* **1986**, *86*, 781.
[28] W. A. Butte, F. H. Case, *J. Am. Chem. Soc.* **1961**, *26*, 4690.
[29] R. Hoogenboom, G. Kickelbick, U. S. Schubert, *Eur. J. Org. Chem.* **2003**, 4887.
[30] R. Hoogenboom, B. c. Moore, U. S. Schubert, *J. Org. Chem.* **2006**, *71*, 4903.
[31] S.-C. Chuang, M. Sander, T. Jarrosson, S. James, E. Rozumov, S. I. Khan, Y. Rubin, *J. Org. Chem.* **2007**, *72*, 2716.
[32] F. Thébault, A. J. Blake, C. Wilson, N. R. Champness, M. Schröder, *New J. Chem.* **2006**, *30*, 1498.
[33] H. Xie, L. Zu, H. R. Oueis, H. Li, J. Wang, W. Wang, *Org. Lett.* **2008**, *10*, 1923.
[34] T. Eicher, S. Hauptmann, *The Chemistry of Heterocycles*, Wiley-VCH, **2003**.
[35] R. N. Castle, *Pyridazines*, Wiley, **1973**.
[36] H. Neunhoeffer, G. Werner, *Tetrahedron Lett.* **1972**, *16*, 1517.
[37] B. L. Schottel, H. T. Chifotides, M. Shatruk, A. Chouai, L. M. Pérez, J. Bacsa, K. R. Dunbar, *J. Am. Chem. Soc.* **2006**, *128*, 5895.
[38] N. Tsukada, T. Sato, H. Mori, S. Sugawara, C. Kabuto, S. Miyano, Y. Inoue, *J. Organomet. Chem.* **2001**, *627*, 121.
[39] C. Yuste, A. Bentama, S.-E. Stiriba, D. Armentano, G. D. Munno, F. Lloret, M. Julve, *J. Chem. Soc., Dalton Trans.* **2007**, 5190.
[40] A. M. M. Lanfredi, A. Tiripicchio, F. Ugozzoli, *J. Chem. Soc., Dalton Trans.* **1988**, 651.
[41] I. Weissbuch, P. N. W. Baxter, I. Kuzmenko, H. Cohen, S. Cohen, K. Kjaer, P. B. Howes, J. Als-Nielsen, J.-M. Lehn, L. Leiserowitz, M. Lahav, *Chem. Eur. J.* **2000**, *6*, 725.
[42] Z. Deng, H.-W. Tseng, R. Zong, D. Wang, R. Thummel, *Inorg. Chem.* **2008**, *47*, 1835.
[43] J. F. Geldard, F. Lions, *J. Am. Chem. Soc.* **1965**, *30*, 318.
[44] D. L. Boger, R. S. Coleman, J. S. Panek, *J. Org. Chem.* **1985**, *50*, 5377.
[45] M. J. Haddadin, S. J. Firsan, B. S. Nader, *J. Org. Chem.* **1979**, *44*, 629.
[46] E. C. Constable, C. E. Housecroft, M. Neuburger, S. Reymann, S. Schaffner, *Eur. J. Org. Chem.* **2008**, 1597.
[47] B. Sarkar, W. Kaim, T. Schleid, I. Hartenbach, J. Fiedler, *Z. Anorg. Allg. Chem.* **2003**, *629*, 1353.
[48] Z. Wang, F. Dötz, V. Enkelmann, K. Müllen, *Angew. Chem. Int. Ed.* **2005**, *44*, 1247.
[49] X. Feng, W. Pisula, M. Takase, X. Dou, V. Enkelmann, M. Wagner, N. Ding, K. Mullen, *Chem. Mater.* **2008**, *20*, 2872.
[50] D. J. Gregg, C. M. A. Ollagnier, C. M. Fitchett, S. M. Draper, *Chem. Eur. J.* **2006**, *12*, 3043.
[51] J. March, *Advanced Organic Chemistry*, 4th ed., Wiley-Interscience, **1992**.
[52] J. C. Roberts, J. A. Pincock, *J. Org. Chem.* **2004**, *69*, 4279.
[53] J. Gerold, U. Holzenkamp, H. Meier, *Eur. J. Org. Chem.* **2001**, 2757.
[54] M. Shi, B. Xu, *J. Org. Chem.* **2002**, *67*, 294.
[55] J. F. Corbett, P. F. Holt, A. N. Hughes, *J. Chem. Soc.* **1961**, 1363.
[56] G. M. Badger, I. S. Walker, *J. Chem. Soc.* **1956**, 122.
[57] J. Shane-Yang, C.-S. Lin, C.-H. Hwang, *Org. Lett.* **2001**, *3*, 889.
[58] S. A. Tucker, J. William E. Acree, M. J. Tanga, S. Tokita, K. Hiruta, H. Langhals, *Appl. Spectrosc.* **1992**, *46*, 229.

Chapter 2

Iron(II) and Ruthenium(II) Complexes of Pyridazine-Centred Ligands

2.1 Introduction

It was clear from the outset of this work that the coordination and ligand chemistry of the compounds discussed in the previous chapter would be of interest. The chelating properties of the 3-(2-pyridyl)-pyridazine moiety are very similar to 2,2'-bipyridine in that both favour bidentate coordination to metal centres. The coordination chemistry of iron is one of the oldest areas of study of inorganic chemistry. In particular the coordination chemistry of bipyridine, terpyridine and phenanthroline have been well-documented since the early work of Blau in the late 19th century.[1, 2] These ligands form complexes with iron under mild conditions. Such complexes of iron(II) have featured widely in various fields of analytical chemistry including the quantitative investigation of enzyme activity.[3] Many authors have investigated the effect of exchanging the bipyridyl ligand for other non-bpy diimine ligands such as bipyrimidine, bipyrazine or bipyridazine. The effect of having an additional heteroatom on the coordinating ring has been investigated with particular regard to the photophysical properties of their respective ruthenium complexes.[4-7] The coordination chemistry of ruthenium complexes of bipyridine and similar ligands is far more extensive than that of iron, mainly due to the unique photochemical and photophysical properties of this metal which are discussed later in this chapter.

This chapter deals with the synthesis and characterization of the Ru(II) *bis* bpy, Ru(II) *tris* and iron(II) *tris* complexes of some of the pyridazine-centred ligands discussed in chapter 1. These ligands have the additional attribute of containing a number of substituents, some of which are electron-withdrawing such as the 4-pyridyl substituents attached to the central pyridazine in **6** and some of which are electron-donating such as the methoxy groups in **11**. The effect of these substituents on the ^{1}H-NMR and UV-Vis spectroscopy of the complexes will be investigated. The systematic synthesis of these complexes lead to one additional problem – the separation of the facial and meridional isomers formed. A combination of column and preparative chromatography was used for their purification and the ^{1}H-NMR, UV-Vis and fluorescence spectra of these isomers were analysed and compared.

2.1.1 Introduction to Ruthenium Chemistry

The chemistry of ruthenium metal complexes continues to be one of the most active areas of research within the realm of inorganic and coordination chemistry. This is due to their interesting photochemical and photophysical properties.[8] 2,2'- bipyridine or bpy is a colourless organic compound which can act as a chelating ligand to many metals and bonds via σ-donor orbitals localised on the nitrogen atoms and π^* acceptor bonds delocalised on the aromatic rings. Ru(II) forms low spin octahedral complexes with 2,2'-bipyridine which exhibit D_3 symmetry. The resulting complexes exist as one of two enantiomers denoted by Δ or Λ. The synthesis of ruthenium *tris* bipyridine ($[Ru(bpy)_3]^{2+}$) is relatively straightforward using the readily available $RuCl_3$. Through ubiquitous use it has become the reference by which all other ruthenium polypyridyl complexes are compared in terms of their photochemical and spectroscopic properties. The chemistry of Ru(II) polypyridyl complexes such as $[Ru(bpy)_3]^{2+}$ has been intensely studied because of the extended excited state lifetimes, excited state reactivity, significant luminescence and interesting redox chemistry associated with this compound. Furthermore, the general chemical stability of $[Ru(bpy)_3]^{2+}$ makes it an ideal compound for examining these photochemical properties and as a result it has found applications in a variety of fields including chemiluminescence,[9] electron transfer,[10] luminescent sensors[11] and molecular machines.[12]

The $[Ru(bpy)_3]^{2+}$ ground state is derived from the $\pi_m e(d)^4 \pi_m a_1(d)^2$ electronic configuration. The excited states of the molecule are brought about by a number of different possible transitions, illustrated in Figure 43.[13]

- The promotion of an electron from the π_M metal orbital to the π_L^* ligand acceptor orbital or metal to ligand charge transfer (MLCT).
- The promotion of an electron from the π_M metal orbital to the σ_M^* orbitals known as metal-centred transitions (MC).
- The promotion of an electron from the π_L orbital to the π_L^* or ligand centred electron transition (LC).
- The promotion of an electron from the π_L to the σ_M^* or ligand to metal charge transfer (LMCT).

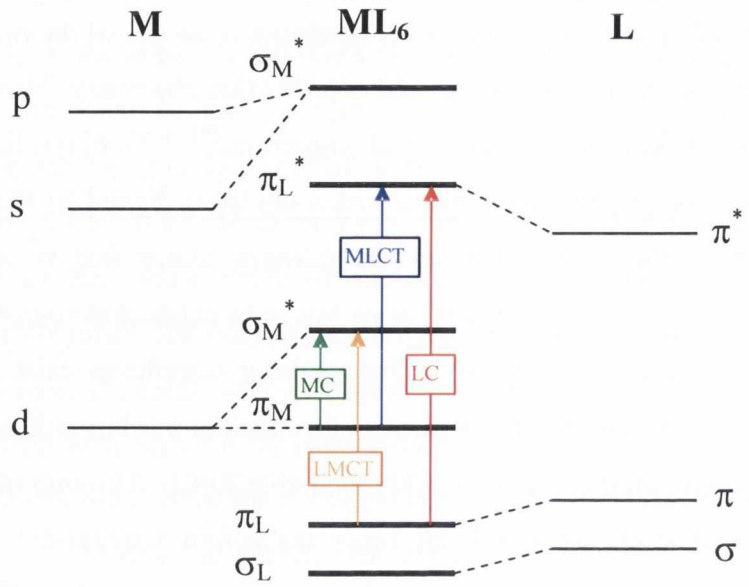


Figure 43: Molecular orbital diagram showing the orbitals for an octahedral complex. The four types of transitions are indicated with arrows.

The MC excited state is strongly displaced with respect to ground state geometry along metal-ligand vibration coordinates. So when the lowest excited state is MC it undergoes fast radiationless decay or ligand dissociation reactions which results in short lifetimes and no luminescence. In the UV-Vis spectrum these transitions are very often masked by stronger MLCT bands.

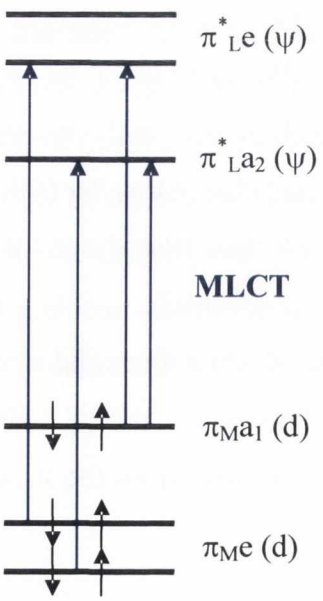


Figure 44: Molecular Orbital diagram showing the orbitals involved in an MLCT transition for Ru(II) polypyridyl complexes.

In contrast LC and MLCT excited state geometries are not strongly displaced and there is no radiationless decay to the ground state. In addition, the excited state lifetimes are significantly longer and luminescence is usually observed. This behaviour is somewhat different at high temperature when the excited electrons can crossover to the MC orbital and return to the ground state via radiationless decay.

The excited state MLCT is more luminescent at room temperature in a fluid medium as the lifetimes of the LC excited state are shortened by intersystem crossing to short lived MC excited states. The orbitals which are involved in the MLCT electron excitation process are the $\pi_M a_1$ (d) and $\pi_M e$ (d) molecular orbitals (HOMO) and the $\pi^*_L a_2$ or the $\pi^*_L e$ orbitals (LUMO) (Figure 44). Transitions between these orbitals result in very intense bands in the UV-Vis spectrum due to the largely singlet nature of both the excited and ground states. In contrast, transitions to triplet excited states are much weaker. For most Ru(II) polypyridyl ligands the lowest excited state is an MLCT, or group of similar MLCT transitions which undergo slow radiationless decay and which have long lifetimes and exhibit luminescence.

For most applications it is therefore desirable to provide π^* acceptor levels on the ligand which are of lower energy, thus reducing the gap between the ground state and the excited state. This can be done by adding electron-withdrawing groups to the polypyridyl ligand which also results in a red-shift in the UV-Vis spectrum.[14] The alternative approach is to stabilise the Ru(III) hole at the metal by adding electron-donating groups directly to the metal. The energy positions of the MC, MLCT and LC transitions are dependent on the ligand properties and the ligand field strength. The choice of ligand is therefore paramount in deciding the energy of the excited states, in particular the orbital nature of the lowest excited state and therefore the resultant UV-Vis spectrum. Any red-shift brought about by the use of anionic or electron donating groups attached to the metal can leave "gaps" in the spectrum, but MLCT bands and $\pi \rightarrow \pi^*$ transitions on other ligands can then be used to fill in these higher energy gaps.[15] Furthermore, switching one of the bpys for another ligand lowers the symmetry of the molecule and removes the degeneracy of the π^* orbitals, which results in a broader UV-Vis spectrum often with various shoulders.[16]

The heteroleptic ruthenium(II) complexes prepared during the course of this work contain two bpy ligands and a third pyridazine –centred ligand of the type discussed in chapter 1. These bidentate ligands are chelated to the metal via a pyridine ring at one point and a

substituted pyridazine ring at the other. Both the extra nitrogen on the pyridazine ring and the substituents bonded to it affect the UV-Vis spectrum of the resulting metal complexes. The effect of replacing the pyridine ring with a pyridazine can be assessed by comparing with similar compounds in the literature.

Ait-Haddou and co-workers are one of the few groups to report the synthesis and characterisation of ruthenium complexes bearing unsubstituted asymmetric diimine ligands (Figure 45). [7] The UV-Vis spectrum of the *bis* bpy complex of 4-(2-pyridyl) pyrimidine (prpm) displays a shoulder at λ 482 nm and a maximum absorption at λ 441 nm. This has been assigned with the help of molecular orbital calculations as an MLCT band mainly delocalised on the asymmetric ligand. Further maxima at λ 280-320 nm and λ 230-260 nm were assigned to $\pi \rightarrow \pi^*$ ligand-centred (LC) and $d \rightarrow d^*$ (MC) transitions respectively. These results were again confirmed *via* calculations although the authors do not specify whether the LC transition is related to the bpy or the 4-(2-pyridyl)pyrimidine ligand.

The Ru(II) *bis* bpy complex of 2-(2'-pyridyl)pyrimidine (pmpy) (Figure 45) has a maximum absorbance at λ 449 nm with a shoulder at λ 425 nm.[16] This transition was assigned to an MLCT ($d\pi \rightarrow \pi_1^*$) absorption. A second transition occurred at higher energy with a maximum at λ 317 nm which was assigned to a second MLCT band ($d\pi \rightarrow \pi^*$). Due to the lower symmetry of the molecule compared to Ru(II) *tris* bpy both of these maxima appear as much broader peaks and could not be assigned to either ligand specifically.

Other groups have made a variety of unsubstituted symmetrical polyazine ligands and compared the absorption properties of the ruthenium complexes of these ligands to Ru(II) *tris* bpy. The *bis* bpy complexes of 3,3'-bipyridazine (bpdz), 4,4'-bipyrimidine (bpm), 2,2'-bipyrazine (bpz) and 2,2'-bipyrimidine (bpym) were prepared by Ernst and Kaim (Figure 45) and the UV-Vis spectra of each compound measured.[17] In addition a number of Hückel Molecular Orbital calculations were carried out and the results compared with the experimental data.[6] In general, it seems the effect of the second nitrogen on the aromatic ring is to increase the electronegativity of the aromatic ring thus lowering the π^* excited state and shifting the MLCT absorption to a lower energy relative to $[Ru(bpy)_3]^{2+}$, which absorbs at λ 451 nm. This suggests that the first electron promoted to the excited state should be localised on the non-bpy ligand.[17] ESR studies on Ru(II) bipyrimidine

complexes further reinforce the idea that the first excited electron is localised on the bipyrimidine ring.[18]

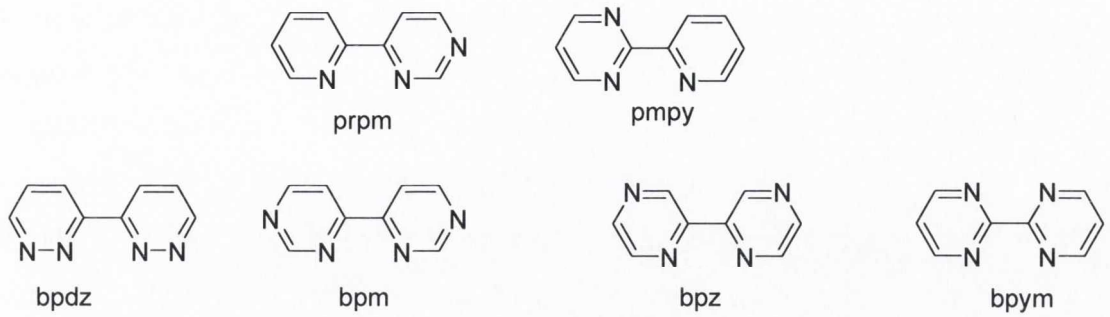


Figure 45: The asymmetric ligands of the Ait-Haddou and Rilemna group (above) and the four symmetrical members of the diazine family studied by Ernst and Kaim (lower).

An important factor in establishing the energy levels of various nitrogen-containing ligands is the σ-donor strength associated with those ligands. A good indication of this is the pKa of the conjugate acid of the ligands which measures the relative affinity of that ligand for H^+. In a metal complex, these weaker σ-donor ligands will cause the metal to have a higher effective nuclear charge which will stabilise the d-orbitals and lower the HOMO. The pKa's of the conjugate acids of the four ligands prepared by Kaim and Ernst are shown in Table 2 along with that of the parent diazines and compared to that of bpy.[6]

Ligand	pK_a of Conjugate Acid	pK_a of Parent Diazine
bpy	4.45	4.30
bpdz	3.37	2.24
bpm	1.50	1.23
bpym	1.20	0.75
bpz	0.45	0.51

Table 2: The pKa's of the ligands discussed here, along with the pKa's of their conjugate acids as compared with those of bpy.

Clearly bpz has the lowest pKa of the series, which results in lower HOMO orbitals for the metal complexes of this ligand. This has been verified by Hückel MO calculations carried out on the chromium and ruthenium complexes of bpz.[4, 6]

The second important factor in the establishment of orbital energy levels concerns the factors influencing the π* LUMO energy. The more electron deficient the π* energy level is, the lower the LUMO energy will be. The most π-electron deficient ligand in Table 2 was calculated to be bpm.[18] This result, coupled with the higher pKa of this ligand compared to bpz, results in a significant bathochromic shift in the MLCT absorbance of

the ruthenium *bis* bpy complex of bpm. This is due to the fact that there is a smaller HOMO-LUMO energy gap for bpm compared to the other ligands, which lowers the energy of the MLCT transition. This result is shown in Table 3 along with the absorption maxima of the $[Ru(bpy)_2L]^{2+}$ complexes of ligands bpdz, bpz and bpym. The complexes of these ligands are only shifted λ 20-30 nm bathochromically relative to $[Ru(bpy)_3]^{2+}$ whereas for the analogous Ru(II) *bis* bpy complex of bpm a shift of λ 75 nm is observed. The shoulder which appears at λ 506 nm in the absorption spectra of the bpm $[Ru(bpy)_2(bpm)]^{2+}$ complex has been assigned to the symmetry allowed MLCT transition to the lowest π* MO of the ligand from the D_3-split (t_{2g}) metal energy level. The fact that this shoulder appears for this complex is attributed to the fact that the bpm has the largest LUMO/SLUMO (Second Lowest Unoccupied Molecular Orbital) or (π_1^*/π_2^*) energy gap of all the ligands which allows for this assignment. This is once again confirmed by Hückel MO calculations which concluded that bpm had the most negative SLUMO and the most positive LUMO of the four. These shoulders are not apparent for the other complexes as the energy gap between the LUMO and SLUMO is too small, and therefore they appear merely as a broadening of the maximum.

$[Ru(bpy)_2(L)]^{2}$	Wavelength (nm) and [absorbance ($M^{-1}cm^{-1}$)]			
L =	MLCT/MC $d\pi \rightarrow \pi^*$	LC $\pi \rightarrow \pi^*$	MLCT $d\pi \rightarrow \pi^*$	Reference
bpy	250 (25000) 238 (30000)	285 (87000)	451 (14000) 428 (13000)	[8]
bpdz	-	-	471 (3830) 409 (3890)	[17]
bpm	-	-	526 (3600) 506 (-) 427 9(3750)	[17]
bpym	360 (6400) 322	294 (48000) 236 (40000)	480 (-) 422 (9700)	[16]
bpz	386 343	283 (63000) 242 (24000)	473 (9900) 414 (1000)	[16]

Table 3: Absorption Maxima of Ru(II) *bis* bpy L heteroleptic complexes in CH_3CN

The other factor influencing the absorption spectra of metal complexes is the presence of substituents attached to the coordinated rings. In mixed diimine complexes such as the Ru(II) *bis* bpy complex of the prpm ligand shown in Figure 45, the excited electron in the MLCT is believed to be located on the non-bpy ring.[7, 17] Therefore the substituents on this ring will have the most influence on the energy maxima of the absorption spectra. Substituents on the bpy ring will be less important, as the electrons will not be localised there in the excited state.

The addition of electron-withdrawing groups such as esters or carboxylic acids makes the ligands more electron-accepting and thus lowers the energy of the LUMOs. This can shift the MLCT absorption band quite considerably to a longer wavelength.[14, 15] Electron-donating groups such as methyl and methoxy functionalities shift the MLCT to a shorter wavelength by raising the energy of the π^* orbital of the LUMO.[19] Campagna and co-workers synthesised a series of Ru(II) *bis* bpy complexes of bis(4-4'-bipyrimidine) (bpm) with and without aromatic substituents at the 6- positions of the chelating rings (Figure 46).[20] The low energy MLCT was shifted from λ 526 nm for the unsubstituted bpm complex to λ 538 nm for the $[Ru(bpy)_2(pbpm)]^{2+}$ which indicates the bathochromic shift arising from the effect of the phenyl substituents. A more significant shift was observed when the phenyl group was replaced by a 2-naphthyl substituent at the same positions (nbpm). This lowers the π^* acceptor orbitals even further due to increased aromaticity of the fused rings and allows for easier acceptance of the excited electron. When the phenyl substituents incorporated methoxy groups at the 3-, 4-, and 5- positions, (mbpm) the

electron donating effect of these substituents effectively raised the π* orbital of the metal complex, thus shifting the MLCT to a higher energy with a maximum absorbance at λ 533 nm. These results are summarised in Table 4.

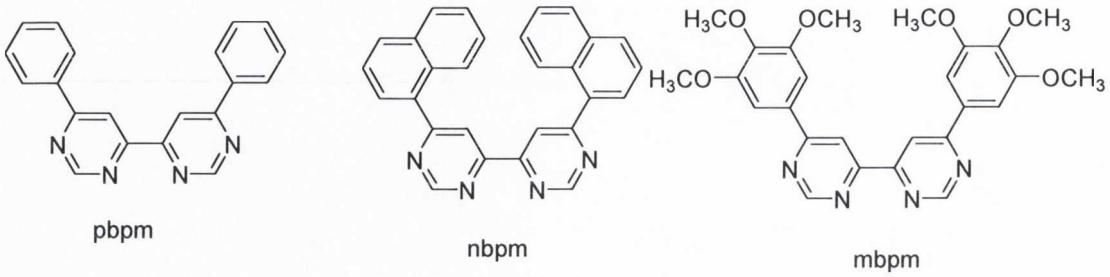


Figure 46: The three ligands prepared by Campagna comparing substituents effects on the absorption spectra.

The Ru (II) *bis* bpy complex of 3, 6- bis-(2'-pyridyl)pyridazine (bppn, Figure 47) was synthesised by Kaim and co-workers and bears the most similarity of all the complexes in the literature to the complexes discussed in this work.[21] The UV-Vis absorption spectra showed a maximum absorbance at λ 480 nm which is a red-shift of λ 30 nm from the Ru (II) *tris* bpy MLCT maximum. There is also a maximum at λ 434 nm which is unassigned, but may be due to a transition to a bpy π* orbital. The wavelength and absorbance of the maxima due to the lowest energy transitions in this Ru(II) *bis* bpy (L) complexes are shown in Table 4 along with those of related compounds.

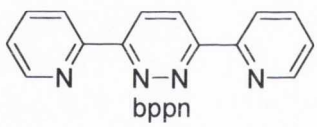


Figure 47: 3, 6- bis(2'-pyridyl)pyridazine (bppn)

Compound $[Ru(bpy)_2(L)]^{2+}$ L =	Wavelength (nm) and [absorbance ($M^{-1}cm^{-1}$)] of low energy maxima	Reference
bpm	526 (3600)	[20]
pbpm	538 (5100) 435 (5500)	[20]
nbpm	542 (2900) 432 (4500)	[20]
mbpm	533 (4700) 432 (5800)	[20]
bppn	480 (2430) 434 (4400)	[21]

Table 4: The low energy absorption maxima of a selection of substituted heteroleptic complexes

2.1.1.1 Luminescence of Ruthenium (II) Complexes

Ruthenium(II) polypyridyl complexes are d^6 metal complexes with fully occupied $\pi_m(t_{2g})^6$ sublevels. Due to the ease of oxidation of the metal centre, the lowest singlet and triplet excited states of Ru(II) *tris* bpy type complexes are MLCT in nature. The MC excited state exhibits no luminescence due to its distorted excited state geometry which results in relaxation via non-radiative deactivation. The luminescence associated with the LC excited states are very often identical to those of the free ligand and are often of low intensity and with no fine structure at high temperature. Only transitions which do not alter the multiplicity are spin allowed. However the presence of a heavy metal, in this case a ruthenium atom, can relax this rule allowing transitions to states with a different multiplicity. Once the excitation has occurred, the electron will return to the ground state via one of several pathways. This decay can occur in some cases via intramolecular reactions or intramolecular radiative and non-radiative deactivations. Any species which is excited to the upper spin-allowed excited states (S_2) undergoes fast 100% radiationless deactivation to the lowest spin allowed excited state (S_1). This lowest excited state relaxes via one of three ways (Figure 48):

- Internal conversion (k_{ic})
- Radiative decay to ground state (fluorescence k_{fl})
- Intersystem crossing to lowest triplet state T_1 k_{isc}, from which it can relax via intersystem crossing or radiative decay (phosphorescence k_{ph}).

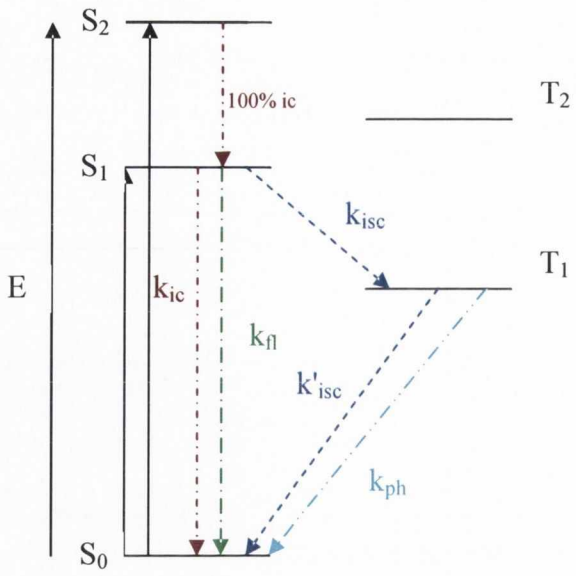


Figure 48: Energy level diagram showing the various pathways of excited state decay.

The luminescence of Ru(II) *tris* bpy is a typical ^{3}MLCT emission and occurs at a much lower energy than the phosphorescence of free bpy. Most Ru(II) polypyridyl complexes exhibit similar luminescence from a ^{3}MLCT state.[22] The energy of this state depends on the reduction potential of the ligand and the charge separation caused by the transition. The σ donor, π donor and π acceptor attributes of the ligand will affect the MLCT excited state and offer some "fine-tuning" of the luminescent emission. The effect of non-bpy diazine ligands on the emission spectrum is related to their effect on the absorption spectrum. As discussed above, most of the diazine ligands are more electronegative than pyridine and result in a bathochromic shift of the MLCT maximum and of the emission maximum.

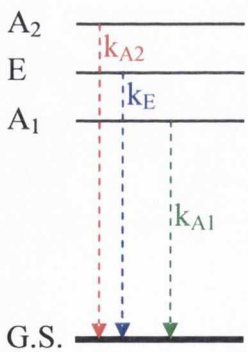


Figure 49: The three closely spaced excited states involved in the luminescence of Ru *tris* bpy.[23]

The emission spectrum of $[Ru(bpy)_2(2,3\text{-bis}(2'\text{-pyridyl})pyrazine)]^{2+}$ is similar to those of ruthenium diazine complexes, with excitation of both the λ 430 nm maximum and the λ 470 nm shoulder in the absorption spectrum resulting in emission at λ 675 nm.[24] This

emission occurs at a lower energy than Ru(II) *tris* bpy due to the lower energy π* LUMO orbital associated with the hetero ligand. The *tris* heteroleptic complexes of various substituted bipyridines theoretically have an individual MLCT absorption maximum for each ligand, although intramolecular charge transfer results in the excited electron ultimately localized on the ligand having the lowest π*-acceptor orbital. However there is only one low energy emission from these complexes which emanates from the ligand with the most positive reduction potential value.[25]

2.1.1.2 Electrochemistry

The redox potential of ruthenium complexes is measured by cyclic voltammetry. This gives an indication of how difficult it is to remove an electron from the metal centre by applying a current through a solution of the complex dissolved in an electrolyte. A cyclic voltammetric sweep is usually carried out between 0 and +2 volts to find the voltage necessary to remove an electron from the metal centre. The current is then reversed, which allows for the reduction of the metal either to its original state, or to some other reduced species. This is also a good indicator of the stability of the complex, as for most applications it is necessary that this process is reversible. In the case of most ruthenium polypyridyl complexes, the oxidation process is metal-centred and results in a Ru(III) low spin $\pi_M(t_{2g})^5$ state.

$$[Ru^{II}(L)_3]^{2+} \rightarrow [Ru^{III}(L_3)]^{3+} + e^-$$

The Ru(II)/(III) redox potential of $[Ru(bpy)_3]^{2+}$ occurs at +1.25 V (*vs.* SCE in acetonitrile). This value is very much dependent on the ligand and its incorporation of electron-donating or -withdrawing groups which lower or raise this value. Therefore, as the removal of the electron during the redox process usually occurs from the HOMO, the redox potential of a particular complex gives valuable information regarding the energy levels within that particular compound. The value of the Ru(II)/(III) redox potential is related to σ-donor strength and is therefore proportional to the pK_a of the ligand.[26] As discussed earlier, a weak σ-donor ligand will stabilize the metal d orbitals in a complex which will lower the HOMO energy levels of this complex.

Reduction is a second electrochemical process which can occur with these complexes. Reduction of the complex can occur by adding an electron to the metal complex in solution. This reduction may be either metal- or ligand-centred, depending on the field strength of the ligand. In the case of ruthenium polypyridine complexes which usually

have a relatively strong ligand field, reduction is ligand based. This reduction occurs on the π^* orbital of the ligand and ensures that the complex maintains its low-spin $\pi_M(t_{2g})^6$ state.

$$[Ru^{II}(L)_3]^{2+} + e^- \rightarrow [Ru^{II}(L)_2(L^-)]^+$$

The electron is localized on one ligand, which is evident from experiments on heteroleptic compounds, where specific reduction peaks indicate the different energies of the π^* orbitals of each individual ligand. Reversibility of these reduction steps is desirable but not always attainable.

Reduction of the ligands is another important indication of the electron transfer processes occurring within a molecule. When an electron is added during the electrochemical process the electron is localised on the LUMO orbital. In the same way, when the complex is oxidised and an electron is removed, it is taken from the HOMO orbital. Therefore, given that the same orbitals are involved in redox transfers as in the MLCT and MC transitions, redox potentials can be used in conjunction with UV-Vis absorption data to assign electronic transitions within a given compound. This relationship can be quantified by the following equation:[14, 18]

$$\Delta E_{1/2} = e[E_{1/2}\,(ox) - E_{1/2}\,(red)]$$

where $E_{1/2}$ (ox) and $E_{1/2}$(red) are the first oxidation and reduction potentials for the complex. If the reduction is centred on the π^* orbital of the ligand and the oxidation centred on the HOMO of the metal as discussed above, then this value should correlate to the low energy MLCT value. In addition to this a linear relationship has been observed between this value and both the emission and absorption of various ruthenium complexes.[14]

In general, complexes containing ligands with lower energy π^* acceptor levels have higher oxidation values as it is more difficult to oxidise the metal due to the stabilization of the metal centred HOMO. Another consequence of this is that the first reduction is attributed to the ligand with the lowest π^* level which is more energetically favourable.

An oxidation potential value of +1.46 V was obtained for the $[Ru(bpy)_2(bpm)]^{2+}$ complex discussed previously (Figure 46).[20] Interestingly, the addition of phenyl, naphtyl and methoxy phenyl substituents to the 6- position of the bipyrimidine ligand cause a decrease in the oxidation potential. These values are summarised below in Table 5.

Compound $[Ru(bpy)_2(L)]^2$ L =	Oxidation *vs* SCE (V)	Reduction *vs* SCE (V)			Reference
bpy	1.25	-1.31	-1.50	-1.77	[8]
bpm	1.46	-0.67	-1.30	-1.59	[20]
pbpm	1.39	-0.69	-1.22	-1.66	[20]
nbpm	1.41	-0.66	-1.24	-1.63	[20]
mbpm	1.37	-0.72	-1.32	-1.69	[20]

Table 5: The oxidation and reduction potentials of the Ru(II) heteroleptic bpy complexes

Crutchley and Lever note a very precise and consistent positive 0.5 V shift in almost all the oxidation and reduction couples of $[Ru(bpz)_3]^{2+}$ compared with the bipyridyl analogue.[5] This is accounted for by the lower basicity and therefore the lower σ-bonding strength of the bipyrazine moiety compared with that of bipyridine, which has the effect of stabilizing the metal orbitals and making the complex more difficult to oxidise.

Similar information regarding the energy levels of ligands has been obtained from the reduction potential values. The first reduction waves of heteroleptic bpy and bpm complexes occur at lower potentials compared to $[Ru(bpy)_3]^{2+}$ which supports the theory that electrons are delocalized on one particular ligand, and that they can be attributed to individual ligands.[26]

2.1.2 The Coordination Chemistry of Iron

Iron, like ruthenium is a d^8 transition metal, of which the Fe(II) and Fe(III) cations are the most prevalent.[27] The chemistry of the Fe(II) species is in many ways similar to that of ruthenium, and the coordination chemistry of both the *bis* and *tris* bpy complexes is well documented.[28] The formation constant for the third bpy ligand of $[Fe(bpy)_3]^{2+}$ is several orders of magnitude higher than that of the first and second ligand. This is believed to be as a result of spin-pairing on changing from a d^6 high-spin to d^6 low spin configuration.[29] Studies have indicated that the excited state of iron(II) polypyridyl complexes are $^5T_2$ and that these states are reached via an MLCT transition from the $^1A_1$ state and have a lifetime of < 700fs.[30] This short lifetime is due to the low lying field states of iron which result in the prompt deactivation of the MLCT excited state. The weaker ligand field of iron ensures that the metal-centred antibonding orbitals e_g are lower than the ligand π* orbitals. This means that unlike ruthenium complexes where the

^{3}MLCT state is populated *via* intersystem crossing and exists for nano to micro seconds, iron complexes crossover to a ligand field state which results in a loss of excited state energy (Figure 50).[31]

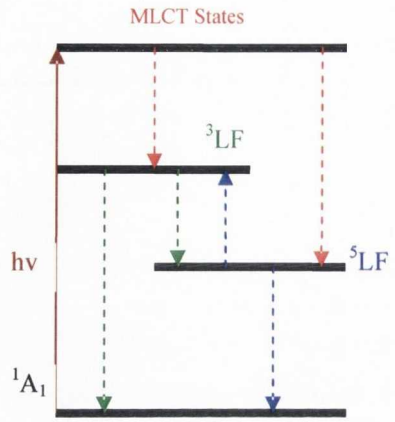


Figure 50:The excited state decay mechanism for iron (II) polypyridyl complexes[31]

The complexes of iron(II) are generally less stable than those of ruthenium(II) and undergo ligand loss easier than their ruthenium analogues. This is partially due to their strong affinity towards anions such as chloride and thiocyanate which increases in the presence of light.

Despite the fact that the majority of photophysical and photochemical studies relate to ruthenium complexes, in recent years an increased interest in the photochemistry of iron has emerged. The use of [Fe(4,4'-dicarboxylic acid-2,2'-bipyridine)$_2$(CN)$_2$] in a dye sensitized solar cell (DSSC) has been investigated by Ferrere.[32] Although this compound has a quantum yield of only 0.4% and a lifetime of 50 ns at room temperature, the quantum yield is near unity when an electron is injected from the excited state into the TiO_2 conduction band. As the cost of iron is less than 1% of ruthenium, if these compounds can be optimized as photosensitizers they would be far more economically efficient than their ruthenium analogues which themselves have exceeded 10% efficiency and are used commercially.[33]

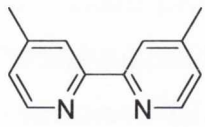
2.1.2.1 *The Spectroscopic Properties of Iron (II) Complexes*

The UV-Vis absorption spectra of $[Fe(bpy)_3]^{2+}$ has three main absorption bands. The highest energy band occurs at λ 298 nm and has been assigned as a $\pi \rightarrow \pi^*$ ligand – centred transition. A second absorption maximum occurs at λ 330 nm which has been assigned a d-d transition. An absorbance at lower energy (λ 520 nm) has been assigned as

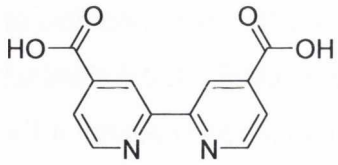
a Laporte allowed MLCT transition. Further shoulders at λ 495, 415 and 387 nm were also assigned as MLCT bands. $[Fe(bpy)_3]^{2+}$ has a relatively short-lived lifetime of 0.8 ns and is not luminescent.[34] The first reduction potential for $[Fe(bpy)_3]^{2+}$ occurs at -1.31 V and the Fe(II/III) oxidation potential occurs at 0.8 V. These are significantly lower than $[Ru(bpy)_3]^{2+}$, due to the decreased backbonding associated with iron complexes.[35]

Due to the decreased stability and shorter lifetimes associated with iron complexes, there is a much smaller body of work in the literature regarding the preparation and characterization of iron(II) non-bpy symmetrical diazine ligands. The synthesis of iron(II) *tris* (2,2'-bipyrimidine) $[Fe(bpm)_3]^{2+}$ has been carried out and its properties compared to that of $[Fe(bpy)_3]^{2+}$.[36] The results are similar to the ruthenium analogue, with the uncoordinated nitrogen on the ring functioning as an electron-withdrawing group. The absorbance spectrum for this compound indicates a low energy MLCT absorbance at λ 530 nm. The *tris* bipyrazine complex has also been prepared and a similar MLCT absorbance occurs at λ 525 nm (Table 6).[37]

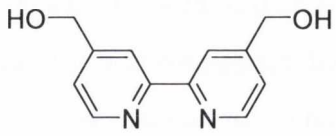
The effect of substituents on the UV-Vis spectroscopy of *tris* bpy type iron complexes is an area in which there is something of a dearth in the literature. Bipyridines with a variety of substituents at the fourth position were synthesised by Ferrere and the iron *tris* complexes subsequently prepared.[38] The low energy maxima of the iron (II) *tris* complexes of 4,4'-dimethyl-2,2'-bipyridine (dmb), 4,4'-dicarboxylate-2,2'-bipyridine (dcb) and 4,4'-bis (hydroxymethyl)-2,2'-bipyridine (dhb) are shown below in Table 6. The effect of di-methyl and hydroxymethyl substituents on the absorption spectra is to shift the absorption maximum of the Fe(II) complex to lower energy; for both complexes the MLCT in the visible region was shifted to λ 528 nm. This shift is larger however for the *tris* dcb iron(II) complex, where the maximum absorption is at λ 535 nm. Clearly the effect of substituents on iron complexes resembles that of their ruthenium analogues, with the addition of electron-withdrawing substituents shifting the absorptions to a lower energy.



dmb



dcb



dhb

$[Fe(L)_3]^{2+}$ L =	Wavelength (nm)	Reference
bpy	523 495 415	[36]
bpym	530 481	[36]
bpz	508 476	[37]
bpdz	520	[39]
dmb	528	[38]
dcb	535	[38]
dhb	528	[38]

Table 6: The low energy absorption maxima of the tris iron(II) complexes of a number of ligands

2.1.3 Isomerism in Coordination Chemistry

The observance and recognition of isomers in coordination compounds is almost as old as the study of coordination chemistry itself. Since the early work of Alfred Werner, the importance of differentiating between the various structural and geometric isomers of coordination compounds has had huge implications for the development of the field. Werner recognised a variety of geometric isomers including the *cis* and *trans* forms of several cobalamine complexes.[40] In the case of ruthenium polypyridyl chemistry the isomerism present in the complexes is based on the chirality of the molecule and can be somewhat more subtle.[41] For example, isomerism in the $[Ru(bpy)_3]^{2+}$ cation is dependent on the direction of the "twist" of the ligands around the central metal complex. There are therefore two distinct enantiomers of this complex, notated as Δ, (right-hand twist), and Λ, (left-hand twist) isomers.

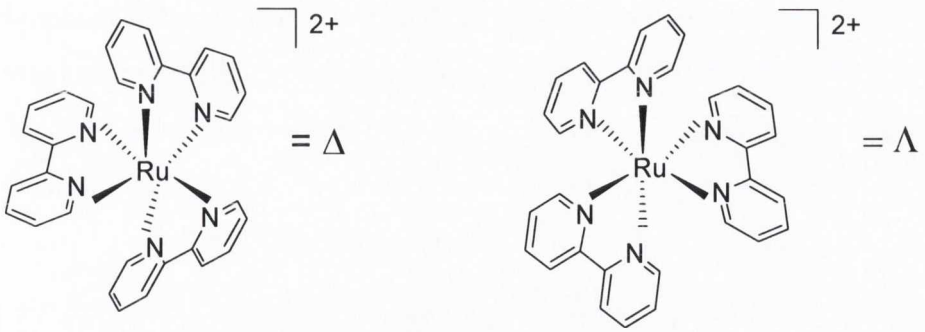


Figure 51: The two enantiomers of the $[Ru(bpy)_3]^{2+}$ cation

There exists an extensive body of work investigating the separation of Λ and Δ enantiomers of both *tris* and *bis* bpy ruthenium complexes. Keene and co-workers prepared a series of ruthenium *bis* bpy and *bis* phenanthroline carbonyl complexes and successfully separated them into their respective enantiomers.[42] The enantiomers were separated by chromatography using Sephadex C-25 as the solid phase and chiral counterions dissolved in the mobile phase. This procedure also proved effective for a number of similar ruthenium *tris* complexes of methyl substituted bipyridine. The effectiveness of the separation is believed to be related to the interaction between the complex, the chiral eluent and the Sephadex support.

Other factors which affect the separation of enantiomers are the degree of aromaticity and chirality of the ligand. This is highlighted by the fact that $[Ru(phen)_3]^{2+}$ separates much better than $[Ru(bpy)_3]^{2+}$ using both the (+)-tartrate salts as eluents and that the order of elution of the two enantiomers of $[Ru(bpy)_3]^{2+}$ is reversed when switching from the (–) tartrate anions to the (+) tartrate anions. The Δ enantiomer has a higher affinity for the (–) salt relative to the Λ isomer which reduces its effective charge and allows for separation.

A number of groups have reacted racemic coordination compounds with enantiomerically pure nucleophiles and produced enantiomerically pure complexes.[43] Similar techniques have been used for the isolation of enantiomerically pure di- and tri- nuclear complexes.[44-46]

As discussed above, the use of three equivalent symmetric ligands coordinated to a metal results in enantiomeric mixtures which can be separated by column chromatography and/or the use of enantiomerically pure chiral salts. This isomerism is further complicated when unsymmetrical ligands are introduced. In this case the facial and meridional isomers are obtained. There is a much smaller body of literature involving the separation of these geometric isomers and much of it has emerged in the past ten years.[47, 48] These two isomers can be distinguished by ^{1}H-NMR spectroscopy due to the different

symmetries associated with each complex. The meridional form has essentially no axis of symmetry (C_1) which results in each proton on each ligand having an individual proton shift. The facial isomer however has a C_3 axis of symmetry which means that the ^{1}H-NMR spectrum is much simpler, as each proton on the ligand is in an identical magnetic environment to the same proton on the other ligands.

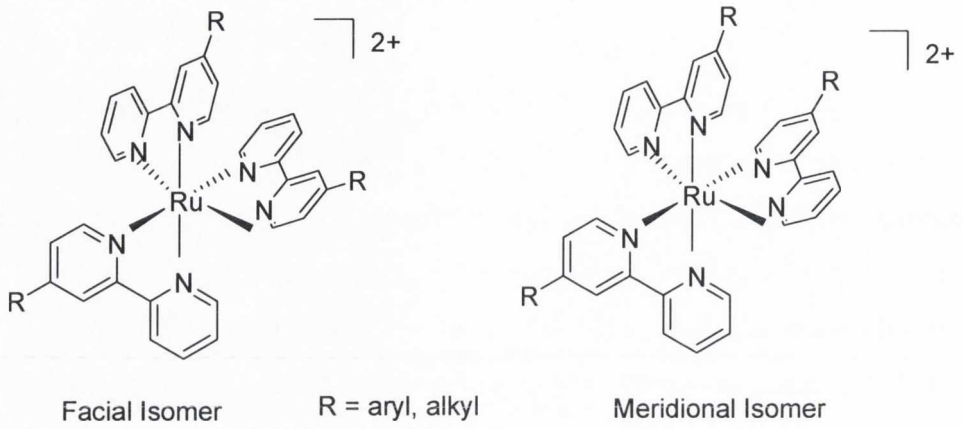


Figure 52: Facial and Meridional Isomers of a Ruthenium Complex

Pure *fac* and *mer* isomers of ruthenium complexes can be prepared via two specific methods. The first involves the synthesis of a mixture of both isomers and their subsequent separation. The second technique involves a more structured preparation of one particular isomer by use of a templated synthetic process. Weizman and co-workers used this technique to synthesise the *fac* isomer of a substituted ruthenium bis bpy complex based on L-alanine derived hydroxamic acid shown in Figure 53.[49] The Ru(II) bpy tripod complex of this ligand was prepared and the chirality of the ligand allowed for separation of the Λ and Δ isomers.

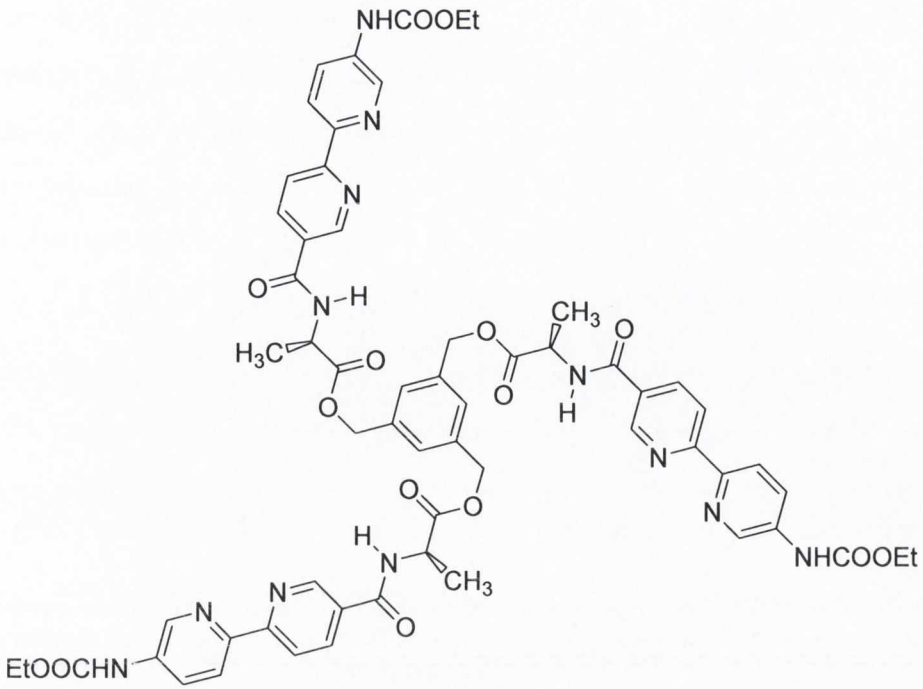


Figure 53: The templated ligand of Weizman[49]

A similar technique was used by Fletcher and co-workers whereby they substituted 2,2'-bipyridine with amino ester functionalities which could be hydrolysed after coordination to give the pure *fac* isomer in good yield.[50]

Apart from the structural control of the ligands before coordination, other techniques have been used to prepare pure *fac* and *mer* isomers without the need for later separation. When other chemical factors are neglected, and the mechanics of the coordination chemistry alone are considered, the statistical ratio of *mer* to *fac* should be 3:1. However this statistical factor is very often overshadowed by reaction conditions and ligand variations. By carrying out the coordination reaction of a number of fluoro-substituted pyridine ligands with $IrCl_3$ at varying temperatures, the ratio of *fac* to *mer* isomer changed considerably. [51] A reaction temperature of 160°C resulted in the mer isomer being isolated as the main product in 45% yield. When the reaction was carried out at 200°C the *fac* isomer was the major product and was isolated in 60% yield. The reason for this is unclear however and no explanation is given by the authors. Ishida and co-workers also noted a variation in the ratio of *mer* to *fac* isomers depending on the nature of the preparation; a 21:79 ratio of *fac* to *mer* is achieved upon microwave irradiation, but under reflux a ratio of 17:83 is observed.[52]

Similar behaviour is observed in the preparation of a number of ruthenium complexes by Fletcher and co-workers, whereby varying both the solvent and the temperature changed the ratio of isomers in the mixture.[47] In particular, when bulky substituents were

attached to the bpy moiety (Figure 54), there was an increase in the proportion of the *fac* isomer. This was further increased when polar solvents or a higher reaction temperature were used. Once again the mechanism behind this phenomenon remains unclear, but the authors propose that the facial geometry may give rise to a hydrophobic cavity brought about by the directionality of the organic moieties on the bpy. Alternatively they propose a greater interaction with the counter-anions than for the *mer* isomer.

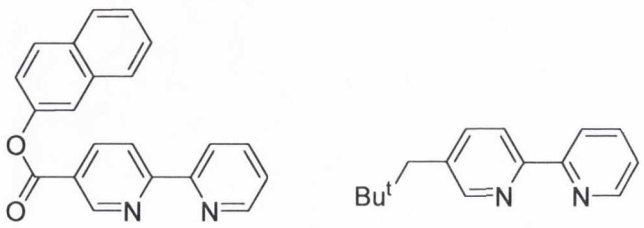


Figure 54: Two of the bulky ligands prepared by Fletcher. The Ru(II) *tris* complex of the ligand on the left favours the *fac* conformation, whilst that on the right was synthesised exclusively in the *mer* configuration

When aliphatic substituents are attached to the bpy, upon increasing the number of carbons in the substituents from methyl to isopropyl, the proportion of *fac* isomer is reduced.[53] When a t-butyl moiety was used, formation of the *fac* isomer was not observed and only the *mer* isomer is obtained. This apparent contradiction only serves to highlight the important role the substituents play in determining the *mer*: *fac* ratio, the plethora of factors which contribute to this variation and most importantly the lack of understanding in the area regarding the theory behind these variations.

The variety of techniques and overall effort that many groups have instilled into preparing isomerically pure *fac* or *mer* isomers of complexes, whether by templated synthesis or by manipulating reaction conditions, gives a good indication of the difficulty in isomer separation after the synthesis has been carried out. Many authors have reported difficulties in separating isomeric mixtures, and many have simply reported the preparation of the mixture of isomers.[53-57]

Of those that have successfully separated facial and meridional isomers of coordination complexes, the techniques usually involve some form of chromatographic procedure. However, in most cases the retardation times of *mer* and *fac* isomers were too similar to be successfully separated by regular silica chromatography. Successful separation techniques used include HPLC techniques or ion exchange chromatography using Sephadex.[52, 53, 58-60] However, difficulties arise with the use of Sephadex in the separation of geometric isomers due to the intrinsic chirality of the Sephadex material itself. It appears in some cases that the use of Sephadex results in enantiomeric resolution

of the Δ and Λ forms of the metal complex occurring in preference to geometric separation of the *fac* and *mer* isomers. This appeared to be particularly relevant when the bpy ligand was functionalised with a methyl ester group.[54] Perhaps in no small part due to the disadvantage associated with Sephadex, the Fletcher group began to use thin layer chromatographic plates to separate *mer* and *fac* isomers. A number of unsymmetrically substituted *tris* bpy complexes of ruthenium(II) were successfully separated into their respective *mer* and *fac* isomers using a mixture of DMF and ethanol or water saturated with ammonium chloride.[47, 54]

2.2 Results and Discussion

2.2.1 Synthesis of Ru(II) *bis* bpy Complexes of Ligands 3, 4, 6, 8 and 11

2.2.1.1 Synthetic Procedure

It was recognised from an early stage that the compounds discussed in chapter 1 would be excellent candidates for coordination chemistry with transition metals. In particular they would be suitable ligands for the synthesis of ruthenium *bis* bpy complexes. As a result the synthesis of the Ru(II) *bis* bpy complexes of **3**, **4**, **6**, **8** and **11** was attempted. The experiments were carried out according to common literature procedures, which involves refluxing the ligand with a suitable ruthenium salt in a high boiling point solvent under inert conditions (Scheme 33).[61] Ruthenium (II) *bis* bipyridine dichloride ($[Ru(bpy)_2Cl_2]$) was chosen as a suitable starting material and the reactions were carried out by refluxing this in a 1:1 mixture of ethylene glycol and water under argon for several hours. The colour of the reaction changed from dark purple to brown. A small excess of ligand was used in the reaction as any excess can be easily removed by washing with dichloromethane. Saturated aqueous KPF_6 was then added to the mixture to precipitate the metal complex, which was then extracted from the aqueous phase in dichloromethane and dried using $MgSO_4$. The *bis* bipyridyl complexes were then purified by column chromatography using a variety of solvents containing saturated potassium nitrate solution.

Compound	% Yields of Ru(II) *bis*-bpy Complex	% Yield of deuterated Complex
22	65	64
23	73	68
24	63	78
25	54	75
26	56	-

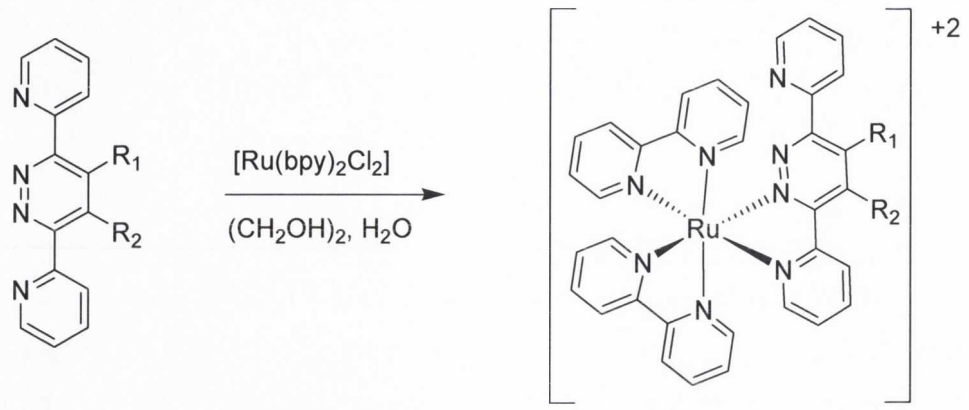
Table 7: Yields obtained for both forms of Ru (II) *bis*-bpy Complexes 22-26

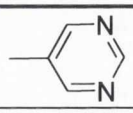
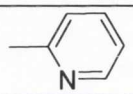
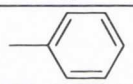
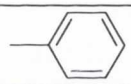
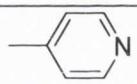
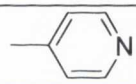
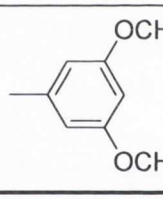
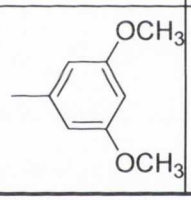
For the isolation and purification of **24** the same solvent mix was used but the quantity of KNO_3 was doubled. In the case of **25** and **26** a more polar mixture of solvents was needed as these compounds did not run in a mixture of acetonitrile and water. This is most likely due to the extra nitrogens on the pyridine rings at the 4- and 5- positions of the pyridazine ring in **25**, and the methoxy substituents on the phenyl rings in **26**. In these cases a mixture of acetone and ammonia was used instead of acetonitrile and water.

2.2.1.2 Characterisation of 22 and 23

As discussed in Chapter 1, the characterisation of ligands **3** and **4** by proton NMR spectroscopy gave rise to a number of complications. In particular, definitively assigning the peaks to specific rings on the compound was not possible despite numerous NOE and ROESY experiments. By coordinating ligands **3** or **4** to a heavy transition metal such as ruthenium, the electron density is dramatically affected. The large metal draws the electrons towards its nucleus and generally results in an overall deshielding effect on ligand protons. Therefore when the ligand is coordinated to a metal at only one site, this brings about a significant difference in the electronic environments of both pyridyl rings at the 3-and 6-positions, which in turn often results in a dramatic shift of the proton signals on the NMR spectra. Furthermore, the coordination to the metal results in restricting one of the rings from moving and fixing the protons in a particular plane. This very often leads to better quality NOESY experiments, as the through-space interaction between the protons can be accentuated.

During the course of the ^{1}H-NMR spectroscopic investigation of these compounds it became apparent that the number of 2-pyridyl rings in the systems resulted in a multitude of protons appearing in the same area of the spectrum, making their assignment difficult. In order to fully assign all the signals in the ^{1}H-NMR spectrum, the Ru(II) bis bpy complexes of the ligands which possess numerous pyridyl ring systems were prepared using a deuterated bis-bipyridyl ruthenium dichloride salt ($[Ru(bpy_{d8})_2Cl_2]$. The reactions and purifications were carried out in the same manner, but the ^{1}H-NMR spectra of the



Ligand	R1	R2	Complex Product
3		H	22
4		H	23
6			24
8			25
11			26

Scheme 33: General scheme for the synthesis of Ru(II) bis bpy complexes of pyridazyl ligands

The solvent mixture used was dependent on the nature of the complex; ligands with two aromatic substituents (**6**, **8** and **11**) require a more polar solvent mix. The ruthenium complexes **22** and **23** were purified using a 10:1.5:1 mixture of acetonitrile:water:sat. KNO_3 on a silica column and were subsequently isolated as their PF_6 salts in 65% and 73% yields respectively (Table 7). In both cases there was a possibility that two isomers would be obtained, given that the ligand could coordinate in one of two possible positions. However only one product was isolated in each case which was then characterized by ^{1}H-NMR spectroscopy, mass spectrometry and X-Ray crystallography.

products contain only the signals which were associated with the pyridazyl ligand in the normal aromatic region of the spectrum (δ 7-9 ppm relative to trimethyl-silyl chloride).

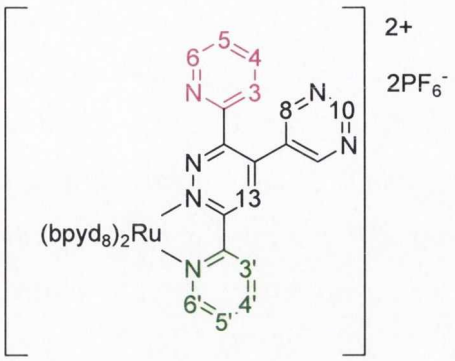


Figure 55: Figure showing the numbering system used for complex 22

Complex **22**: A comparison of the ^{1}H-NMR spectra of ligand **3**, the deuterated *bis* bpy ruthenium (II) complex **22d$_8$** and the non-deuterated complex, **22** is shown in Figure 56. The signals of the pyrimidyl ring H^{8} and H^{10} are only slightly shifted from those of the free ligand. In contrast the signal H^{13} is shifted downfield by δ 0.5 ppm to δ 8.7 ppm due to its proximity to the metal. In differentiating between the two pyridyl rings, it was thought that the most deshielded proton was most likely belonging to the coordinated ring in accordance with previous observations.[62]

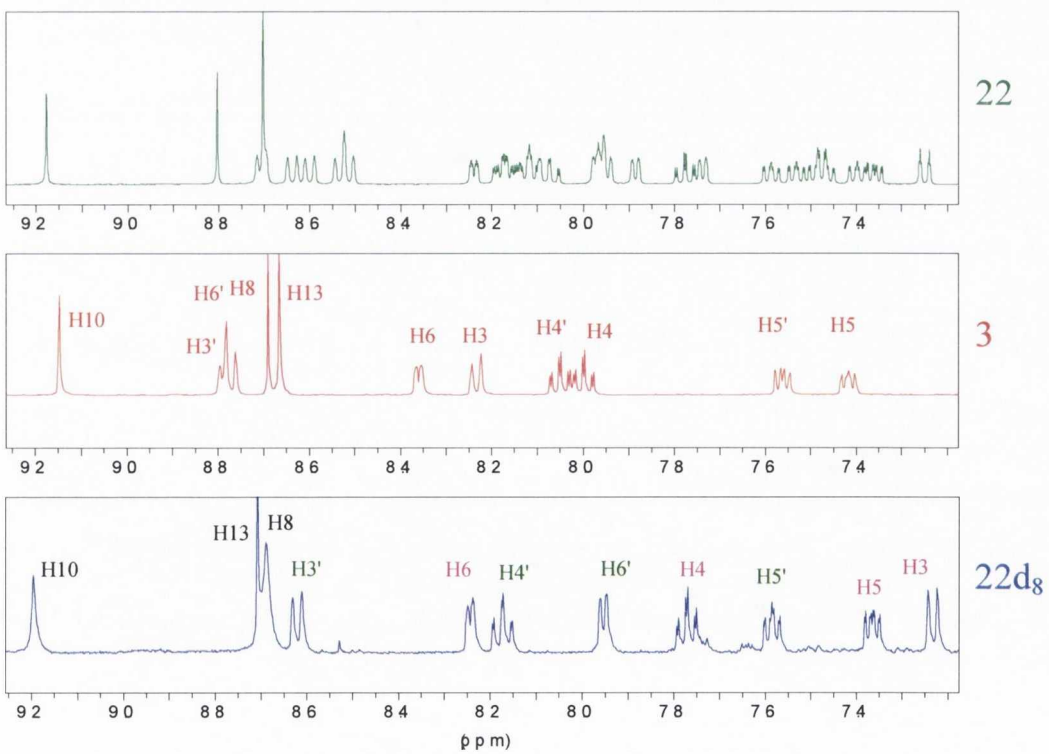


Figure 56: The ^{1}H-NMR spectra of the non-deuterated bpy complex 22 in green in CD_3CN, with the free ligand 3 (red) and the deuterated bpy Ru(II) Complex 22d$_8$ in blue (δ 7.3-9.2 ppm shown)

The ROESY experiment shown in Figure 57 clearly indicates a through-space interaction between the proton H^{13} and the $H^{3'}$ proton which is on the coordinated pyridyl ring. In addition, a 1-D NOe experiment (Figure 58) clearly shows an interaction between these protons. From these experiments the two pyridyl rings could be assigned precisely. The $H^{6'}$ proton from the coordinated pyridyl ring is shifted quite far upfield to δ 7.95 ppm. The $H^{3'}$ proton however is shifted only slightly upfield to δ 8.6 ppm, which compares favourably to other examples in the literature.[20] The other major shift is that of the H^3 proton on the uncoordinated pyridyl ring, which is shifted upfield from δ 8.2 ppm in the free ligand to almost δ 7.2 ppm on the complex. This may be due to coordination resulting in a slight restriction of rotation of the pyrimidyl ring, and this H^3 proton being under the influence of the ring current from the pyrimidine. Further evidence of this is the slight broadening of the pyrimidyl signals in the proton NMR of the complex. The other signals associated with both pyridyl rings are shifted to a much lesser extent.

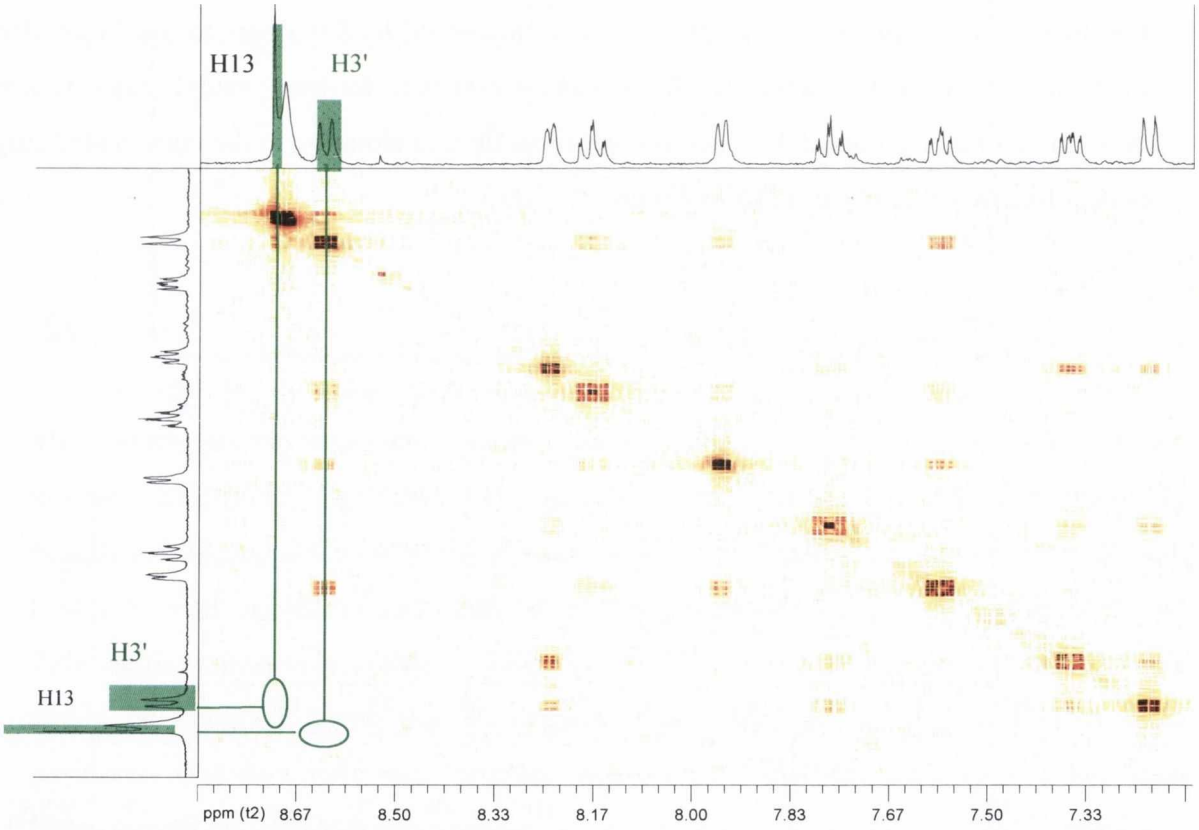


Figure 57: ROESY experiment showing the through - space interaction between $H^{3'}$ and H^{13} in 22_{d8} (δ 7.2-8.8 ppm shown)

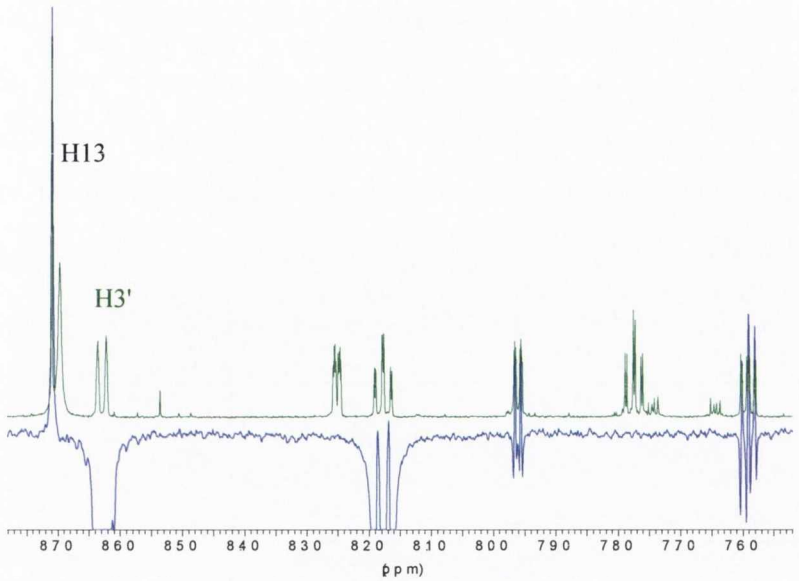


Figure 58:NOe experiment showing the same interaction between the $H^{3'}$ and H^{13} of 22_{d8}

Complex **22** was also characterised by mass spectroscopy and yielded the peak associated with the sodium salt. The mass calculated for this peak was m/z = 726.1518, and the mass obtained experimentally was 726.1516.

Complex **23**: The analysis of the proton NMR spectrum of **23** was assisted by comparison with the spectrum of the deuterated bpy complex. Figure 59 shows the ^{1}H-NMR spectrum of the free ligand **4** and the spectra of the deuterated and non-deuterated ruthenium(II) complexes, $\mathbf{23d_8}$ and **23**.

The use of 2-D NMR ^{1}H-^{1}H COSY experiments was necessary to determine the three separate 2-pyridyl ring systems labelled A, B and C in Figure 59. The identity of each individual ring was assigned on the basis that the most downfield H^3 proton belongs to the ring on the 6 position, (labelled A in Figure 59) as it is deshielded by coordination to the metal and a similar shift was seen for the same proton in **22**. From this and other information obtained from the ^{1}H-^{1}H COSY the other A protons could be assigned. The H^6 proton on this ring experiences the greatest shift, appearing at δ 7.95 ppm compared with δ 8.8 ppm in the free ligand. Both the H^4 and the H^5 protons on the same ring are shifted only slightly upon coordination. Despite the use of ROESY and NOe experiments, the pyridyl rings in position 3- and 4- of the pyridazine could not be definitively distinguished. In Figure 59 these rings have been labelled B and C and the signals have been assigned on the basis of a slight upfield shift of each H^6 proton from the chemical shift of the free ligand. Unfortunately, no other systematic spectral evidence could be

found to support this proposition despite numerous attempts. Therefore these assignments are somewhat more tenuous than for ring A.

Complex **23** was also characterised by mass spectrometry, with an accurate mass obtained for the ruthenium complex of 725.1572 and an isotopic distribution pattern typical of ruthenium-containing complexes. This is in good agreement with the calculated mass of 725.1589.

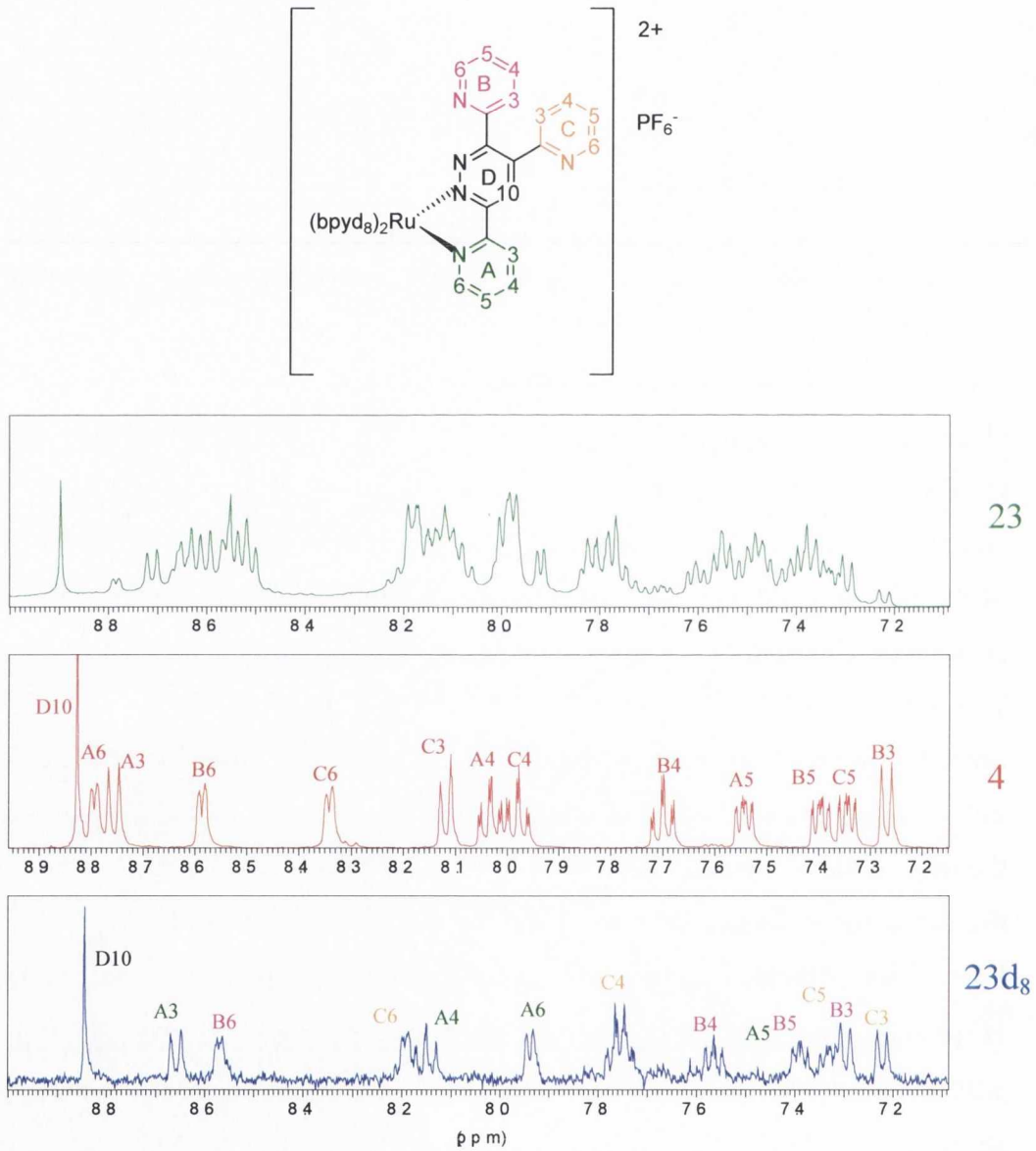


Figure 59: The non-deuterated *bis* bpy Ru(II) complex in green with the free ligand 4 shown in red, and the deuterated Ru(II) *bis* bpy complex $23d_8$ in blue (δ 7.1-8.9 ppm shown)

2.2.1.3 Characterisation of Compounds 24, 25 and 26

24, 25 and **26** were fully characterised by mass spectrometry and proton NMR spectroscopy. In the case of **24**, the peak at 399.47 in the electrospray mass spectrum was assigned as the m/z peak for the $[M\text{-}2PF_6]^{2+}$ complex ion which was close to the calculated value of m/z = 400.09 for this complex.

Complex **24:** The proton NMR spectrum of **24** was extremely complicated due to the quantity of aromatic signals and the unsymmetrical nature of the heteroleptic complex. The deuterated Ru(II) d_8 *bis*-bpy complex **24d$_8$** was therefore synthesised as an aid to assign the proton NMR of complex **24**. Figure 60 shows separate plots of the uncoordinated ligand **6** in deuterated acetonitrile above the proton spectrum of the deuterated ruthenium complex (**24d$_8$**) and the original spectrum of the ruthenium complex (**24**).

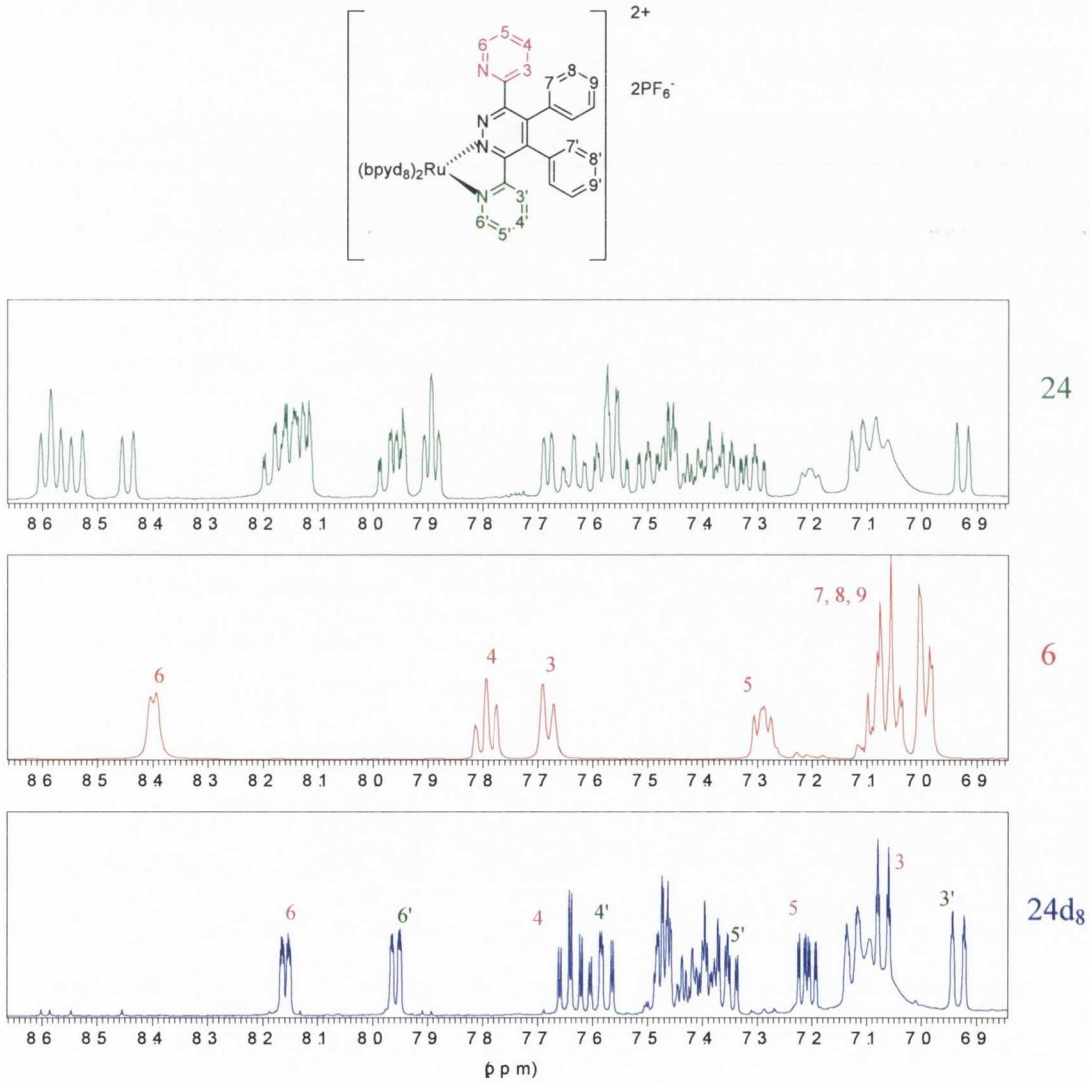


Figure 60: The ^{1}H-NMR spectrum in CD_3CN of the Ru(II) *bis* bpy complex 24 in green, ligand 6 in red, with the deuterated *bis* bpy Ru(II) complex 24d$_8$ in blue (δ 6.9-8.6 ppm shown)

Coordination to the ruthenium centre at one bidentate site on the ligand results in the loss of the inherent symmetry of the ligand as both the phenyl and pyridyl rings are in different chemical environments. NMR TOCSY experiments were carried out to assign the peaks relative to their neighbours on each individual ring. The final difficulty in assigning this spectrum was to differentiate between the two pyridyl rings. This was achieved again by considering the fact that the $H^{3'}$ proton of the coordinated ring is more shielded than the H^3 of the uncoordinated pyridyl ring (δ 6.8 compared to δ 7.1 ppm). This is due to the fact that the uncoordinated ring can twist in such a way that the shielding effect of the phenyl ring is less significant (Figure 61 (a)). The coordinated ring on the other hand is unable to rotate, leaving the H^3 proton more exposed to the ring current of the neighbouring phenyl ring (Figure 61 (b)).

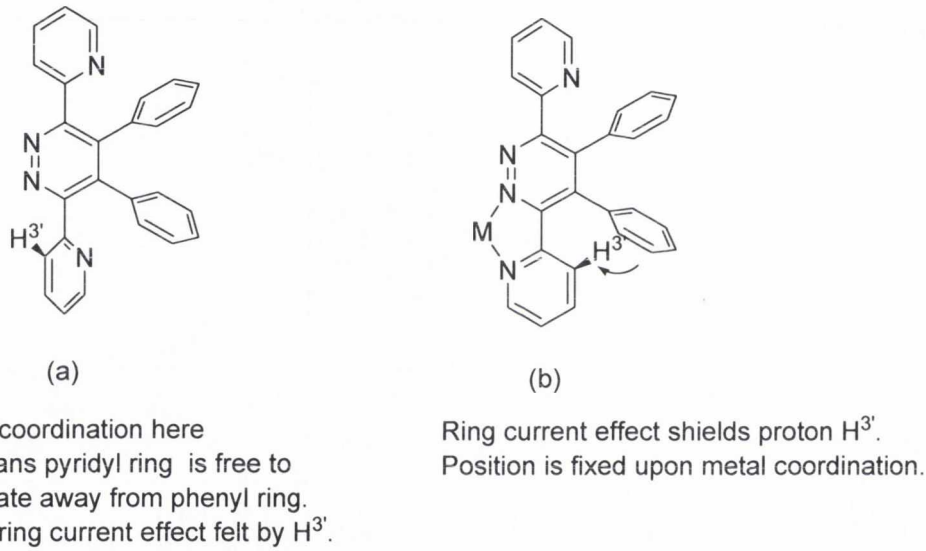


Figure 61: Graphic showing the shielding effect prevalent in 24, 25 and 26

With this in mind, the most shielded signal was assigned as the coordinated $H^{3'}$ proton and from the TOCSY experiments the remaining proton signals on this ring were also assigned.

As can be seen from Figure 60, the H^6 and $H^{6'}$ protons have been shifted upfield upon coordination, with the coordinated pyridyl $H^{6'}$ appearing at δ 7.9 ppm and the "free" H^6 appearing at δ 8.18 ppm. The H^4 protons have also shifted upfield from the free ligand, with both signals appearing at about δ 7.6 ppm. The $H^{5'}$ signal of the coordinated ring is shifted downfield to δ 7.36 ppm and the uncoordinated ring $H^{5'}$ is shifted upfield to δ 7.21 ppm from the free ligand. This could be due to the fact that the ring current effect of the neighbouring phenyl ring is negligible at this position and the overwhelming influence on the chemical shift of this is coordination to the metal. The phenyl signals appear as

multiplets at δ 7.45 and 7.10 ppm but it is unclear which signals belong to which phenyl ring. It is likely however that the most downfield signals are those of the H^7 protons due to the deshielding effect of the pyridazine ring. On the spectrum of the original ruthenium *bis* bpy complex **24** it is now possible to assign some of the peaks belonging to the bipyridine rings by process of elimination. The four signals between δ 8.4 and 8.6 ppm are the H^3 signals from the coordinated bpy rings. Equally, some of the H^6 and the H^4 signals can be identified from their unique splitting patterns at δ 7.9 and 8.1 ppm.

Complex **25**: The assignment of the proton NMR spectrum of **25** was also complicated due to the presence of the two 4-pyridyl rings on the back of the ligand. Once again the deuterated bipyridyl analogue was prepared to assist in the NMR assignment (**25d$_8$**). Figure 62 shows the relevant ^{1}H-NMR spectra.

As for **24**, the symmetry which existed for the free ligand is no longer present on coordination. In addition in the case of **25** there is an apparent loss of symmetry of the 4-pyridyl substituents on the back of the ligand. The reason for this loss of symmetry is discussed in a later section. The two most downfield $H^{8'}$ signals are from the same ring and couple to the $H^{7'}$ signal at δ 7.1 ppm. The H^8 signals are shifted only slightly downfield from the free ligand to δ 8.3 ppm. However these signals are extremely broad and are poorly resolved. The same applies to the H^7 signal from the same ring which is shifted upfield from δ 6.9 ppm on the free ligand to δ 6.8 ppm on the complex; this signal is also very weak and broad. The same logic was applied to the assignment of each individual 2-pyridyl ring as for **24**. The more intense ring current effect would be felt by the coordinated ring; hence the most shielded ring was assigned as that of the coordinated system.

From the spectrum of non-deuterated **25** the most downfield signals of the bpy ligands can be identified from their coupling constants as the H^3 signals. The other bpy signals are difficult to distinguish as they tend to be grouped together. However a number of bpy multiplets are clearly present at δ 8.1, 7.9, 7.7 and 7.35 ppm.

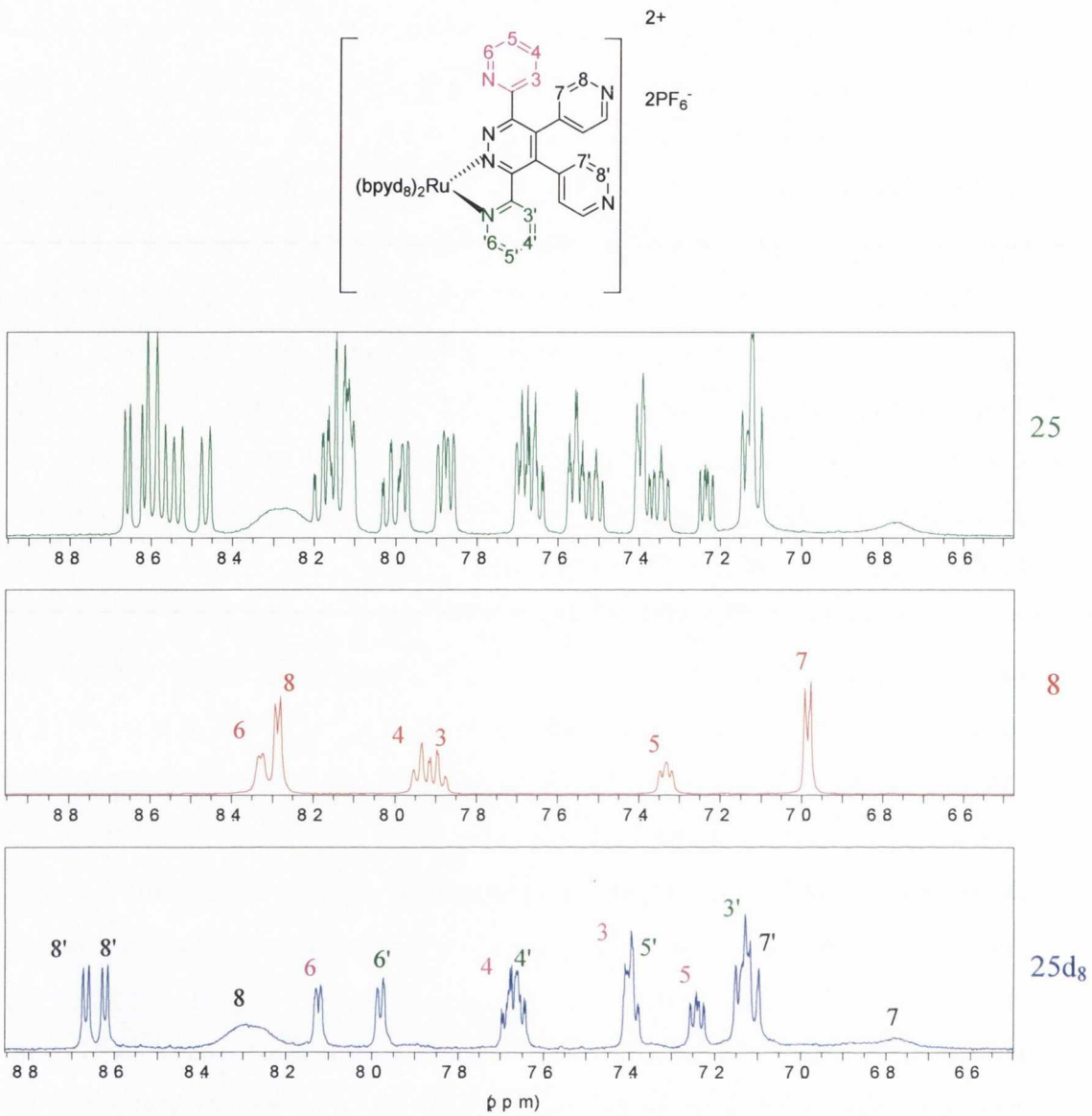
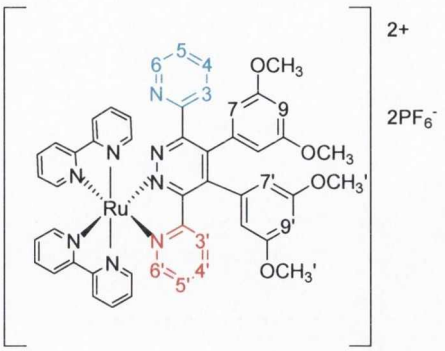


Figure 62: The ^{1}H-NMR spectrum in CD_3CN of the regular Ru (II) bis bpy complex 25 in green, ligand 8 in red, with the deuterated bis bpy Ru(II) complex $25d_8$ in blue (δ 6.6-8.8 ppm shown)

Complex **26**: To fully characterise **26** by ^{1}H-NMR spectroscopy it was not necessary to compare it to a deuterated bpy analogue. This was because the methoxy groups ensured that the phenyl signals from the pyridazine ligand occurred significantly upfield from the pyridyl signals and that there were only six pyridyl rings in the downfield region from δ 7.0 to 8.6 ppm. The four rings belonging to the bpy ligands were identifiable, as the H^3 signals from these rings and were almost identical in chemical shift to those observed in **24**. TOCSY experiments allowed the other signals on the rings to be identified. The most upfield of the remaining two ring signals was assigned to the coordinated pyridyl ring. Figure 63 shows the ^{1}H-^{1}H COSY NMR experiment which was carried out in the aromatic region of the spectrum. As discussed above, the most upfield ring has been

assigned to the coordinated pyridyl ring. The other uncoloured signals are those associated with the two bpy ligands.



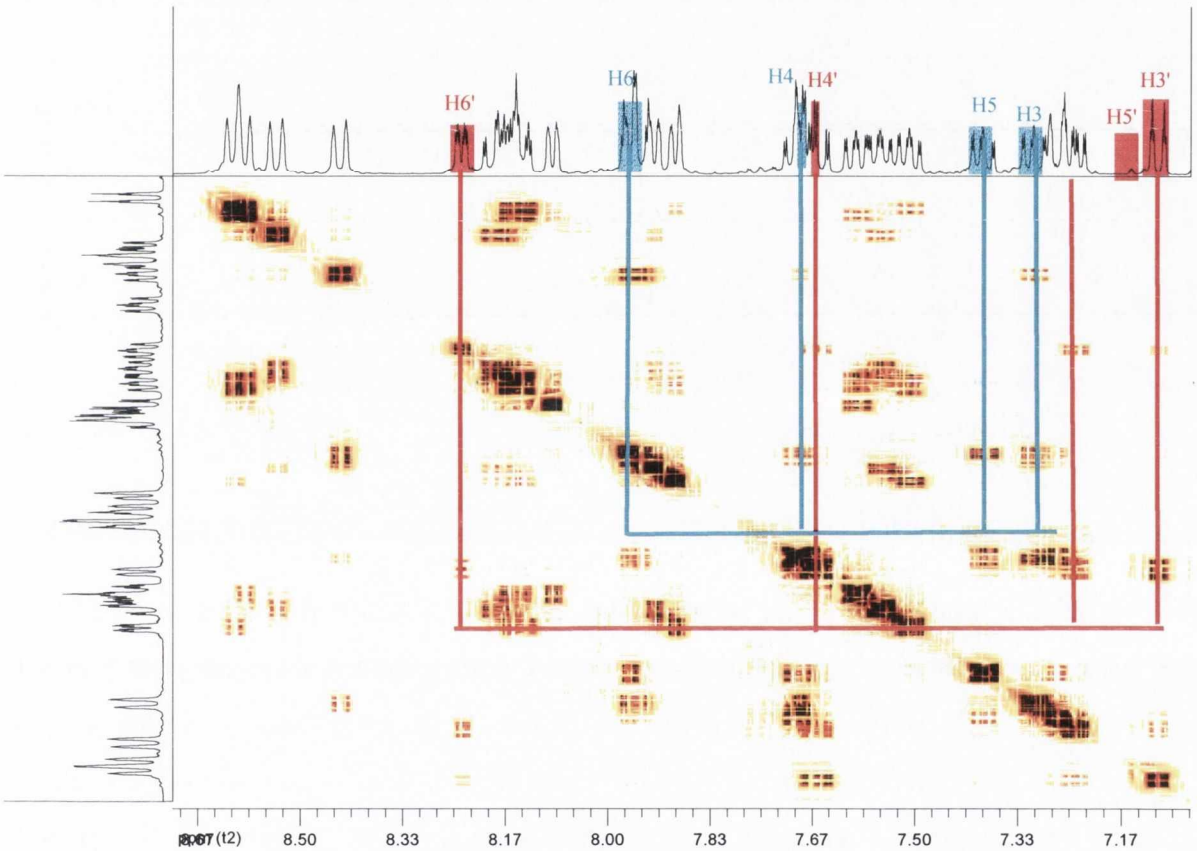


Figure 63: ^{1}H-^{1}H COSY spectrum showing the two 2-pyridyl rings on 26

Figure 64 shows the proton NMR spectrum of ligand **11** as compared with that of the bpy complex **26**. The most upfield signals are those of the methoxy functional group which resonate at δ 3.5 ppm in the free ligand. When the ligand is complexed these methoxy protons lose their symmetry. However there appears to be a further complication as there are now three signals for these protons rather than two as expected. One of the signals is quite broad, while the other two are very sharp. This is due to the fact that the individual rings have also lost their axis of symmetry, giving rise to a broad signal for one ring and

two individual resonances for the other. This effect is explained in greater detail in a later section.

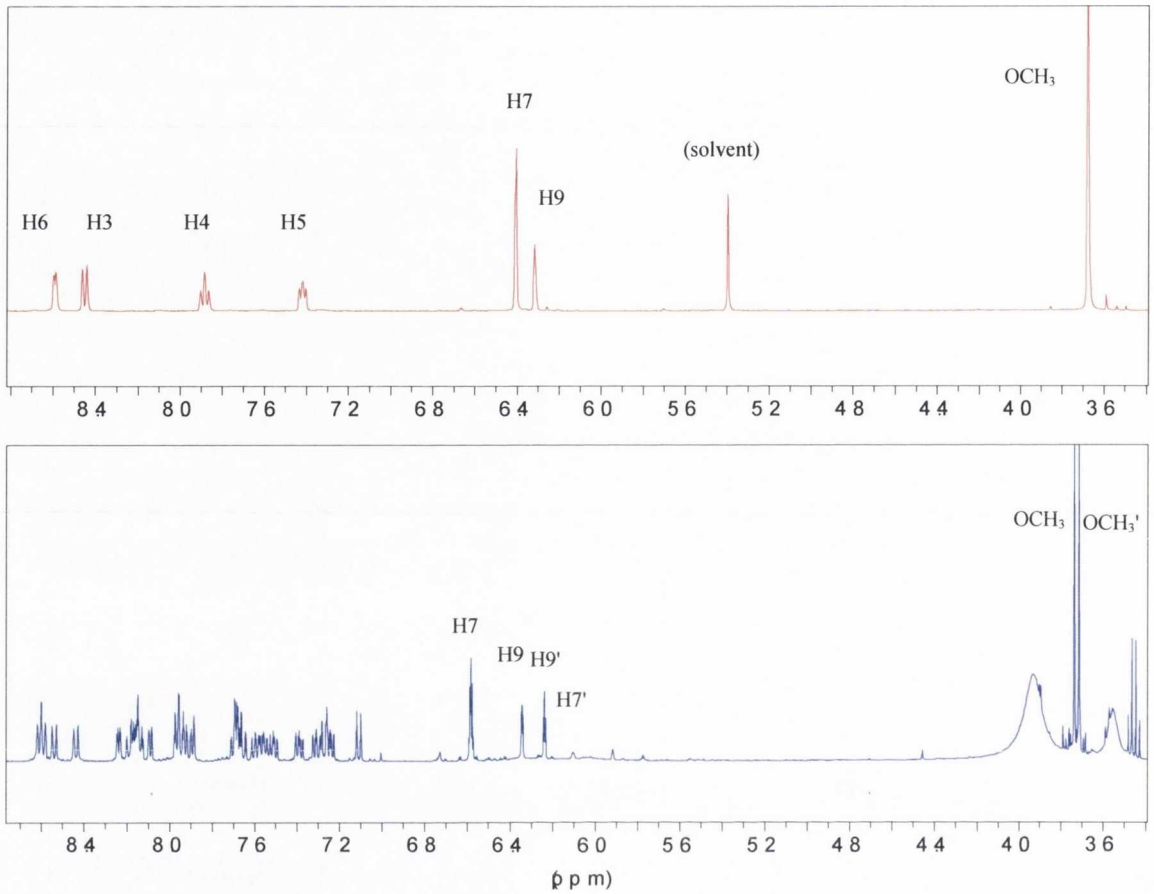


Figure 64: The ^{1}H-NMR spectra on CD_3CN of 11 in red with the related Ru(II) bis bpy complex 26 in blue ((δ 3.6-8.5 ppm shown)

A similar broadening effect is noticed for the proton labelled $H^{7'}$ which is most likely the signal from the ring furthest from the point of coordination. This signal is very broad and shifted δ 0.3 ppm upfield from the free ligand. Both the H^9 and $H^{9'}$ proton signals are shifted only slightly from the uncoordinated ligand, one slightly upfield and the other slightly downfield. Figure 65 shows the aromatic region of the free ligand and the complex and allows for comparison of these shifts. The H^6 and $H^{6'}$ protons are shifted upfield by δ 0.4 and 0.6 ppm, with the $H^{6'}$ of the coordinated ring resonating at the more downfield shift. The most significant shift upon coordination is apparent for the H^3 proton which is shifted from δ 8.45 ppm on the free ligand to δ 7.10 and 7.28 ppm for the coordinated and uncoordinated rings respectively. This dramatic shift most likely occurs as a result of the ring current effect brought about by the proximity to the phenyl rings on the back of the pyridazine. The shielding effect is more intense for the $H^{3'}$ proton on the coordinated ring, as this is unable to rotate away from the ring due to coordination, as

was the case for **24** and **25**. Both the $H^4/H^{4'}$ and $H^5/H^{5'}$ protons differ only slightly from the ligand signals with upfield shifts of between δ 0.1 and 0.3 ppm. Table 8 below summarises the chemical shifts associated with the 2-pyridyl ring systems of compounds **24**, **25** and **26** relative to their respective ligands.

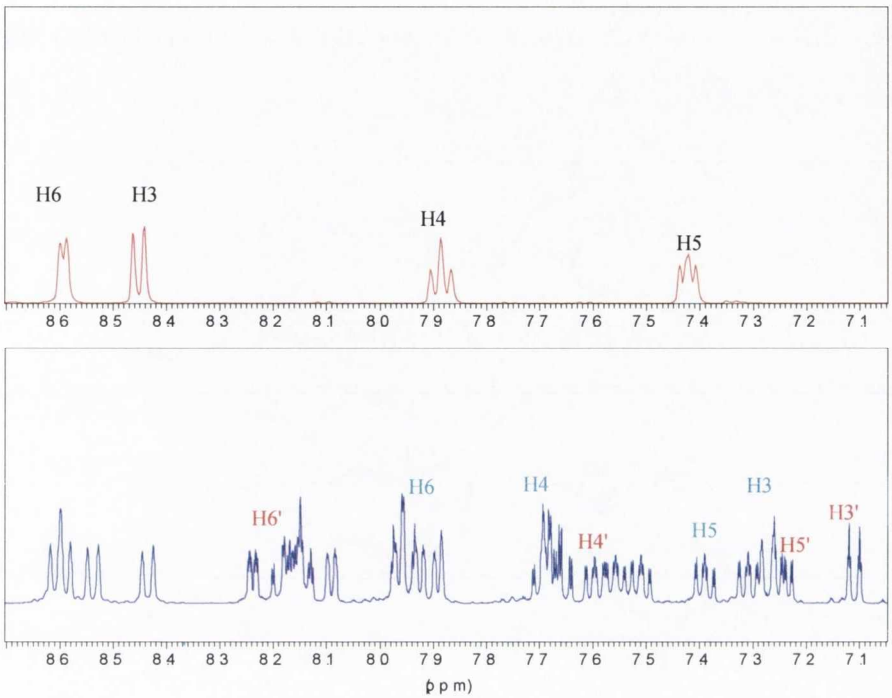


Figure 65: The aromatic regions of the ^{1}H-NMR spectra of 11 and 26 in CD_3CN (δ 7.1-8.7 ppm shown)

Compound	Chemical Shifts of 2-pyridyl Protons in CD_3CN in δ ppm			
	H6, H6'	H5, H5'	H4, H4'	H3, H3'
6	8.40	7.29	7.80	7.68
24	8.16, 7.96	7.21, 7.33	7.66, 7.56	7.06, 6.93
8	8.33	7.33	7.91	7.91
25	8.12, 7.98	7.24, 7.39	7.67, 7.66	7.39, 7.12
11	8.59	7.41	7.89	8.45
26	7.97, 8.24	7.40, 7.24	7.70, 7.64	7.28, 7.10

Table 8: The ^{1}H-NMR shift of the two 2-pyridyl ring systems in compounds 24, 25 and 26 and their respective ligands

2.2.1.4 X-Ray Crystallographic Determination of 22 and 23

Crystals of 22 were grown by slow evaporation of ether into an acetone solution of the complex. The asymmetric unit of **22** consists of Ru(II)(**3**)$(bpy)_2$ species along with two PF_6^- and an acetone molecule. The complex crystallized in a monoclinic space group, $P2_1/c$. The ligands are coordinated in an octahedral arrangement around the central metal as shown in Figure 66.

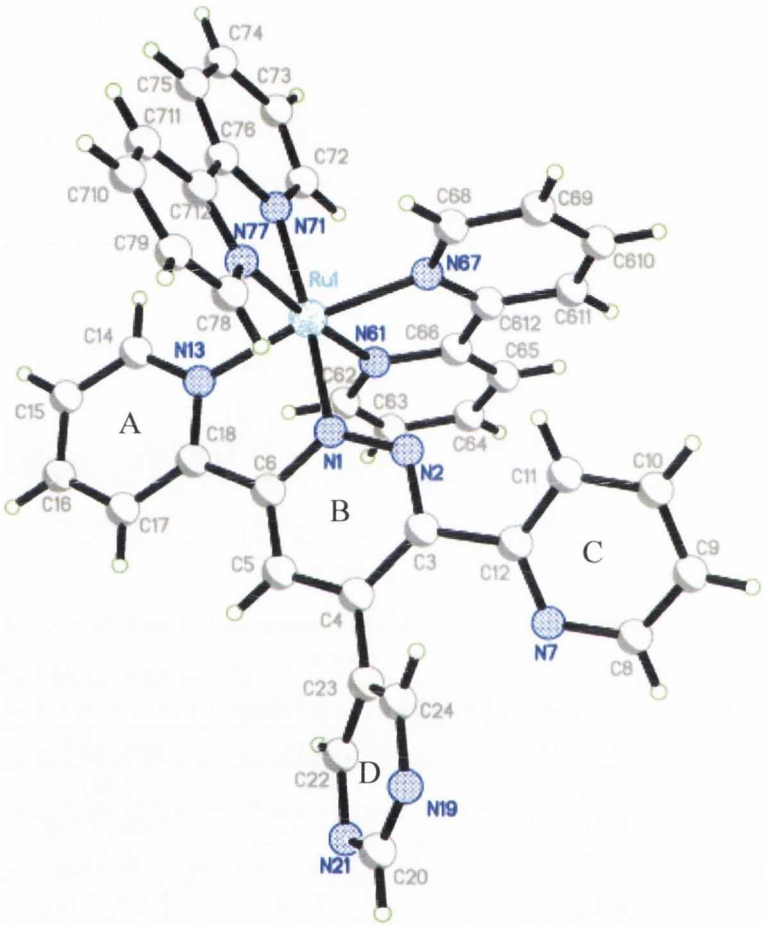


Figure 66: Perspective view of the crystal structure of 22

Rings C and D are tilted at angles of 33.45° and 48.61° respectively from the plane of the coordinated rings A and B. The Ru-N bond lengths vary between 2.014Å and 2.067Å.

In the crystal lattice, four molecules of **22** undergo self-assembly through the formation of C-H···N hydrogen bonds involving both the 2-pyridyl (H···N, 2.38 Å) and the pyrimidyl units (H···N, 2.56 Å). This leads to the formation of a host framework, with two acetone molecules and two $PF6^-$ anions occupying the void space. The pictorial representation of the resulting host assembly is given in Figure 67.

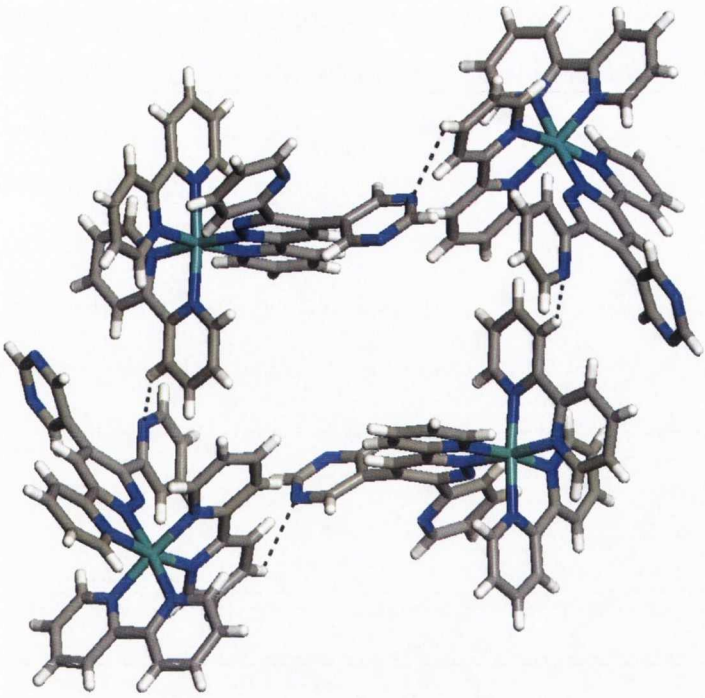


Figure 67: The host framework formed in the crystal lattice of 22 showing the C-H···N hydrogen bonds.

The guest species is held to the host-framework through C-H···O (H···O, 2.42, 2.45 Å) and several C-H···F (with H···F distance varying from 2.31 to 2.53 Å) interactions. Unlike in various porous assemblies generally observed, the void space is not extended further to form a channel. This host-guest complex is shown in Figure 68.

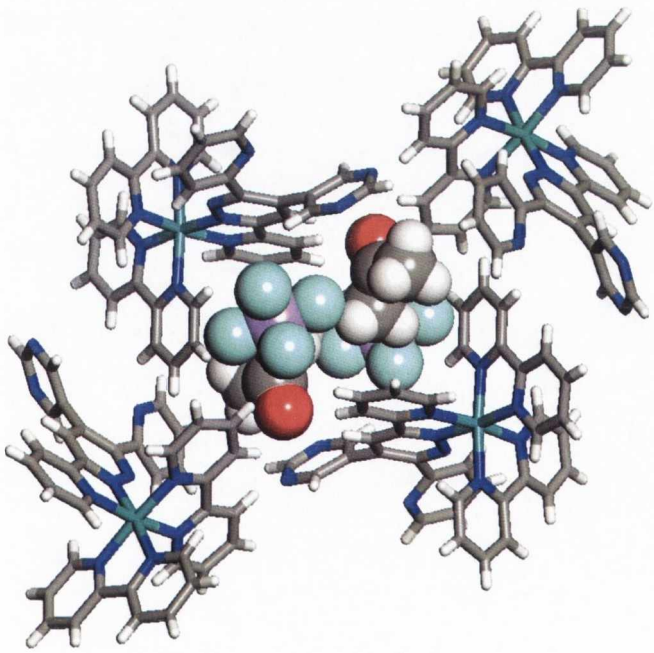


Figure 68: The host-guest complex of 22

Crystals of **23** were grown by slow evaporation of ether into an acetone solution of the complex. This mixture yielded an isostructural complex with that of **22**, crystallising in the same space group, $P2_1/c$. In the complex, the Ru(II) metal centre is bound by two bpy units and a **4** unit as shown in Figure 69. There is a small dihedral angle between rings A and B (2.26°). The dihedral angles between rings A and C, and A and D are 39.54° and 42.50° respectively. The Ru-N bond lengths measure between 2.013 Å and 2.073Å.

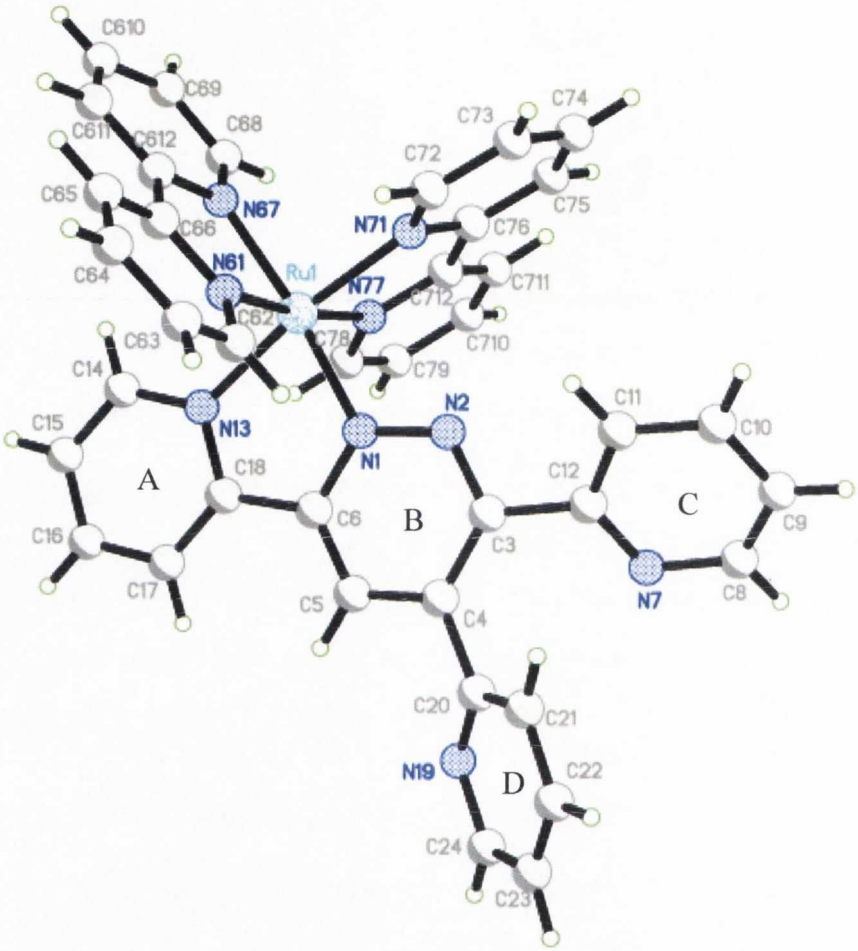


Figure 69: Perspective view of 23

In the crystal lattice, the complex undergoes self-assembly to form a host framework stabilized by C-H···N hydrogen bonds varying between 2.38Å to 3.69Å. This is shown in Figure 70.

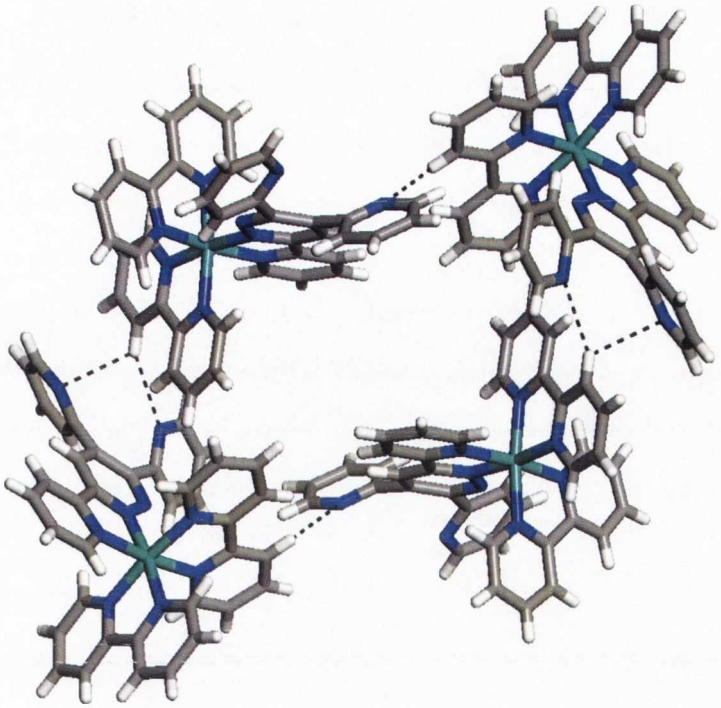


Figure 70: The host framework assembly formed in the crystal lattice of 23

The void space is occupied by two PF_6^- units and two acetone molecules as observed in **22**. The guest molecules are stabilized by several intermolecular interactions formed with the host-framework. This framework is shown in Figure 71.

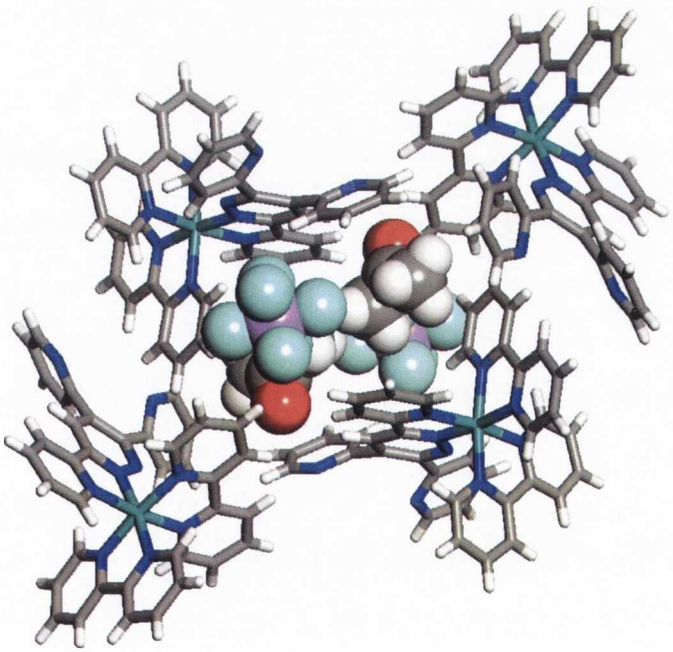


Figure 71: The host-guest complex observed in the crystal lattice of 23

2.2.1.5 UV-Vis and Fluorescent Spectroscopy of 22-26

The UV-Vis absorption spectra of **22** and **23** are show in Figure 72 along with that of Ru(II) *tris* bpy. The high energy regions of the spectra are very similar to the homoleptic *tris* bpy analogue. The absorption at λ 230 nm has been assigned to an MLCT spin allowed $\pi \rightarrow \pi^*$ transition for *tris* bpy and is most likely a transition to the excited state of the bpy ligand in **22** and **23**. The transition at λ 285 nm is also very similar for all three compounds with an extinction coefficient indicative of a spin allowed LC transition ($\varepsilon > 1000 M^{-1}cm^{-1}$). This is most likely a combined LC transition involving both the bpy and pyridazine ligands which is indicated by the increased width of the absorption in both spectra.

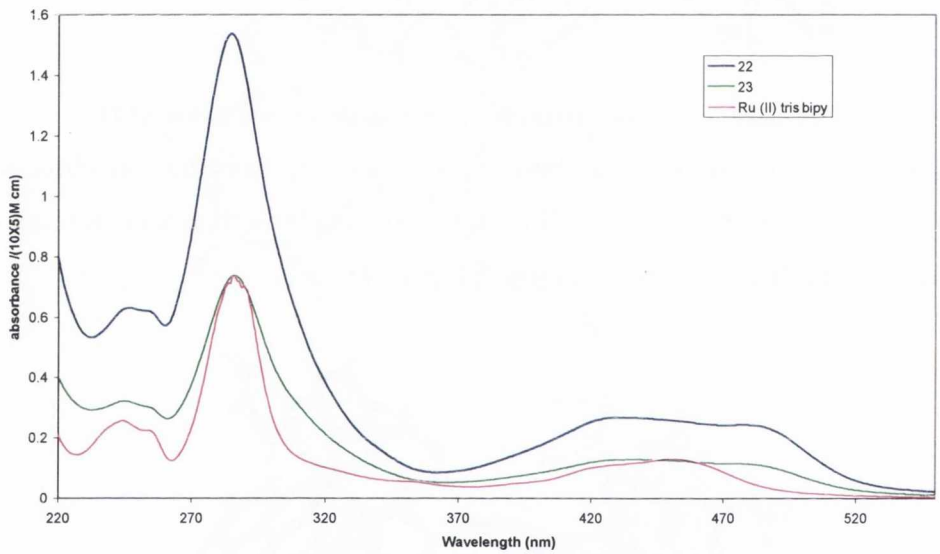


Figure 72: UV-Vis Absorption Spectra of 22, 23 and Ru tris bpy in CH_3CN

The most interesting feature of the UV-Vis spectra occurs in the visible region, where there are two distinct maxima for both complexes (Figure 73). The first occurs at λ 428 nm for **22** and λ 432 nm for **23**, whilst the second occurs at λ 480 nm for **22** and λ 478 nm for **23**. The second maxima are bathochromically shifted almost λ 30 nm from the *tris* bpy maximum. This is in agreement with much of the literature which indicates a lower energy maximum for ruthenium complexes containing other diazines. In this case it is clear that the pyridazine has led to this λ 30 nm shift, and that these transitions can be assigned as $d\pi \rightarrow \pi^*$ transitions located primarily on the pyridazine ring.

The maxima at λ 428 and λ 432 nm and the broad area of high absorbance between the two maxima is most likely due to the $d\pi \rightarrow \pi^*$ transition of the bpy ligand and the possible

SLUMO $\pi_2 \rightarrow \pi^*$ transition of the pyridazyl ligand.[17] This agrees with the assertion that the LUMO/SLUMO gap is so small for pyridazyl complexes that this transition appears in the UV-Vis spectra merely as a shoulder. The effect of the various substituents on the pyridazine ring of the ligands is hard to determine precisely but they appear to have very little effect on the energy of the absorption maxima. This can be deduced from the similarity between the low energy spin allowed MLCT of **22** compared with **23** in the visible region.

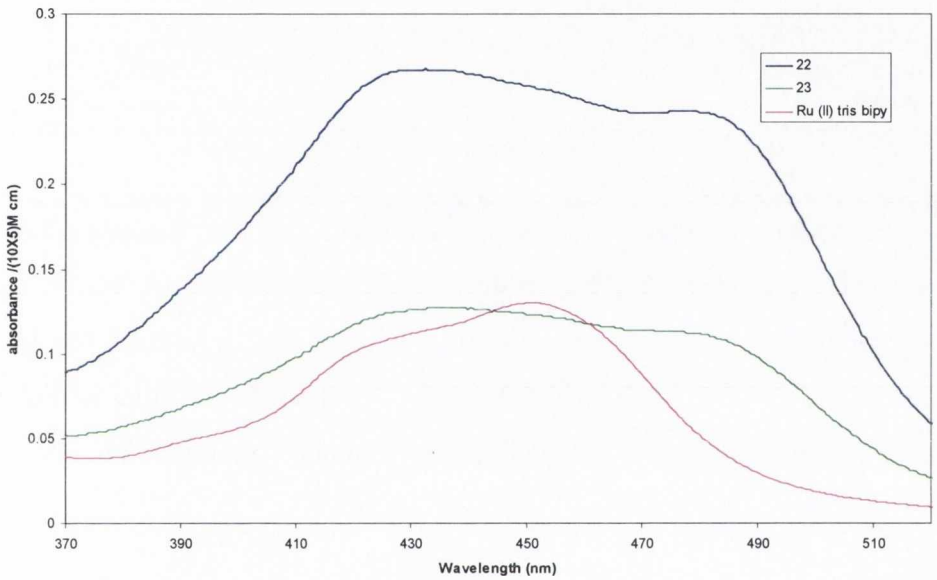


Figure 73: The MLCT Region of the UV-Vis Spectra of 22, 23 and $[Ru(bpy)_3]^{2+}$ in MeCN

The luminescence emission spectra of **22** and **23** are shown in Figure 74. The measurements were carried out using a $1cm^3$ glass cuvette at concentrations of 2×10^{-5} M. As expected the emission is bathochromically shifted relative to $[Ru(bpy)_3]^{2+}$. Both compounds are only weakly luminescent, hence the low signal to noise ratio. **22** has a slightly lower energy maximum (λ 698 nm) than that of **23** (λ 692 nm). Excitation of both the shoulder at λ 427/426 nm and the peak at λ 470/483 nm in the absorbance spectra results in the same emission.

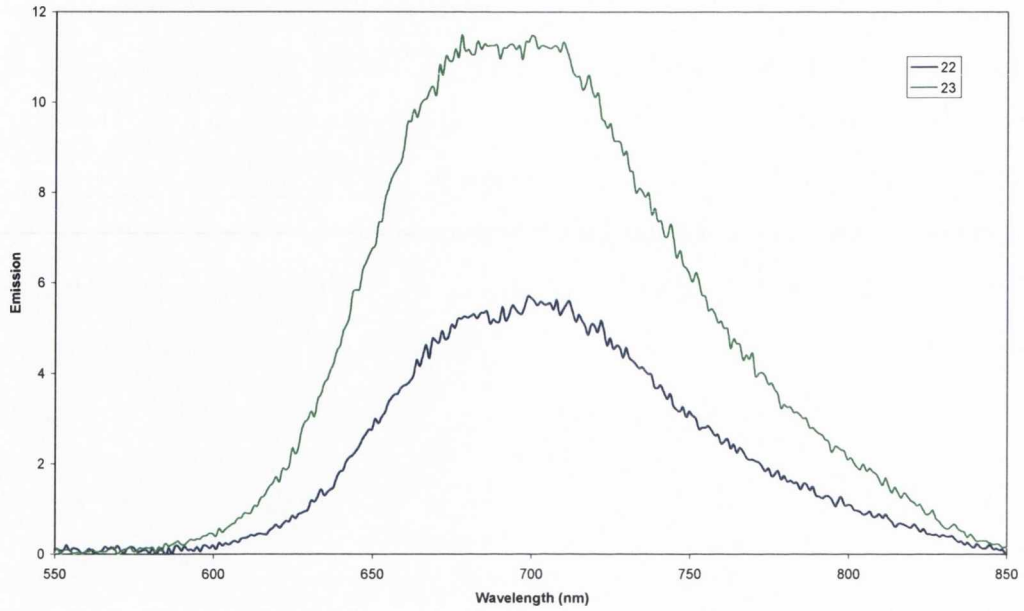


Figure 74: The normalised luminescence Emission spectra of 22 and 23 in MeCN excited at λ 464 nm.

The tetrasubstituted pyridazine *bis* bpy ruthenium complexes shown below exhibit similar transitions to that of Ru(II) *tris* bpy. The high energy region of the UV-Vis spectra for both **24** and **25** indicates a spin allowed $d\pi \rightarrow \pi^*$ transition similar to that of the *tris* bpy complex with a maximum at λ 240 nm and a shoulder at around λ 252 nm.

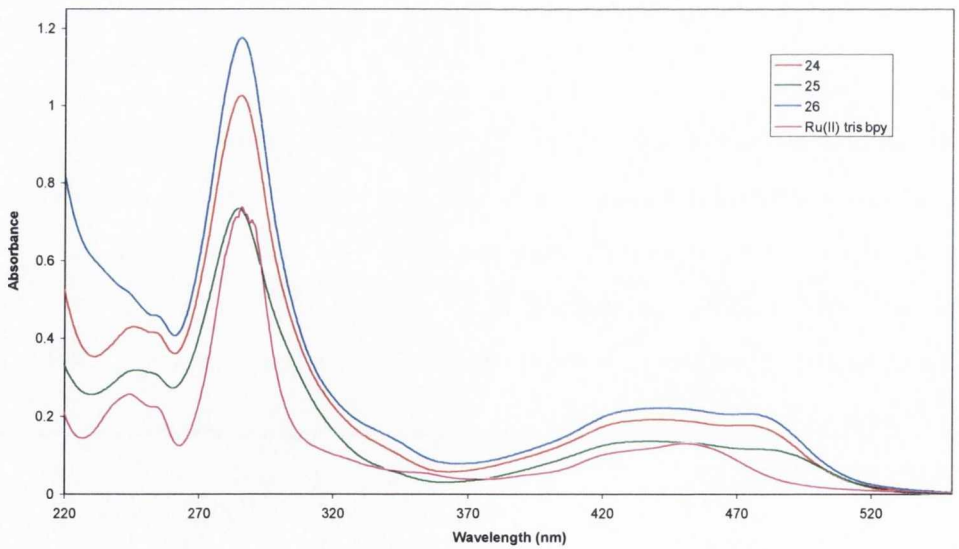


Figure 75: The UV-Vis Absorption Spectra of 24, 25 and 26 in MeCN

This maximum at λ 240 nm appears only as a shoulder in the spectrum of **26**. This may be brought about by the presence of the methoxy groups on the phenyl substituents, which have the effect of raising the energy of the π^* orbital for this ligand. The shoulder

at λ 240 nm may be caused by an electron occupying this orbital on the pyridazyl ligand and subsequently "hopping" to the π* orbital on the bpy ligand, hence the appearance of a second shoulder at λ 254 nm.

The spin allowed LC transition is similar for all three compounds and absorbs at the same maximum as that of the *tris* bpy complex. This peak is quite broad, which may indicate the overlap of a LC transition for the pyridazyl ligands as well as that of a bpy.

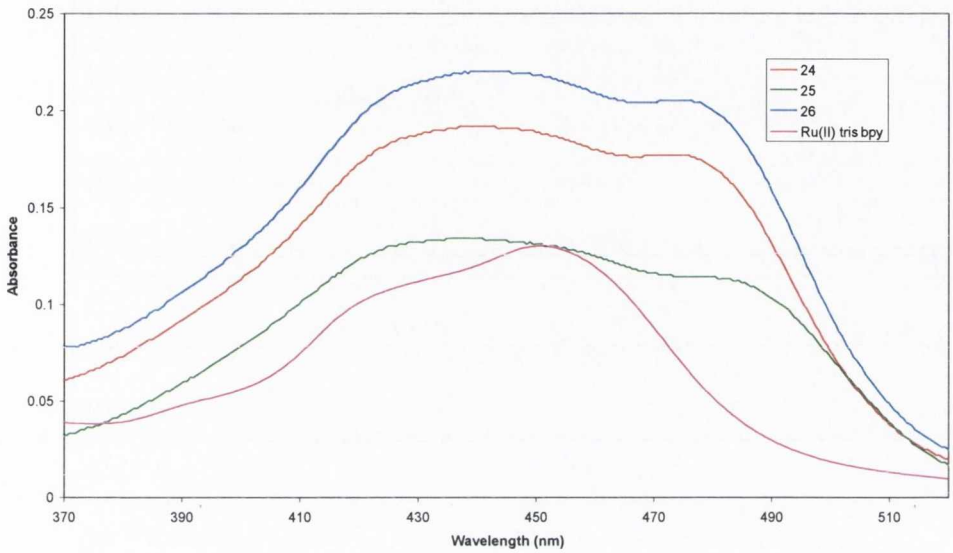


Figure 76: The Low Energy Region of the UV-Vis Spectra of 24, 25 and 26 in MeCN

The visible region of the spectra is shown in Figure 76 and displays similar bands to the absorbance spectra of **22** and **23**. The broad area which occurs between λ 428 nm and λ 470 nm for the three complexes is most likely as a result of the spin-allowed MLCT π→π* transitions of the bpy ligand as well as the HOMO→SLUMO of the pyridazyl ligands. This would account for the broader plateau-like maxima which is not present for the *tris* bpy complex. The most significant difference between the three heteroleptic complexes and the *tris* bpy complex is the distinctive bathochromic shift which results from the lower π* level of the pyridazine ligands (λ 10 nm for **24** and **26**, λ 20 nm for **25**). The shift may be greater for **25** due to the effect of the nitrogen atoms on the ligand substituents.

Nonetheless, the absorption spectra of the five heteroleptic complexes here have shown a significant bathochromic shift in the visible region in comparison with Ru(II) *tris* bpy, and this is thought to be brought about primarily by the lower energy π* orbital of the pyridazyl ring, with the substituents contributing to a much lesser extent.

Complexes	Wavelength *nm* (absorbance $M^{-1}cm^{-1}$)		
	MLCT $d\pi \rightarrow \pi^*$	LC $\pi \rightarrow \pi^*$	MLCT $d\pi \rightarrow \pi$
Ru *tris* bpy	250 (25000) 238(30000)	285 (87000)	451 (14000) 428 (13000)
22	246 (62900) 255 (61200)	286 (15000)	427 (26600) 470 (24200)
23	244 (31500) 255 (30300)	286 (72400)	426 (13100) 483 (11300)
24	246 (43000) 256 (40400)	286 (102100)	437 (19100) 477 (17500)
25	245 (31700) 254 (30500)	286 (72400)	426 (13100) 485 (11100)
26	- 256 (44600)	287 (11600)	435 (21800) 465 (20400)

Table 9: The absorbance maxima of 22, 23, 24, 25, 26 and Ru(II) tris bpy

The emission spectra of **24**, **25** and **26** are shown below in Figure 77. Once again these measurements were carried out using a $1cm^3$glass cuvette at a concentration of 2 X 10^{-5}M. The spectra of **24** and **26** differ only slightly in intensity and have an almost identical emission maximum at around λ 670 nm. The emission of **25** is of slightly lower energy with an emission maximum at λ 707 nm. This is in good agreement with the absorption spectra where the low energy maximum of **25** was shifted bathochromicaly by 10 nm. The excitation of both low energy peaks of these complexes resulted in the same emission maximum on each complex, which is in agreement with the literature contention that the lowest π* orbital is responsible for the fluorescent emission. [13, 24, 25] The intensity of the absorption maxima of **25** is lower than that of **24** and **26** which may be due to increased non-radiative decay of the excited state, although why this should occur to a greater degree in this compound is unclear.

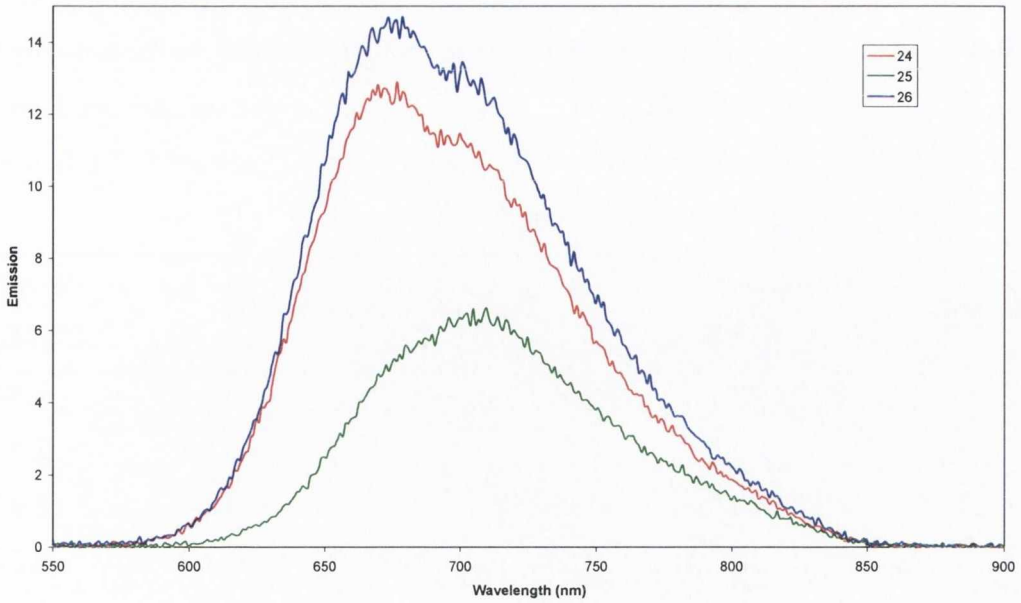


Figure 77: The normalised emission spectra of 24, 25 and 26 in MeCN excited at λ 464 nm

2.2.1.6 Electrochemistry of 22-26

The ruthenium *bis*-bpy complexes **22** and **23** were analysed via cyclic voltammetry in order to investigate the redox potentials of these complexes and the reversibility of both the ruthenium oxidation process and the ligand reductions. Voltammetry experiments were also carried out on the free ligands for comparative purposes. The voltammongrams were run on 1mM solutions of the complexes in acetonitrile using 0.1 M *tert*-butyl ammonium hexafluorophosphate as the supporting electrolyte. A Pt wire counter electrode and a AgCl reference electrode were used, but results are quoted with respect to a Standard Calomel Electrode (SCE) which appears to be the most common reference in the literature. The experiments were carried out with a scan rate of between 0.1 and 0.4 V/s.

The ligand reductions of the five complexes were found to be largely reversible, as were the reductions of the free ligands. They also had lower reduction potentials on ruthenium complexation. This is to be expected as the loss of negative charge on the ligand due to σ-bonding with the metal upon coordination, and the overall positive charge of the metal complex, renders the ligands more electron-accepting.[63] In accordance with similar work in the literature the first ligand reduction peak of the heteroleptic complexes was assigned to the pyridazine-centred ligand, as their lower π* orbitals ensure that they are easier to reduce.[6] From the literature the second and third reduction peaks are generally assigned

to the two bipyridine ligands although there are some cases, particularly involving pyrimidyl ligands, where the second reduction is thought to occur on the non-bpy ligand preferentially.[20] The values obtained in this work for the second and third reduction potentials compare very favourably with literature values obtained for heteroleptic ruthenium complexes and were assigned to the bpy ligands.

Complex	Oxidation *vs* SCE (V)	Reduction *vs* SCE (V)			$\Delta E_{1/2}$ (V) (E_{ox}-E_{red})
22	+1.48	-0.92	-1.39	-1.64	2.40
23	+1.34	-0.98	-1.43	-1.64	2.32
24	+1.39	-1.04	-1.42	-1.66	2.43
25	+1.36	-0.91	-1.46	-1.67	2.27
26	+1.43	-1.07	-1.42	-1.67	2.51

Note: A second less significant oxidation was obtained in the case of **22** at +1.20 V which was irreversible. This was also apparent on the oxidation sweep of the ligand.

Table 10: Electrochemistry results for compounds 22-26 in CH_3CN

The oxidation potential values for **22** to **26** are shown in Table 10. Clearly the pyridazine centre in these complexes has a large effect on the oxidation potential, as its lower pK_a and consequent lower σ-bonding strength result in a higher oxidation potential than for $[Ru(bpy)_3]^{2+}$ which occurs at +1.29 V. However the oxidation potentials follow the series **22** > **26** > **24** > **25** > **23**. It may appear surprising that the heteroleptic complex with electron-donating methoxy substituents, **26**, has a higher oxidation potential than that of **23** and **25**, which both contain electron-withdrawing groups in the form of pyridyl substituents. However, as discussed in Chapter 1, the electron-donating effect of the methoxy groups at the *meta* position is most prominent at the neighbouring carbons, not at the point of substitution with the pyridazine ring. Therefore, it may be that electron donation has no influence over the energy of the metal HOMO and hence the oxidation potential is not as low for **26** as might be anticipated. Nonetheless, it is still significantly higher than for complexes **23** and **25** which contain electron-withdrawing pyridyl substituents. As an example, the cyclic voltamogramm of **23** is shown in Figure 78.

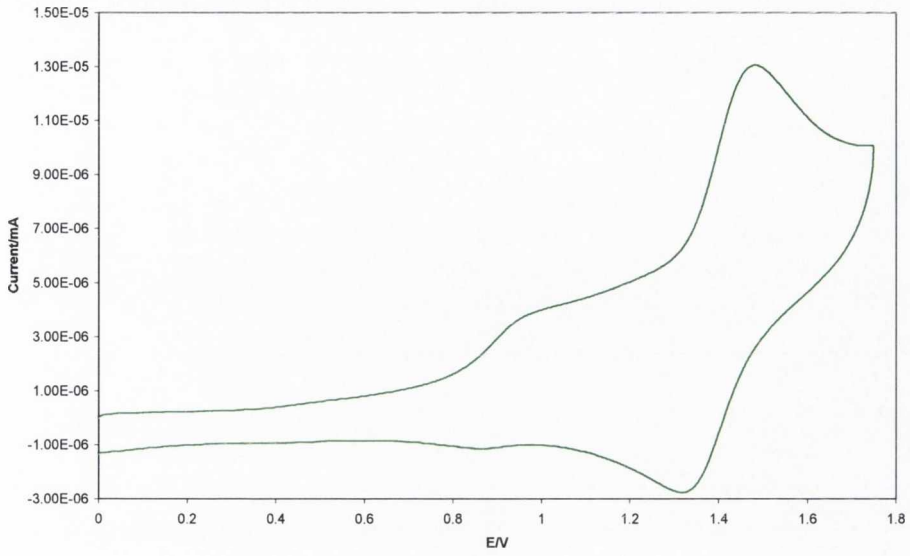


Figure 78: Cyclic voltammogram of 23 showing the Ru(II/III) redox peak (1 mmol in MeCN *vs.* SCE)

A small additional irreversible oxidation peak was often encountered between 1 and +1.5 volts in the oxidation sweep of some of the compounds. However oxidation sweeps on the free ligands showed similar oxidative phenomenon. This may be due to the presence of the pyridyl and pyrimidyl substituents on the ligands and a possible oxidation process occurring on the heteroatoms. This feature can be seen very clearly in the cyclic voltamogramm of **26** which is shown in Figure 79.

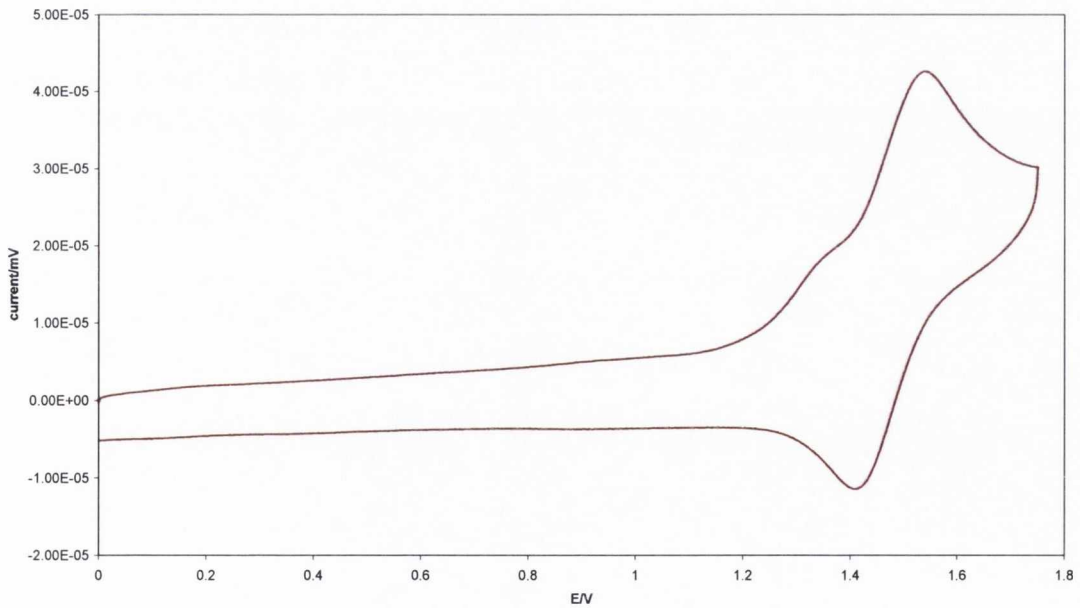


Figure 79: The Cyclic voltamogram of 26 showing the Ru(II/III) redox peak (1 mmol in MeCN *vs.* SCE)

The reduction potentials of all the above complexes were generally reversible although some were only quasi-reversible. The reduction potential of **23** is shown in Figure 80.

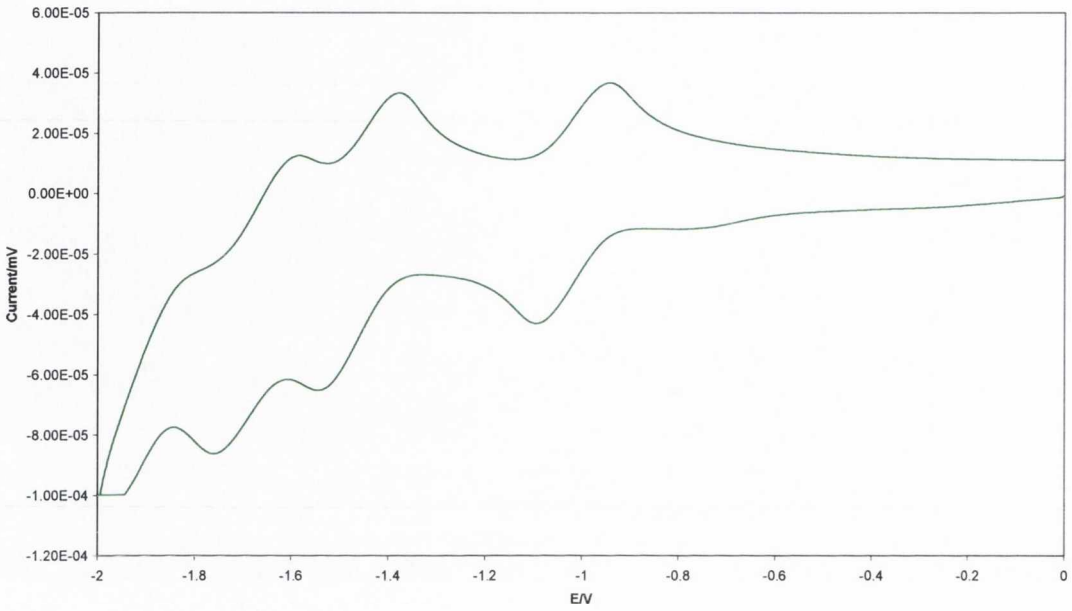


Figure 80: The Cyclic voltamagram of 23 showing the ligand-based reduction peaks (1 mmol in MeCN *vs.* SCE)

As discussed above, these reduction processes are believed to occur on the π^* orbital of the ligand, therefore the electron-donating or withdrawing effects of substituents appear to be more influential on the reduction potential values. For example, the electron-donating effects of the methoxy groups in **26** give rise to a more negative reduction potentials for this complex compared to the others. Equally, the electron-withdrawing pyridyl and pyrimidyl groups on complexes **22**, **23** and **25** ensure that these complexes are easier to reduce than **24** (Figure 81).

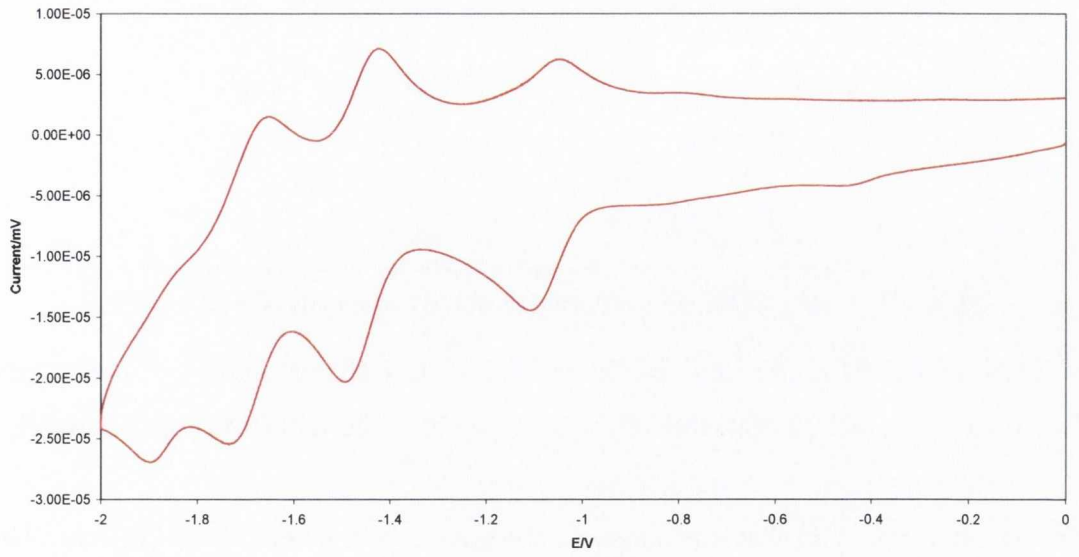


Figure 81: Cyclic voltammogram of 24 showing the ligand-based reduction peaks (1 mmol in MeCN *vs.* SCE)

The magnitude of the second and third reduction potentials for these heteroleptic compounds is consistent with literature values of bpy reductions. The second reductions occur between around -1.40 and -1.45 V which is similar to those obtained for other heteroleptic complexes.[21, 64] The third reduction falls within the range -1.73 to -1.77 V and is also consistent with further reduction of the bpy ligands on similar compounds in the literature.[15, 21]

The final column in Table 10 shows the $\Delta E_{1/2}$ values for the five complexes which is calculated by subtracting the first reduction potential of the complex from the oxidation potential, as discussed in the introduction. These values should give an indication of the HOMO-LUMO energy of the complexes, and correlate with the MLCT in the visible region of the UV-Vis and fluorescence spectra. Indeed, complex **26**, which had the highest energy absorption of all the complexes in the visible region (λ 465 nm) also has the largest $\Delta E_{1/2}$ (2.51 V). Similarly, the complex with the lowest energy absorption in the visible region, **25** (λ 485 nm), has the smallest $\Delta E_{1/2}$ value (2.27V).

Table 11 compares the reduction potential of the five ligands **3-11** used in the preparation of the Ru(II) bis bpy complexes **22-26**.

Compound	Reduction Potential vs SCE (V)
3	-1.63
4	-1.58
6	-1.50
8	-1.56
11	-1.39

Table 11: Reduction Potentials of the five ligands *vs.* SCE

The presence of the large metal and the overall positive charge on the complexes ensures a much easier reduction than that of the free ligands. The reductions of the free ligands are generally about 0.6 V lower than that of their complexes.

Surprisingly, ligand **11** has the most positive reduction potential of the five. This is somewhat counterintuitive given that the presence of electron-donating methoxy groups might be expected to make this compound harder to reduce. However this unusually low negative value may be explained by the fact that the electron-donating substituents and the electron-withdrawing substituents occupy opposite sides of the compound ensuring that the π^* orbital is easier to occupy.

2.2.2 Synthesis of Ruthenium (II) Tris Complexes of 27, 28 and 29

2.2.2.1 Synthetic Procedure

The success of the synthetic preparation of the ruthenium *bis* bpy complexes led to a desire to prepare other coordination compounds such as homoleptic ruthenium *tris* complexes. Although the synthesis of these *tris* complexes was relatively straightforward, the presence of isomers in the product mix would give rise to significant challenges in terms of separation. Early investigations regarding the separation of iron (II) *tris* complexes of **3** and **4** led to the realisation that multiple products were being obtained. This was most likely the result of the presence of multiple binding sites (see Figure 82). In particular, the likelihood of successful isolation of any symmetrical isomers would be significantly reduced. Without the benefit of a crystal structure the characterization of unsymmetrical isomers of this type is almost impossible due to the sheer quantity of peaks in the aromatic region of the proton NMR. As a result, ligands **3** and **4** were omitted from this synthetic project, and no *tris* isomers of this type were isolated or characterised.

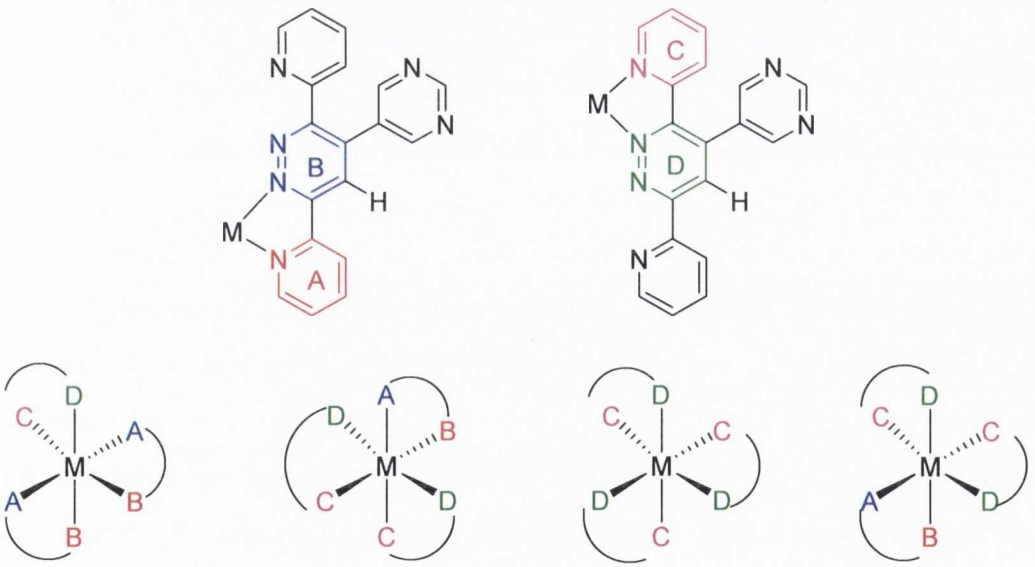


Figure 82: Schematic showing some of the isomers which would result from the synthesis of metal *tris* complexes using compound 3 as the coordinating ligand.

In contrast, despite the presence of two coordination sites in compounds **6**, **8** and **11**, their inherent symmetry results in coordination on either site resulting in the same geometric configurations. In this way, there are only two possible variations; the unsymmetrical meridional isomer or the symmetrical facial isomer. Figure 83 below attempts to emphasise this point.

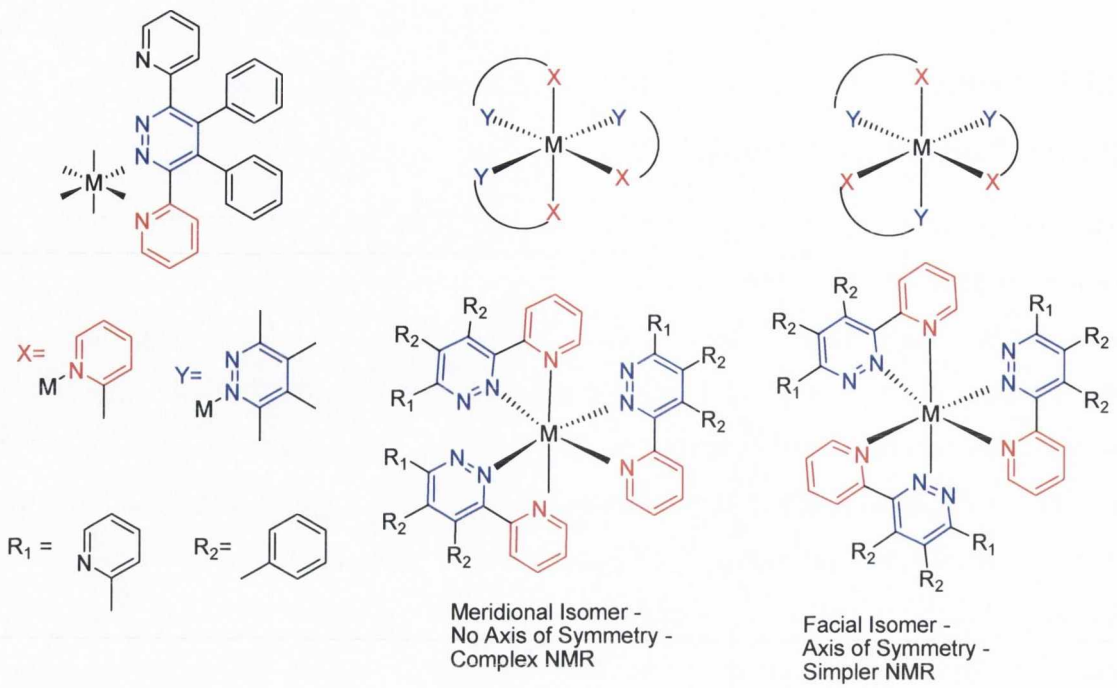
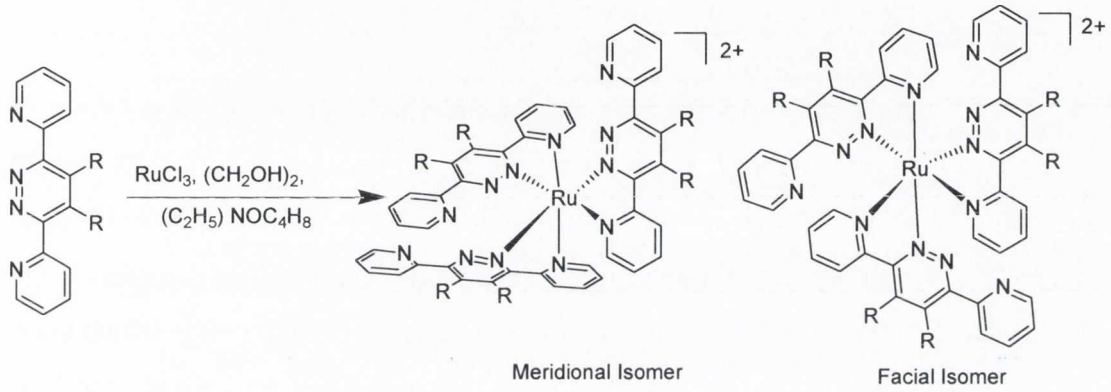


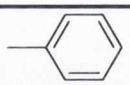
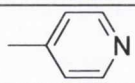
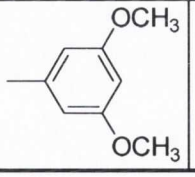
Figure 83: Schematic showing the symmetry present in the meridional and facial isomers

The synthesis was carried out by refluxing the relevant ligand and ruthenium tri chloride hexahydrate in ethylene glycol with a small quantity of n-ethyl morpholine as a reducing agent. The reaction turned from a dark purple colour to a dark orange and was monitored by TLC. In all cases the reaction was left for 72 hours to ensure maximum yield. A small quantity of water was added to the reaction after the vessel had cooled, and the excess ligand was then removed by washing with dichloromethane. Saturated KPF_6 was added to the remaining mixture to precipitate the metal complex. This was separated from the aqueous layer by washing in dichloromethane. Separation of the isomers proved to be quite difficult given the extreme sensitivity of the process to even the slightest change in the solvent mixture. In addition to separating the two isomers from each other it was also necessary to separate them from the excess metal salt. Unfortunately both isomers and the excess metal salt had a tendency to streak on the column and move very close together. This made any large scale synthesis of these complexes very difficult, as they would need to be further purified on thick silica plates which have a maximum loading capacity of < 50 mg. Thus when these reactions were carried out using quantities in excess of this, the reaction mixture was initially purified using a long column.

This however led only to a greater number of impure fractions, which were either re-columned or directly applied to thick silica plates. In either case, each successive column or plate resulted in a significant loss of yield partially brought about by the streaking of the products.

The choice of mobile phase for these reactions was a difficult one and involved a delicate balance of separating the isomers from each other adequately, separating them from other minor undesirable products (ethylene glycol itself forms purple ruthenium complexes) and from the unreacted metal salt as well as minimising any streaking. A solvent mixture which achieved all this proved difficult to find. Instead, a plate was run which moved the *fac* isomer more slowly than the *mer* isomer and other products. In this way the *fac* isomer could be separated and the residue reloaded onto another plate and run using a different solvent mix to isolate the pure *mer* isomer. In general a more polar mix was needed for the second plate, e.g. replacing the water with ammonia. Scheme 34 summarises the preparation of complexes **27**, **28** and **29**.



Ligand	R	*Tris* Ru (II) Complex
6		27
8		28
11		29

Scheme 34: Synthesis of 27, 28 and 29

In the case of **27** a mixture of acetone, water and saturated KNO_3 was used to separate the facial isomer (R_f = 0.35) on a thick silica plate. The residue was then reloaded onto a second silica plate and a mixture of acetonitrile, ammonia and saturated KNO_3 allowed for the isolation of the meridional isomer (R_f = 0.15).

In the isolation of *fac* and *mer* isomers of **28**, the more electron-rich ligand resulted in the complexes moving more slowly on the plate and as a result a higher percentage of water and ammonia was used for both plates. In the case of **29** the methoxy functional groups

ensured that both isomers moved quite rapidly, so a larger amount of water and ammonia was not needed. Furthermore, in this case the separation of the facial isomer was significantly better than the other complexes (R_f = 0.34) – with the result that a column could be used. The yield of this complex was still very poor. The meridional isomer required separation using a thick layer silica plate. Characterisation was carried out by proton NMR spectroscopy and mass spectrometry.

Table 12 compares the percentage yields obtained for each isomer of complexes **27**, **28** and **29**.

Compound	% Yield of *Mer* Isomer	% Yield of *Fac* Isomer
27	29	12
28	14	10
29	5	3

Table 12: Yields obtained of each isomer for compounds 27, 28 and 29

The yields of both isomers of **27** are substantially higher than those of **28** and **29**. In particular the meridional isomer was obtained in a relatively good yield. This is due to the fact that this isomer streaked far less on the silica plate than the other complexes. This in turn ensured a higher density of the complex in a thin band on the plate which could be readily isolated and removed from the silica. Nonetheless the overall streaking of products and loading and re-loading onto plates resulted in poor yields.

2.2.2.2 Characterisation of Compounds 27, 28 and 29 by Mass Spectrometry and NMR Spectroscopy

Both isomers of each compound were characterised by mass spectrometry and ^{1}H-NMR and ^{13}C-NMR spectroscopy. The peaks at m/z 630.18 in the electrospray mass spectra of both isomers of **27** were assigned to the $[M\text{-}2PF_6]^{2+}$.

In the case of all three ruthenium (II) *tris* complexes, the meridional isomer moved quicker on the column and plates, however as discussed above, it was usually easier to isolate the facial isomer from the first plate before purifying the meridional isomer.

Complex **27** *mer*: The ^{1}H-NMR spectrum of the meridional isomer of **27** shown in Figure 84 demonstrates the complexity associated with the spectra of these complexes. In the case of **27** the spectrum should integrate for fifty-four individual signals in the proton NMR spectrum; many of these signals are broad at room temperature. In the case of **27** most of the ^{1}H signals appear in the multiplet between δ 7.0 and 7.8 ppm. This large mass

of signals accounts for all the phenyl protons on the back of the pyridazine as well as all of the H^4 and H^5 protons associated with the pyridyl rings. The signals shifted downfield of this can be identified by their coupling constants as the H^6 protons, nearest the nitrogen on the pyridyl rings. The peaks upfield of the large multiplet have been identified as the H^3 protons on the pyridine ring, as these typically possess a coupling constant of around seven or eight hertz.

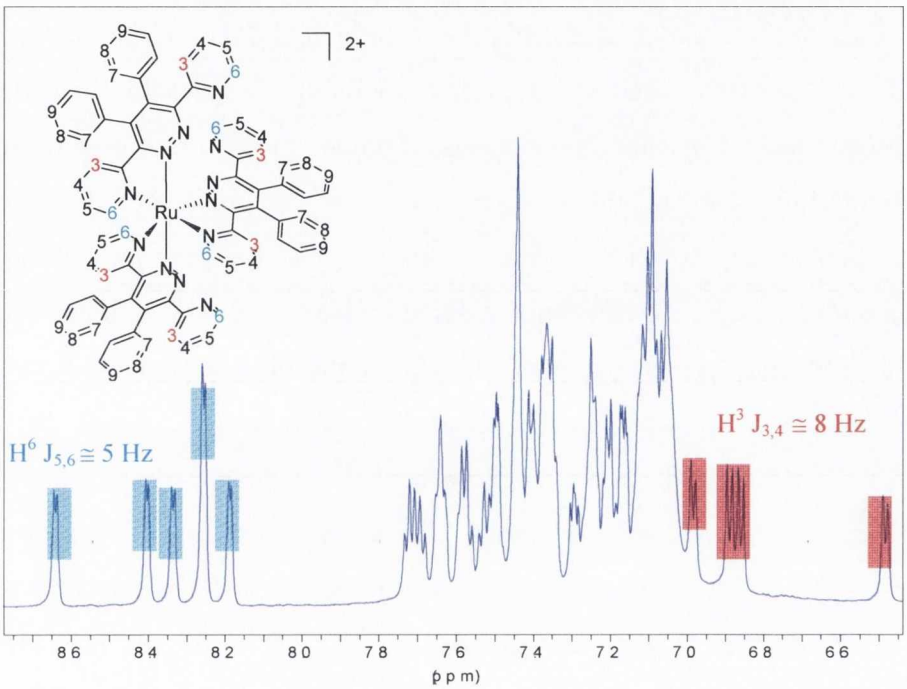


Figure 84: The ^{1}H-NMR spectrum of the *mer* isomer of 27 in CD_3CN (δ 6.5-8.7 ppm shown)

Although the ^{13}C-NMR spectrum of this compound was obtained, it was impossible to identify most of the peaks. There were up to seventy-eight signals observed in the aromatic region.

The ^{1}H-NMR spectra of the facial isomers of **27**, **28**, and **29** were less complicated due to their C_3 symmetry. This ensured that although the symmetry of the individual ligand was broken due to coordination at one position, each proton had an identical shift to the same protons on the other two ligands. Thus rather than six individual phenyl and six pyridyl systems in the spectrum as was the case for the meridional isomer, there are now only two sets of phenyl and two sets of pyridyl signals present.

Complex **27** *fac*: A ^{1}H-^{1}H COSY experiment was used to assign each peak in the spectrum of the *fac* isomer of **27** relative to its neighbours and is shown in Figure 85. There are clearly two separate pyridyl ring systems in this spectrum. In a similar situation to the ruthenium *bis* bpy complexes discussed above, the H^3 protons were shielded by the ring current effect of the neighbouring phenyl rings. It was expected that the $H^{3'}$ of ring A (the coordinated ring) would experience this effect to the greatest extent, as it has the least freedom to rotate. Therefore the most shielded signal was assigned to this position. From this, all eight pyridyl signals could be identified. The remaining two phenyl ring systems exhibited two unexpected features which were unusual for these metal complexes. It would perhaps have been expected that these spectra would resemble the free ligand, but that the loss of symmetry of the two phenyls would result in double the number of signals. However, it is clear from the ^{1}H-NMR spectrum that there are a number of other factors which result in the unusual splitting and broadness associated with these signals. These are related to a "slow exchange" phenomenon which is believed to be occurring on both phenyl rings.

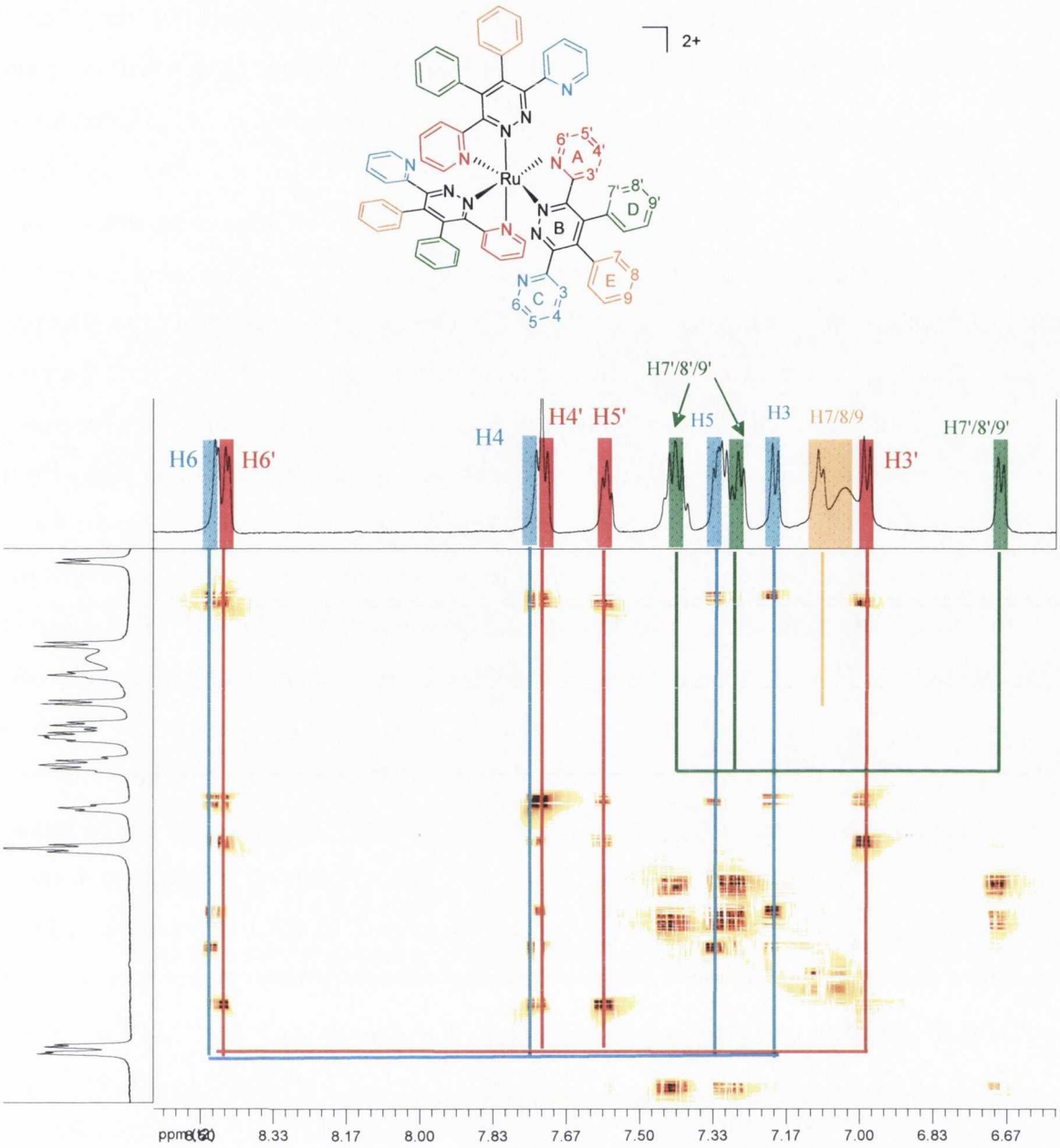


Figure 85: ^{1}H-^{1}H COSY showing the two pyridyl and two phenyl systems of the *fac* isomer of 27

2.2.2.3 Chemical Exchange in NMR

Chemical exchanges which occur in NMR spectra can be divided into two different timeframes; fast and slow.[65] If, for example which possibly occurs in the case of **6** and **8**, the rings are rotating at a rate faster than the Larmor frequency of the protons, then the protons are flipping between two magnetic environments at such speed that the frequency of neither state can be accurately measured, and the result is an average of the two frequencies. Therefore, if for example one *ortho* proton is resonating at 400 MHz, and the other at 401 MHz, but they are flipping between the two states too fast for either

frequency to be accurately represented in the free induction decay (FID), the NMR will see a resonance at 400.5 MHz and the Fourier Transformation of this will be a single peak which will be an average of the two positions. This situation is complicated however if the rings are hindered in some way and the "flipping" occurs at a rate slower than the NMR resonance timescale. In this case, if we assume the same frequencies for the protons, the spectrometer will measure a resonance of 400 MHz for a certain period of time, followed by a resonance at 401 MHz for another certain period of time. The proton will then flip back to its original position and resonate again at 400 MHz and the process repeats itself again. The Fourier Transform of this process will result in two separate and distinct peaks for each proton. Thus two very closely spaced but individual peaks for each *ortho* proton will be seen in the spectrum. This scenario is complicated by the fact that this process is occurring to several molecules at the same time at different stages of the ring flip. Thus, some rings will be flipping from the 400 to the 401 MHz position as another ring is still resonating at 400 MHz. In fact, there will be a multitude of resonances at various positions in the process. This will result in destructive interference and when the various waves are combined in the FID it will decay quicker. This in turn will lead to a broad signal in the Fourier Transform. If the ring flip rate can be increased to the point where the process becomes a fast-chemical exchange phenomenon then the broadness will be eliminated and one average signal will be obtained as discussed above. This can be done by increasing the temperature. The temperature at which this transition from slow to fast process occurs is known as the coalescence temperature, T_c. Thus, as this temperature is approached the broadness in the NMR spectrum begins to disappear and the peaks sharpen, as the ring flip becomes too fast for the timescale of the spectrometer. However, below T_c, an increase in the flip rate has the opposite effect of broadening the signals. This is because if the ring is flipping more often from one frequency to the other, then there is an increase in destructive interference between the waves and the FID will decay at a faster rate.

2.2.2.4 Application to the Characterisation of the facial Isomer of 27

In the ^{1}H-NMR spectrum of the facial isomer of **27** there are two separate sets of signals for the two phenyl rings on the ligand as expected. However these two rings appear to be in quite different chemical environments and their resulting peaks are quite different. The ^{1}H-^{1}H COSY spectrum which is shown in Figure 85 was used to assign each phenyl peak to its neighbours on the ring. It was found that one of the phenyl rings exhibits three sharp peaks at δ 7.42, 7.35 and 6.68 ppm. The peaks associated with the other ring are much broader and there appears to be a sharp signal at δ 7.10 ppm, followed by a much broader signal at δ 7.05 ppm and an extremely broad signal at δ 6.0 ppm. Given that the NMR spectra were run at room temperature and the inherent broadness of some of the peaks, it seems a fair assumption that this broadness and unusual splitting pattern is due to a slow chemical exchange phenomenon. It is therefore more likely that the ring assigned to the broader sets of signals is that ring which is flipping faster, as this would lead to increased destructive interference in the FID. The ring which is flipping at a slower rate would incur less destructive interference in the FID and the signals would appear sharper as a result. Looking at the structure of **27**, it would appear that the presence of the metal on one side of the ligand is most likely the largest single obstacle to the free rotation of these rings. Furthermore, it seems likely that the phenyl ring adjacent to the coordinated pyridyl ring, labelled as ring D below, is the more hindered of the two rings and consequently rotates at a slower rate. It was therefore assumed that this was the ring with the three sets of sharper peaks and is coloured green in the spectrum. The other phenyl ring (ring E) is not adjacent to a rigid ring, and its neighbouring pyridyl ring is reasonably free to rotate, so it is most likely rotating at a faster rate than ring D. This faster rotation means that there is an increase in the amount of destructive interference incurred in the FID and hence a faster deterioration of the signal. This will lead to broader signals in the final spectrum. The fully assigned ^{1}H-NMR spectrum is shown in Figure 86.

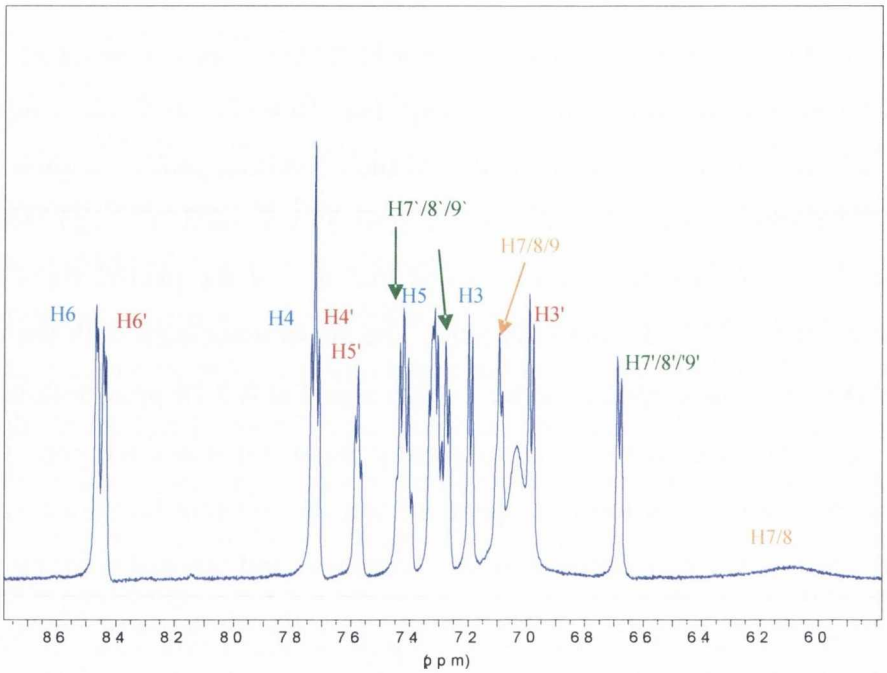


Figure 86: ^{1}H-NMR spectrum of the *fac* isomer of 27 in CD_3CN (δ 5.9-8.7 ppm shown)

In order to investigate the coalescence temperature of these compounds, the ^{1}H-NMR spectrum was run at 60°C (blue) and compared to the room temperature spectrum (green, Figure 87).

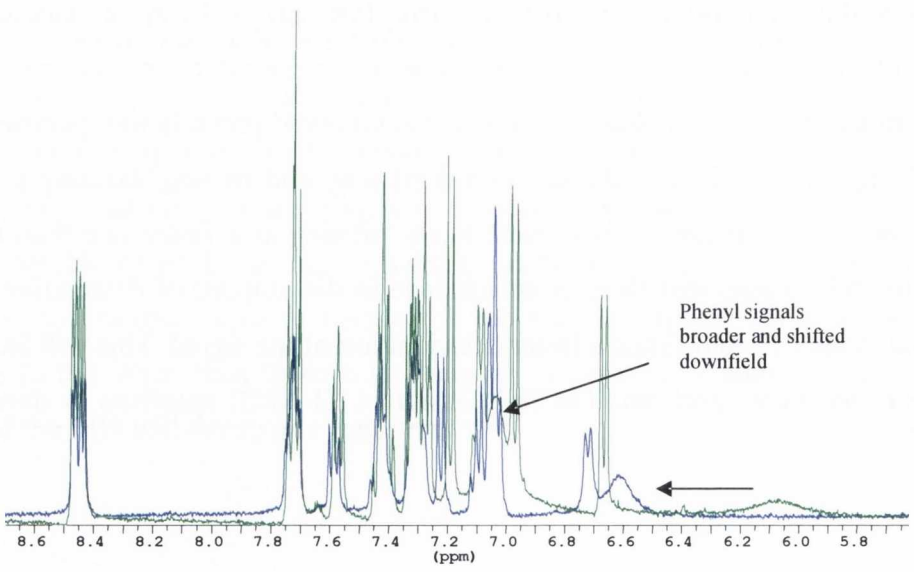


Figure 87: A 60°C ^{1}H-NMR spectrum of the *fac* isomer of 27 (blue) superimposed on the room temperature spectrum (green) (δ 5.7-8.6 ppm shown)

There are a number of significant differences between the spectra in terms of the chemical shift and the intensity. There are clearly slight downfield shifts in the signals assigned to ring D such as the peak at δ 7.18 ppm which is shifted to δ 7.22 ppm at 60°C. There is a more dramatic difference however in the peaks assigned to ring E. The broad signal at δ 7.05 ppm is much sharper at higher temperature and perhaps most significantly the broad signal at δ 6.1 ppm is now shifted downfield to δ 6.5 ppm and is sharper. The fact that ring E is changed more considerably adds further weight to our assignment of this ring, as a more dramatic change in the sharpness in signal implies a faster rotation below the coalescence temperature which changes when the ring flip speed increases enough to approach the fast exchange region. Ring D is less affected by this change in temperature because its signals are already sharp due to the slow rotation of the rings and there is less destructive interference of the FID. In addition, at higher temperature the coordinated pyridyl ring (ring A) is fixed in position, so even at higher temperature ring D is restricted to some extent from rotating. Thus the increased temperature will have a less dramatic effect on this ring than ring E, which is freer to rotate at a higher frequency. The carbon signals associated with the *fac* isomer of **27** were assigned with the aid of a 2 D ^{13}C-^{1}H COSY experiment. The ^{13}C-NMR spectrum is shown below in Figure 88; the C^6 and $C^{6'}$ carbons are the most downfield due to the deshielding effect of the neighbouring nitrogens. The $C^{6'}$ of ring A is most deshielded with a chemical shift at δ 152 ppm, with the C^6 slightly more shielded at δ 149 ppm. The next pair of peaks were assigned to the C^4 and $C^{4'}$ carbons and appear around δ 137 ppm. The most upfield signals at δ 124 ppm were assigned to the C^3 and C^5 on ring C.

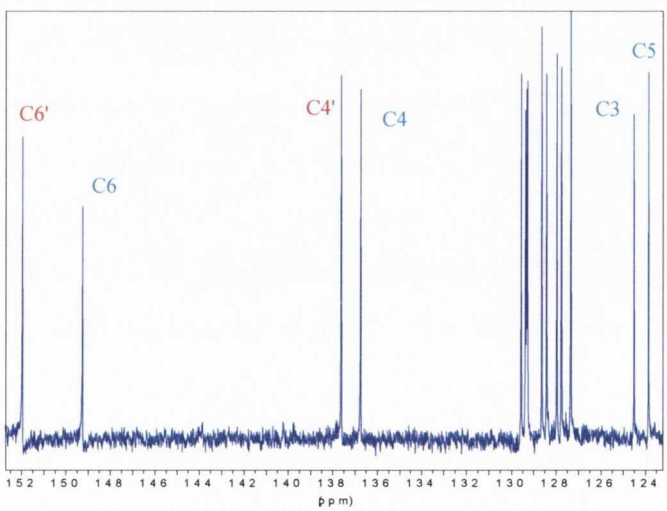


Figure 88: ^{13}C-NMR spectrum of the *fac* isomer of 27 in CD_3CN (δ 124-152 ppm shown)

There are a number of peaks which appear between δ 127 and 130 ppm. This area of the spectrum has been expanded and is shown in Figure 89. Once again, a ^{13}C-^{1}H COSY experiment was used to assign these signals. Interestingly, there are five individual carbon peaks for the five carbons assigned to the phenyl ring D. This is further evidence that this ring is rotating slowly and that destructive interference is minimal. The carbons associated with ring E are at δ 128 and 127 ppm. There are also two peaks associated with the pyridyl ring A in this area which have been assigned as the $C^{3'}$ and $C^{5'}$ from this ring.

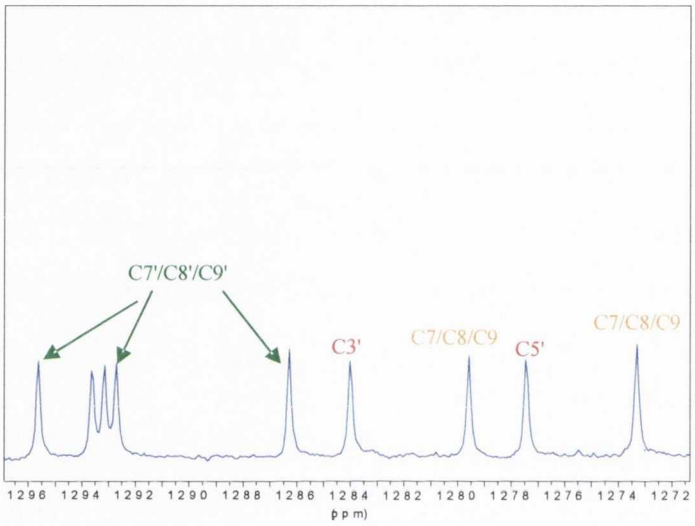


Figure 89: The region between 127 and 130 ppm in the ^{13}C-NMR spectrum of the *fac* isomer of 27

2.2.2.5 X-Ray Crystallographic Determination of the facial Isomer of 27

A crystal suitable for single crystal X-ray diffraction was grown by slow diffusion of ether into an acetone solution of the facial isomer of **27**. The crystal grew in a P-3 hexagonal space group. The dihedral angles of the various rings are shown in the table below. There were two complex molecules in a unit cell along with one solvent molecule and eight PF_6^- counterions. There appear to be two different types of counterions in the cell, with six anions making up the six corners of the unit cell, and two anions in the centre. The bond angles between the metal centre and the ligands are all between 88.70° and 88.74° which is expected for octahedral complexes. The bond length between the ruthenium metal and the nitrogen donor atoms is approximately identical; 2.049Å and 2.005Å. The asymmetric unit of the crystal cell is shown in Figure 90.

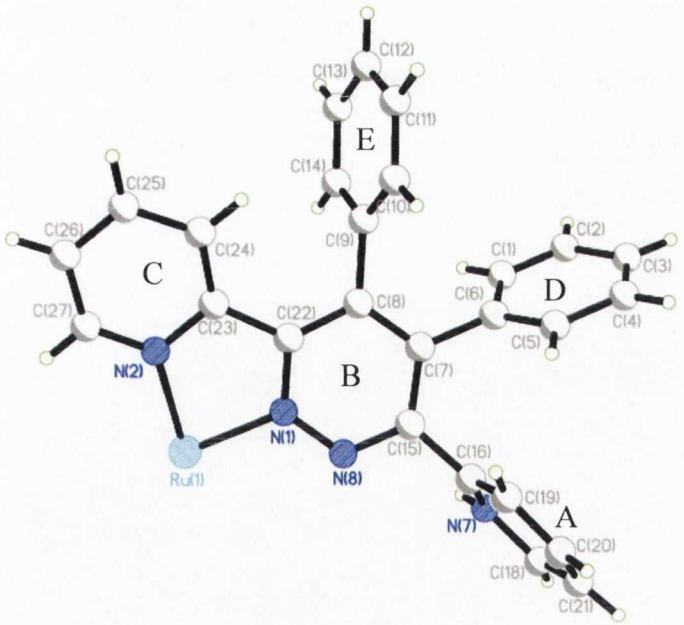


Figure 90: Perspective view of the asymmetric unit of the fac isomer of 27. The PF_6^- anions and the methanol molecule have been removed for clarity

Dihedral Angle Relative to Central Pyridazine Ring (B)			
B-A	**B-C**	**B-D**	**B-E**
70.91°	17.33°	66.70°	66.80°

Table 13: The Dihedral Angles Associated with the *fac* isomer of 27

The coordination sphere along with the two PF_6^- counterions and the methanol molecule is shown in Figure 91. The three ligands have been given different colours for clarity.

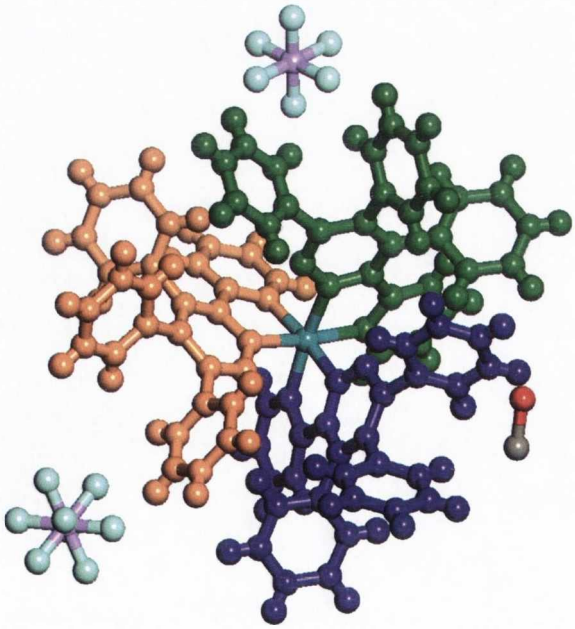


Figure 91: The coordination sphere of the *fac* isomer of 27

The complex forms a hexagonal porous assembly which is characterized by the two unique PF_6^- anions in the crystal lattice. One of these counterions plays a crucial role in stabilizing the framework while the other one occupies a one-dimensional channel. This assembly is shown in Figure 92. The guest anions and methanol molecules are represented in space fill mode.

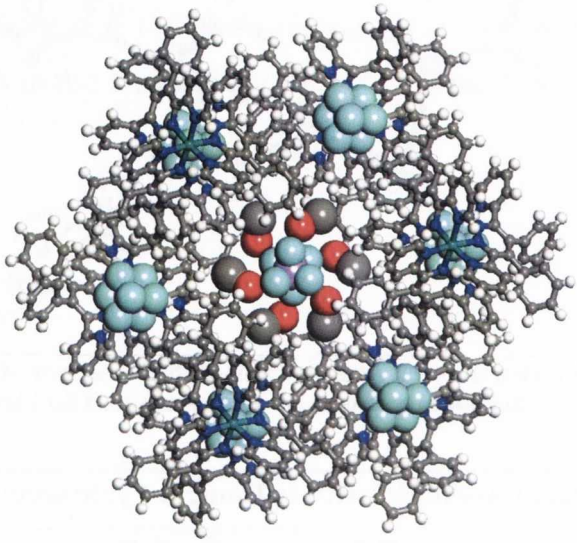


Figure 92: The porous assembly formed by the self-assembly process in the *fac* isomer of 27

The host framework is stabilized by weak C-H···π and π···π interactions whereas the system as a whole is stabilised by the intermolecular interactions involving the PF_6^- counterions. These C-H···F interactions are in the range (2.63-3.01 Å). This interaction is shown on the left in Figure 93. The schematic on the right shows the second PF_6^- unit which occupies the channels and is stabilized by six C-H···F hydrogen bonds with hexagonal symmetry.

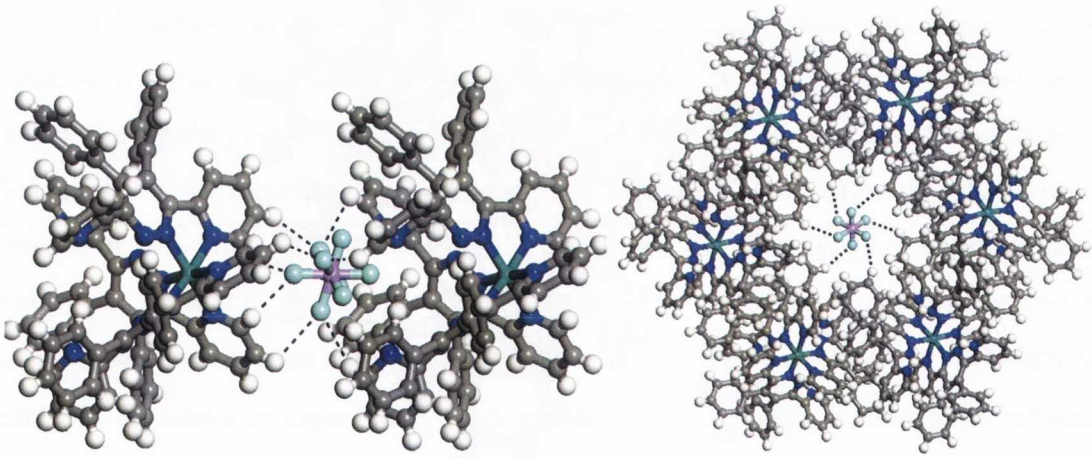


Figure 93: The intermolecular interactions between the PF_6^- anions and the complexes. The schematic on the left depicts the C-H···π and π···π interactions which stabilise the host framework. On the right is the PF_6^- anion which occupies the one-dimensional channel.

Figure 94 shows the hexagonal host framework which is represented in space filling mode. The one-dimensional channels occupied by the PF_6^- anion can be clearly seen. The PF_6^- have been removed for clarity, along with the methanol molecules.

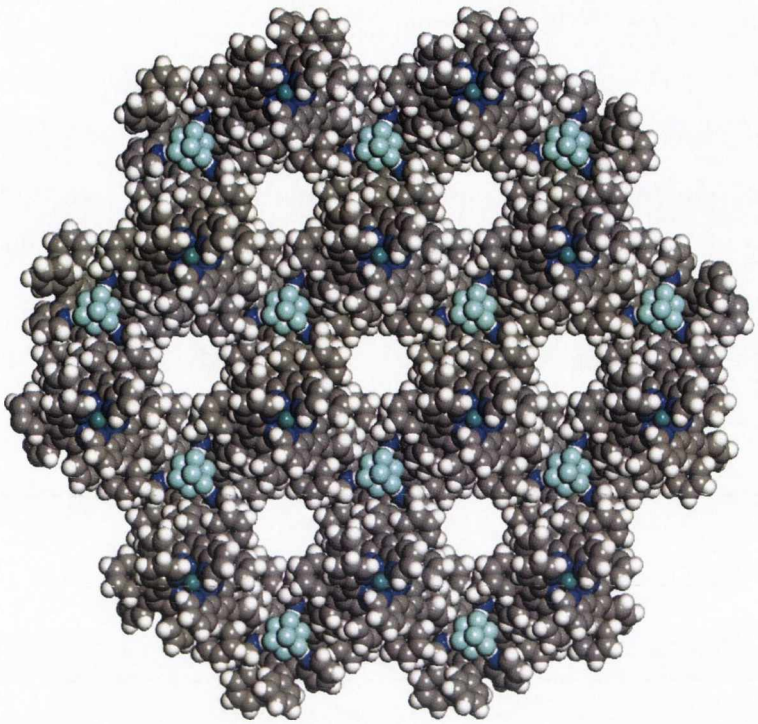


Figure 94: The hexagonal host framework of the *fac* isomer of 27 in space filling mode

2.2.2.6 Characterization of 28 and 29 by NMR Spectroscopy

The two isomers of **28** were isolated and characterised by electrospray mass spectrometry and proton and carbon NMR spectroscopy.

Complex **28** *mer*: The ^{1}H-NMR spectrum of the meridional isomer was complicated and only some of the signals could be assigned from their coupling constants. The ^{1}H-NMR spectrum associated with this isomer is shown in Figure 95. The most downfield signals belong to the H^{6} and H^{8} protons which are most deshielded due to their proximity to the nitrogens on the rings. The most upfield signals are due to the H^{3} protons which are shielded by the ring current effect of the nearby 4-pyridyl ring. The other protons occur in groups of multiplets between these two extremes but could not be assigned.

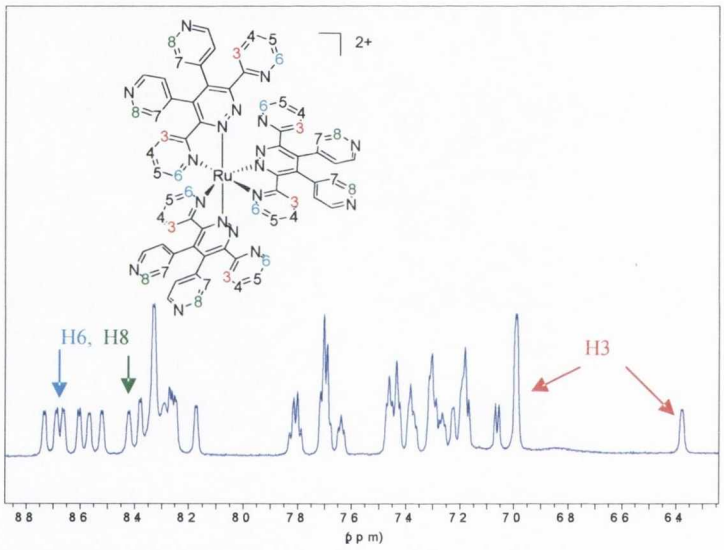


Figure 95: The ^{1}H-NMR spectrum of the mer isomer of 28 in CD_3CN (δ 6.3-8.8 ppm shown)

Complex **28** *fac*: The facial isomer of **28** gave a ^{1}H-NMR spectrum that was easier to assign. There are two sets of ring systems in the aromatic region as was the case for **27**. It was assumed that the most shielded H^{3} of the 2-pyridyl ring was that belonging to ring A. From the 2 dimensional ^{1}H-^{1}H COSY each pyridine ring could then be fully assigned. The 4-pyridyl ring systems appear to behave in a similar way to the phenyl rings in **27** and their signals show similar splitting and broadening patterns. As before, one of the 4-pyridyl rings, labelled as E is extremely broad and its signals are difficult to see in the spectrum, especially the more shielded H^{7} signal. This is assumed to be related to the increase in the destructive interference in the resonating protons due to a faster ring flip of this ring. In comparison, ring D is thought to rotate more slowly due to its proximity to

the rigid coordinated 2-pyridyl ring and thus destructive interference of the resonating protons is reduced.

The most downfield ^{1}H-NMR signals of **28** have been assigned as the $H^{8'}$ protons on ring D. One might anticipate that there would be only one signal for these protons, but clearly the ring flip is slow enough that the spectrometer can measure the decay of two distinct resonances. The multiplet at δ 8.35 ppm was assigned to the two $H^{6'}$ protons from ring A and the two H^8 protons from ring E. The H^4 and $H^{4'}$ protons have a chemical shift around δ 7.8 ppm. The most upfield shifts associated with the pyridyl rings are the H^3/$H^{3'}$ and H^5/$H^{5'}$ protons which appear between δ 7.2 and 7.6 ppm. The H^7 and $H^{7'}$ protons on rings D and E are the most shielded signals appearing at δ 6.8 and 7.2 ppm. The H^7 protons associated with ring E are very broad, but those of ring D are much sharper, indicating that the ring flip of ring D is slower.

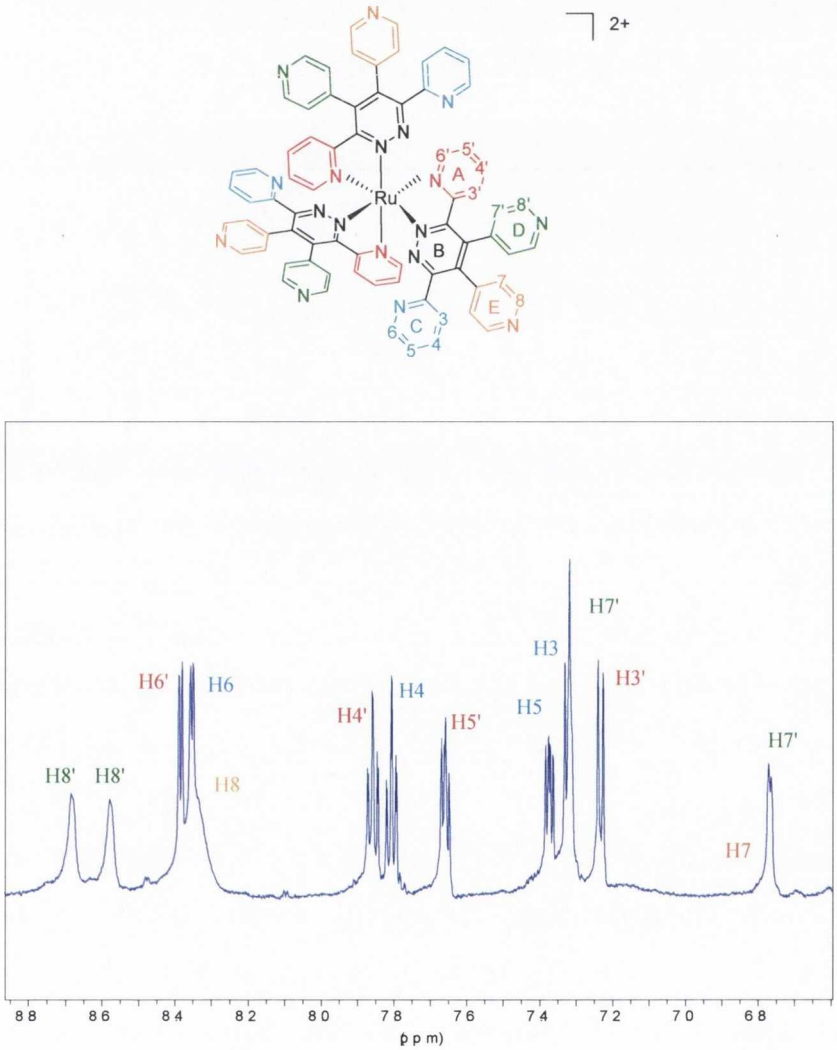


Figure 96: The ^{1}H-NMR spectrum of the *fac* isomer of 28 in CD_3CN (δ 6.6-8.8 ppm shown)

The DEPT spectrum of the *fac* isomer of **28** is shown in Figure 97 and the peaks have been assigned with the aid of a ^{13}C-^{1}H COSY. As was the case for **27**, the spectrum is unusual in that there are four individual carbon peaks for the four C-H carbons atoms on ring D. The peaks associated with $C^{8'}$ on this ring are deshielded by the nitrogen in the 4-position and are thus shifted to δ 151 ppm. The C^{6} and $C^{6'}$ carbons are similarly deshielded and shifted to δ 149 and 152 ppm respectively. The signals of the C^{8} carbons of ring E are extremely weak and are shifted to δ 147 ppm. The other signals are assigned in Figure 97. C^{7} is of note as it is weak, broad and shifted upfield due to the rotation of ring E.

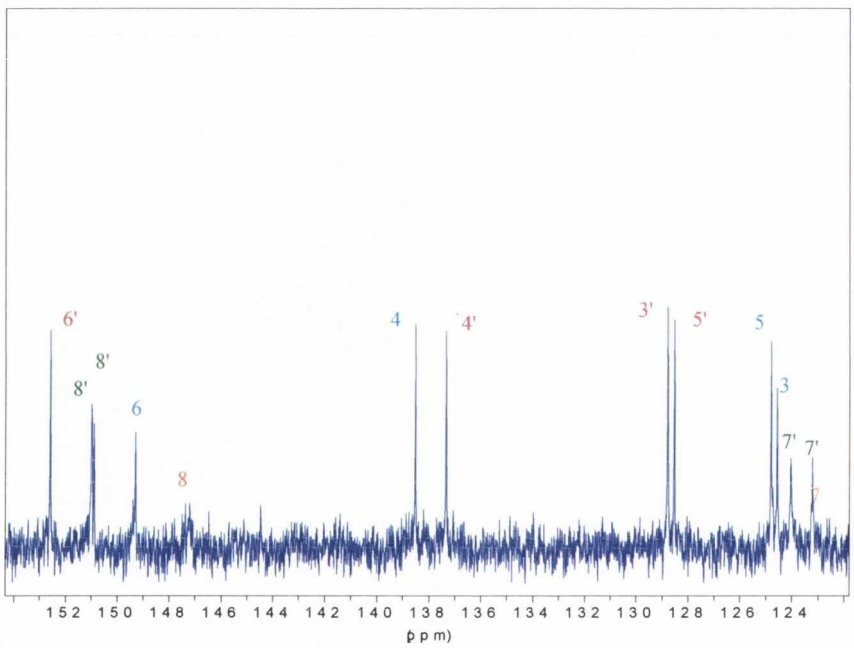


Figure 97: The ^{13}C-NMR DEPT of the *fac* isomer of 28 in CD_3CN (δ 123-153 ppm shown)

Complex **29** *mer*: The ^{1}H-NMR spectrum of the meridional isomer of **29** is shown in Figure 98 and is somewhat easier to interpret than that of **27** and **28**. This is mainly due to the fact that the electron-donating methoxy substituents on the phenyl rings shield the phenyl positions at H^{7} and H^{9} and they are now shifted upfield between δ 6.0 and 6.5 ppm. This has the effect of reducing the quantity of signals which appear between δ 7 and 9 ppm in the spectrum. Nonetheless, due to the lack of symmetry in this molecule there are still six different 2-pyridyl systems which could not be individually identified. It was obvious from the coupling constants of the most downfield signals that the latter were those of the H^{6} protons deshielded by the nitrogen on the ring. The group of signals

between δ 7.6 and 7.8 ppm consist of some of the H^4 and H^5 signals from the pyridyl rings, with the H^3 and remaining H^5 signals occurring around δ 7.2 ppm. The H^7 and H^9 signals occur as a cluster of peaks between δ 6.2 and 6.8 ppm and the methoxy protons are the most shielded signals at δ 3.6 ppm

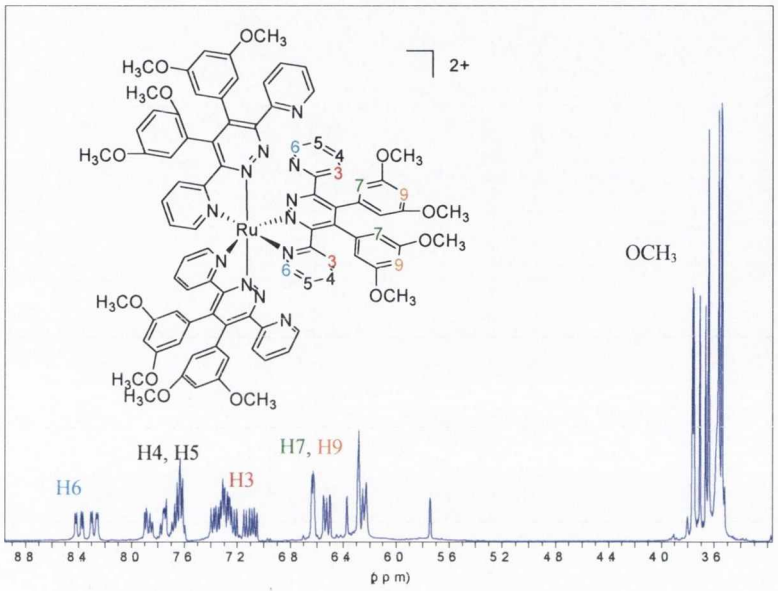


Figure 98: The ^{1}H-NMR spectrum of the *mer* isomer of 29 in CD_3CN (δ 3.5-8.8 ppm shown)

Complex **29** *fac*: The facial isomer of **29** has a C_3 axis of symmetry and the ^{1}H-NMR spectrum of this complex is therefore relatively simple when compared to that of the meridional isomer. As was the case for the latter, the identification of all the peaks is made easier by the fact that the methoxy groups shield the phenyl signals and they are therefore shifted between δ 6.0 and 6.5 ppm. This ensures that there are only two ring systems shifted downfield of δ 7 ppm in the spectrum, and these were assigned using the ^{1}H-^{1}H COSY which is shown in Figure 99. The H^6 and $H^{6'}$ signals are the most downfield appearing at around δ 8.4 ppm. As before the two rings were differentiated by the increased shielding effect felt by the coordinated ring A, in particular on the chemical shift of $H^{3'}$ of this ring. This was the most upfield shifted proton at δ 7.17 ppm, with the H^3 of ring C downfield at δ 7.33 ppm. The other pyridyl signals could be identified by a combination of their coupling constants and the information obtained from the two dimensional spectra.

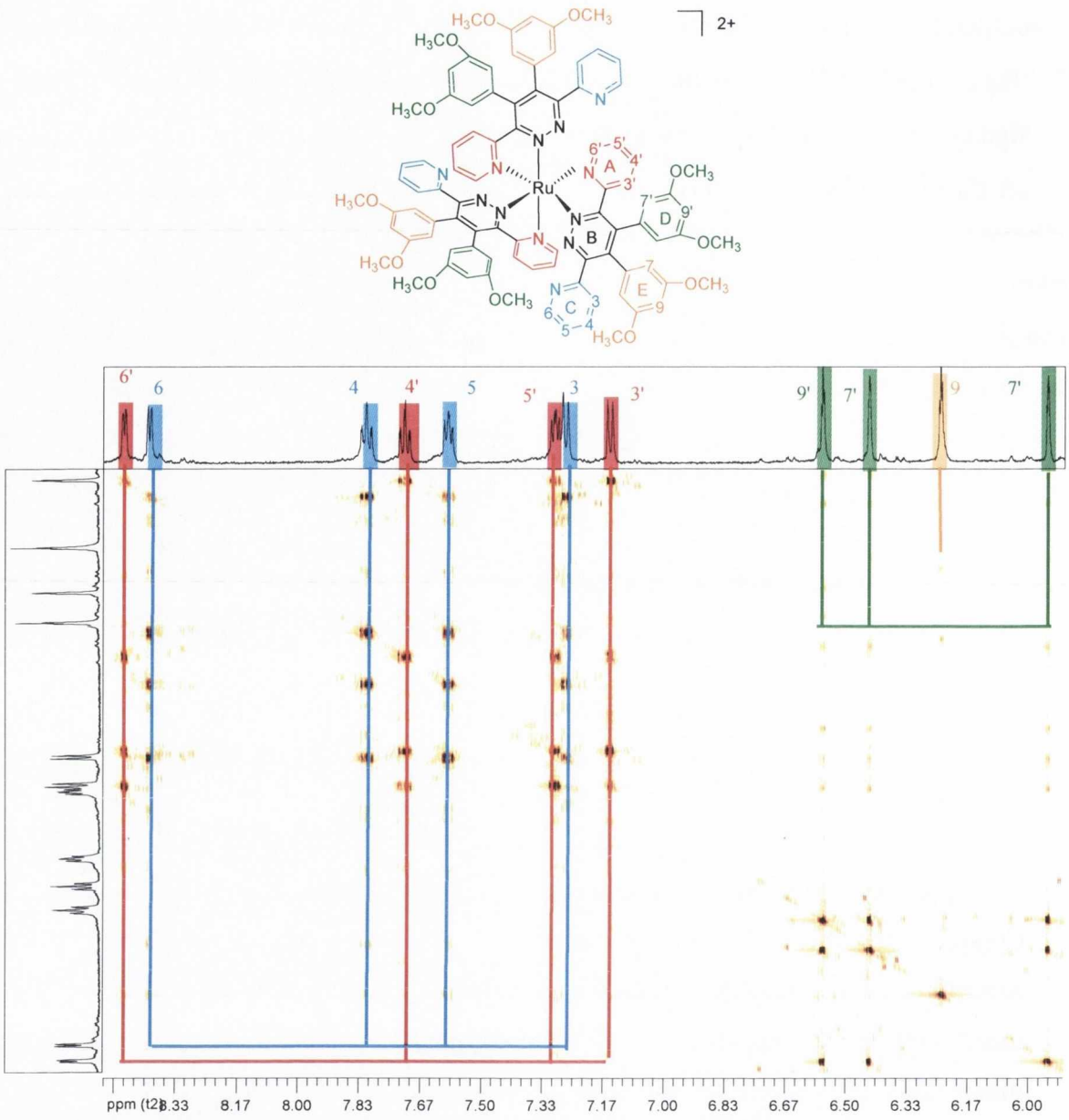


Figure 99: ^{1}H-^{1}H COSY showing the two 2-pyridyl systems and the two phenyl systems of the *fac* isomer of 29 in CD_3CN ((δ 6.0-8.4 ppm shown)

The most interesting feature of the ^{1}H-^{1}H COSY is the splitting pattern associated with the peaks of rings D and E. The two rings appear to exhibit similar slow chemical exchange behaviour as was seen for **27** and **28**. One of the rings has three quite sharp peaks, which indicates that the ring flipping is occurring at a slow enough rate for the protons to resonate at different Larmor frequencies. Applying the same logic as before, this ring has been designated as that which is closest to the metal, ring D. Only one peak is visible in the spectrum for ring E, that of H^9. Because this proton is in the *para* position, its resonance frequency does not change when the ring flips. The H^7 peaks however, which are in the *ortho* position are in different magnetic environments when they rotate, and thus are precessing between two different Larmor frequencies. The

destructive interference which is incurred by the process of many H^7 protons switching between two different frequencies at different intervals results in increased decay of the FID and subsequent broadness in the ^{1}H-NMR spectrum for these proton signals, with the result that they cannot be identified in the spectrum at room temperature.

A similar phenomenon is observed for the methoxy signals of which the two at δ 3.69 and 3.65 ppm are coupled on the same ring according to the ^{13}C-^{1}H COSY. Both of these signals integrate for three protons, whereas the methoxy signal for the other ring is a single peak which is shifted to δ 3.55 ppm and integrates for six protons. The ring which has two distinct methoxy resonances was thought to be ring D, as the rotation of this ring would be the more hindered leading to two distinct magnetic environments brought about by the neighbouring fixed rings. Table 14 shows the comparative chemical shifts of the two 2-pyridyl ring systems of the *fac* isomers of **27**, **28** and **29**.

Compound	Chemical Shifts of 2-pyridyl Protons in CD_3CN in ppm			
	H6, H6'	**H5, H5'**	**H4, H4'**	**H3, H3'**
27 ***fac***	8.16, 7.96	7.21, 7.33	7.66, 7.56	7.06, 6.93
28 fac	8.38, 8.35	7.38, 7.79	7.83. 7.79	7.28, 7.20
29 ***fac***	8.40, 8.46	7.59, 7.27	7.81, 7.70	7.27, 7.14

Table 14: ^{1}H-NMR data of the two 2-pyridyl rings of the *fac* isomers of 27, 28 and 29

The ^{1}H-NMR spectrum of the *fac* isomer of **29** was run again at 60°C in order to investigate any changes in the phenyl and methoxy peaks as they approach the coalescence temperature. The methoxy region of the spectrum is shown at room temperature below in green, with the high temperature superimposed in blue. All three signals appear to be shifted between δ 0.2 and 0.3 ppm downfield at higher temperature. The signals are also distinctly narrower, due to the fact that as the coalescence temperature is approached the ring flip is occurring so fast that the spectrometer can only measure the average of two proton resonances, so there is negligible destructive interference in the signal as the ring flips between the two positions. The lower aromatic regions of the spectra of the *fac* isomer of **29** at room temperature and at 60°C are shown below in Figure 100. It is clear from the overlay that as the coalescence temperature is approached, the phenyl signals are all shifted slightly downfield by between δ 0.2 and 0.3 ppm. The peaks also become narrower, but the most distinctive difference between the two spectra is the appearance of a broad signal at δ 5.8 ppm which most likely correlates to the H^7 protons on ring E. Evidently, as the coalescence temperature is approached, the destructive interference is reduced and the peak is more pronounced.

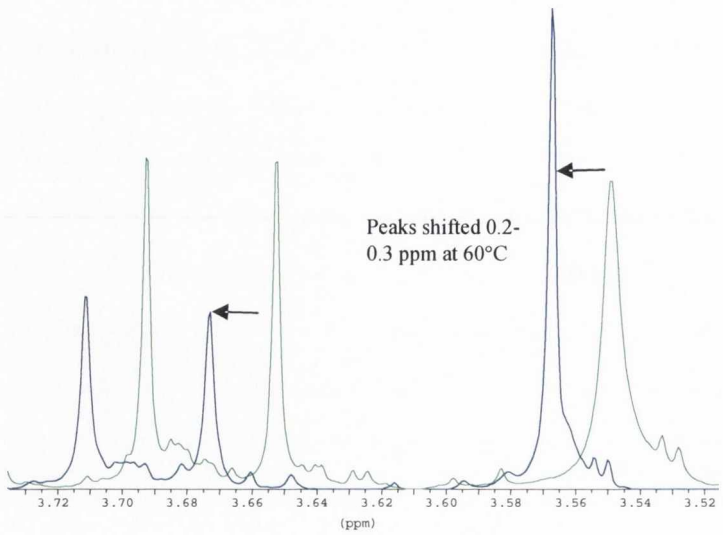


Figure 100: The methoxy peak shifts of the *fac* isomer of 29 run at room temperature (green) and at 60°C (blue) in CD_3CN

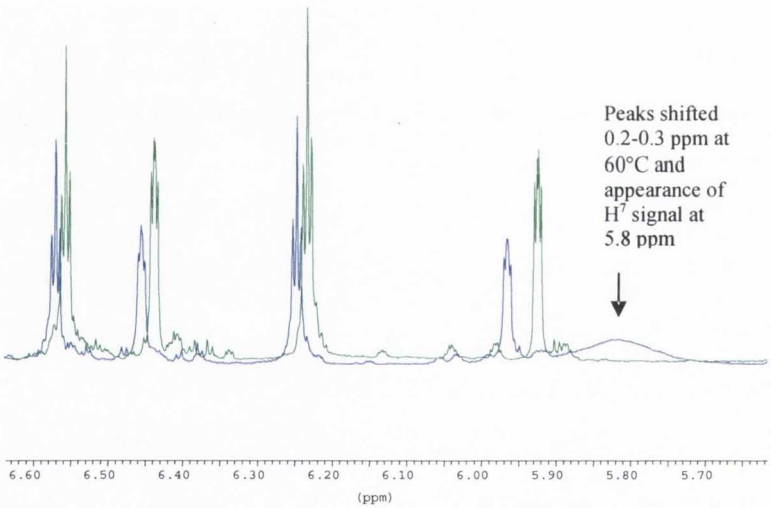


Figure 101: The aromatic region of the ^{1}H-NMR spectra of the *fac* isomer of 29 run at room temperature (green) and at 60°C (blue) in CD_3CN (δ 5.6-6.6 ppm shown)

The ^{13}C-NMR spectrum and the DEPT spectra of the facial isomer were also obtained and although the quaternary protons could not be assigned, all the non quaternary protons were identified with the help of a ^{13}C-^{1}H COSY. The pyridyl protons were the most downfield, with the C^6 and $C^{6'}$ carbons the most deshielded due to their proximity to the nitrogen on the ring. The methoxy carbons appear as two closely spaced peaks at δ 55 ppm. Three signals appeared for the three carbons from ring D in the lower aromatic region, but only two carbon peaks were observed for C^7 and C^9 on ring E.

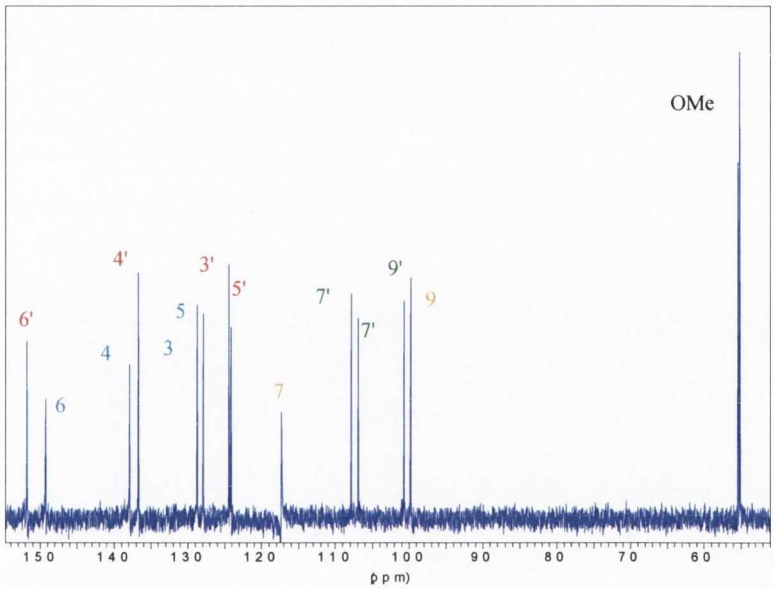


Figure 102: The ^{13}C-NMR of the *fac* isomer of 29 in CD_3CN (δ 55-150 ppm shown)

2.2.2.7 UV-Vis Absorption Spectra of Ru (II) tris *Isomers*

The absorption spectra of homoleptic *tris* polyazine complexes often have features in common with their heteroleptic *bis* bpy counterparts, but due to the presence of only one type of ligand in the homoleptic complexes, it is often easier to assign the absorption maxima to particular excited states. In addition, heteroleptic ruthenium complexes and homoleptic complexes containing asymmetric ligands are less symmetric compared with Ru(II) *tris* bpy and therefore the degeneracy of the π* orbitals is removed which lead to broadening of the MLCT bands.[16]

Although significant differences have been observed for the UV-Vis absorption spectra of facial and meridional isomers of certain iridium complexes, the existing literature seems to indicate substantially less difference between the spectra of isomers of ruthenium complexes.

In the case of iridium, the *fac* and *mer* isomers of a variety of cyclometalated fluorophenyl substituted pyridyl *tris* complexes showed different spectroscopic properties.[51, 66] The *fac* isomers appeared to have a higher energy MLCT compared to their *mer* counterparts. These MLCT shifts are more pronounced in more polar solvents indicating a stronger solvent interaction in the case of the *fac* isomers. This could be because the *fac* isomer is more polar; with its polar functional groups aligned along the three-fold axis it is more sensitive to solvent polarity.

There appears to be very little precedent for similar variations in the UV-Vis absorption spectra of *mer* and *fac* ruthenium complexes. The synthesis of *fac* and *mer* isomers of Ru(II) *tris* complexes of 5'-amino-2,2'-bipyridine-5-carboxylic acid was carried out by Ishida and co-workers.[52] Both isomers showed absorption maxima at λ 463 nm. Other derivatives of these complexes showed no variation in the absorption spectra of both isomers.

Fletcher and co-workers found there to be no significant difference in the spectra of the *fac* and *mer* isomers of the Ru(II) *tris* 5-hydroxymethyl-2, 2'-bipyridine benzoate and 5-hydroxymethyl-2,2'-bipyridine naphthoate ligands.[54] Not only did both isomers of each complex have the same absorption maxima at λ 452 nm, but the complexes showed little variation in their absorption spectra, which seemed to indicate that the functionality at the 5-position had very little impact on the excited state chemistry of the complex.

A slight difference was observed in the UV-Vis spectra between the *mer* and *fac* isomers of the Ru *tris* 5, 6-dimethyl-3-(pyridin-2-yl)-1,2,4-triazine complex.[64] In this case the *mer* isomer displayed a slight bathochromic shift relative to the *fac*, with a maximum at λ 442 nm compared with λ 434 nm for the latter. The authors provide no explanation for this difference, and the isomers of other related ligands were not successfully separated and thus could not be individually measured.

2.2.2.8 The UV-Vis Absorption Spectra of fac and mer isomers of 27, 28 and 29

The UV-Vis spectra of **27**, **28** and **29** show some fundamental differences from that of Ru(II) *tris* bpy. The single biggest factor causing this difference is the pyridazine ring which is coordinated to the metal. As discussed in the introduction, complexes containing pyridazine ligands tend to absorb at lower energies than their pyridyl analogues due their low-lying π* orbitals.[4] The UV-Vis absorption spectra of the *fac* and *mer* isomers of **27**, **28** and **29** are shown in Figure 103. The high-energy MLCT which occurs in Ru(II) *tris* bpy at λ 243 nm is shifted slightly to longer wavelength for compounds **27** and **28** and is absent from **29**. This absence may be due to the electron-donating methoxy groups increasing the energy of the LUMO on the ligand and thus increasing the HOMO-LUMO energy gap for this transition. A similar logic could explain the slightly higher energy absorption of the LC absorption which occurs in **29** at around λ 280 nm – this transition occurs at a higher energy because the LUMO of the methoxy-containing ligand is higher in energy. The opposite is true for the electron-withdrawing 4-pyridyl substituents on the

ligand on complex **28**; this complex absorbs at a slightly longer wavelength as the ligand centred LUMO is at lower energy due to the electron-withdrawing effect of the pyridyl substituents in the ligand. Another point of interest is the small but consistent bathochromic shift in the spectra of the *mer* isomer of each complex compared to the *fac* analogue. This may be due to the lack of symmetry associated with the *mer* isomer which results in the loss of degeneracy of the π^* orbital on the ligands and accounts for lower energy LUMO orbitals. This results in slightly lower energy transitions to these orbitals from metal-centred HOMOs.

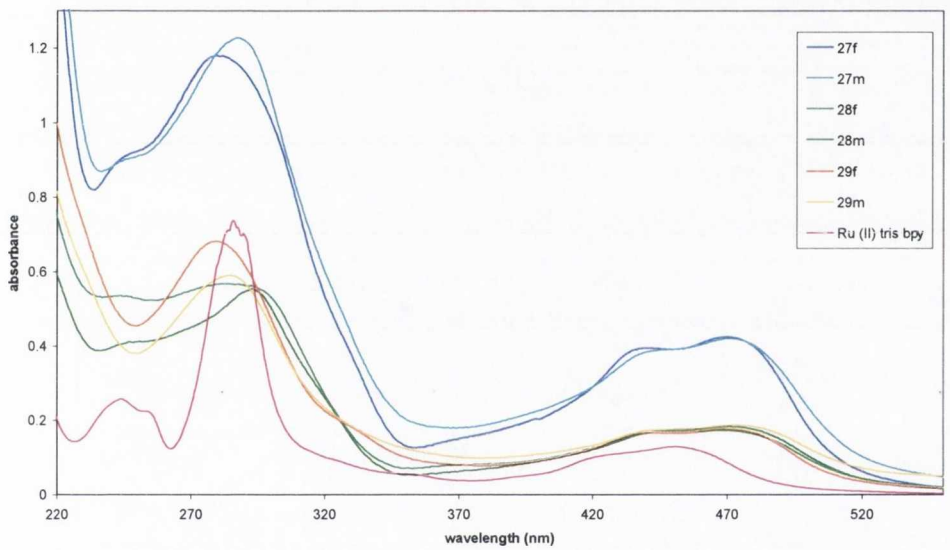


Figure 103: The UV-Vis absorption spectra of the meridional and facial isomers of 27, 28 and 29 in MeCN

Figure 104 shows the visible region of the UV-Vis spectra of both *mer* and *fac* isomers of complexes **27**, **28** and **29**. The same general trends apply in this region of the spectra; the lower energy π^* orbitals of the pyridazine ring system result in a bathochromic shift of the MLCT in this region compared to Ru(II) *tris* bpy. A similar trend is observed in the visible region with regard to the *mer* and *fac* isomers of each complex- the *mer* is slightly red-shifted compared to the *fac* analogue – although this shift appears to be less significant in this region of the spectra. Nonetheless, this is further evidence of the lower energy π^* LUMO orbitals associated with the *mer* complexes compared to the *fac*, resulting in longer wavelength absorptions.

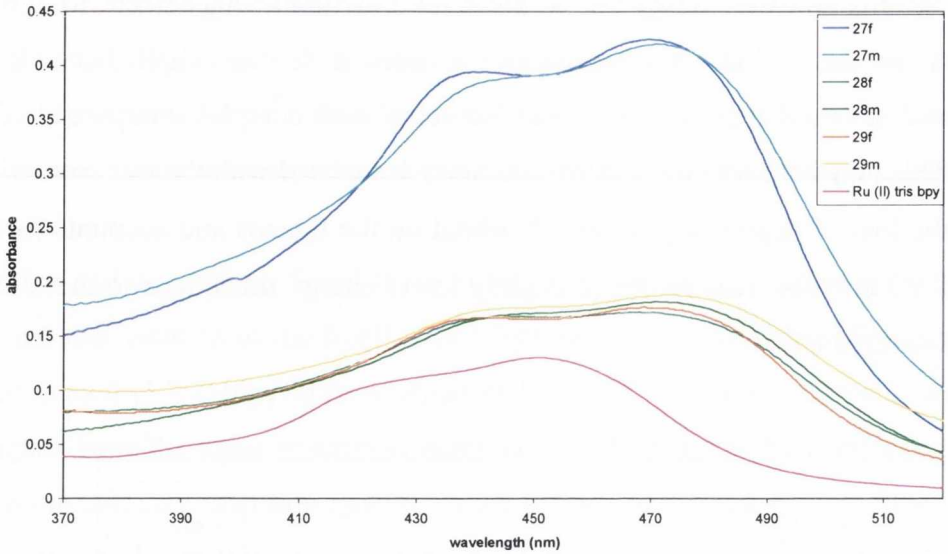


Figure 104: The Low Energy Region of the UV-Vis spectra of 27, 28 and 29

The absorption maxima associated with these complexes are summarised in Table 15.

Compound	Wavelength *nm* (absorbance $M^{-1}cm^{-1}$)		
	MLCT $d\pi \rightarrow \pi^*$	LC $\pi \rightarrow \pi^*$	MLCT $d\pi \rightarrow \pi$
Ru *tris* bpy	250 (25000) 238(30000)	285 (87000)	451 (14000) 428 (13000)
27 fac	244 (90,410)	279 (118,300)	469 (41,860) 436 (38,970)
27 mer	241 (88,4500	286 (122,410)	468 (41,790) 441 (38,460)
28 fac	244 (53,340)	282 (56,6700	470 (17,600) 439 (17,200)
28 mer	246 (40,900)	293 (54,4000	471 (18,700) 443 (17,500)
29 fac	-	280 (68,300)	470 (17,600) 440 (17,300)
29 mer	-	285 (59,000)	472 (18,800) 444 (17,500)

Table 15: Summary of the absorption bands of $[Ru(bpy)_3]^{2+}$ and both isomers of 27, 28, 29 and in MeCN

2.2.2.9 Emission Spectra of the fac and mer isomers of 27, 28 and 29

The UV-Vis Emmission spectra were carried out in acetonitrile using a $1cm^3$ glass cuvette with the complexes at concentrations of 2 X 10^{-5} M. Figure 105 shows the emission spectra of the *fac* and *mer* isomers of **27**, **28** and **29**.These spectra reflect a similar pattern to the absorption spectra, where there is a small but consistent bathochromic shift of the maximum of each *mer* isomer relative to the *fac*. This difference (λ 27 nm) is most apparent in the *fac* and *mer* spectra of **27**. The *fac* complex of **28** has the lowest energy emission of the three *fac* isomers (λ 638 nm) This could be due to the lower energy excited state orbitals arising from the electron-withdrawing effect of the 4-pyridyl substituents on the ligands.

The *fac* isomers of each complex are uniformLy blue shifted and more intense than their *mer* analogues which reflects the higher energy π* orbitals of the *fac* isomers and a subsequent increase in emission on returning to the ground state HOMO.

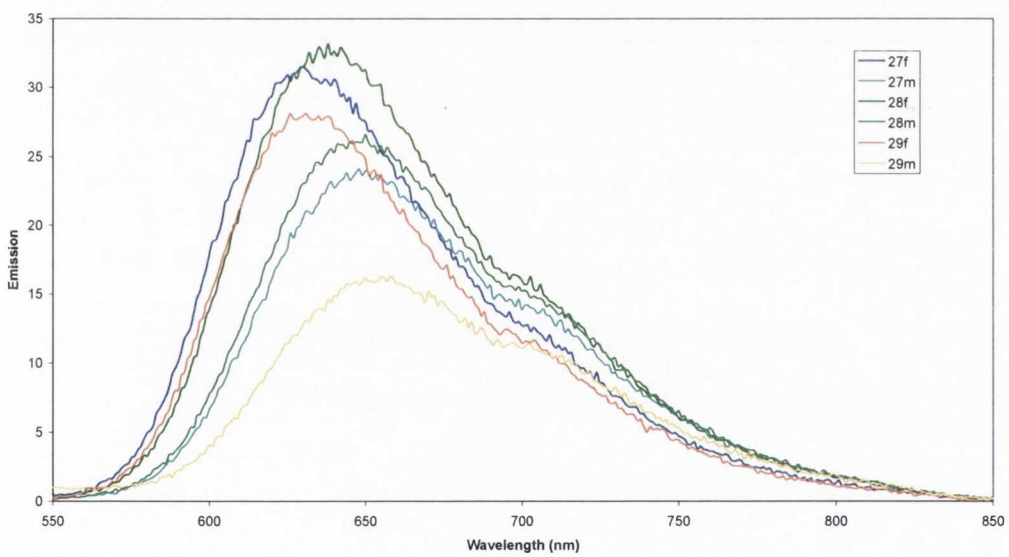
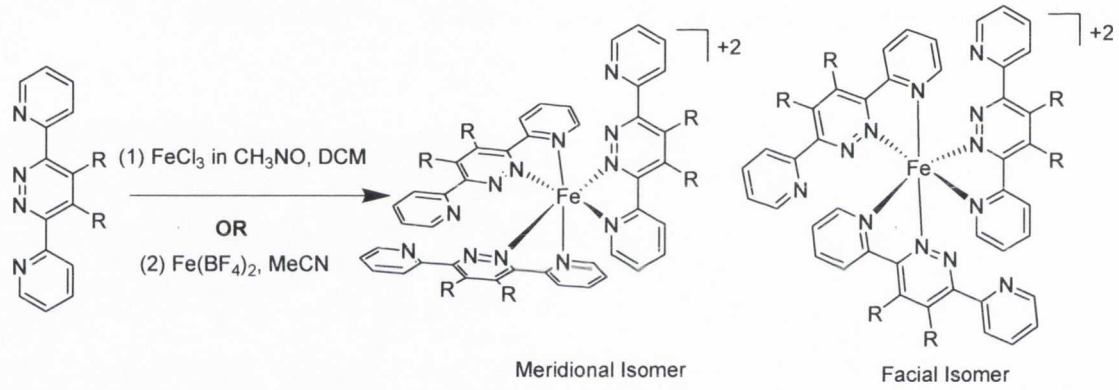


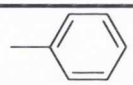
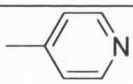
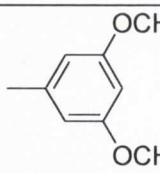
Figure 105: Emission Spectra of both Isomers of 27 28 and 29 in MeCN

2.2.3 The Synthesis of Iron (II) Complexes 30, 31 and 32

2.2.3.1 Synthetic Procedure

The ligands prepared in Chapter 1 were designed as candidates for cyclodehydrogenation. This was attempted with compounds **3**, **4**, **6** and **8** and was not successful despite employing a variety of methods. One method involved $FeCl_3$ catalysed oxidative cyclodehydrogenation in dichloromethane. The result in this case was the formation of a dark iron-containing reaction mixture which on TLC was shown to comprise a number of products. These were thought initially to be a series of isomeric iron complexes. To investigate this further, $Fe(BF_4)_2$ was chosen for direct reaction with ligands **6**, **8** and **11** and the result was metal complexes **30**, **31** and **32** produced using a metal to ligand ratio of 1:3 in acetonitrile (Scheme 35).



Ligand	R	Tris Fe (II) Complex
6		30
8		31
11		32

Note: In the case of **11** only method (2) produced pure iron *tris* complexes

Scheme 35: Schematic showing the two methods (1) and (2) of the synthesis of the iron (II) tris complexes of ligands 6, 8 and 11

The $Fe(BF_4)_2$ reaction involving ligand **6** generated two well-separated spots on the plate when using acetone, water and a saturated solution of KNO_3 in a 100:10:1 ratio as eluent. A column was run using this solvent mixture and two isomers of the iron complex were

isolated. The meridional isomer (24% yield) was the fastest moving with an R_f value of 0.74 and the facial isomer (11% yield) was isolated more slowly (R_f = 0.26, Table 16).

The purification of the two isomers of **31** was carried out using a more polar mixture of solvents, using ammonia to replace the water and an increase in the amount of saturated KNO_3. The two isomers moved very closely, and could not be separated using a standard column. Separation was possible however using a thick layer silica plate. The meridional isomer was isolated in a 16% yield, and unusually, the facial isomer was isolated in a 42% yield. This was not expected as statistically the meridional isomer should be prepared in a 3 to 1 excess over the facial isomer. The statistical ratio is known to be affected by bulkier substituents, but it is not clear why this ratio was not seen consistently for all three complexes.

Compound	% Yield of Mer Isomer	% Yield of Fac Isomer
30	24	11
31	16	42
32	37	20

Table 16: Isolated yields of each isomer of the Fe(II) tris complexes 30, 31 and 32

The two isomers of **32** were isolated using a mixture of water, methanol and saturated KNO_3. The meridional isomer was isolated in 37% yield and the facial isomer in 20% yield. Interestingly, when the synthesis of this complex was attempted using $FeCl_3$ the two isomers of **32** could not be obtained. This was thought to be due to possible partial cyclodehydrogenation of the ligand as discussed in Chapter 1. Although no crystals suitable for X-ray crystallography were obtained, all complexes were characterised by ^{1}H-NMR and UV-Vis spectroscopy and electrospray mass spectrometry.

2.2.3.2 Characterisation of 30, 31 and 32 by NMR Spectroscopy

Many of the issues which featured in the NMR spectra of the ruthenium *tris* homoleptic complexes of ligands **6**, **8** and **11** were apparent in their respective iron complexes. For example the asymmetric nature of the meridional isomers led to several overlapping signals in the ^{1}H-NMR spectrum.

Complex **30** *mer*: The ^{1}H-NMR spectrum of the meridional isomer of **30** is shown below in Figure 106 as an example.

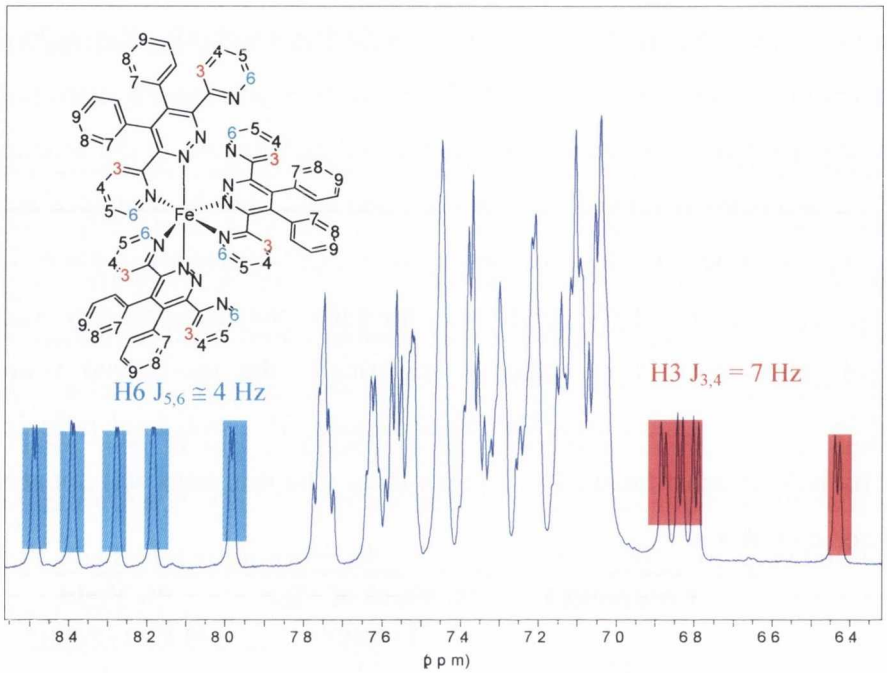


Figure 106: ^{1}H-NMR spectrum of the mer isomer of 30 in CD_3CN (δ 6.4-8.5 ppm shown)

The most downfield shifted proton signals between δ 8.0 and 8.5 ppm were assigned as the H^6 of the 2-pyridyl rings based on their coupling constants of 4–5 Hz and the fact that they are deshielded by neighbouring nitrogen atoms. The most upfield signals were assigned as the H^3 protons based on their coupling constants of 7-8 Hz. The other pyridyl signals appear together with the phenyl signals as groups of overlapping multiplets between δ 7.0 and 7.8 ppm. The integration of these peaks could not be determined accurately. The high resolution mass spectra of both the *fac* and *mer* isomers were obtained. The calculated mass for both isomers is 1214.3944. The mass obtained for the *mer* isomer was 1214.3938 and for the *fac* isomer was 1214.3936.

Complex **30** *fac*: The ^{1}H-NMR spectrum of the facial isomer of **30** is shown in Figure 107 and bears many similarities to the ruthenium *tris* complex of the same ligand. The rings were differentiated using a ^{1}H-^{1}H COSY experiment and ring A was assigned based on the assumption that the $H^{3'}$ of this ring is likely to be more shielded than the H^3 of ring C due to the fact that coordination to the metal restricts ring rotation. The signals associated with the H^6 and $H^{6'}$ protons are the most deshielded, with the signal of ring C appearing at δ 8.5 ppm and that of ring A at δ 8.2 ppm.

The H^4/$H^{4'}$ and H^5/$H^{5'}$ pyridyl signals were assigned from the ^{1}H-^{1}H COSY spectrum and appear between δ 7.3 and 7.8 ppm. The signals associated with the phenyl rings like those of the ruthenium analogue, exhibit one ring with particularly broad peaks at δ 6.0 and 7.0

ppm and the other ring with a set of unusual splitting patterns with peaks at δ 6.65, 7.35 and 7.45 ppm. It was assumed that the broader peaks occurred as a result of destructive interference brought about by the quicker ring-flip of ring E. The signal at δ 6.65 ppm integrates for one proton which could indicate that it is the $H^{9'}$ proton at the para position on ring D. However it seems unusual that this proton would be so shielded; it is possibly one of the $H^{7'}$ protons shielded by the neighbouring 2-pyridyl ring.

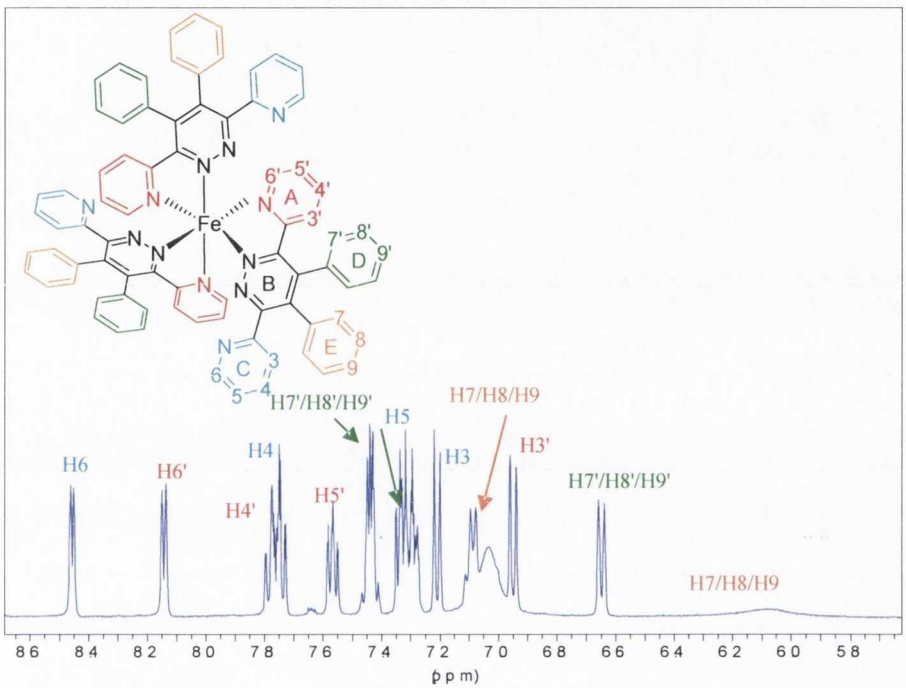


Figure 107: The ^{1}H-NMR spectrum of the *fac* isomer of 30 in CD_3CN (δ 5.8-8.6 ppm shown)

The meridional and facial isomers of **31** were also characterised by mass spectrometry. The complex has a calculated mass for the di-cation of 1220.3659, and a mass of 1220.3659 was obtained for both the meridional and the facial isomer. The isotropic distribution of the peak was consistent with that expected of Fe(II) complexes.

Complex **31** *mer*: The ^{1}H-NMR spectrum of the meridional isomer is shown in Figure 108. The C_1 symmetry associated with meridional isomers ensures that the ^{1}H-NMR spectrum should integrate for 48 protons. However, due to the broadness associated with some of the 4-pyridyl signals, the overall integration of the spectrum is difficult to calculate accurately.

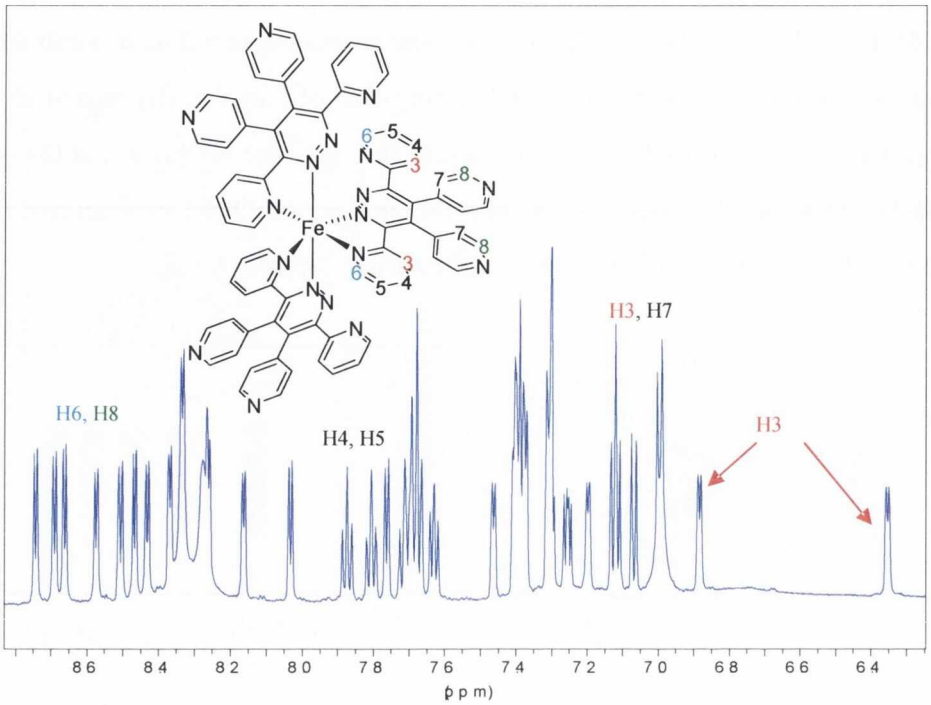


Figure 108: The ^{1}H-NMR spectrum of the mer isomer of 31 (δ 6.3-8.7 ppm shown)

Only some of the peaks can be identified by assessing their coupling constants and chemical shift. The most downfield signals from δ 8.0 to 8.8 ppm have been assigned as the H^{6} protons of the 2-pyridyl rings and the H^{8} protons of the 4-pyridyl rings, as their coupling constants are around 4 Hz. There are two signals which are shifted quite far upfield at δ 6.35 and 6.90 ppm. These are two of the H^{3} protons which are most likely to be on the rings coordinated to the iron, and are thus shielded by the ring current of the neighbouring 4-pyridyl ring. The other signals occur in groups of doublets and multiplets between δ 7.0 and 8.0 ppm, and many can be assigned from their coupling constants.

Complex **31** *fac*: The proton NMR spectrum of the facial isomer of **31** is shown in Figure 109. The 4-pyridyl ring labelled as D shows unusual splitting as was the case for the ruthenium analogue. The two $H^{8'}$ signals of D are the most downfield signals and appear around δ 8.6 ppm. The corresponding $H^{7'}$ signals are shifted upfield to different degrees, with one proton shifted to δ 7.25 ppm and the other to δ 6.67 ppm. The H^{8} and H^{7} signals associated with ring E are much broader due to the increased freedom of rotation of this ring, and consequent increase in destructive interference. In particular the H^{7} signal at δ 6.1 ppm is very broad. As before the two 2-pyridyl rings were differentiated by the assumption that the most upfield H^{3} shift is that of the coordinated ring A. Thus a ^{1}H-^{1}H COSY experiment was performed in order to establish which signals were associated

with rings A and C. The results of the assignment are shown in Figure 109. A ^{1}H-NMR spectrum of this isomer was also obtained at 60°C in order to assess the behaviour of the signals as they approach the coalescence temperature. As expected the signals associated with ring D and E were sharper and shifted by δ 0.2 to 0.3 ppm downfield.

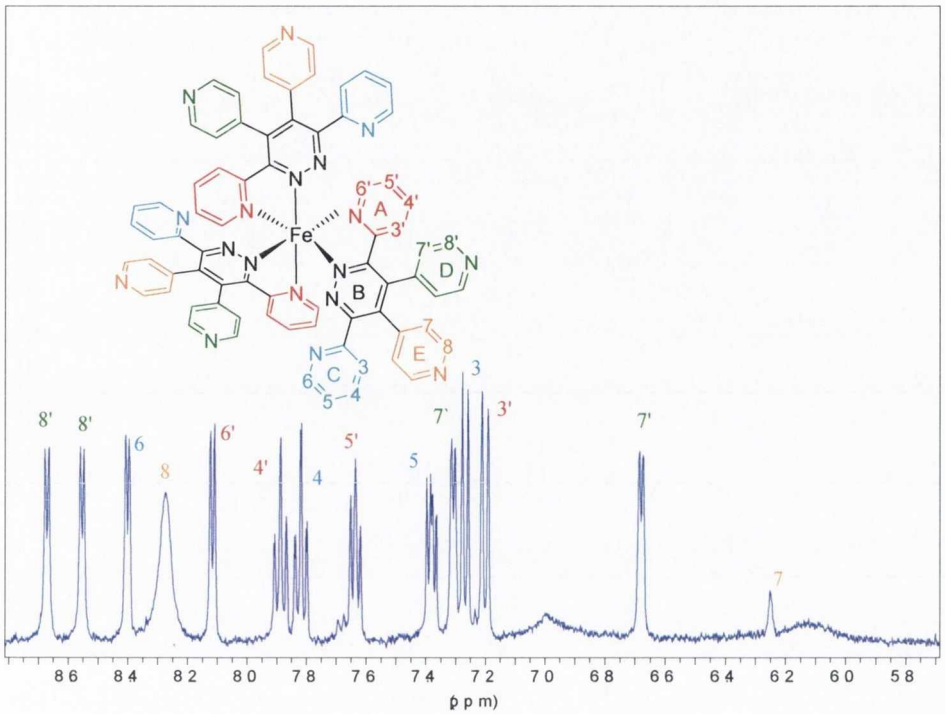


Figure 109: The ^{1}H-NMR spectrum of the facial isomer of 31 in CD_3CN (δ 5.8-8.7 ppm shown)

The two geometric isomers of **32** were isolated and characterised by mass spectrometry, proton NMR spectroscopy and UV-Vis spectroscopy. The accurate mass spectra of both the meridional and the facial isomers of **32** were obtained. The calculated mass of the dicationic complex was 1620.4906, and the mass obtained for the meridional isomer was 1620.4902, with a value of 1620.4956 obtained for the facial isomer.

Complex **32** *mer*: The proton NMR of the meridional isomer of **32** is shown in Figure 110, and is similar to its ruthenium analogue. There is no symmetry within the complex, which results in several overlapping peaks due to the large number of 2-pyridyl proton signals. Nevertheless, the methoxy groups shield the phenyl protons to such an extent that they are shifted upfield to between δ 5.8 and 6.8 ppm. The H^6 protons from the pyridyl rings appear as a closely bunched group of doublets between δ 8.2 and 8.4 ppm. The H^4 and H^5 protons appear in two large groups of multiplets between δ 7.1 and 7.5 ppm and between δ 7.6 and 7.9 ppm. The most upfield pyridyl signals are the H^3 protons of the coordinated rings at δ 7.1 ppm due to the shielding effect of the neighbouring phenyl

rings. The methoxy groups appear as a group of singlets appearing upfield at around δ 3.6 ppm.

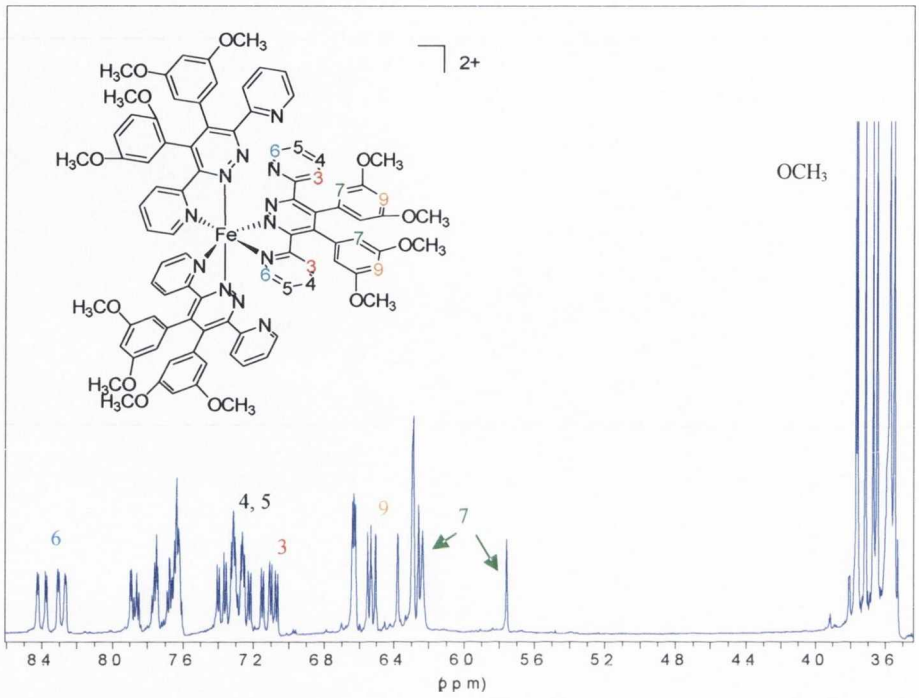


Figure 110: The ^{1}H-NMR spectrum of the *mer* isomer of 32 in CD_3CN (δ 3.6-8.4 ppm shown)

Complex **32** *fac*: The facial isomer of **32** was also analysed by ^{1}H-NMR spectroscopy and is shown in Figure 111. There are two sets of 2-pyridyl signals and these were assigned with the help of a two dimensional ^{1}H-^{1}H-COSY experiment. The two sets of phenyl signals exhibited a similar splitting pattern as seen in the analogous ruthenium complexes. One ring, which was assigned as ring E exhibited a very broad signal at δ 5.4 ppm which was assigned to the H^7 protons. The H^9 of this ring is at δ 6.2 ppm whereas the equivalent signal of ring D is more downfield at δ 6.6 ppm. The unusual splitting pattern which was a feature in the ruthenium complex of this ligand is also a feature here, with two signals appearing for the H^7 protons at δ 5.9 and 6.45 ppm. As before the signals associated with this ring are much sharper for ring E. There are three methoxy signals present between δ 3.5 and 3.7 ppm. Two of these signals were assigned to ring D, and the most upfield signal which integrates for six protons was assigned to ring E, which has more rotational freedom. Table 17 displays chemical shifts of the 2-pyridyl protons for the facial isomers of **30**, **31** and **32**.

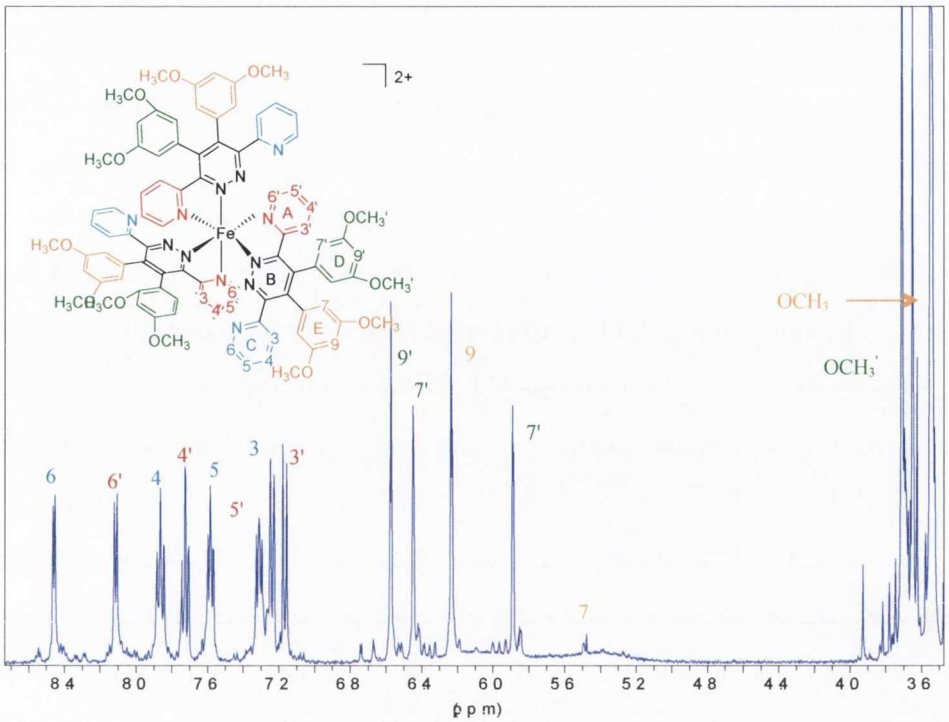


Figure 111: The ^{1}H-NMR spectrum of the *fac* isomer of 32 in CD_3CN (δ 3.6-8.5 ppm shown)

Compound	Chemical Shifts of 2-pyridyl Protons in CD_3CN in δ ppm			
	H6, H6'	H5, H5'	H4, H4'	H3, H3'
30 ***fac***	8.45, 8.14	7.31, 7.57	7.74, 7.75	7.20, 6.94
31 fac	8.40, 8.11	7.38, 7.63	7.82, 7.88	7.26, 7.20
32 ***fac***	8.46, 8.11	7.58, 7.30	7.86, 7.72	7.23, 7.16

Table 17: NMR data for the 2-pyridyl systems in the facial isomers of 30, 31 and 32 in CD_3CN

2.2.3.3 UV-Vis Absorption Spectra of the facial and meridional Isomers of 30, 31 and 32

The UV-Vis absorption spectra of both geometric isomers of **30**, **31** and **32** are shown in Figure 112. The high energy region of the spectra is dominated by a ligand centred $\pi \rightarrow \pi^*$ transition which in $[Fe(bpy)_3]^{2+}$ appears at λ 298 nm.[35] In general the same trends were observed for the iron complexes as were seen in the analogous spectra of the ruthenium complexes. The electron-withdrawing effect of the 4-pyridyl substituents in **31** appears to lower the energy of the π^* orbital and shift the absorbance maxima to a lower energy. The LC absorption maxima for the *fac* and *mer* isomers of **32** occur at slightly higher energy (λ 280 nm) than those of the other complexes. This can be attributed to the electron-donating effect of the methoxy substituents. The broadness in these LC absorptions may be due to reduction in symmetry arising from metal complexation by the ligands. This may give rise to a number of closely-spaced individual π^* orbitals on the ligand which would result in broadness in the absorption spectrum. A consistent shift is observed for all the complexes when comparing the facial with the meridional isomers of each compound. The meridional isomers appear to have a slightly lower energy absorbance maximum than their facial analogues.

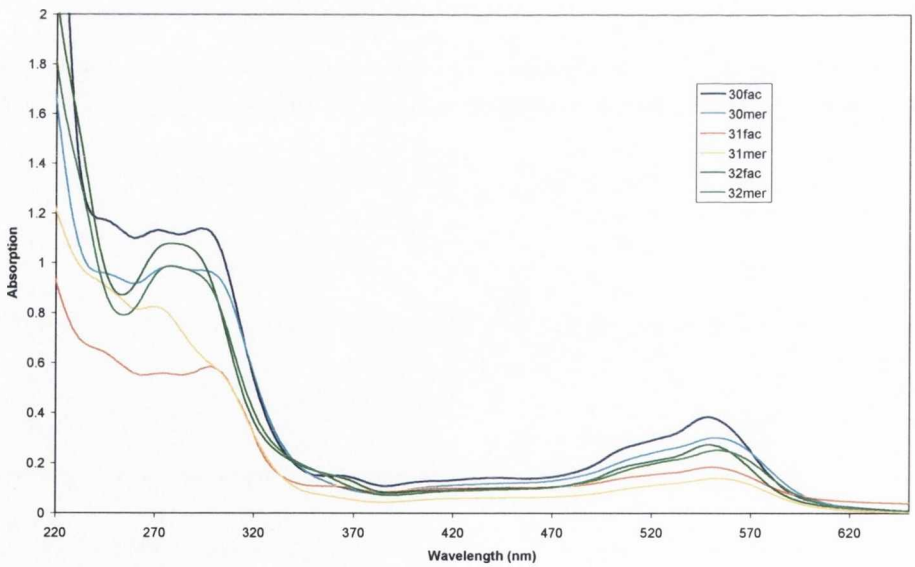


Figure 112: UV-Vis Absorption Spectra of both isomers of 30, 31 and 32 in MeCN

The visible region of the absorption spectra of compounds **30**, **31** and **32** is shown in Figure 113. The MLCT absorption is at lower energy for the *mer* isomers compared to the *fac* isomers of each complex. The facial isomers also have a consistently higher extinction coefficient which arises due to the slightly higher LUMO orbitals on the ligand

for these complexes. The electron-donating effect of the methoxy, and the electron-withdrawing effect of the 4-pyridyl substituents can be observed by the slight shift in the absorption maxima of the MLCT for these compounds compared with the phenyl substituted pyridazine ligands in **31**.

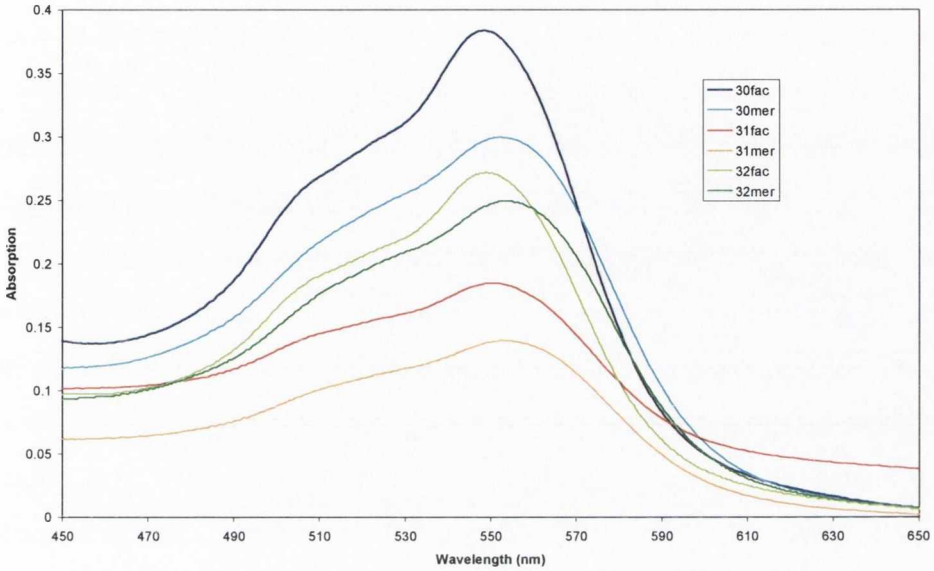


Figure 113: The Low Energy Region of the UV-Vis Spectra of *fac* and *mer* isomers of 30, 31 and 32 in MeCN

The absorption maxima are summarised in Table 18:

Compound	Wavelength *nm* (absorbance $M^{-1}cm^{-1}$)		
	LC $\pi\rightarrow\pi^*$	MLCT $\pi\rightarrow\pi^*$	MLCT $d\pi\rightarrow\pi$
30 *fac*	291 (113,270)	365 (13,700)	547 (38,290) 505 (25,600)
30 *mer*	297 (95,500) 276 (98,400)	-	550 (29,860) 508 (21,280)
31 *fac*	296 (60,500) 272 (55,800)	363 (12,200)	549 (18,480) 508 (14,350)
31 *mer*	267 (82,380)	-	552 (13,950)
32 *fac*	280 (107,500)	360 (13,300)	549 (27,100) 513 (19,500)
32 *mer*	278 (98,600)	-	556 (26,400)

Table 18: The UV-Vis Absorption maxima associated with the Fe (II) *tris* Iron Complexes 30, 31 and 32

2.3 Conclusion

Five Ru(II) *bis* bpy complexes have been prepared and characterised and their electrochemical and spectroscopic properties examined. The ^{1}H-NMR spectral assignment of these complexes was successfully carried out by comparison with the deuterated *bis* bipyridyl analogues. The UV-Vis spectroscopy and electrochemistry of these compounds were compared to those of similar compounds in the literature.

The ruthenium *tris* complexes of three ligands were carried out as was the subsequent separation of the meridional and facial isomers. Some differences were noted between the facial and meridional isomers of each complex, with the *mer* isomer of each complex consistently absorbing and emitting at lower energy. The substituents on the 4- and 5-positions of the pyridazine ring of the ligand had only a small effect on the absorption spectra of these compounds.

The iron analogues of these pyridazine centred ligands were also prepared and characterised. The spectroscopic properties of both *fac* and *mer* isomers of these iron(II) complexes were also measured and compared.

2.4 References

[1] F. Blau, *berichte* **1888**, *21*, 1077.

[2] F. Blau, *Monatshefte fuer Chemie* **1898**, *19*, 647.

[3] F. Li, M. Wang, P. Li, T. Zhang, L. Sun, *Inorg. Chem.* **2007**, *46*, 9364.

[4] S. Ernst, W. Kaim, *Inorg. Chim. Acta* **1986**, *114*, 123.

[5] R. J. Crutchley, A. B. P. Lever, *Inorg. Chem.* **1982**, *21*, 2276.

[6] S. Ernst, W. Kaim, *J. Am. Chem. Soc.* **1986**, *108*, 3578.

[7] H. Ait-Haddou, E. Bejan, J.-C. Daran, G. G. A. Balavoine, F. Berruyer-Penaud, L. Bonnazzola, H. Smaooui-Chaabouni, E. Amouyal, *J. Chem. Soc., Dalton Trans.* **1999**, 3095.

[8] A. Juris, V. Balzani, F. Barigalletti, C. S., P. Belser, A. Von Zelewsky, *Coord. Chem. Rev.* **1988**, *84*, 85.

[9] A. Islam, H. Sugihara, L. P. Singh, K. Hara, R. Katoh, Y. Nagawa, M. Yahigda, Y. Takahashi, S. Murata, H. Arakawa, *Inorg. Chim. Acta* **2001**, *322*, 7.

[10] R. Konduri, H. Ye, F. M. MacDonnell, S. Serroni, S. Campagna, K. Rajeshwar, *Angew. Chem. Int. Ed.* **2002**, *41*, 3185.

[11] M. K. Brennaman, T. J. Meyer, J. M. Papanikolas, *J. Phys. Chem. A* **2004**, *108*, 9938.

[12] V. Balzani, A. Juris, M. Venturi, S. Campagna, S. Serroni, *Chem. Rev.* **1996**, *96*, 759.

[13] V. Balzani, S. Campagna, *Photochemistry and Photophysics of Coordination Compounds I*, Springer, **2007**.

[14] F. Barigelletti, L. d. Cola, V. Balzani, P. Belser, A. v. Zelewsky, F. Vogtle, F. Ebmeyer, S. Grammenudi, *J. Am. Chem. Soc.* **1989**, *111*, 4662.

[15] P. A. Anderson, R. F. Keene, T. J. Meyer, J. A. Moss, G. F. Strouse, J. A. Treadway, *J. Chem. Soc., Dalton Trans.* **2002**, 3820.
[16] D. P. Rillemna, C. B. Blanton, R. J. Shaver, D. C. Jackman, M. Boldaji, S. Bundy, L. A. Worl, T. J. Meyer, *Inorg. Chem.* **1992**, *31*, 1600.
[17] S. D. Ernst, W. Kaim, *Inorg. Chem.* **1989**, *28*, 1520.
[18] S. Ernst, W. Kaim, *Angew. Chem. Int. Ed.* **1985**, *24*, 430.
[19] R. J. Crutchley, A. B. P. Lever, *J. Am. Chem. Soc.* **1980**, *102*, 7128.
[20] E. Ioachim, E. A. Medlycott, G. S. Hanan, F. Loiseau, V. Ricevuto, S. Campagna, *Inorg. Chem. Commun.* **2005**, *8*, 559.
[21] S. Ghumann, B. Sarkar, S. Patra, K. Parimal, J. v. Slageren, J. Fiedler, W. Kaim, G. K. Lahiri, *J. Chem. Soc., Dalton Trans.* **2005**, 706.
[22] G. Denti, S. Campagna, L. Sabatino, S. Serroni, M. Ciano, V. Balzani, *Inorg. Chem.* **1990**, *29*, 4750.
[23] G. D. Hager, G. A. Crosby, *J. Am. Chem. Soc.* **1975**, *97*, 7031.
[24] C. H. Braunstein, A. D. Baker, T. C. Strekas, H. D. Gafney, *Inorg. Chem.* **1984**, *23*, 857.
[25] P. A. Anderson, G. B. Deacon, K. H. Haarmann, F. R. Keane, T. J. Meyer, D. A. Reitsma, B. W. Skelton, G. F. Strouse, N. C. Thomas, J. A. Treadway, A. H. White, *Inorg. Chem.* **1995**, *34*, 6145.
[26] D. P. Rilemna, G. Allen, T. J. Meyer, D. Conrad, *Inorg. Chem.* **1983**, *22*, 1617.
[27] F. A. Cotton, G. Wilkinson, C. A. Murillo, M. Bochmann, *Advanced Inorganic Chemistry*, Sixth ed., Wiley-Interscience, **1999**.
[28] E. Konig, *Coord. Chem. Rev.* **1968**, *3*, 471.
[29] H. Irving, D. H. Mellor, *J. Chem. Soc.* **1962**, *1962*, 5222.
[30] J. K. McKusker, K. N. Walda, R. C. Dunn, J. D. Simon, D. Magde, D. N. Hendrickson, *J. Am. Chem. Soc.* **1993**, *115*, 298.
[31] M. A. Bergkamp, B. S. Brunschwig, P. Gutlich, T. L. Netzel, N. Sutin, *Chem. Phys. Lett.* **1981**, *81*, 147.
[32] S. Ferrere, *J. Am. Chem. Soc.* **1998**, *120*, 843.
[33] M. K. Nazeeruddin, A. Kay, I. Rodicio, R. Humphrey-Baker, E. Müller, P. Liska, N. Vlachopoulos, M. Grätzel, *J. Am. Chem. Soc.* **1993**, *115*, 6382.
[34] C. Creutz, M. Chou, T. L. Netzel, M. Okumura, N. Sutin, *J. Am. Chem. Soc.* **1980**, *102*, 1309.
[35] R. A. Kirgan, D. P. Rillemna, *J. Phys. Chem. A* **2007**, *111*, 13157.
[36] R. R. Ruminski, J. D. Petersen, *Inorg. Chim. Acta* **1985**, *97*, 129.
[37] A. B. P. Lever, J. Lewis, R. S. Nyholm, *J. Am. Chem. Soc.* **1964**, 1187.
[38] S. Ferrere, *Inorg. Chim. Acta* **2001**, *329*, 79.
[39] D. Onggo, A. D. Rae, H. A. Goodwin, *Inorg. Chim. Acta* **1990**, *178*, 151.
[40] A. Werner, A. Hantsch, *Berichte der Deutschen Chemischen Gesellschaft* **1890**, *23*, 11.
[41] N. C. Fletcher, *J. Chem. Soc., Perkin Trans. 1* **2002**, 1831.
[42] T. J. Rutherford, P. A. Pellegrini, J. Aldrich-Wright, P. C. Junk, F. R. Keene, *Eur. J. Inorg. Chem.* **1998**, 1677.
[43] D. Hesekittoshi, Y. Inoue, S. R. L. Everitt, H. Ishida, M. Kunieda, M. G. B. Drew, *Inorg. Chem.* **2000**, *39*, 317.
[44] F. R. Keene, *Chem. Soc. Rev.* **1998**, *27*, 185.
[45] A. v. Zelewsky, O. Mamula, *J. Chem. Soc., Dalton Trans.* **2000**, 219.
[46] L. S. Kelso, D. A. Reitsma, F. R. Keene, *Inorg. Chem.* **1996**, *35*, 5144.
[47] E. A. P. Armstrong, R. T. Brown, M. S. Sekwale, N. C. Fletcher, X.-Q. Gong, P. Hu, *Inorg. Chem.* **2004**, *43*, 1714.

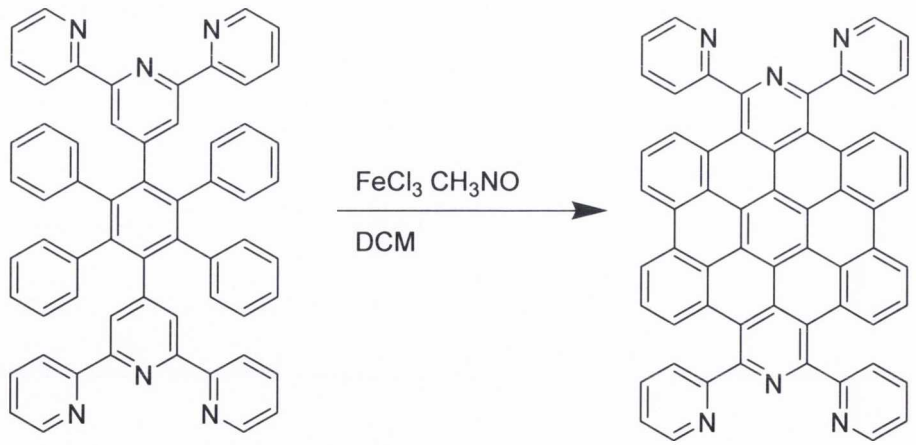
[48] M. Kyakuno, S. Oishi, H. Ishida, *Inorganic Chemistry* **2006**, *45*, 3756.
[49] H. Weizman, J. Libman, A. Shanzer, *J. Am. Chem. Soc.* **1998**, *120*, 2188.
[50] N. C. Fletcher, M. Nieuwenhuyzen, *J. Chem. Soc., Chem. Commun.* **2002**, 1188.
[51] R. Ragni, E. a. Plummer, K. Brunner, J. W. Hofstraat, F. Babudri, G. M. Farinola, F. Naso, L. D. Cola, *J. Mater. Chem.* **2006**, *16*, 1161.
[52] M. Kyakuno, S. Oishi, H. Ishida, *Inorg. Chem.* **2006**, *45*, 3756.
[53] N. C. Fletcher, M. Nieuwenhuyzen, S. Rainey, *J. Chem. Soc., Dalton Trans.* **2001**, 2641.
[54] R. T. Brown, N. C. Fletcher, M. Nieuwenhuyzen, T. E. Keyes, *Inorg. Chim. Acta* **2005**, *358*, 1079.
[55] T. L. Borgne, P. Altmann, N. Andre, J.-C. G. Bunzli, G. Bernadinelli, P.-Y. Morgantini, J. Weber, C. Piguet, *J. Chem. Soc., Dalton Trans.* **2004**, 723.
[56] J. G. Eaves, H. S. Munro, D. Parker, *Inorg. Chem.* **1987**, *26*, 644.
[57] M. Krejcik, S. Zalis, J. Klima, D. Sykora, W. Matheis, A. Klein, W. Kaim, *Inorg. Chem.* **1993**, *32*, 3362.
[58] G. Tresoldi, S. L. Schiavo, P. Piraino, *Inorg. Chim. Acta* **1997**, *254*, 381.
[59] G. Predieri, C. Vignali, G. Denti, S. Serroni, *Inorg. Chim. Acta* **1993**, *205*, 145.
[60] S. Torelli, S. Delahaye, A. Hauser, G. Bernadinelli, C. Piguet, *Chem. Eur. J.* **2004**, *10*, 3503.
[61] E. C. Glazer, Y. Tor, *Angew. Chem. Int. Ed.* **2002**, *41*, 4022.
[62] G. Orellana, C. A. Ibarra, J. Santoro, *Inorg. Chem.* **1988**, *27*, 1025.
[63] F. Barigelletti, A. Juris, V. Balzani, P. Belser, A. v. Zelewsky, *Inorg. Chem.* **1987**, *26*, 4115.
[64] R. Hage, J. H. v. Diemen, G. Ehrlich, J. g. Haasnoot, D. J. Stufkens, T. L. Snoeck, J. G. Vos, J. Reedijk, *Inorg. Chem.* **1990**, *29*, 989.
[65] J. K. M. Sanders, B. K. Hunter, *Modern NMR Spectroscopy - A Guide For Chemists*, Oxford University Press, **1987**.
[66] I. R. Laskar, S.-F. Shu, T.-M. Chen, *Polyhedron* **2005**, *24*, 189.

Chapter 3

Phenyl-Centred Fluorenol Derivatives and Related Compounds

3.1 Introduction

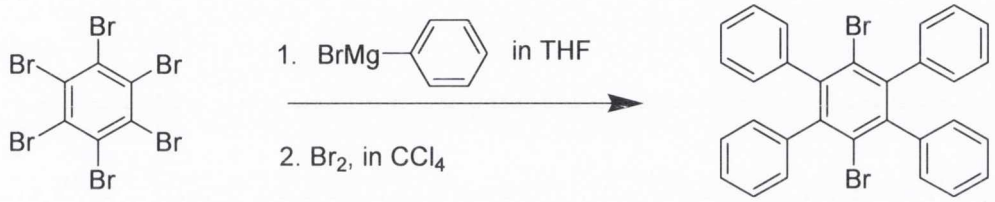
The pyridazine centred ligands prepared in chapter 1 were synthesised as precursors to novel N-HSB type target compounds. However despite several attempts using many different methods, the cyclodehydrogenation step was largely unsuccessful and cyclisation of the ligands did not occur. The reasoning behind this is unclear - however it was evident from similar work in the group that difficulties arise when heteroatoms are present in the central ring.[1] This may be because preferential protonation of the nitrogen atoms reduces the possibility of subsequent protonation of the phenyl rings. These protonated nitrogen rings are also very poor nucleophiles, which makes the ring-closure step difficult as the bonds between the all-carbon and nitrogen-containing aromatic rings cannot be formed.[2] Clearly, the success of the initial work on the cyclodehydrogenation of carbon-centred polyphenylene compounds and the nitrogen containing heterosuperbenzenes implies that the reaction can be quite successful when phenyl-centred precursors are employed.[3, 4] This led the synthetic aims of the project to change track, and a move away from pyridazine-centred ligands in favour of phenyl centred precursors which incorporated heteroatoms at the periphery. In particular, the incorporation of a terpyridine unit on either side of a tetraphenyl-substituted benzene was seen as a suitable precursor for a novel nitrogen containing heterosuperbenzene (Scheme 36).



Scheme 36: The proposed synthesis of a novel nitrogen containing phenyl centred aromatic hydrocarbon

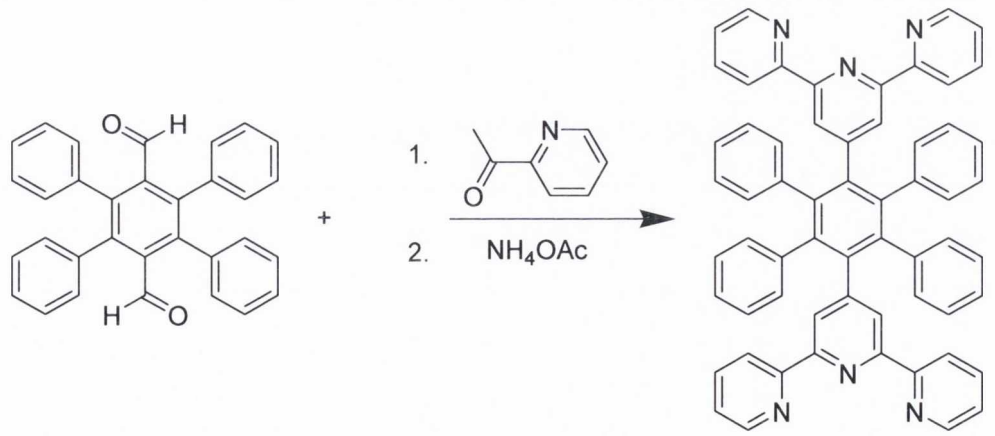
The synthesis of 1,4-di-4'-(2,2':6',2"-terpyridyl)-2,3,5,6-(tetraphenyl) benzene could be undertaken in a number of ways. There are two fundamental strategic methods possible in the synthesis of functionalised terpyridines – palladium catalysed cross-coupling addition

of the functional group to the terpyridine such as Stille, Suzuki or Negishi coupling reactions, or the *in situ* formation of a terpyridine via ring-assembly condensation type reactions. If the former were to be employed in this case it would require two separate syntheses of a functionalised terpyridine and of an appropriately functionalised tetraphenyl substituted benzene. The functionalisation of terpyridines with halides, boronic acids and various other groups has been well-documented in the literature. The synthesis of suitably functionalised tetraphenyl benzenes is far less prevalent. Indeed, with regard to functional groups suitable for coupling reactions, the only precedent was the preparation by Hart and co-workers of 1,4-dibromo-2,3,5,6-tetraphenyl benzene (Scheme 37).[5]



Scheme 37: The synthesis of 1,4-dibromo-2,3,5,6-tetraphenyl benzene

This one step multi-Grignard reaction yields the desired product in 50% yield, however the inaccessibility and cost of the starting material precluded this starting point. The most straightforward synthetic route therefore was deemed to be *via* a ring-formation type synthesis starting with a tetraphenyl substituted dicarboxaldehyde (Scheme 38).



Scheme 38: The synthetic route towards 1,4-di-4'-(2,2':6',2''-terpyridyl)-2,3,5,6-(tetraphenyl) benzene

This dicarboxaldehyde had not been previously reported, and the first part of this chapter describes some of the methods used in its attempted synthesis. Most of the chemistry attempted here involved a Diels-Alder reaction using a cyclopentadienone functionalised at the 1- and 4- positions and reacting this with diphenyl acetylene to form the central

benzene ring. This was followed by the attempted oxidation at the *para* positions of the resulting substituted benzene in order to prepare the carboxaldehyde. It was also desirable to incorporate heteroatoms into the system and to this end, 1,2-bis-(5-pyrimidyl)ethyne was used as an alternative dienophile in the Diels-Alder reaction stage of the process. This would allow for the potential to cyclodehydrogenate these smaller phenyl-centred compounds, with the possibility of using them as ligands in metal complexes.

3.1.1 Introduction to Terpyridines

The synthesis of terpyridines has been known since the early 1930s but the recent explosion of interest in the area of supramolecular chemistry has seen a dramatic increase in the popularity of these compounds. Most of this has arisen due to the interesting photophysical properties associated with the metal complexes of these ligands. 2,2':6',2''-terpyridine is a tridentate chelating ligand and extensive coordination chemistry has been carried out involving transition metals.[6]

Although other isomers of terpyridine exist, this is the most common variant in the literature due to the strategic positioning of the donor atoms and the possibility of functionalisation at the 4'- position. Hence, the term terpyridine or tpy shall refer only to this isomer during the course of this work.



Scheme 39: 2,2':6'2'' terpyridine

The properties of the metal complexes of terpyridine compounds are particularly sensitive to the electronic influences of the substituents on the terpyridyl unit. Electron withdrawing groups can improve the luminescent properties of metal complexes and this feature has been used in the development of sensitizers for energy conversion.[7] Aryl substituents increase the extinction coefficient of the metal to ligand charge transfer in terpyridyl metal complexes.[8] Chiral terpyridines are currently being used in the area of enantioselective synthesis, and functionalised terpyridines have been applied in asymmetric catalysis.[9, 10] Terpyridines have a wide range of applications in medicinal chemistry, as DNA binding agents and in anti-cancer research.[11, 12] In addition, lanthanide complexes of terpyridines have been used as protein labelling agents and the ligand has also been used in the colorimetric determination of metals.[13] However it is the

recent shift from molecular to supramolecular chemistry that has seen terpyridine assume a role at the forefront of chemical research. Diterpyridines which have the capability to coordinate linearly to two metals have potential applications as molecular nanowires, and similar "back to back" ligands coordinated to different metals such as ruthenium and osmium exhibit highly efficient energy transfer properties.[14, 15] When the terpyridyl unit includes a non-linear functionality, the possibility of two- and three- dimensional structures with applications as light-harvesting devices has been investigated.[16]

3.1.2 Synthetic Routes Towards Terpyridines

3.1.2.1 Coupling Methods

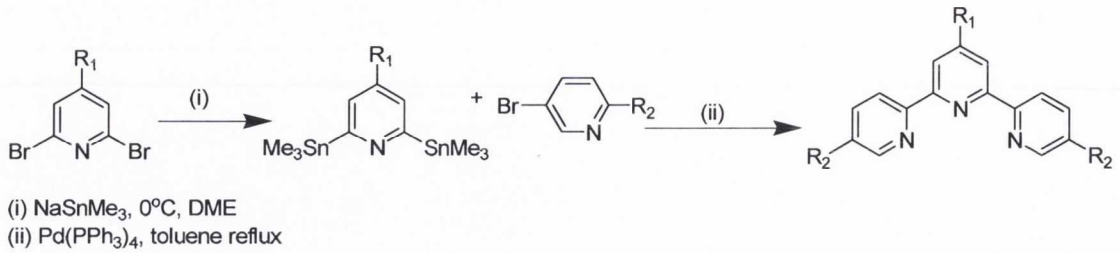
The earliest reported synthesis of a terpyridyl molecule was that of Morgan and Burstall in 1932.[17] In their efforts to improve the large scale synthesis of 2,2'-bipyridine first reported by Blau in the late 19th century, they reacted pyridine and iron(III) chloride at high temperature and pressure and obtained over twenty products. One of these was identified as 2,2':6',2''-terpyridine which formed in poor yield initially as an iron complex but which was later isolated by treatment with caustic soda. Later attempts using copper, iodine or Raney nickel as coupling agents typically resulted in yields lower than 10%.[18] Subsequent methods involved the coupling of 6-bromo-2,2'-bipyridine with a lithiated pyridine to give terpyridine in 36% yield.[19]



Scheme 40: The coupling of 6-bromo 2,2' bipyridine with pyridine[19]

With the use of a slight modification involving a sulfinyl moiety in place of the bromo group, and the use of a Grignard reagent rather than a lithiation, this yield was increased to 65%.[20] More modern coupling techniques include palladium catalysed Stille and Negishi style reactions.[21, 22] The Stille coupling in particular has found favour with terpyridine synthetic chemists, due to its ease of scale-up and the possibility to functionalise at various positions on the pyridyl rings (Scheme 41). For example a variety of functional groups were employed in the synthesis of 4- substituted terpyridines by stannylating the 2,6-dibromo-4-substituted pyridyl precursor and reacting this with a halogenated pyridine in a 1:2 ratio in the presence of a palladium catalyst.[23] In this way a number of functionalities could be incorporated into the 4'- position such as carboxylic

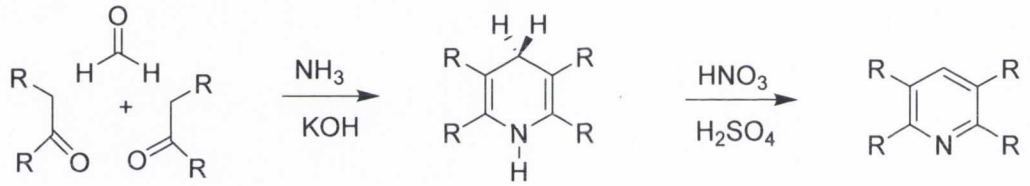
acids and esters. In addition, other functional groups could be incorporated onto the two terminal pyridine rings giving rise to a large array of substituted terpyridines via this method.



Scheme 41: The Stille coupling of substituted terpyridines

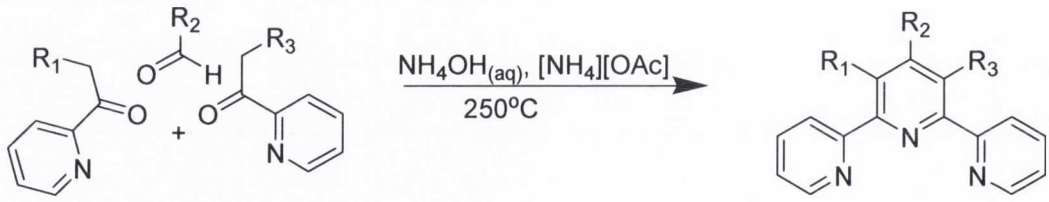
3.1.2.2 Ring Formation

The most popular method for the formation of pyridyl ring systems is known as the Hantzsch synthesis.[24] This involves the condensation of two equivalents of a 3-oxocarboxylate ester with one equivalent of an aldehyde followed by a ring closing step using a base such as ammonia and a final oxidation step (Scheme 42).



Scheme 42: The Hantzsch synthesis of pyridines

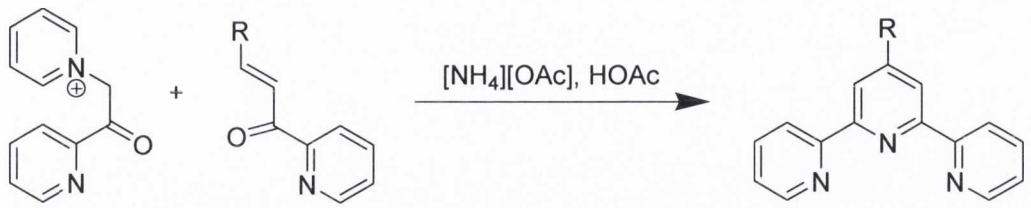
This method was further developed by Tschitschibabin which allowed for the one step isolation of the tpy using harsher conditions (Scheme 43).[25] Unfortunately this often results in lower yields and the potential for alternative products, due to the possible different arrangements of the precursors prior to the condensation step.



Scheme 43: The Tschitschibabin terpyridine synthesis

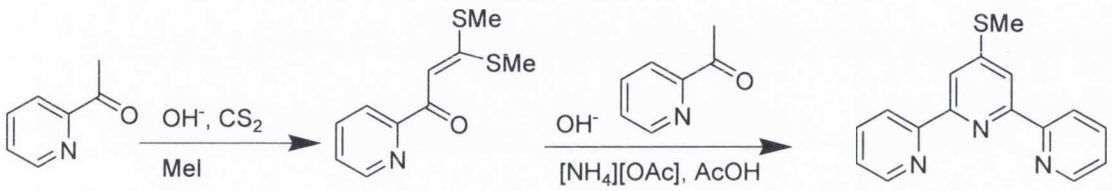
Multi-step syntheses were thus required in order to improve overall yields and also to allow for more subtle control of substituents, particularly if asymmetric tpy synthesis was to become a reality. To this end, the use of acylpyridinium salts has been investigated by Kröhnke.[26] These salts are prepared by reacting 2-acetyl pyridine with halides in

anhydrous solvent, and can then be reacted with suitably functionalised enones and ammonium acetate to give substituted tpys (Scheme 44).



Scheme 44: The Kröhnke use of pyridinium salts in tpy synthesis

The Potts method is another popular synthetic route to terpyridine compounds.[27] This procedure results in a high yield of 4'-methylthio-2,2':6':2"-terpyridine. 2-acetyl pyridine is reacted in basic media with CS_2 and MeI to form an α-oxoketene dithio acetal. This can then be reacted again with 2-acetyl pyridine and subsequent ring closure results in the terpyridine product (Scheme 45).



Scheme 45: The Potts Method of tpy Synthesis

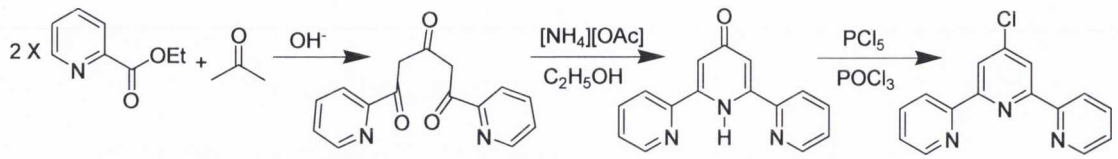
Recently many groups have taken on a "greener" approach towards the synthesis of a variety of terpyridines by simply grinding the ketones and the aldehyde with solid NaOH for 20 minutes in good yields and therefore avoiding the use of solvent or any large-scale reaction waste.[28]

3.1.2.3 Functionalised Terpyridines

One of the advantages of 2,2':6',2" terpyridine is the ability to add substituents to the 4'-position of the ligand and thus tune the properties of its metal complexes. In addition to this a variety of functional groups can be added to the two terminal pyridine rings including the formation of asymmetrical tpy compounds via the multistep methods discussed above. The recent surge in interest in supramolecular chemistry has only served to increase the desire for ligands with many functionalities and donor sites. As a consequence many functionalised tpy compounds have been prepared for a variety of applications.

Many of these compounds are prepared from the 4'-chloro-tpy and terpyridone first reported by Constable in the early 1990s.[29] By reacting two equivalents of ethyl 2-

pyridine with acetone in the presence of a strong base, 1,5-bis(2'-pyridyl)pentane-1,3,5-trione was formed. Subsequent ring closure with ammonium acetate gave a novel di-pyridyl substituted terpyridone, which was further reacted with phosphorous pentachloride in refluxing phosphoric trichloride to give 4-chloro-2,2':6',2" terpyridine.



Scheme 46: The synthesis of 4'-chloro-2,2':6',2" terpyridine

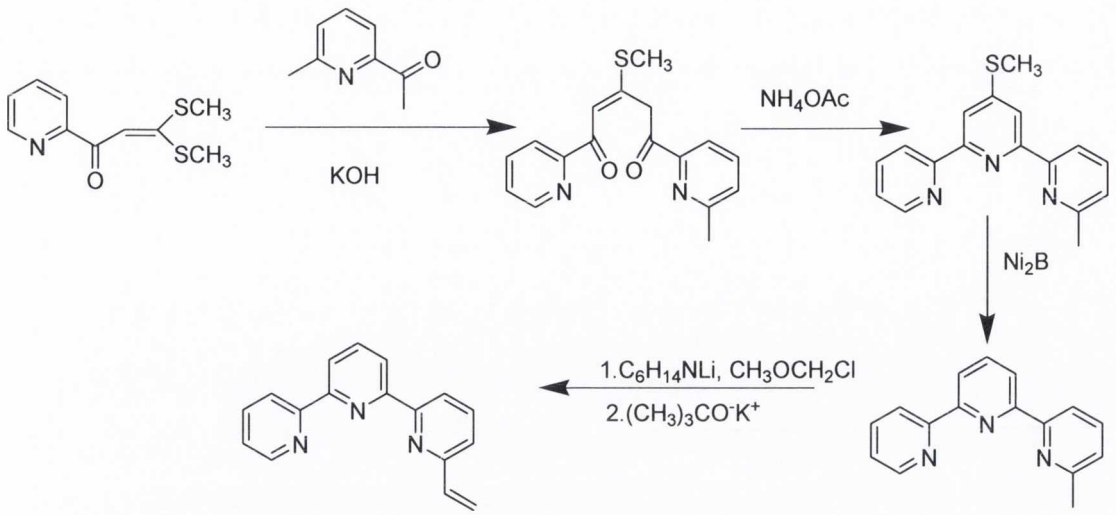
This halogenated terpyridine has proven to be a very useful starting material for the synthesis of a large array of 4'-functionalised tpy compounds.[30, 31]

A number of palladium-catalysed coupling reactions have been carried out using the bromo tpy analogue, notably the addition of ethynyl groups at the 4-position of tpy.[32]

Other useful functionalities at the 4'- position of tpy include the addition of a triflate group which was prepared directly from the terpyridone by reaction with triflouromethanesulfonic anhydride in pyridine.[33] This also proved to be a useful compound for interconversion of functional groups and can be used as a starting material in a palladium-catalysed coupling reactions.[34]

Substituents at the 4'- position on tpy can also be introduced using the central ring formation synthetic routes to tpy.[35] This method has worked for a variety of other functional groups such as *t*-butyl and *t*-butyl-phenyl and is limited only by the ability to functionalise the aldehyde or ketone.[36] Other functionalities added at the 4'- position via a ring formation reaction include phenyl and fluorophenyl groups.[37, 38]

Introducing substituents onto one of the outer rings of the tpy unit has also been achieved. Potts reports the synthesis of vinyl substituted tpy compounds by incorporating a methyl functionality in the 6- position at the ring formation stage by reacting 2-acetyl-6-methyl pyridine with Potts' dithioacetal compound discussed earlier (Scheme 47).[27]

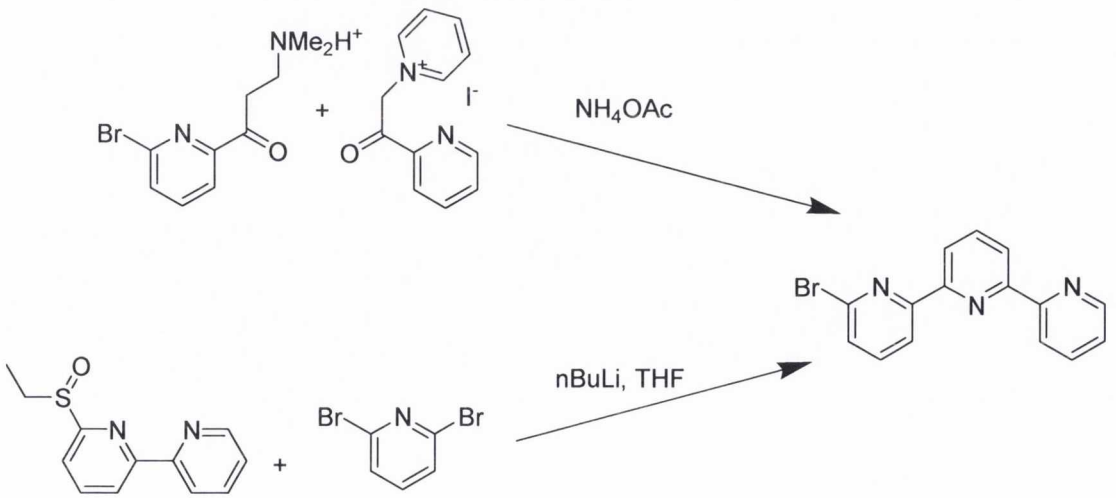


Scheme 47: The Potts method applied to asymmetricly substituted tpy compounds[27]

After the desulfurization step the methyl at the 6-position can be functionalised as required. In this case a chloromethyl ether is added in the presence of a base, and the ether is then removed to leave the vinyl substituted tpy.

Uenishi and co-workers prepared the useful 6-bromo tpy via coupling of 2,6-dibromo pyridine with ethyl bipyridyl sulfoxide in the presence of n-BuLi.[39] This provided a good platform for further functionalisation of the 6-position given the ability of the bromide to operate as an excellent leaving group in nucleophilic reactions.

Constable and co-workers prepared the same compound via a ring formation reaction using a pyridinium salt, and went on to use this tpy in the nickel templated synthesis of 2,2':6',2":6",2"':6"',2"":6"",2"""-sexipyridine.[40] Both of these methods of preparing mono-brominated tpy are summarised below in Scheme 48.

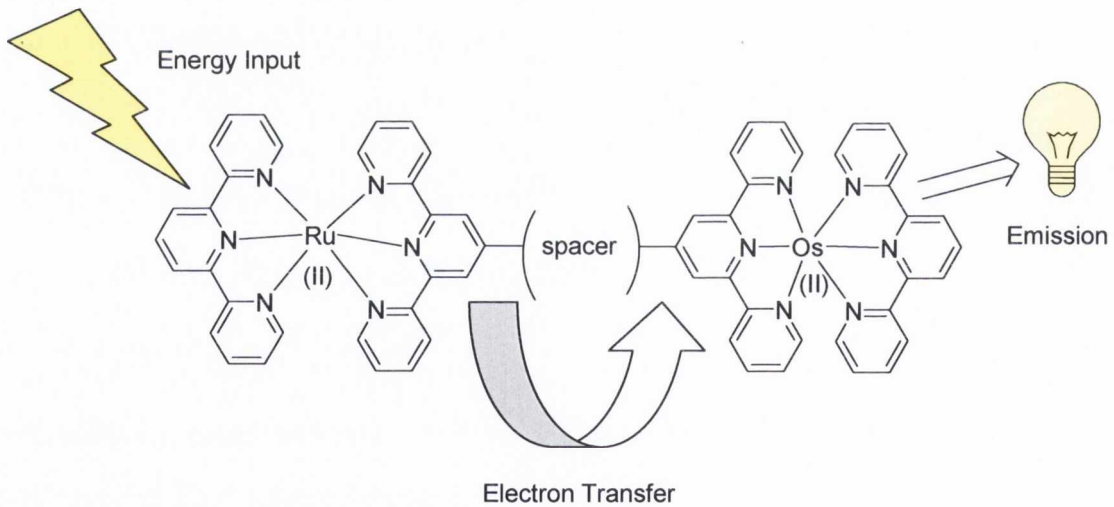


Scheme 48: Two alternative syntheses of 6-bromo-2,2':6':2'' terpyridine

Ring formation reactions are the preferred method of choice for the formation of symmetrically substituted tpy compounds. The alternative palladium coupling method could lead to difficulties due to the necessity to react at two positions on the molecule. Ring formations have the advantage of allowing the substituents to be added prior to formation of the tpy, and thus the number of by-products can be reduced.

3.1.2.4 Diads and "back-to-back" tpy ligands

Di-terpyridyl back-to back ligands have the capacity to coordinate to two metal centres and depending on the nature of the connectivity, these metals can interact with each other. Of particular interest is the interaction between a species coordinated with a ruthenium metal centre at one side and osmium at the other. If a $[Ru(tpy)_2]^{2+}$ species is connected to a similar species containing an osmium metal centre, excitation of the ruthenium species can result in the energy being transferred to the osmium species. This can then be measured in the osmium emission spectrum. These types of complexes are of particular interest due to their applications as energy transfer species or "molecular nanowires". Scheme 49 shows this principle in pictorial form.



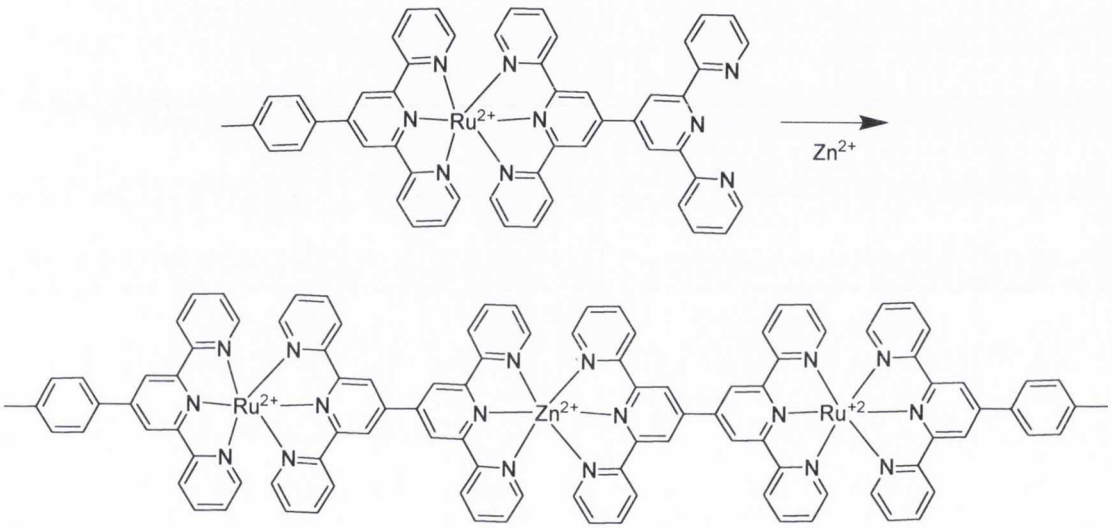
Scheme 49: The principle of electron transfer from ruthenium to osmium in terpyridine species

Many groups are investigating the effect of incorporating different unsaturated functional groups such as ethynyl units between two tpy moieties and investigating their ability to promote electron transfer.[41]

In addition to this, the possibility for novel supramolecular architectures and the preparation of a wide variety of macrocyclic systems with these ligands is extensive. Here the functional groups between the tpy units are required to be much more flexible

than the rigid frameworks required for molecular wire synthesis. Ether groups and long alkyl chains have been used extensively for this purpose.[6]

As early as 1959, Goodwin and Lions reported the synthesis of the first back-to-back tpy ligand, 2,3,5,6-tetrapyridylpyrazine. They also reported that binuclear complexes of this ligand could not be formed, although more recent studies have had more success in this area using ruthenium.[42] Constable reported the synthesis of 6',6"-bis(2-pyridyl)-2,2':4',4":2",2"'-quaterpyridine in a nickel-catalysed reaction from 4'-chloroterpyridine.[29] Although the *bis* ruthenium complex of this ligand was essentially non-luminescent, the coordination of zinc at the open tpy end of the molecule resulted in a ten-fold increase in the species luminescence (Scheme 50).[43]



Scheme 50: The coordination of Zn to a $[Ru(tpy)_2]^{2+}$ system

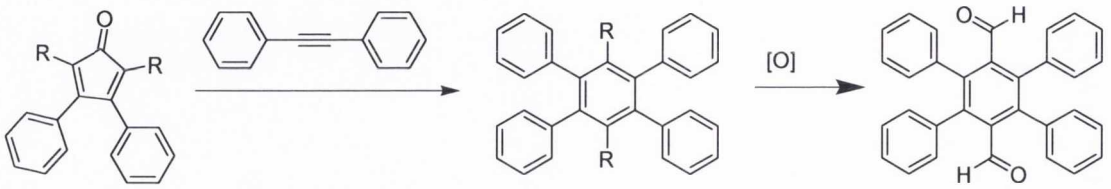
Further investigations in this area have included the incorporation of other coordinating units such as bpy between the linear tpy moieties. This appears to improve the luminescence when protonated.[44]

Back to back tpy ligands have also featured prominently in macrocyclic chemistry, with a variety of functional groups placed between the two tpy units resulting in numerous crystal structures of grids, racks and macrocycles.

3.1.3 Precursors to Phenyl-centred Terpyridyl Compounds

Of the possible routes available for the synthesis of terpyridines it was decided to adopt the ring formation Hantzsch-type synthesis involving a phenyl-centred dialdehyde and 2-acetyl pyridine (Scheme 38). The synthesis of this aldehyde would most likely involve a two-step procedure, whereby the first step would involve formation of the phenyl-centred

core with aromatic substituents in four positions, and two groups in two *para* positions which could be converted to aldehydes in a second step (Scheme 51). There is an enormous amount of literature available regarding the preparation of aldehydes from other functional groups, which allows for some variation in the preparation of the phenyl-centred precursors. These precursors are most accessible via Diels-Alder reactions of suitably substituted cyclopentadienones with acetylenes.

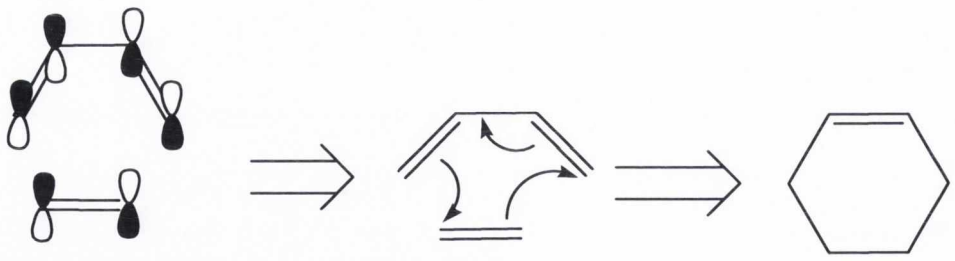


Scheme 51: Synthetic route towards 1,4-dicarboxy tetraphenyl benzene

3.1.4 Diels-Alder Reactions (Normal-Electron Demand)

Although Diels-Alder reactions have been introduced in Chapter 1, some of the following work discussed in this chapter involves a different form of this reaction commonly known as the "normal electron demand" Diels-Alder reaction.

In these reactions the appropriate π orbitals of the diene and the dienophile must overlap, and the electrons then move from the HOMO of the diene to the LUMO of the dienophile. In doing this the carbon atoms change from sp2 to sp3 hybridisation and two new σ-carbon bonds are formed in what is generally considered to be a concerted mechanism.[45]



Scheme 52: Schematic showing the overlap of p orbitals and the subsequent movement of electrons to form the new ring

Although the classic example used in these reactions is butadiene, any conjugated system can operate as the diene. The only requirement is that the orbitals of the diene and dienophile can overlap effectively and that the HOMO and LUMO energy difference between the two is small enough to allow for the transfer of electrons. To this end cyclic

dienes are commonly employed in this type of Diels-Alder reaction. Figure 114 highlights the relative reactivities of some common dienes towards Diels-Alder reactions.

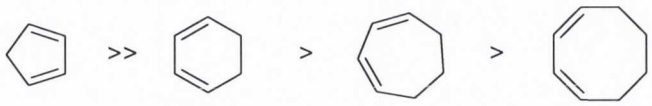


Figure 114: The relative reactivities of various cyclic dienes

The reactivity is reduced as the ring size increases due to the increased steric difficulty of overlap with the p or π orbitals of the dienophile. This overlap is most suitable in the case of cyclopentadiene which is consequently highly reactive towards Diels-Alder reactions. Indeed this compound reacts with itself in a Diels-Alder reaction at room temperature to form a bridged cyclic compound (Scheme 53).

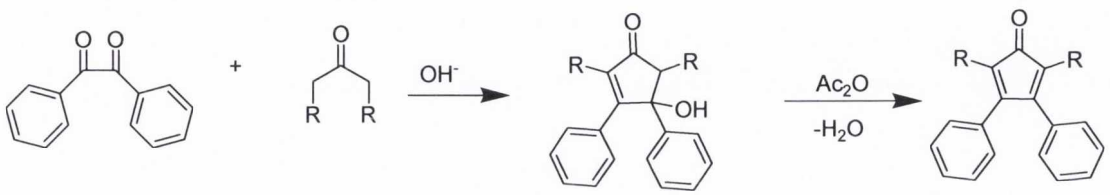


Scheme 53: The dimerization of cyclopentadiene at room temperature

Cyclopentadiene is also an effective diene when reacted with other dienophiles such as substituted alkenes and some acetylenes. The same trend applies here as discussed in Chapter 1 for the inverse-electron demand Diels-Alder reactions i.e. acetylenes are less reactive as dienophiles in comparison with their vinyl analogues.

When cyclopentadiene is functionalised at the methylene bridge with a carbonyl, the resulting compound known as cyclopentadienone, is also an excellent diene in Diels-Alder reactions. Furthermore, with the loss of CO gas during the reaction, it is also an excellent route towards substituted benzenes.

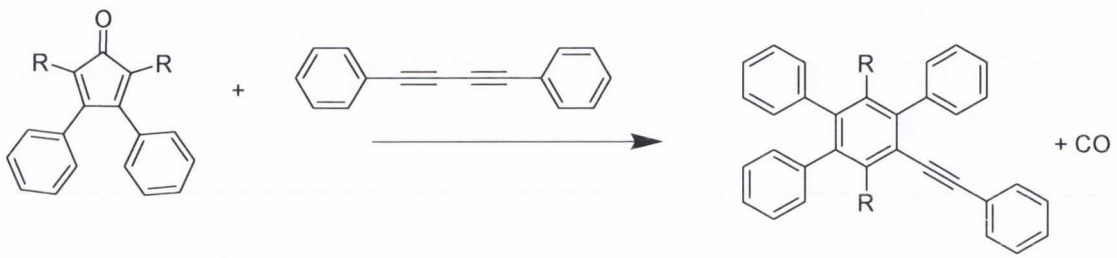
Substituted cyclopentadienones have been known since the 1940s and their use in the synthesis of substituted polyphenylenes has been discussed in Chapter 1.[46] The synthesis of these compounds is usually carried out via a Knoevenagel condensation followed by a dehydration step (Scheme 54).



Scheme 54: The synthesis of a tetra substituted cyclopentadienone

Functional groups at the 2'- and 5'- positions on the central ring of the cyclopentadienone can be introduced from the monoketone starting material. When these R groups are small

the compound can further react to form a dimer as was the case for cyclopentadiene. In the case of larger groups, such as phenyl rings, or methyl ester functionalities this is not sterically feasible and the compound can be quite easily isolated as a monomer.[47] The cyclopentadienone monomer can then react with acetylenes or vinyl compounds in Diels-Alder reactions to give substituted benzene-centred compounds. The relative reactivity of phenyl, methyl and methylester substituted cyclopentadienones towards Diels-Alder reactions with diphenylbutadiyne is compared in Scheme 55. Those with smaller functional groups in the 2- and 5- positions are found to be more reactive.[48]



R Group	Reaction Temperature (°)	Yield (%)	Ref
Me	130	92	[48]
COOMe	180	70	[48]
Ph	315	60	[47]

Scheme 55: The relative reactivitites of three substituted cyclopentadienones towards Diels-Alder reactions with an acetylenic dienophile[47, 48]

Although this chemistry dates back to early in the last century, the advent of the "nano-age" and the desire to find novel nano-sized conducting materials has led to something of a renaissance in the synthesis of polyphenylene compounds. The normal-demand Diels-Alder reactions discussed offer very reliable, highly efficient synthetic routes towards polyphenylenes and they have played and continue to play an integral part in modern synthetic materials chemistry. The versatility of these reactions allows for a wide variety of functional groups to be incorporated onto the phenyl core, and in the context of this work, provides a number of different routes towards aldehyde synthesis.

3.1.5 Synthetic Routes Towards Aldehydes

There are two major routes for the preparation of aromatic aldehydes.[49] The first involves the direct addition of the formyl group to the aromatic ring, the second route is a less direct method which involves the conversion of other functionalities to aldehydes. This second route is more pertinent to the work reported here.

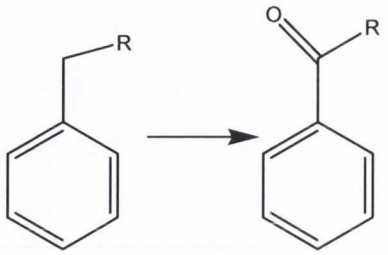
The aldehyde functionality is an extremely useful chemical group due its ability to act as a nucleophile and its easy conversion to dithioacetal, cyanohydrin and dithiane functional groups as well as its inherent ability to accept electrophiles.

The most common indirect synthetic route to preparing aromatic aldehydes is through oxidation of a methyl or alcohol group. The most popular method involves refluxing the methyl- or alcohol-functionalised starting material with chromium oxide in an acidic environment.[50]

Other reagents employed in converting methyl functional groups to aldehydes or ketones include dichloro dicyano quinone (DDQ) and potassium persulfate with copper sulfate.[51, 52] These methods are summarised in Scheme 56.

One of the difficulties in the direct oxidation of methyl groups to aldehydes is controlling the reaction such that the alcohol or carboxylic acid groups are not formed. The alternative is the formation of aldehydes via reduction of either the carboxylic acid or the ester.

The most common reagent used in the reduction of esters to aldehydes is a form of aluminium reducing agent, such as diisobutyl aluminium hydride (DIBAl).[50] Other aluminium reagents can be more effective e.g. the reduction of ethyl benzoate to benzaldehyde in 94% yield using lithium aluminium hydride.[53]



(R = H or alkyl)

Reagents	Reference
CrO_3, Ac_2O	[54]
CrO_3, HOAc, H_2SO_4	[54, 55]
$KMnO_4$, KOH, $(n\text{-}Bu_4N)HSO_4$	[56]
O_2, cat.	[57]
$RuCl_2(PPh_3)_3$, t-BuO_2H	[58]
DDQ	[52]
$K_2S_2O_8$, $CuSO_4$, H_2O	[51]

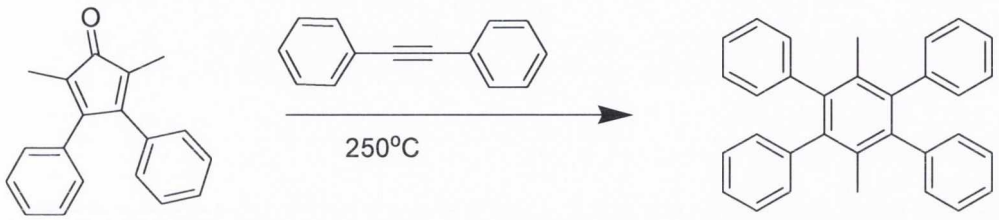
Scheme 56: Various literature methods of converting alkyl groups to aldehydes and ketones.

A number of reagents containing lithium have also been used in the reduction of carboxylic acids to aldehydes. Lithiumethylamine reduces a variety of saturated carboxylic acids but with limited stereospecificity.[59] Bedenbaugh and co-workers later improved on this by using a basic media which allowed for the isolation of the imine intermediate which was further hydrolysed to the aldehyde in good yield.[60] Other groups have used lithium tri-tert-butoxyaluminium hydride (LTBA) via the initial formation of the acid chloride using thionyl chloride and subsequently reducing this with LTBA.[61].

3.2 Results and Discussion

3.2.1 Diels-Alder Reactions of 2,4-dimethyl-3,5-diphenyl cyclopentadienone

The first approach taken towards the synthesis of the dicarboxaldehyde shown in Scheme 38 was to synthesise 1,2,4,5-tetraphenyl-3,6-dimethyl benzene (**33**) and attempt to oxidise the methyl functionalities to aldehydes. The synthesis of **33** was carried out via the Diels-Alder reaction between 2,4-dimethyl-3,5-diphenyl cyclopentadienone and diphenyl acetylene (Scheme 57).

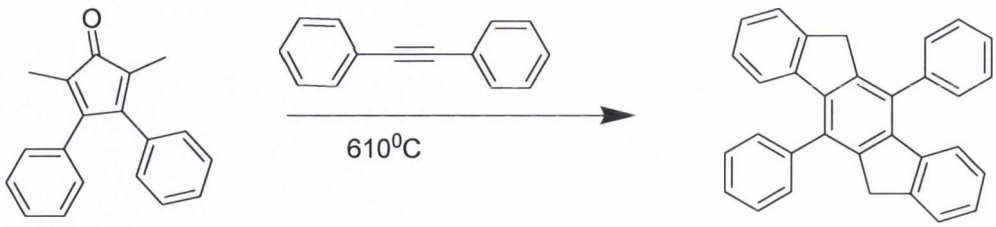


33

Scheme 57: The synthesis of 33

The cyclopentadienone exists as a dimer at room temperature and was reacted neat with a large excess of diphenylacetylene at 250°C for two hours. After washing with hexane the product was obtained in almost 100% yield. Compound **33** has been known since the 1960's, but has received some attention recently due to its use as a building block in hydrogen bonded molecular crystals.[62, 63] The compound was characterised by I.R. spectroscopy, melting point measurement and proton and carbon NMR spectroscopy.

This reaction was also carried out at a higher temperature (610°C) and TLC analysis after the reaction showed a different fluorescent product. The product was recrystallised from toluene and analysed by NMR spectroscopy and mass spectrometry. It was found to be the indenoflourene **34** (Scheme 58) which was obtained in 26% yield. This is a rather surprising result given that there is no base present in the reaction mixture to act as a proton acceptor. Nonetheless there is some precedent for these types of reactions in the literature.



34

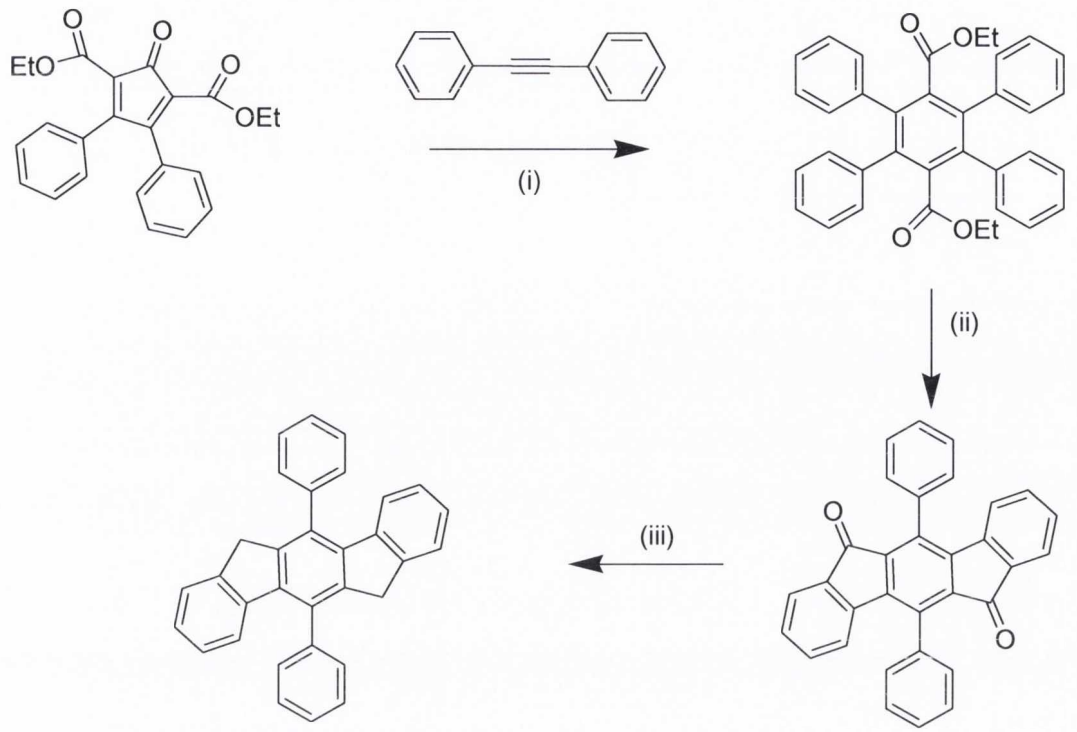
Scheme 58: The synthesis of 34

This reaction type may be described as a thermal cyclodehydrogenation, and was first discovered by Graebe when he prepared phenanthrene from stilbene at high temperature.[64]

Thermal cyclodehydrogenations usually occur in the gas–phase as a flash-vacuum pyrolysis (FVP) reaction. Very high temperatures are required for these reactions, although some reports indicate cyclodehydrogenation can occur at room temperature as observed by Bodwell in his investigation into the aromaticity of pyrene systems.[65] Scott investigated the mechanism associated with FVP reactions and concluded that the cyclodehydrogenation occurs via a [4n+2] electrolytic closure step.[66] However it remains unclear whether or not this can be applied to reactions in the liquid phase.

It seems unlikely that a gas phase reaction could occur at 650°C with these compounds. There appears to be no other reports in the literature of these types of reactions occurring in the liquid phase without the use of any other reagent.

At any rate this is a novel and simple route towards substituted indenofluorenes; as most literature preparations involve multistep syntheses. A number of substituted indenofluorenes, including **34**, were prepared by Wang and co-workers via a Diels-Alder reaction between diphenylacetylene and 2,5-diethylcarboxylate-3,4-diphenyl cyclopentadienone.[67] This was then oxidised to the carboxylic acid and converted to the diketone. A subsequent Wolf-Kischner reduction resulted in the indenoflourene in good yield (Scheme 59).



(i) DCM, reflux, 12 h, (78%). (ii) glacial AcOH, HBr, reflux, 48 h, then H_2SO_4 (90%), (iii) $N_2H_4.H_2O$, KOH, diethylene glycol, reflux, 24 H, (95%).

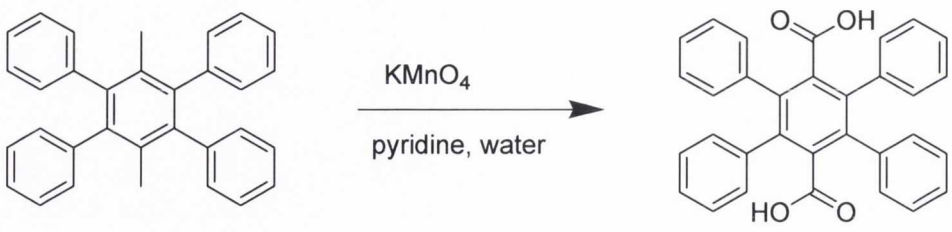
Scheme 59: The synthetic method of Wang towards substituted indenofluorenes

3.2.2 Attempted Oxidation of 33

Following the successful Diels-Alder formation of **33**, the following step towards a novel tpy compound involved the transformation of the two methyl substituents to aldehydes. **33** was refluxed in dry acetic acid with a large excess of chromium oxide, however no carboxaldehyde was retrieved. The same reaction was attempted using Brederick reagent, (*tert*-butoxy *bis*-dimethylamino-methane) in dry DMF and only the starting material was recovered.

Given the apparent failure of these reagents, it was decide to use harsher conditions and reagents, and if necessary to prepare the carboxylic acid and subsequently attempt a reduction. **33** was refluxed in dioxane with a large excess of SeO_2 and was then filtered after cooling. No product could be isolated from this mixture.

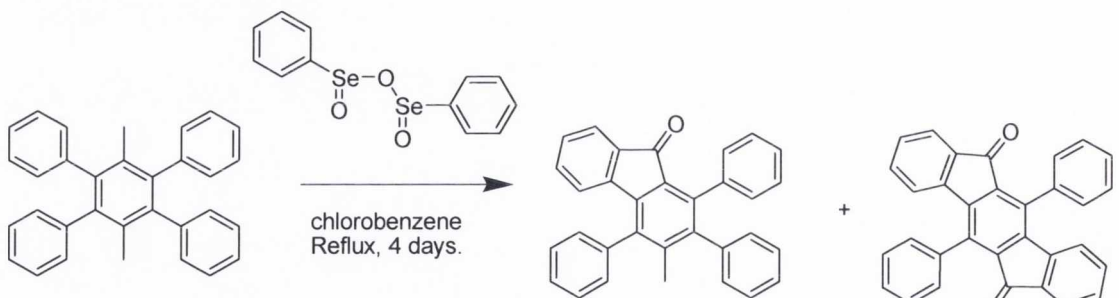
33 was then reacted with a large excess of $KMnO_4$ in pyridine and water and filtered while hot. The solvent was reduced *in vacuo* and a white precipitate formed upon addition of concentrated HCl. This solid was collected by filtration and analysed by ^{1}H-NMR and I.R. spectroscopy. It was found to be 1,2,4,5-tetraphenyl-3,6-dicarboxylate benzene (**35**).



33 **35**

Scheme 60: The synthesis of 35 via oxidation of 33

In a final attempt to oxidise the methyl functionalities directly to aldehydes, **33** was reacted with benzene seleninic anhydride in chlorobenzene. The reaction was refluxed for five days and the solvent was subsequently removed. TLC analysis clearly showed two new products. Purification by column chromatography yielded two products; one yellow compound in 37% yield and one red in 21% yield. The yellow product was subsequently identified by NMR spectroscopy and X-Ray crystallography as a novel compound, 1,2,4-triphenyl-3-methyl flouren-9-one (**36**). The red compound was identified as 5,11-diphenyl indeno[1,2b] fluoren-6,12-dione (**37**). This compound has been previously reported coincidentally in Wangs' synthesis of **34** (Scheme 59) but through a different synthetic route.[67] It was also reported by Padwa as an intermediate en route to a number of polysubstituted β-Napthols.[68]

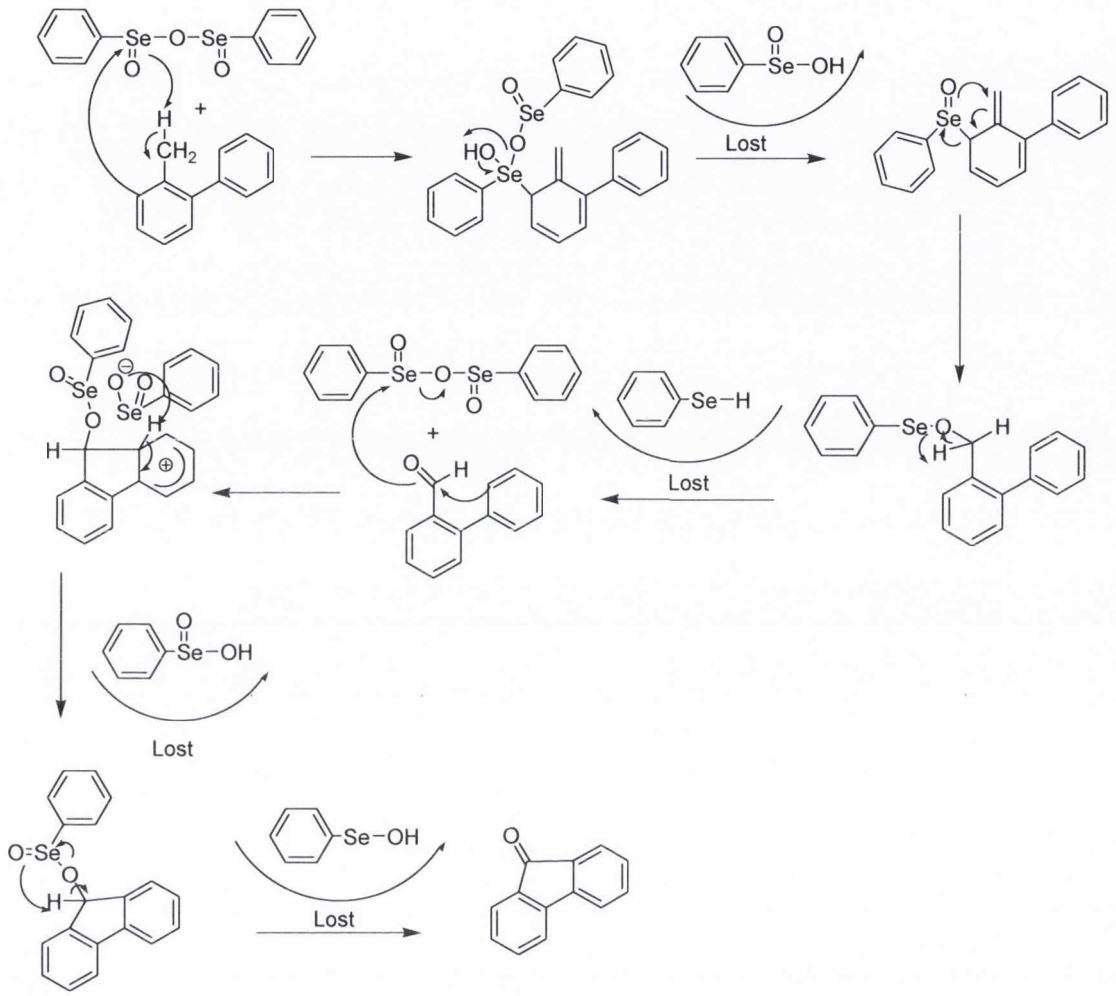


33 **36** **37**

Scheme 61: Synthesis of 36 and 37 from 33

One possible mechanism for this reaction is described in Scheme 62; the selenium reagent removes a proton from the methyl group and forms a bond with the neighbouring carbon on the central benzene ring. Subsequent loss of seleninic acid and nucleophilic attack of the remaining oxygen on the alkene carbon results in formation of an ether bond. Another equivalent of seleninic acid is then lost with removal of another proton from the methylene group which results in aldehyde formation. A second equivalent of benzene seleninic anhydride then attacks the carbonyl forming an SeO bond and resulting in nucleophilic attack from the *ortho* carbon on the neighbouring benzene ring on the

aliphatic carbon. One equivalent of seleninic acid is then lost in the (IV) oxidation state by removal of the proton on the adjacent *ortho* benzene ring. Finally, another equivalent of seleninic acid is lost with the removal of the remaining proton on the aliphatic carbon and allowing for the formation of a carbonyl bond, resulting in fluorenone formation.



Scheme 62: Proposed mechanism for the oxidative ring cleavage of 33 with benzene seleninic anhydride

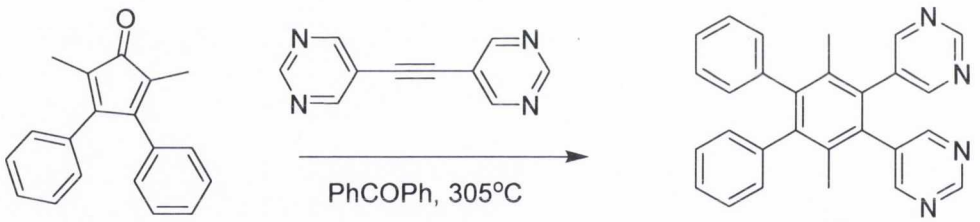
It must be stressed that there is no direct evidence for this mechanism; for example, no evidence of the aldehydic moiety was ever observed. Nonetheless, although this specific reaction appears to be unique in the literature, the pathway outlined above bears a lot of similarity with other selenium induced oxidations in the literature. MLochowski and co-workers review the oxidation mechanism of benzene seleninic anhydride and propose that they occur by the formation of an ester bond between the carbon and the selenium reagent, and the subsequent loss of both oxidation states of benzene seleninic acid.[69] A similar procedure was used by Barton and co-workers in the oxidation of alcohols to ketones, and their proposed mechanism bears much similarity to that outlined in Scheme 62.[70] This selenium reagent has also been used in the oxidation of methylene groups

directly to ketones by Rabideau and co-workers.[71] In this case aza-acenapthenes were converted to the corresponding quinones with the use of two equivalents of benzene seleninic anhydride.

Thus the overall formation of an ester bond followed by the removal of a proton and subsequent loss of acid appears to be well-documented. Less conclusive however is the likelihood of the removal of the proton on the *ortho* position of the neighbouring phenyl ring, and also the susceptibility of the aldehyde to nucleophilic attack by the selenium reagent. With regard to the latter, isolation of the mono-ketone **36** and the inability to isolate any aldehyde functionality would appear to indicate that the aldehyde is extremely unstable in the reaction environment and that stability is only brought about by fusion of the rings.

3.2.3 Incorporating other Functionalities onto the Phenyl centre

In an attempt to incorporate heteroatoms into the polyaromatic core, 1,2-bis-(5-pyrimidyl)ethyne was added to 2,5-dimethyl-3,4-diphenylcyclopentadienone in a Diels-Alder reaction in a similar matter to diphenylacetylene.

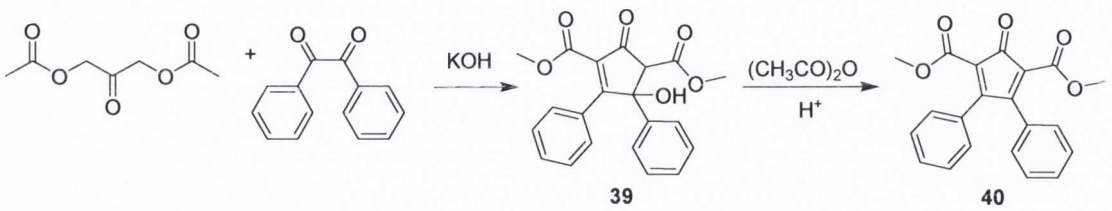


38

Scheme 63: The Diels-Alder reaction resulting in the formation of 38

The reagents were refluxed in benzophenone for 300 mns and purified by column chromatography to give a 72% yield of 3,6-dimethyl-1,2-di-(5-pyrimidyl)-4,5-diphenyl benzene (**38**).

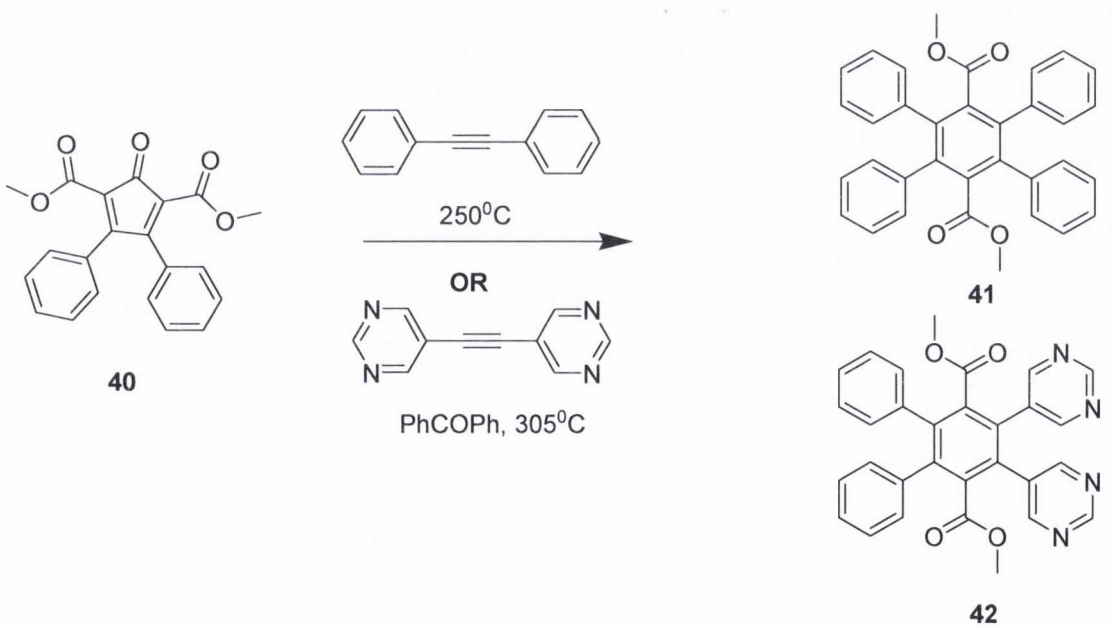
Given the lack of success with the oxidation of **33** to a di-aldehyde, it was desirable to incorporate other functional groups onto the benzene ring. One possibility was to prepare the 3,6-dimethyl ester benzene and attempt a reduction to the aldehyde. In order to do this, it was necessary to prepare the cyclopentadienone suitably functionalised with ester groups. This was carried out via a Knoevenagel condensation reaction and subsequent dehydration reaction.[48]



Scheme 64: The synthetic route towards di-ester substituted cyclopentadienone

The ester and diketone were heated with a base in ethanol for 24 hours and the product (**39**) was isolated by filtration. This compound was then added to a solution of acetic anhydride with one drop of concentrated H_2SO_4 and heated. The product, 2,5-dicarboxymethyl-3,4-diphenylcyclopentadienone (**40**) was recrystallised from acetic acid and characterised.

40 was then used as the diene in Diels-Alder reactions with diphenyl acetylene and 1,2-bis-(5-pyrimidyl)ethyne. The reaction with diphenyl acetylene was carried out by heating the two reagents at 250°C for 2 hours and then washed with hexane. The product, 1,2,4,5-tetraphenyl-3,6-dicarbomethoxy-benzene (**41**), was isolated in 88% yield. The reaction with 1,2-bis-(5-pyrimidyl)ethyne was carried out in benzophenone at 305°C for 5 hours. The product (**42**) was purified by column chromatography in 23% yield.



Scheme 65: The Synthetic routes towards 41 and 42

3.2.4 Reduction of Esters to Aldehydes

Given the lack of success with oxidation of methyl functional groups to aldehydes, another possible route was the reduction of the dicarbomethoxy ester **41**. Prasad and co-

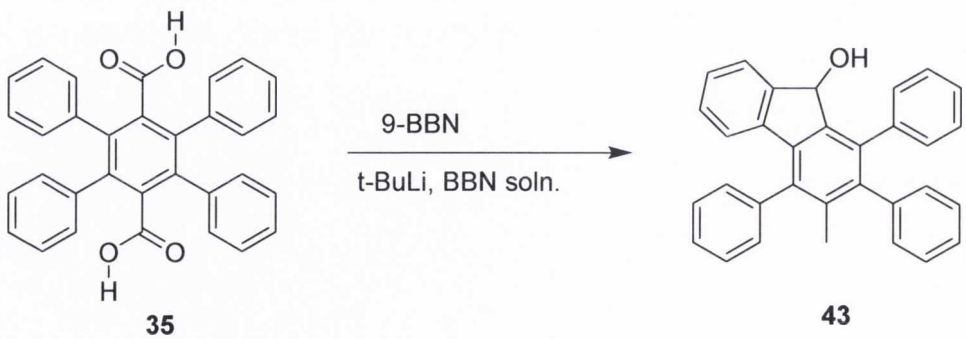
workers used $Ca(BH_4)_2$ successfully as a reducing agent of certain carboxylic acids to aldehydes.[72]

$Ca(BH_4)_2$ was prepared by the reaction of $NaBH_4$ with $CaCl_2$ in dry THF and was then directly added to a refluxing solution of **41** in THF containing a catalytic amount of COD. The COD catalyst is believed to improve reactivity by formation of the more stable BH_4^- moiety *in situ* which allows for more rapid exchange of the hydride species. The mixture was refluxed for 24 hours and quenched with methanol, however no product was obtained.

A second method was attempted using Red-Al and n-methyl piperazine as reducing agents. N-methyl piperazine was added to a toluene solution of Red-Al at 0°C. This was then added to a toluene solution containing **41** at -20°C and stirred for one hour. After quenching the reaction with water, only starting material was recovered.

3.2.5 Attempted Reduction of Carboxylic Acid to Aldehyde

After trying several attempts at reducing **41** to an aldehyde, it was hoped that the dicarboxylic acid **35** would be more reactive towards reduction. A solution containing 9-BBN dimer and **35** was cooled to -20°C, and t-BuLi and a second solution of 9-BBN was added.[73] The reaction was allowed to return to room temperature and stirred overnight. After quenching with water the reaction was purified by column chromatography, however no aldehyde was recovered. A 52 % yield of 2,3,5-tri phenyl-4-methyl fluorenol (**43**) was obtained, however. This compound was characterised by X-ray crystallography, mass spectrometry and NMR spectroscopy. The characterisation is discussed in the next section. Unusually, none of the equivalent di-fluorenol was obtained.

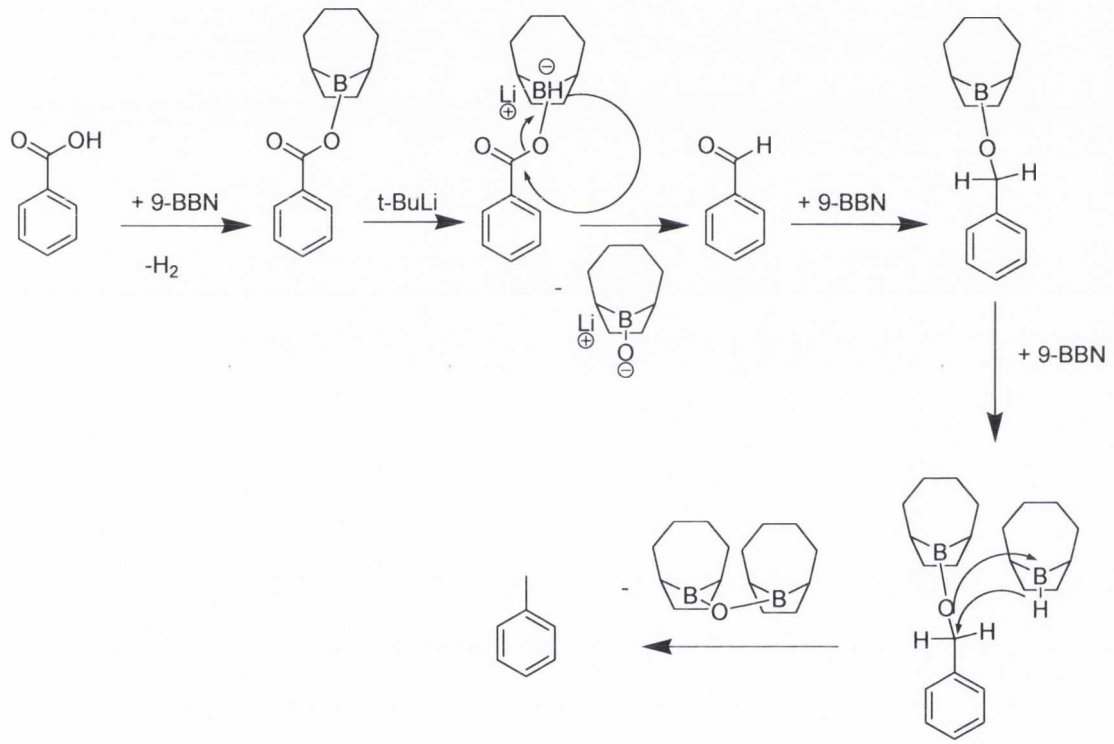


35 **43**

Scheme 66: The reduction of 35 to give fluorenol 43

In their reduction, Cha and co-workers claim that the second addition of 9-BBN encourages the migration of the hydride from the 9-BBN moiety to the carbon, but in this case, it appears the aldehyde may have been reduced again to an alcohol at one end and a

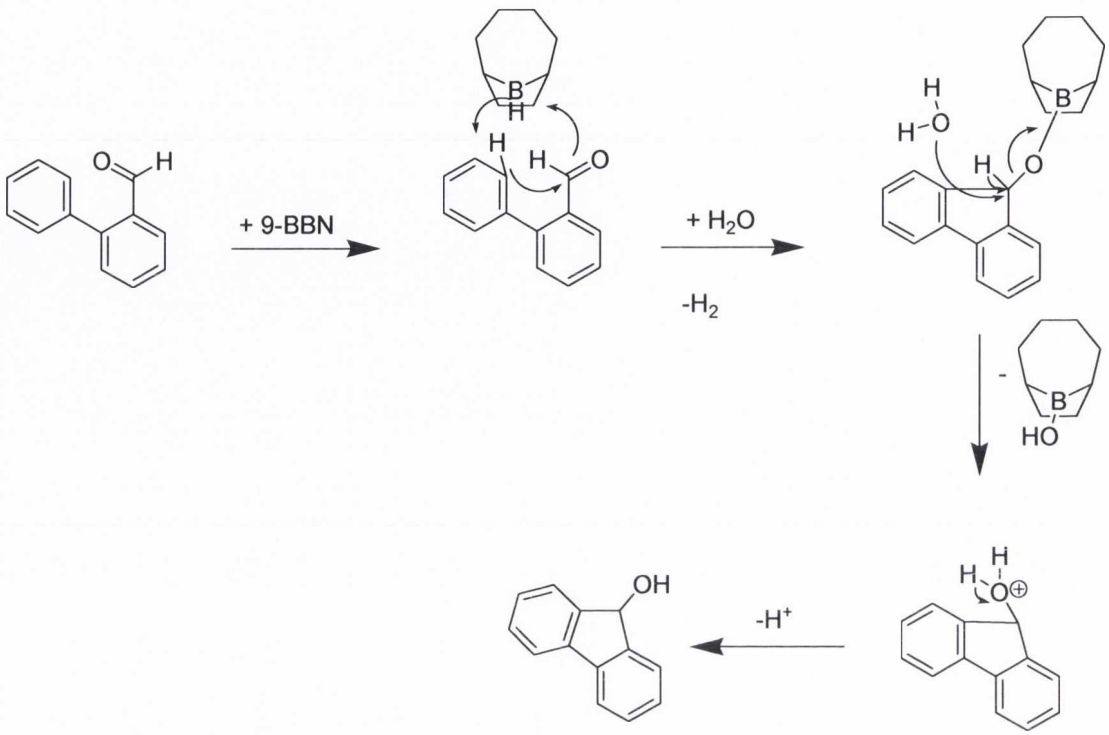
methyl functionality at the other.[73] There appears to be no precedent for such a reductive ring cleavage reaction in the literature but a possible reaction mechanism for the reduction to a methyl group is outlined in Scheme 67. The addition of 9-BBN to the carboxylic acid eliminates hydrogen gas by nucleophilic attack of the hydride. Subsequent addition of t-BuLi results in the formation of the lithium salt. According to Cha and co-workers addition of a second equivalent of 9-BBN solution at this point improves the overall yield of the aldehyde. However, in this case, the lithium borohydride may hydrolise *in situ* and result in the formation of the aldehyde. Subsequent addition of two equivalents of 9-BBN results in further hydride addition and the elimination of a boronic ester resulting in formation of the methyl group.



Scheme 67: The proposed reaction mechanism for the formation of 43

Clearly another mechanism is responsible for the reductive cyclisation and formation of the fluorenol functional group on one end of **43**. A possible mechanism for this ring fusion is shown in Scheme 68. The mechanism is similar to Scheme 67 up to the formation of the aldehyde. At this point, a 9-BBN molecule removes a proton from the neighbouring phenyl ring by nucleophilic attack of a hydride. The resulting carbanion attacks the aldehydic carbon and forms a bond. The boron forms an ester bond with the oxygen and subsequent hydrolysis with water results in the loss of hydroxy 9-BBN and formation of a fluorenol. Once again, no aldehyde product was observed in this reaction

and the proposed mechanism is based purely on previous literature and likely mechanistic routes.[73, 74]



Scheme 68: The proposed route for the formation of fluorenols by reduction with 9-BBN

3.2.6 Attempted Cyclodehydrogenation of Phenyl-Centred Compounds

A number of attempts were made to cyclodehydrogenate some of the phenyl-centred compounds prepared above. A similar procedure was used as for the ligands prepared in chapter 1. In the case of compounds **38** and **42** only starting material was retrieved, while in the case of **33** only an insoluble black material was recovered.

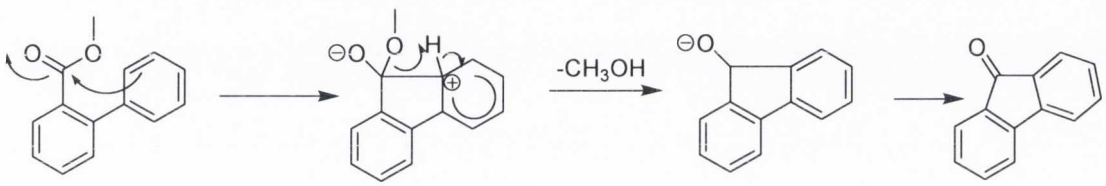
However when the same procedure was applied in the case of **41**, a new spot was seen on the TLC after the usual work-up. After purification via column chromatography a yellow compound was isolated and identified as 1,2,4-triphenyl-3-carbomethoxy-fluoren-9-one (**44**) (Scheme 69).



41 **44**

Scheme 69: The synthetic preparation of 44

Ring closure between the phenyl rings has not occurred. Instead a coupling reaction was seen between the carbon of the ester group and the neighbouring *ortho* phenyl carbon as was seen previously in the case of compounds **36** and **43**. A proposed mechanism for this reaction is given in Scheme 70. According to the mechanism discussed in chapter 1 which was first reported by Kovacic, the initial step involves protonation of a benzene ring and formation of an arenium cation.[75] However in this case the carbonyl undergoes nucleophilic attack from an electron pair on the neighbouring benzene ring. This results in fusion of the carbon from the carbonyl moiety and the adjacent benzene ring. Subsequent loss of methanol results in the formation of a substituted fluorenone. Once again, no di-fluorenone product was isolated, and there appears to be no evidence of any other cyclodehydrogenated products.



Scheme 70: Proposed mechanism for the formation of 44

3.3 Characterisation of Phenyl-Centred Compounds

3.3.1 NMR Spectroscopy

The ^{1}H-NMR spectrum of **33** is shown in Figure 115. Due to the high level of symmetry within the compound, only one methyl peak at δ 1.83 ppm is observed integrating for six protons, and two peaks associated with the phenyl protons at δ 7.17 and 7.09 ppm integrating for eight and twelve protons respectively.

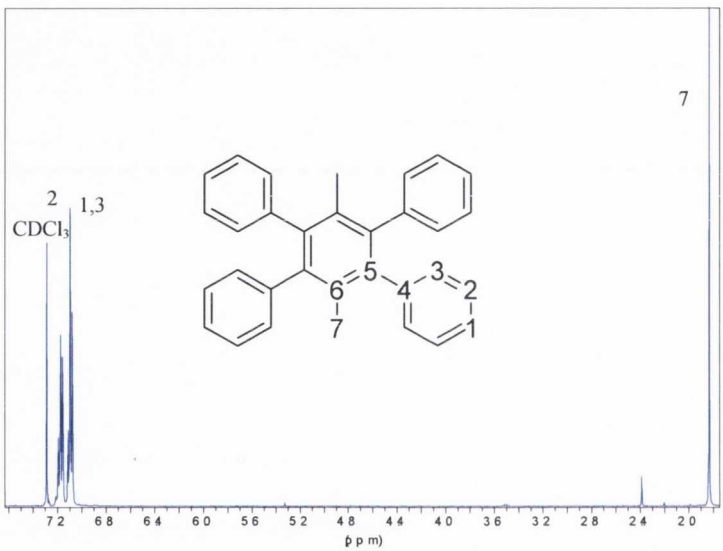


Figure 115: The ^{1}H-NMR spectrum of 33 in $CDCl_3$ (δ 1.9-7.3 ppm shown)

The ^{13}C-NMR spectrum comprises three quaternary carbon peaks and three C-H peaks in the aromatic region, in addition to one methyl peak at δ 19 ppm.

The ^{1}H-and ^{13}C-NMR spectra of **34** were also obtained. The most upfield signal of the ^{1}H-NMR spectrum is that associated with the methylene protons of the fluorene at δ 3.76 ppm which integrates for four protons. The aromatic region is shown in Figure 116; the most significant feature is the upfield shift associated with the signal of the H^5 proton. This is believed to be due to the shielding effect brought about by the neighbouring phenyl ring. The protons H^2, H^3 and H^4 were identified with the help of a ^{1}H-^{1}H COSY experiment. H^3 and H^4 are split into doublets of doublets and the outer proton signals are doublets. The signals associated with the phenyl rings are the most shielded and exist as a multiplet at around δ 7.6 ppm which integrates for ten protons as anticipated.

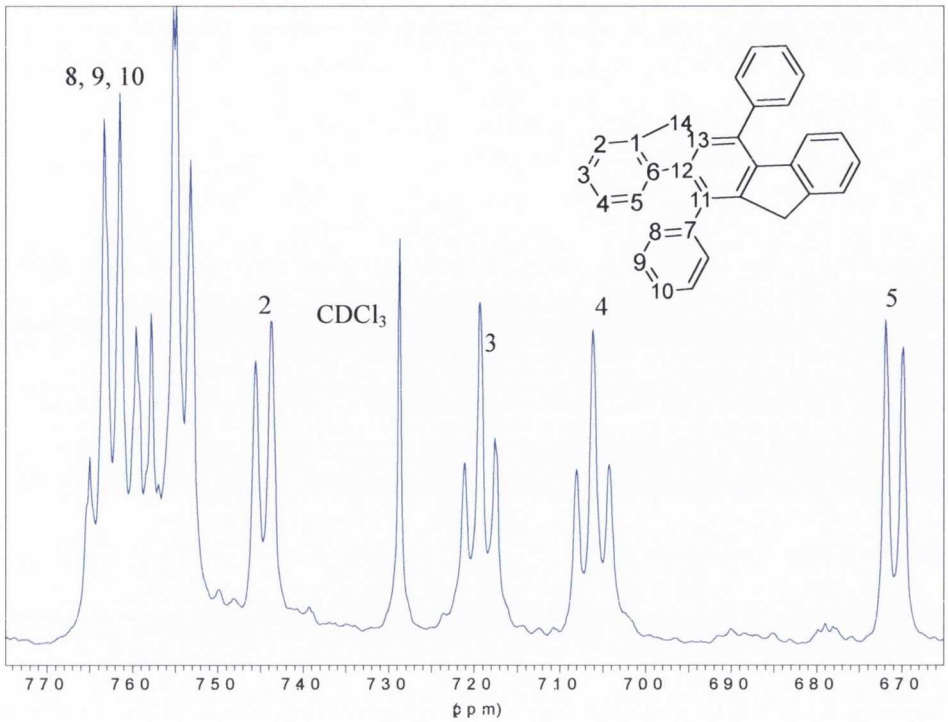


Figure 116: The aromatic region of the ^{1}H-NMR spectrum of 34 in $CDCl_3$ (δ 6.7-7.7 ppm shown)

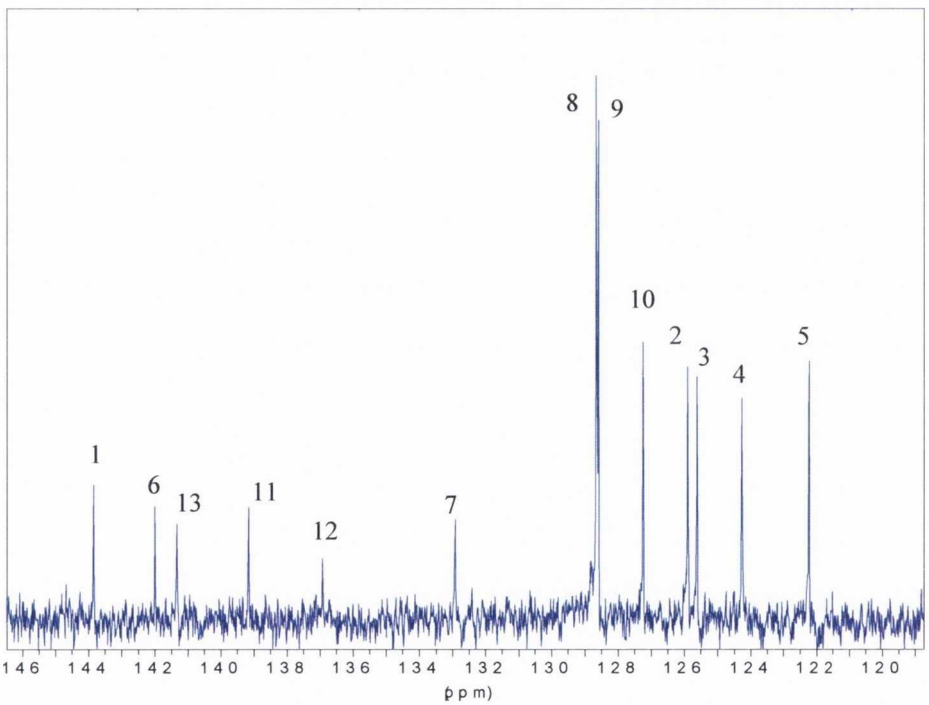


Figure 117: The aromatic region of the ^{13}C-NMR spectrum of 34 in $CDCl_3$ (δ 119-146 ppm shown)

The ^{13}C-NMR spectrum of **34** was assigned with the help of ^{13}C-^{1}H COSY and long-range ^{13}C-^{1}H COSY experiments. The most downfield signals are the quaternary carbons at chemical shifts between δ 133 and 144 ppm. The C-H carbons associated with the

phenyl rings are shifted between δ 127 and 129 ppm, and the most upfield signals are the C-H carbons of the fluorene which appear between δ 122 and 127 ppm.

Solubility problems with **35** made characterisation by NMR difficult, and a full ^{13}C-NMR analysis was not possible. The ^{1}H-NMR spectrum of **35** is very simple due to the high degree of symmetry in the molecule, and contains one multiplet appearing between δ 7.1 and 7.2 ppm. The ^{13}C-NMR DEPT spectrum contains three aromatic peaks appearing between δ 127 and 130 ppm.

For compound **36** there were three separate sets of phenyl rings and one set of fluorene proton signals, as well as a methyl signal at δ 1.90 ppm which integrated for three protons in the ^{1}H-NMR spectrum. The fluorene peaks could be assigned with the help of a ^{1}H-^{1}H COSY experiment. The most upfield signal was assigned as proton H^{5}, which is believed to be shielded by the ring current effect of ring D in Figure 118. From the ^{1}H-^{1}H COSY the other signals of ring A could then be fully assigned. The most downfield phenyl signals were assigned as those of ring B based on its proximity to the fluorene and relative distance from the methyl group. The signals of ring C and D could not be differentiated from each other and are labelled as C/D in Figure 118.

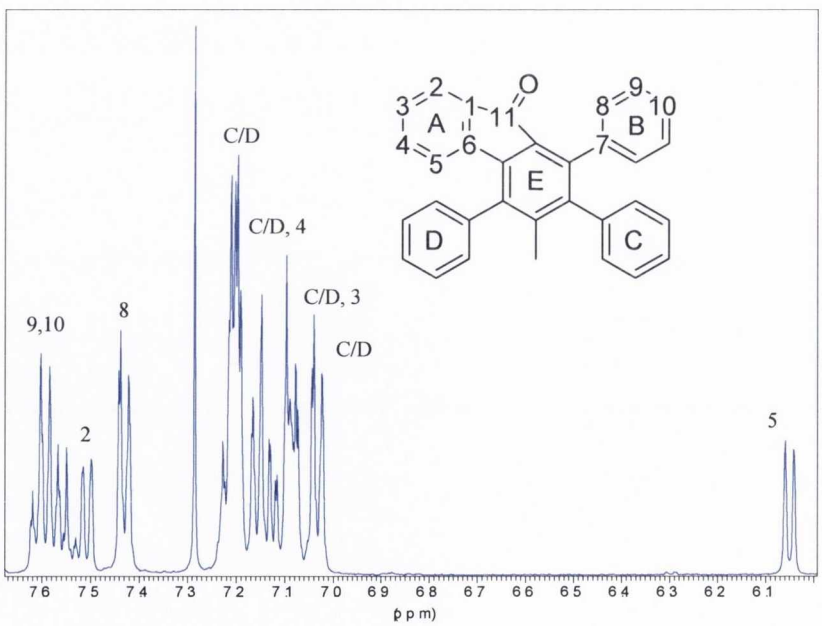


Figure 118: The aromatic region of the ^{1}H-NMR spectrum of 36 in $CDCl_3$ (δ 6.0-7.6 ppm shown)

The ^{13}C-NMR spectrum was complex and many of the peaks could not be specifically assigned, although the quaternary peaks appear in the region between δ 133 and 143 ppm.

The C-H peaks, being more shielded, appear between δ 122 and 130 ppm and the methyl peak is observed at δ 19.6 ppm.

37 with its C_{2v} symmetry gave ^{1}H- and ^{13}C-NMR spectra which could be fully assigned. As before in the case of **36,** the fluorene proton H^5 was shielded by the adjacent phenyl ring and with the help of a ^{1}H-^{1}H COSY experiment the other peaks associated with this ring could be assigned. The *meta* and *para* protons of the phenyl rings were the most deshielded appearing at δ 7.6 ppm.

In the ^{13}C-NMR spectrum the carbonyl peak appears at δ 192.30 ppm. The aromatic region is shown in Figure 119.

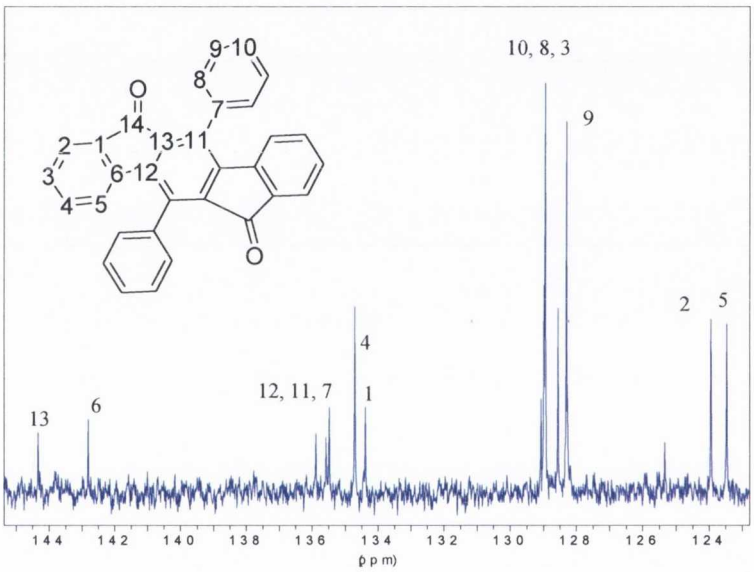


Figure 119: The aromatic region of the ^{13}C-NMR spectrum of 37 in $CDCl_3$ (δ 123-145 ppm shown)

The quaternary signals are most deshielded with C^{13} and C^6 appearing at δ 143.1 and 143.7 ppm respectively. The most shielded signals are those of C^2 and C^5 which appear at δ 123.4 and 123.9 ppm. There are two further sets of carbon peaks, which consist mainly of the C-H peaks associated with the phenyl and fluorinyl rings. Both the proton and carbon spectra are in agreement with the literature data.[67]

The spectra associated with **38** have been fully assigned with the help of 2-dimensional NMR spectra. The ^{1}H-NMR spectrum is shown in Figure 120.

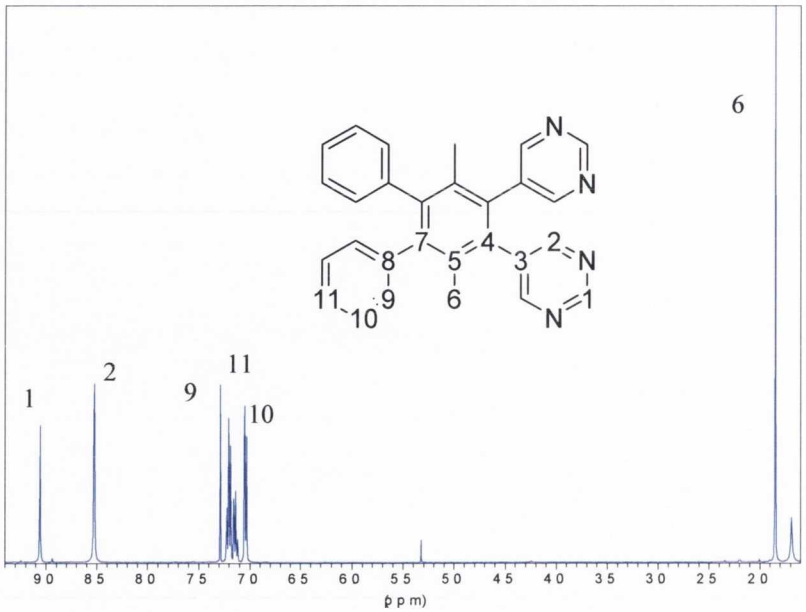


Figure 120: The ^{1}H-NMR spectrum of 38 in $CDCl_3$ (δ 1.8-9.1 ppm shown)

The most downfield signals are those of the pyrimidine rings. H^1 which sits directly between two nitrogens is the most deshielded of the two and integrates for two protons; the other pyrimidyl signal appears at δ 8.5 ppm and integrates for four. The three phenyl signals occur between δ 7.0 and 7.3 ppm and were differentiated by their integration and coupling constants. The most upfield signal is that of the methyl group which is shifted to δ 1.85 ppm. The ^{13}C-NMR spectrum was also completely assigned. The pyrimidyl C-H signals were the most downfield, appearing at around δ 157 ppm. The quaternary signals are shifted between δ 132 and 143 ppm with the three phenyl signals appearing at chemical shifts between δ 125 and 130 ppm. The methyl carbon is the most shielded signal appearing at δ 1.9 ppm.

Compounds **39** and **40** were characterised by ^{1}H- and ^{13}C- NMR spectroscopy and the data was compared to that published.[48] The ^{1}H-NMR spectrum of **40** contains only one set of phenyl signals and one methoxy peak at δ 3.7 ppm which integrates for six protons. The ^{13}C-NMR spectrum consists of five quaternary peaks and four C-H peaks as expected. The most shielded carbon is that of the methoxy group which appears at δ 52 ppm.

The ^{1}H-NMR spectrum of **41** consists of one aromatic multiplet at δ 7.14 ppm and one methoxy signal at δ 3.19 ppm. The ^{13}C-NMR spectrum of **41** is shown in Figure 121. The most deshielded carbon is the C^7 of the ester functionality which is at δ 169 ppm. The

other quaternary signals C^4, C^5 and C^6 are at chemical shifts between δ 136 and 138 ppm. The phenyl C-H signals occur between δ 126 and 130 ppm while the most shielded signal is that of the methoxy C^8.

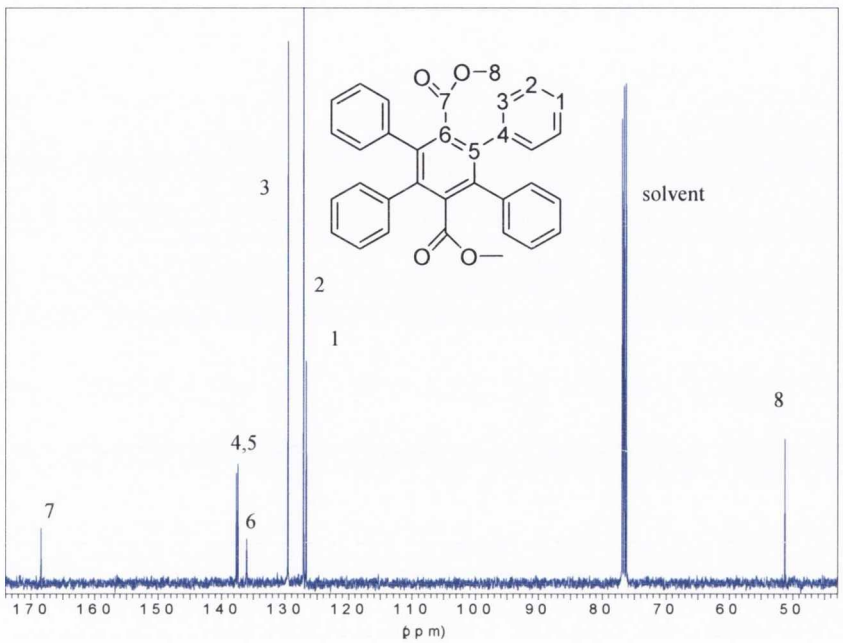


Figure 121: The ^{13}C-NMR spectrum of 41 in $CDCl_3$ (δ 45-170 ppm shown)

The ^{1}H-NMR spectrum of **42** is shown in Figure 122. The most downfield signals are those of the pyrimidyl signals which are deshielded due to the nitrogen atoms on the rings. The phenyl signals appear between δ 7.1 and 7.3 ppm and the methoxy signal is observed at δ 3.26 ppm.

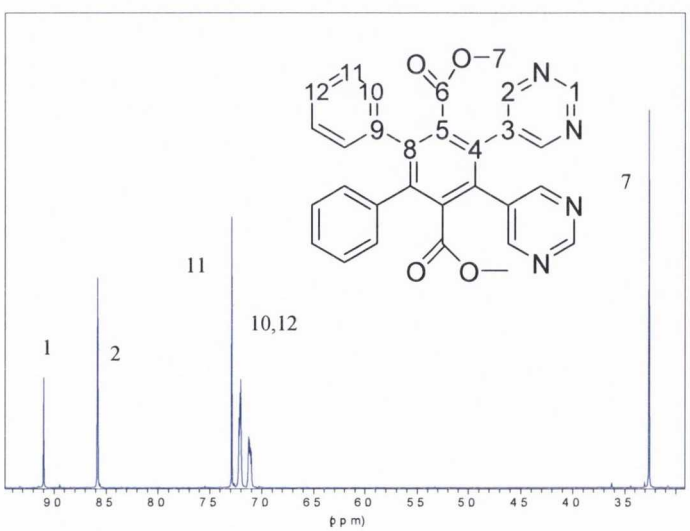


Figure 122: The ^{1}H-NMR spectrum of 42 in $CDCl_3$ (δ 3.6-9.2 ppm shown)

The ^{13}C-NMR spectrum of **42** is also relatively simple with the most downfield quaternary and pyrimidyl C-H signals between δ 157 and 167 ppm. The methoxy carbon signal appears at δ 53 ppm with the phenyl C-H signals are at δ 127 ppm.

The ^{1}H-NMR and ^{13}C-NMR spectra of fluorenol **43** reflect the unsymmetrical nature of the molecule. There are several overlapping phenyl signals in the ^{1}H-NMR spectrum between δ 7.0 and 7.5 ppm (Figure 123). The most downfield aromatic signals are those of ring B and H^2 of ring A. The rings C and D could not be distinguished from each other but with the help of 2-dimensional COSY experiments the remaining signals on ring A were assigned as shown in Figure 123. Not all the peaks in the ^{13}C-NMR spectrum could be assigned, particularly the quaternary peaks which occur between δ 135 and 145 ppm, and the peaks associated with rings C and D which appear between δ 125 and 130 ppm. The carbons C^2 and C^5 appear at δ 124 and 122 ppm, with C^{11} appearing at δ 73 ppm. The most shielded signal is that of the methyl carbon which appears at δ 18 ppm.

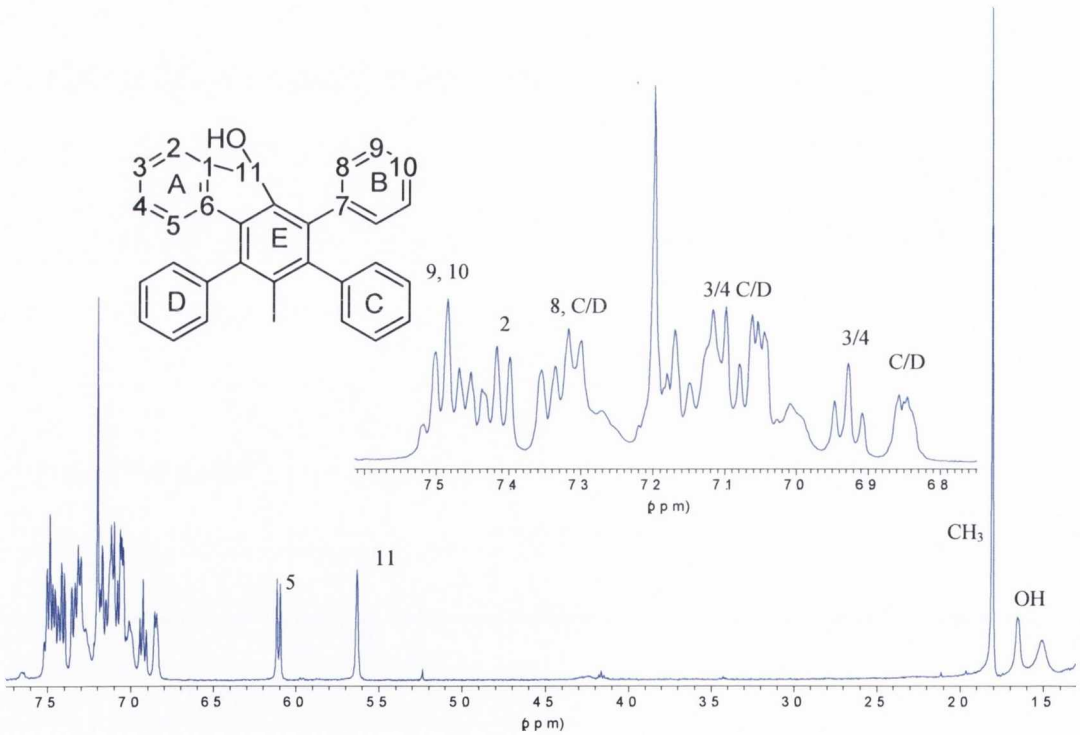


Figure 123: The ^{1}H-NMR spectrum of 43 in $CDCl_3$(δ 1.5-7.5 ppm shown)

The ^{1}H-NMR spectrum of **44** in $CDCl_3$ bears some similarity to the fluorene and fluorenone compounds discussed earlier. The most noticeable similarity is the characteristic aromatic doublet which is shielded by ring D, resonates at δ 6.3 ppm and

integrates for one proton (Figure 124). The other aromatic signals appear as two sets of multiplets at δ 7.2 and 7.5 ppm. The more downfield shifted multiplet consists of the peaks associated with ring B and the H^2 signal from ring A. The other multiplet was assigned to H^3 and H^4 and the protons of rings B and C by 2-D TOCSY experiment. The methoxy ester peak appears at δ 3.3 ppm.

The ^{13}C-NMR spectrum consists of a number of very similar aromatic peaks. However, some of the C-H peaks could be assigned from 2-D COSY experiments. The methoxy ester carbon peak appears at δ 51 ppm due to the shielding effect of the electron pairs on the oxygen atoms. The most downfield aromatic peaks were those assigned to C^2 and C^5 of ring A, as was the case for compounds **36** and **43**. Most of the other C-H carbon peaks associated with rings B, C and D appear between δ 122 and 135 ppm, with the quaternary peaks appearing more downfield to δ 145 ppm. The two carbonyl peaks are the most deshielded signals.

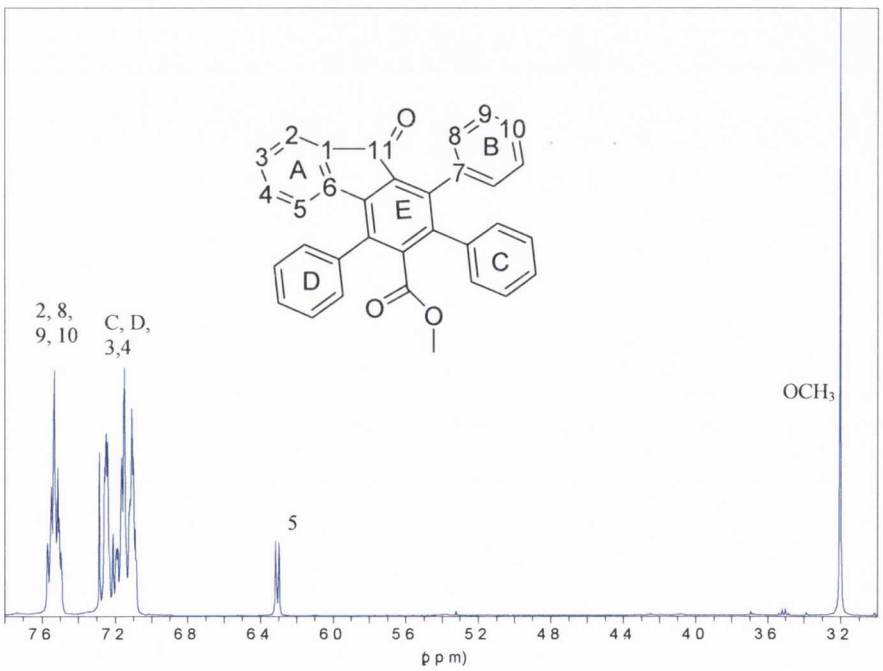


Figure 124: The ^{1}H-NMR spectrum of 44 in $CDCl_3$ (δ 3.2-7.6 ppm shown)

3.3.2 Characterisation of 36 and 43 by X-Ray Crystallography

Crystals of **36** obtained by slow evaporation of a dichloromethane solution crystallised in the triclinic space group *P*$\bar{1}$. The asymmetric unit of the compound is given in Figure 125. The methyl functionality is found to be disordered. The structural analysis revealed that while the fluorenone moiety is almost planar with only a slight torsion angle between rings A and E of 1.5°, the other rings (B, C and D) deviate from planarity. The torsion angles of rings B, C and D with respect to the central ring E are 61.6°, 70.3° and 89.9° respectively. These contrast with those published for octaphenyl substituted fluorenone by Pascal and co-workers where a torsional angle of around 30° between the two phenyl rings of the fluorenone unit was observed.[76]

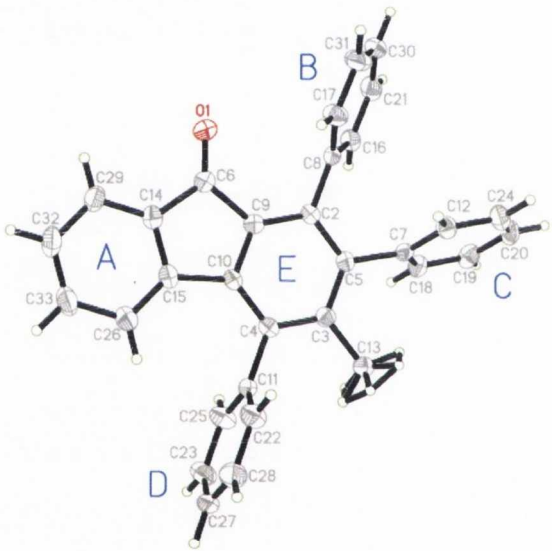


Figure 125: The asymmetric unit in the crystal structure of 36 with selected labelling.

In the crystal lattice the molecules form a layered assembly. In an individual layer, the molecules are held together in dimers by centrosymmetric C-H...O (H...O 2.72Å) hydrogen bonds, making use of the carbonyl group and an aromatic H-atom of the fluorenone moiety as shown in Figure 126.

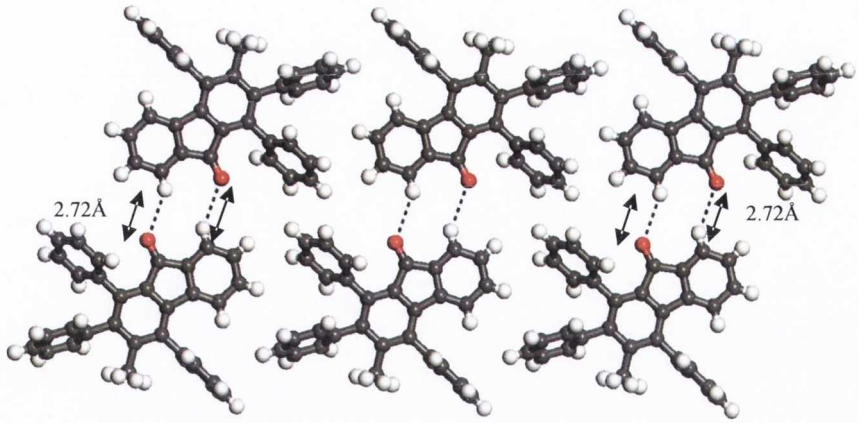


Figure 126: A row of the crystals of 36 showing the interaction between the oxygen atom and one of the hydrogen atoms of the neighbouring molecule

These rows of dimers are stabilized by various weak π-π and hydrophobic interactions. The molecules in adjacent layers are stabilized by C-H…π interactions, in the range 2.95 -3.34Å (Figure 127).

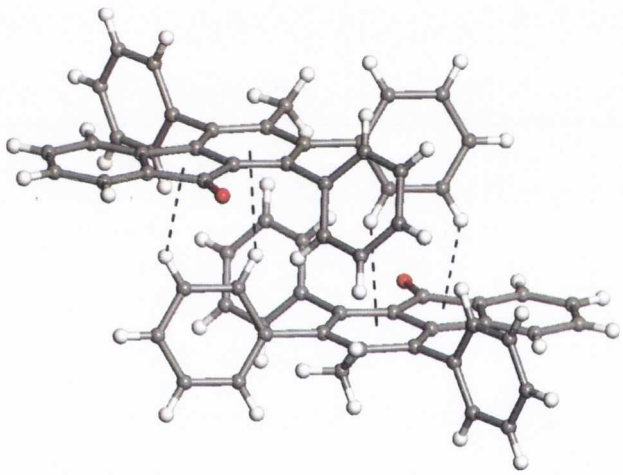


Figure 127: Diagram showing the inter-columnar CH-π interactions between two molecules of 36

One of these CH…π interactions involving ring D has a torsion angle of nearly 90° and creates a gap between two adjacent layers (~4.91Å) as shown in Figure 128. In order to avoid steric crowding, each alternating unit is stacked in such a way that the bulky phenyl rings point away from each other and the almost planar fluorenone units can pack closer together.

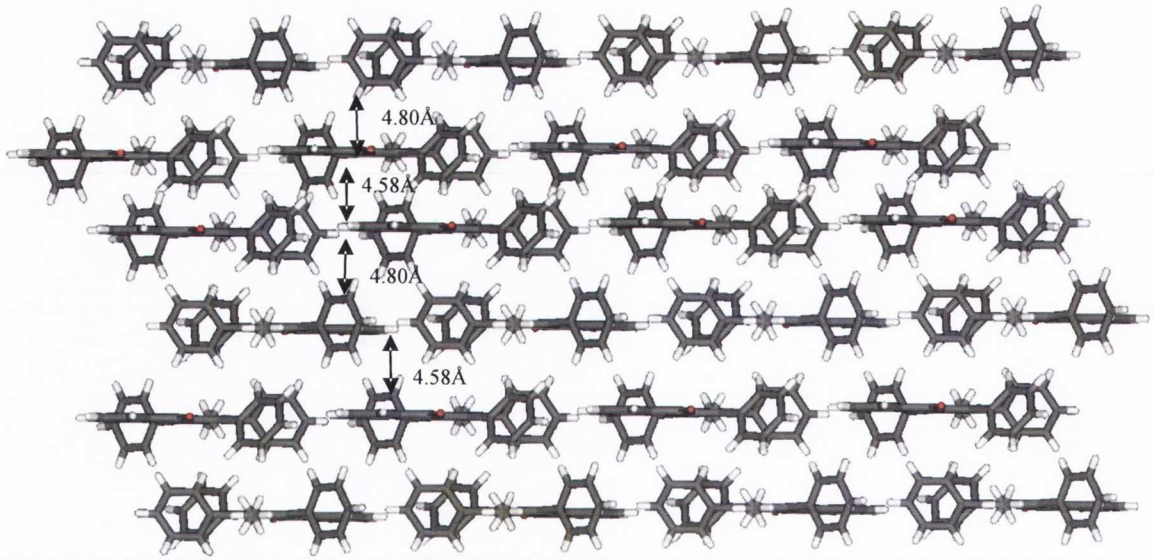


Figure 128: The packing arrangement of the molecules of 36

43 was obtained as crystals by slow evaporation of a dichloromethane solution and crystallised in the monoclinic space group C2/*c*. The asymmetric unit of the crystal is given in Figure 129. As in compound **36** the fluorenol unit is almost planar, with a torsion angle in this case of 1.9° between rings A and E. The torsion angles between the central ring and rings B and C are 72.8° and 75.8° respectively. The torsion angle between the central ring and ring D is much greater at 89.1°. The bond lengths of the C-O and O-H bonds are consistent with other fluorenol crystals in the literature at 1.41Å and 0.82Å respectively. [77]

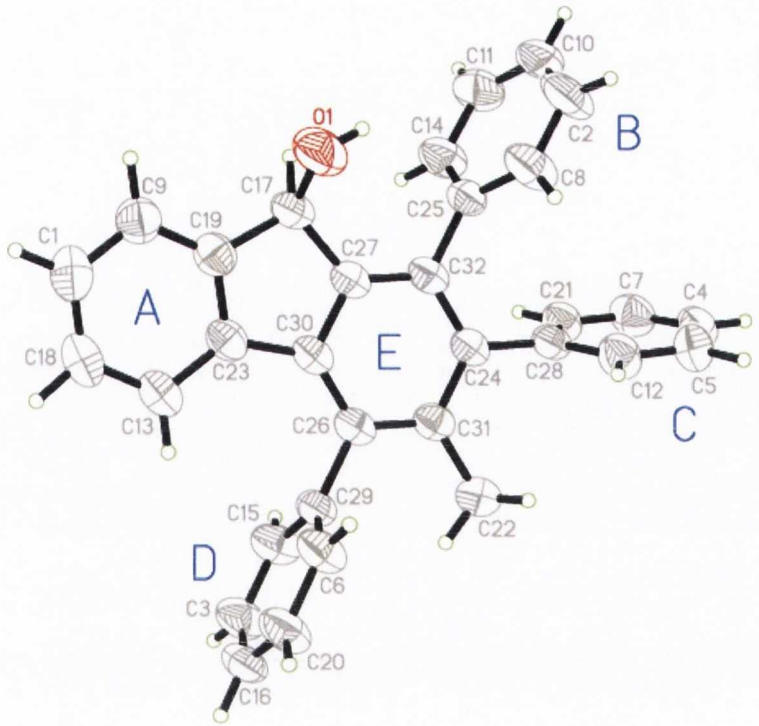


Figure 129: The asymmetric unit of 43 with selected labelling

The crystals are arranged in dimeric units which are held by inter molecular bonds between the oxygen of one molecule and one of the ortho protons on ring A of another (Figure 130). The distance between the two units of the dimer is 2.55Å.

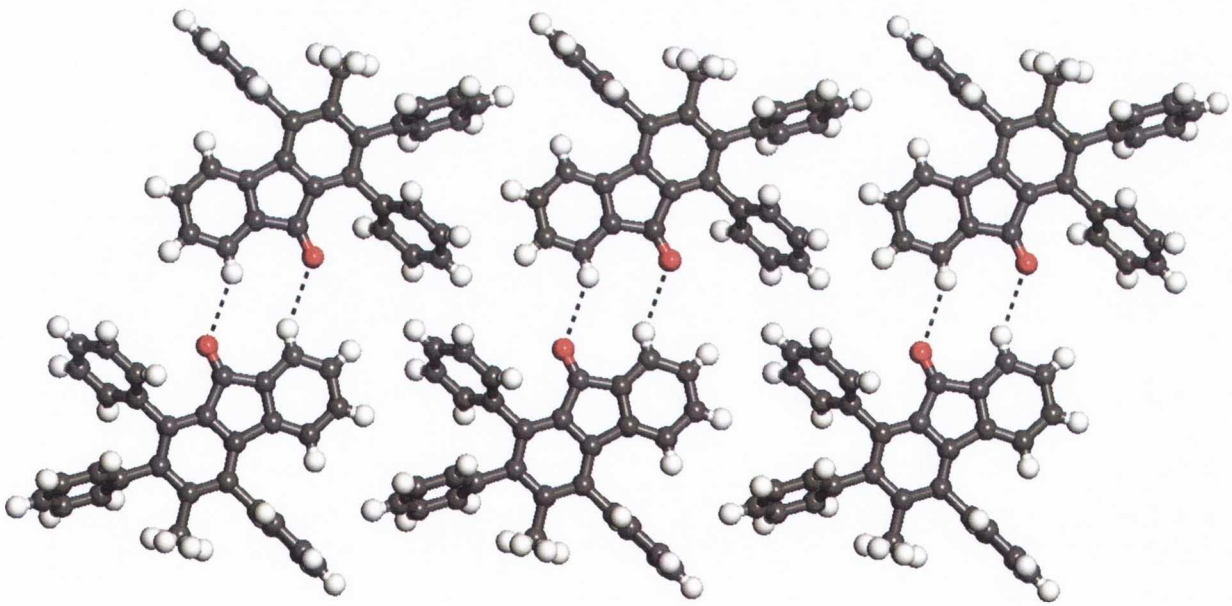


Figure 130: The intra-layer interactions of 43 with the hydroxyl hydrogens removed for clarity

In addition to this, intermolecular C-H…π interactions in the range of 2.05 – 3.33Å exist between the different columns in the crystal-packing which result in the staggered stacking of the molecules (Figure 131).

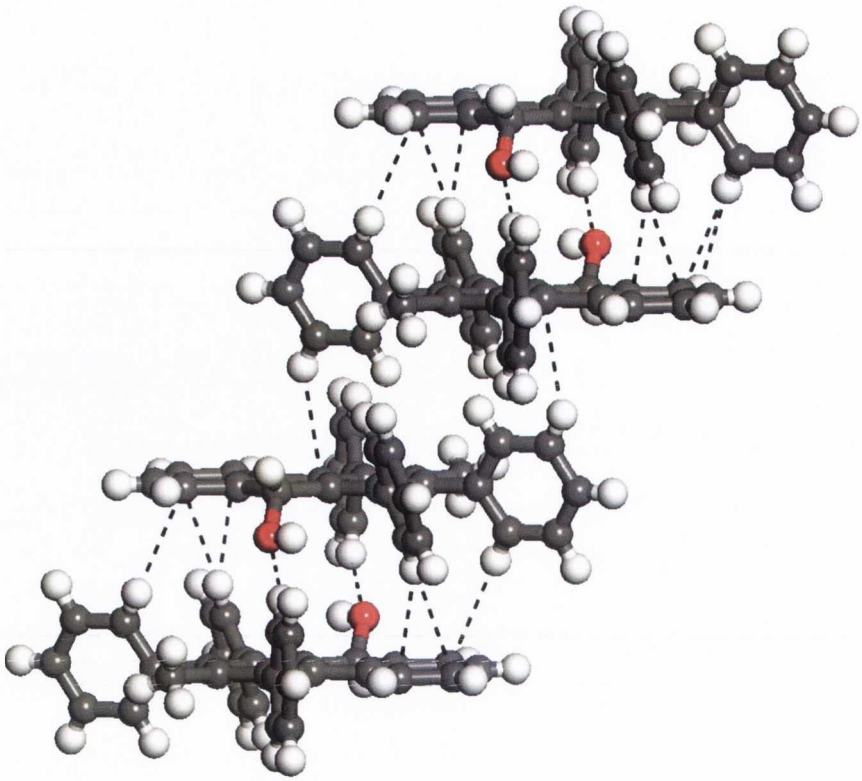


Figure 131: Diagram showing the CH-π intermolecular bonds which results in staggered columnar stacking in 43

These intra-columnar interactions result in the molecules arranging themselves in an ABAB pattern with a distance of 4.83Å between layers A and B and a distance of 4.58Å between these repeating units. The packing of the molecules is shown in Figure 132 viewed along the y-axis. The layered assembly formed by the molecules is shown in Figure 133.

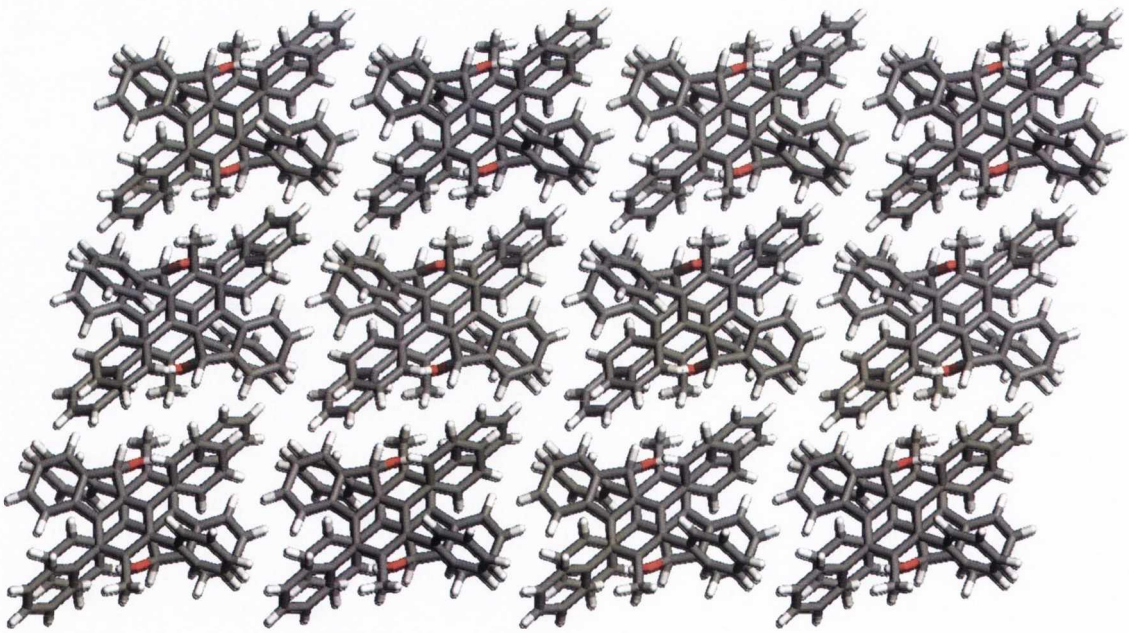


Figure 132: The packing of 43 viewed along the y axis

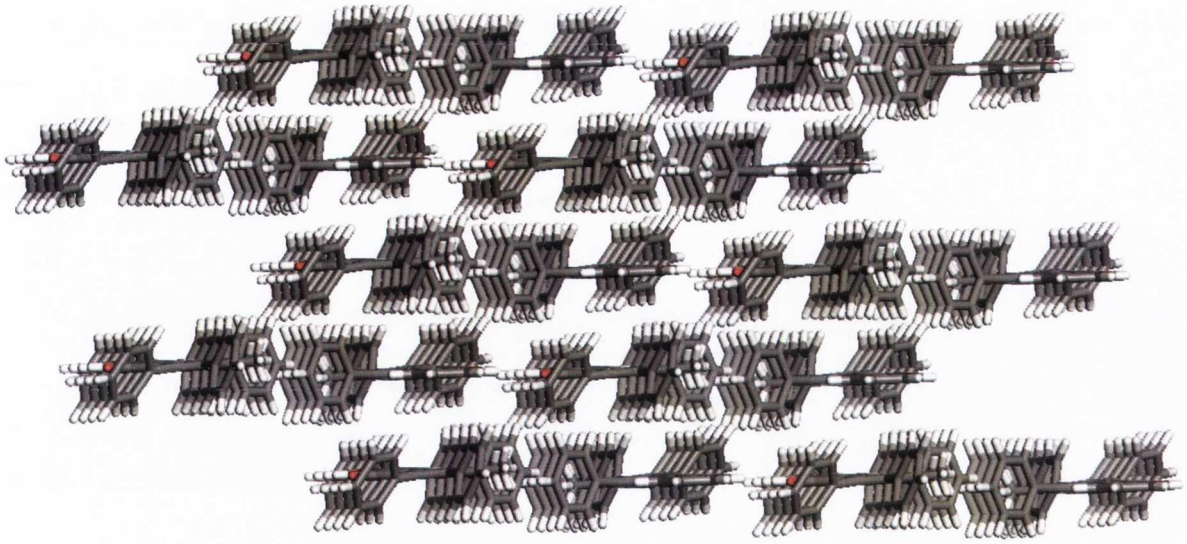


Figure 133: The layered packing viewed along the z axis of 43

3.3.3 Characterisation of Fluorenyl/Fluorenonyl Compounds by UV-Vis Spectroscopy

The fluorene and fluorenone moieties are known to possess interesting photophysical properties.[78] As a result the UV-Vis and fluorescence spectra of compounds **34**, **36**, **37**, **43** and **44** were measured. The UV-Vis spectra of these compounds are shown in Figure 134. The absorption maxima of all the compounds was assigned as an $n \rightarrow \pi^*$ transition with the exception of **34** which has a lower energy maximum that was assigned to a $\pi \rightarrow \pi^*$ transition from comparison to literature assignments.

The photochemistry of fluorenone has been widely discussed in the literature due to its interesting dependence on solvent polarity.[79] This is due to the fact that the first singlet excited state is believed to be a $\pi \rightarrow \pi^*$ transition in polar solvents, whereas in non-polar solvents the first singlet excited state is thought to be a $n \rightarrow \pi^*$ transition. There are two triplet excited states lower in energy than these which are believed to have $\pi \rightarrow \pi^*$ character. Radiationless transitions occur from the lowest excited singlet $n \rightarrow \pi^*$ state to the ground state via these triplet states. The shape of the fluorenone spectra is influenced by the carbonyl moiety which introduces non-bonding electrons into the π^* orbitals which gives rise to the $n \rightarrow \pi^*$ transitions.[78]

The addition of substituents to the fluorenone unit may also influence the absorbance wavelength. Electron-withdrawing substituents increase the permanent ground-state dipole moment which decreases the energy gap between the ground and excited states, and shifts the absorbance to a lower energy maximum. For example the absorption

maximum of 2-nitrofluorenone is bathochromically shifted compared to that of fluorenone.[80] Fluorenone itself has two maxima in cyclohexane, at λ 292 and 306 nm.[81] Figure 134 shows the absorbance maxima of the substituted fluorenone compounds **36** and **44** in addition to compounds **34**, **37** and **43**. The maximum absorbance of **36** and **44** is significantly shifted to a higher energy than that of fluorenone, with an absorbance for the n→π* transition at λ 264 nm and a shoulder at around λ 250 nm. This shoulder may be due to a transition to the S_2 (π→π*) state from the ground state, as a similar weak absorbance has been assigned in the case of fluorenone.[82]

The spectrum of fluorene **34** has been obtained previously.[67] Clearly the absorbances within this molecule are at much lower energy and are most likely due to π→π* transitions from the fluorenyl unit.

Although the synthesis of compound **37** has been reported before, neither report refers to the photochemistry of this molecule.[67, 68] Comparison with other unsubstituted difluorenone compounds indicate that the absorbance maximum of **37** is similar to that of difluorenone, with the phenyl substituents giving rise to only a slight blue shift in the absorbance maximum.[83] In contrast the absorbance maxima of **43** are broader and less intense. This is most likely due to the C-O single bond ensuring that this molecule has a smaller contribution from the non-bonding electrons and resulting in a weaker n→π* transition.

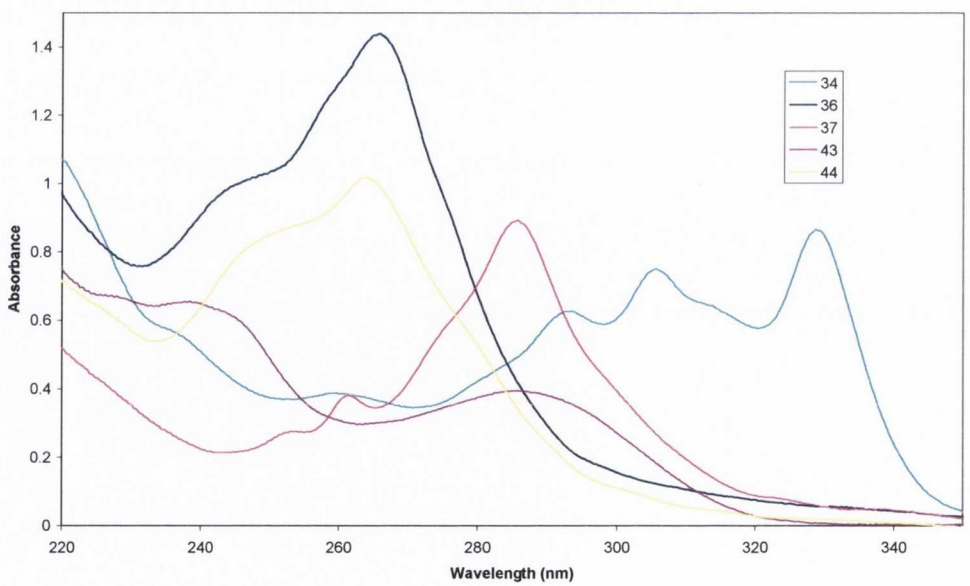


Figure 134: The UV-Vis Absorption Spectra of Compounds 34, 36, 37, 43 and 44 in cyclohexane

Although the fluorescence of these compounds was measured, the emission of all but **34** was extremely low and barely above the baseline noise. This may be due to the fact that when an $n \rightarrow \pi^*$ transition is the lowest excited singlet state, and there is a triplet $\pi \rightarrow \pi^*$ state below this, the fluorescence of the molecule is often quenched.[84]

The fluorescence of **34** was measured in acetonitrile at a concentration of 2×10^{-5}M and found to be in agreement with that previously reported, with a strong emission at λ 350 nm.[67]

3.3.4 Characterisation of Compounds 33-44 by I.R. Spectroscopy and Mass Spectrometry

The compounds discussed above were also characterised by I.R. spectroscopy, and due to the presence of a number of distinctive functional groups, this proved to be a useful characterisation tool. All the compounds contained characteristic aromatic C-H stretches at around 3020 cm^{-1} as well as the C=C aromatic stretches at ν 1600, 1495 and 1450 cm^{-1}. However due to the presence of functionalities such as methyl, carboxylic acids and esters in some of the compounds, a number of unique absorptions were observed with several of the samples. Some of these absorptions are summarised in Table 19.

Compound	I.R. Absorbance ν (cm^{-1})	Corresponding Functional Group
33	2961, 2867	CH_3 methyl stretch
35	3057 1707	OH stretch C=O stretch
36	2984 1719	C-H methyl stretch C=O stretch
37	1713	C=O stretch
38	1549, 1398, 773, 702	C=N stretch of pyrimidine
41	2950, 1735 1190,1180	methyl ester stretch CC(=O)-O stretches
42	2950, 1190, 1730 1180 1548, 702	CC(=O)-O stretches methyl ester stretch C=N stretches
43	3553 1442, 1368 1023	O-H stretch O-H bend C-O stetch
44	2921 1732, 1712 1222, 1172	C-H methyl stretch C=O stretches C-O stretch

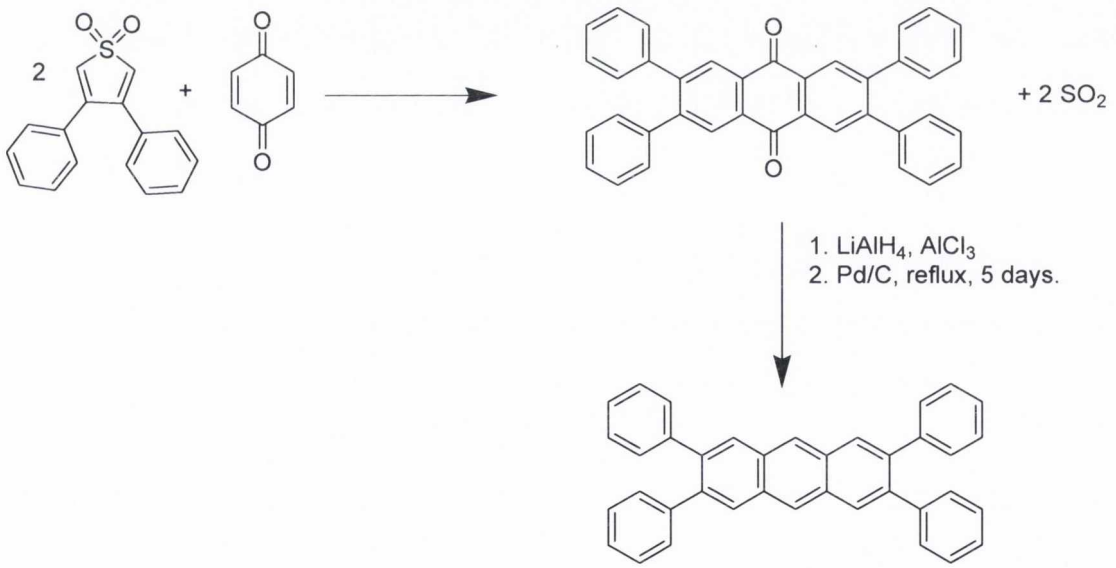
Table 19: Some of the assigned absorptions observed in the I.R. spectra of compounds 33-44

The mass spectra of compounds **33** – **44** were obtained using electrospray mass spectrometry, with the $[MH]^+$ or $[MNa]^+$ peak of the molecules appearing in the spectra. No mass spectra were obtained for compounds **33** and **35**. In the case of **33**, the sample could not be ionised and therefore did not fly to the detector. The issue with **35** appears to be negligible solubility in most common laboratory solvents which made input into the spectrometer extremely difficult. Melting points for all compounds were obtained and are outlined in the experimental section. Due to the highly fused nature of many of these compounds melting points were generally higher than 200°C.

3.4 Introduction to Part II

After the synthesis of 1,2,4,5-tetraphenyl substituted dicarboxaldehydes had been attempted without success, other routes towards phenyl-centred N-HSB compounds were investigated. It was observed that the proximity of the phenyl rings *ortho* to the central benzene ring made specific reactions at this point very difficult. In particular, the acidity of the adjacent protons from the *ortho* phenyl rings, the willingness of these protons to act as leaving groups and the tendency for the resulting carbanions to couple to the nearby methyl carbon seemed to be responsible.

In order to reduce the steric hindrance around the *para* positions of the benzene ring, spacer groups between the phenyls and the central benzene ring were introduced. This lead to a desire to functionalise phenyl-substituted anthracenes with aldehyde groups at the 9- and 10- positions. It was hoped that the functionalisation of these phenyl substituted anthracenes would be easier than the phenyl substituted carboxaldehyde discussed earlier. The synthesis of 2,3,6,7-tetraphenyl anthracene was previously carried out in three steps by Williams (Scheme 71).[85, 86]



Scheme 71: The synthetic route towards 2,3,6,7-tetraphenyl substituted anthracene

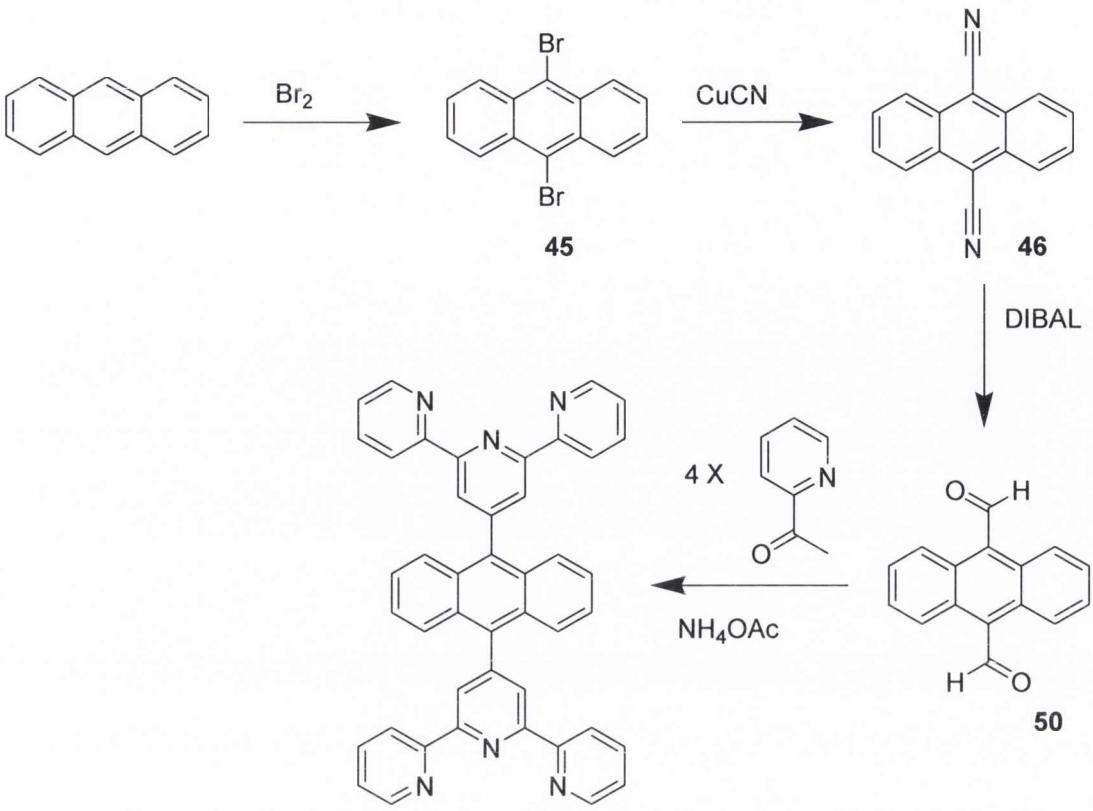
It was hoped that functionalising the 9- and 10- positions of this substituted anthracene compound with carboxaldehyde groups would lead to a novel di-terpyridine compound with interesting coordination and photophysical properties.

However, the overall yields of this anthracene were quite low, and before embarking on a potentially low-yielding synthesis of a starting material which could be required in bulk, it was decided to work with the unsubstituted anthracene.

3.5 Results and Discussion of Part II

Although a number of literature preparations for 9,10-anthracene dicarboxaldehyde are available, the most straightforward appears to be direct bromination and subsequent cyanation of anthracene itself. Other routes include the oxidation of the methyl chloride, oxidation of the dimethyl anthracene or conversion of the anthraquinone, but all three methods are either low-yielding, involve the lengthy synthesis of precursors or use expensive reagents.[70, 87, 88]

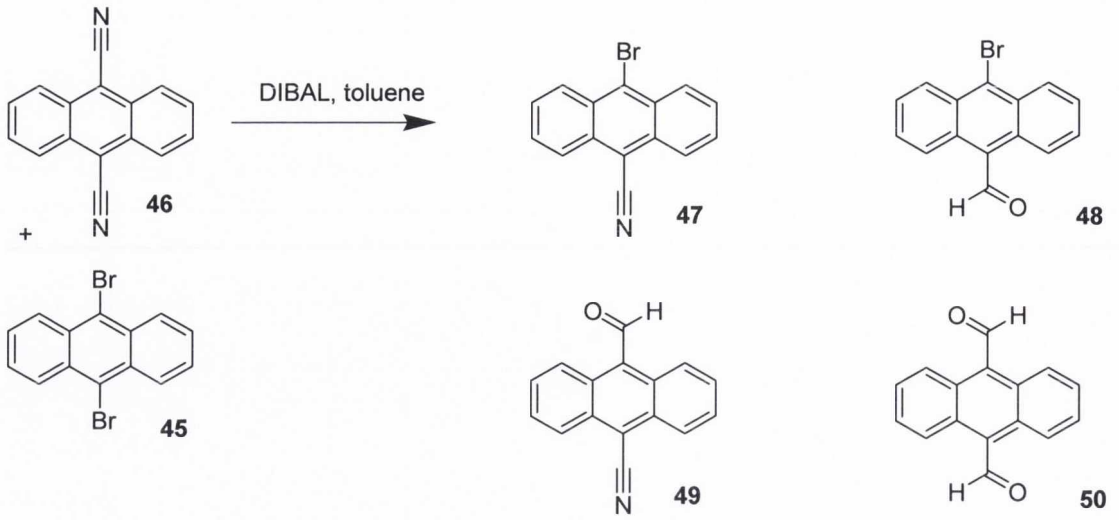
The bromination of anthracene at the 9- and 10- positions can be carried out in high yield according to the method of Cakmak and co-workers.[89] This involves the cooling of a dichloromethane solution of anthracene to 0°C and the addition of Br_2 in the absence of light. The solution was stirred for one hour and the solvent removed. As there appeared to be only one spot on the TLC, no chromatography was necessary, and the mixture was recrystallised from chloroform. 9,10-dibromoanthracene (**45**) was identified by NMR spectroscopy and mass spectrometry and was obtained in 99% yield. This was then refluxed in DMF with an excess of CuCN.[90] After quenching with aqueous ammonia the mixture was extracted into dichloromethane and washed with acid and water. The product, 9,10-dicyanoanthracene (**46**) was recrystallised from DMF and characterised by NMR spectroscopy. A six molar excess of di-isobutyl aluminium hydride (DIBAL) was added to a toluene solution of **46** and this was stirred for 20 hours. After quenching the reaction, purification by column chromatography revealed a number of products.



Scheme 72: The route towards novel anthracene-centred di-terpyridyl compounds

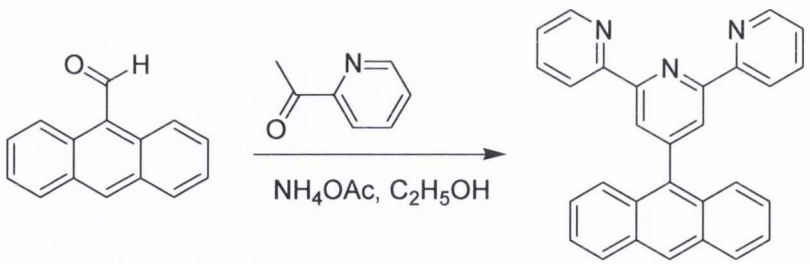
The resulting compounds were characterised and were identified as a combination of brominated, cyanated and aldehydic disubstituted anthracene compounds (Scheme 73). It was clear from this result that the cyanoanthracene used in this reaction contained a significant amount of dibromoanthracene. As evidence of this, the first compound off the column was identified as 9-bromo-10-cyanoanthracene (**47**) which was isolated in 11% yield. The second compound to be isolated was 9-bromo-10-anthracenecarboxaldehyde (**48**) in 17% yield. 9-cyano-10-anthracenecarboxaldehyde (**49**) was the third compound to be eluted from the column in 14% yield. Finally, the desired product, 9,10-dicarboxaldehyde (**50**) was isolated in 5% yield after recrystallisation from toluene.

Despite numerous attempts, this yield could never be improved; indeed, on several occasions, the product did not extract into the organic phase despite attempted neutralisation with a number of bases.



Scheme 73: The synthesis of a number of substituted anthracenes

Nonetheless, a small amount of **50** was isolated and a number of attempts were made to synthesise the di-tpy compound. However prior to this, the previously reported 4'-(9-anthryl)-2,2':6',2"-terpyridine (**51**) was prepared in order to investigate the ideal conditions for this reaction before expending precious starting material.[91] 9-anthracenecarboxaldehyde was refluxed overnight in ethanol with two equivalents of 2-acetylpyridine and an excess of NH_4OAc (Scheme 74). The solution turned dark red upon heating and a green precipitate began to form. The precipitate was collected by filtration and recrystallised from ethanol. The product was identified as compound **51** and was isolated in 31% yield.

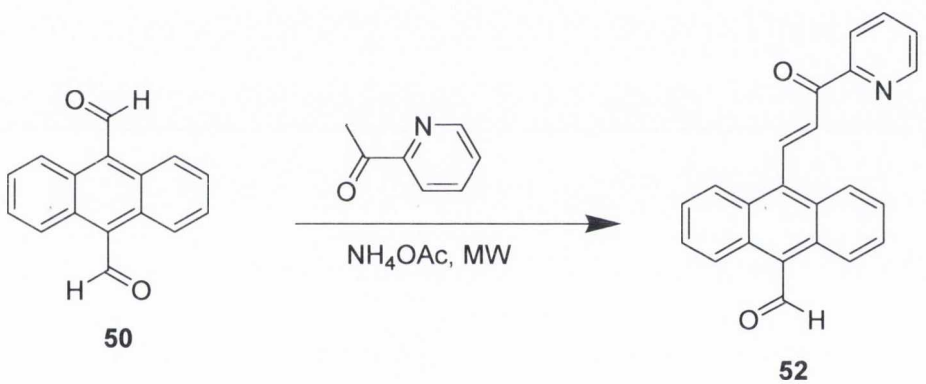


51

Scheme 74: The synthesis of 51

A similar method was attempted with **50** by refluxing with four equivalents of 2-acetyl pyridine and an excess of KOH in ethanol and water, however despite several attempts only the starting material was isolated. It must also be noted that this reaction could only be performed on a milligram scale due to the poor yield of **50**. The literature appears to suggest that the reaction works better on a multigram scale as the product can then be isolated directly by filtration.

Other groups have achieved high yields of terpyridine ligands via a microwave irradiation synthesis. Tu and co-workers report yields of up to 92% of certain substituted terpyridines by heating the starting materials in a microwave for ten minutes.[92] This method was an attractive option due to the higher yields reported and the ability to work on a smaller scale. Compound **50** was added to a sealed tube with a fourfold excess of 2-acetyl pyridine and an excess of ammonium acetate. The mixture was heated for a number of minutes in a microwave and subsequently purified by column chromatography. The intermediate 9-anthracenyl(10-al)-1-(2-pyridyl) propen-2-one (**52**) was isolated in low yield (Scheme 75). Despite lengthier irradiations and several attempts at this reaction no other products were obtained. At this point it seemed appropriate to find alternative routes towards tpy synthesis given the lack of reactivity of the dialdehyde towards ring formation reactions with 2-acetyl pyridine.

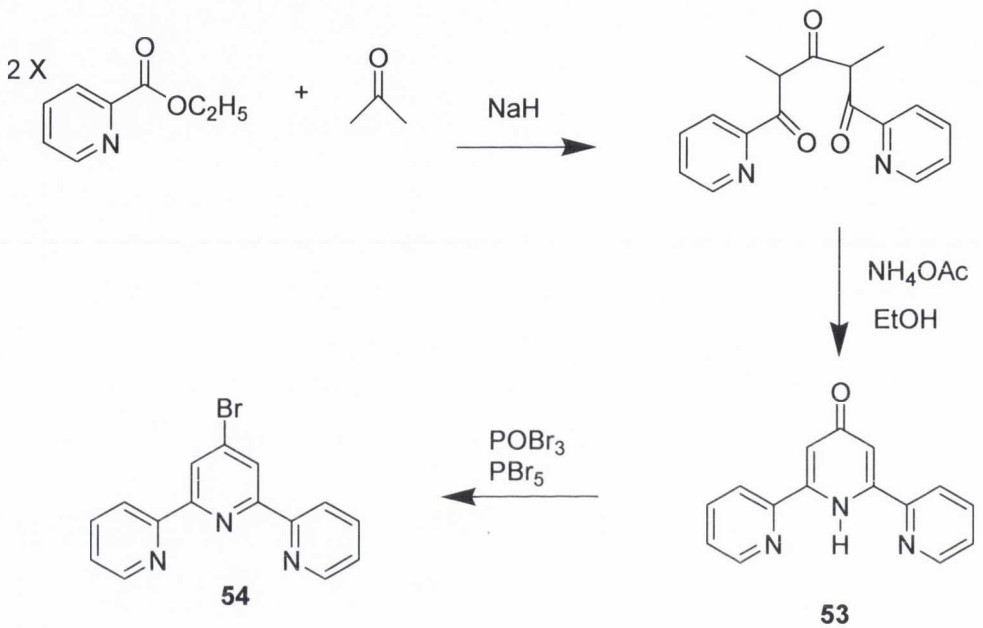


50 **52**

Scheme 75: The synthesis of 52

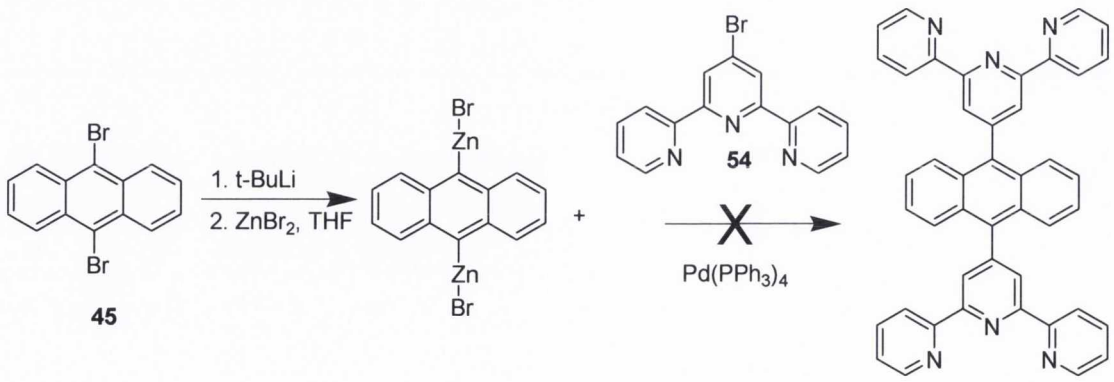
A number of coupling reactions have been applied in the synthesis of terpyridines as discussed in the introduction. In particular the use of various palladium catalysed reactions has been applied with some success. Given that the dibromoanthracene had already been prepared, it seemed feasible to prepare a suitably substituted tpy moiety separately and attempt a coupling reaction with **45**. With this in mind, two bromo substituted tpy compounds were prepared. The first of these was 4'-bromo-(2,2':6',2")-terpyridine, which was prepared from 2-*bis*-(2-pyridyl)-4-pyridone. This compound was prepared from the literature procedure of Constable and co-workers.[29] A 50cm^3 dimethoxyethane solution of acetone and pyridine carboxylate were added via canula to a dimethoxyethane solution of NaH. The mixture was heated gently until hydrogen gas was evolved and then refluxed overnight. The solvent was removed *in vacuo* and the mixture dissolved in water and neutralised with HCl. A yellow precipitate formed and was

collected by filtration and dried. This was then refluxed with an excess of ammonium acetate in ethanol overnight, and the solvent was again removed. The resulting solid was recrystallised from ethanol to give 2,6-bis(2-pyridyl)-4-pyridone (**53**). This was then heated with $POBr_3$, and PBr_5 at 120°C overnight and water was added after cooling.[93] The reaction was neutralised with KOH, extracted into chloroform and washed with activated charcoal to give a 75% yield of 4'-bromo-(2,2':6',2'') terpyridine (**54**) (Scheme 76).



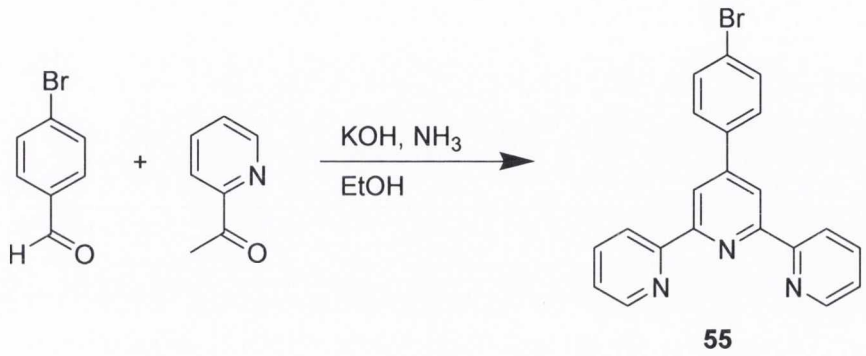
Scheme 76: The synthetic route towards 53 and 54

This was then used in a Negishi-style coupling reaction with **45**.[94] This reaction was carried out by lithiating **45** at the 9- and 10- positions and adding $ZnBr_2$ (Scheme 77). The anthracene was then added to a THF solution containing **54** and palladium tetra-kis triphenylphosphine. This was refluxed overnight at 78°C and quenched with water. However no product was isolated.



Scheme 77: The unsuccessful Negishi-coupling of 45 and 54

A similar reaction was attempted with 4-bromo-4'-phenyl-(2,2':6',2") terpyridine, which was prepared according to the literature preparation of Hovinen and Hakala.[95] This was carried out via a Hantzsch style ring formation reaction between 4-bromo benzaldehyde and 2-acetyl pyridine in basic ethanol solution (Scheme 78)



55

Scheme 78: The synthesis of 55

The product was isolated in a 62% yield, and was then used in a similar Negishi reaction with **45** but again this was unsuccessful. It was hoped that a Suzuki coupling would also be possible, but isolation of boronic anthracenes proved problematic.

3.6 Characterisation of Anthracene and Tpy Compounds

The substituted anthracene and terpyridine compounds discussed in this section were characterised by ^{1}H- and ^{13}C-NMR spectroscopy, as well as I.R. spectroscopy and melting point analysis. Where possible these compounds were also characterised by mass spectrometry.

The ^{1}H- and ^{13}C-NMR spectra of the di-substituted anthracene compounds **45-50** were compared with literature spectra where possible, and the peaks were duly assigned from these.[96] The various aldehyde, cyano and bromo substituents had differing but consistent effects on the chemical shifts of the neighbouring protons of the anthracene moiety. The ^{1}H- and ^{13}C-NMR spectra of **49** are shown in Figure 135 and Figure 136 as an example. The singlet at δ 11.5 ppm in the ^{1}H-NMR spectrum was assigned to the aldehyde proton. The two most downfield aromatic doublets are H^3 and H^6 which are shifted differently due to the effects of the substituents at the 9- and 10- positions of the anthracene. The anthracene function provides a greater deshielding effect with the result that the neighbouring proton H^6 appears downfield at to δ 8.81 ppm. This proton has a similar chemical shift in compounds **48** and **50** where there is also an aldehyde present on the 9-position. The deshielding effect of the cyano group is less severe, with the neighbouring proton on the H^3 position appearing at δ 8.53 ppm. This is also reflected in the other cyano containing compounds **46** and **47**. The deshielding effect of the bromo substituents is more extreme than the cyano group but less than the aldehyde with the neighbouring protons resonating at around δ 8.6 ppm, depending on the relative effect of the opposite substituents. The H^4 and H^5 protons exist as a multiplet at δ 7.8 ppm in the case of **49** and there is only a slight shift from compound to compound depending on the substituents. These effects are summarised in Table 20.

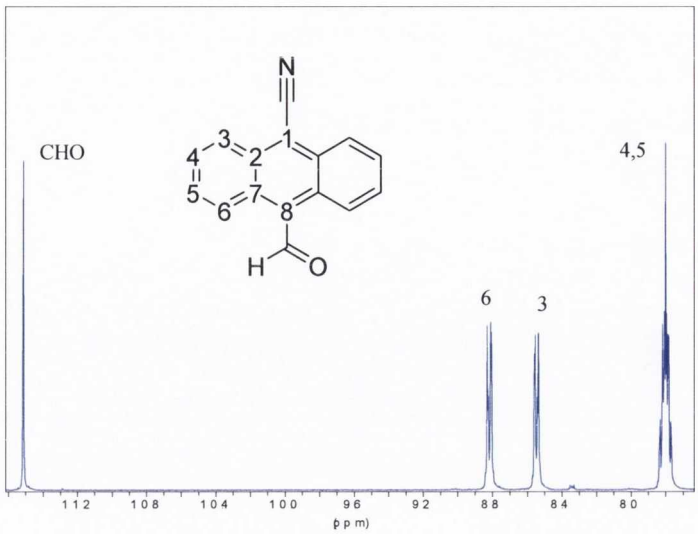


Figure 135: The ^{1}H-NMR spectrum of 49 in $CDCl_3$ (δ 7.8-11.4 ppm shown)

The ^{13}C-NMR spectrum of **49** consists of one aldehyde carbon peak at δ 192.97 ppm and several aromatic peaks between δ 124 and 132 ppm, with two additional peaks between δ 110 and 120 ppm. The region between δ 110 and 135 ppm is shown in Figure 136. The most downfield aromatic signals are the quaternary carbons C^2, C^7 and C^8 followed by the four C-H signals. The most shielded signals are the cyano carbon and the adjacent carbon on the anthracene, C^1. A similar trend can be seen here regarding the effect of the substituents on the carbon shifts of these compounds, and this is summarised in Table 21.

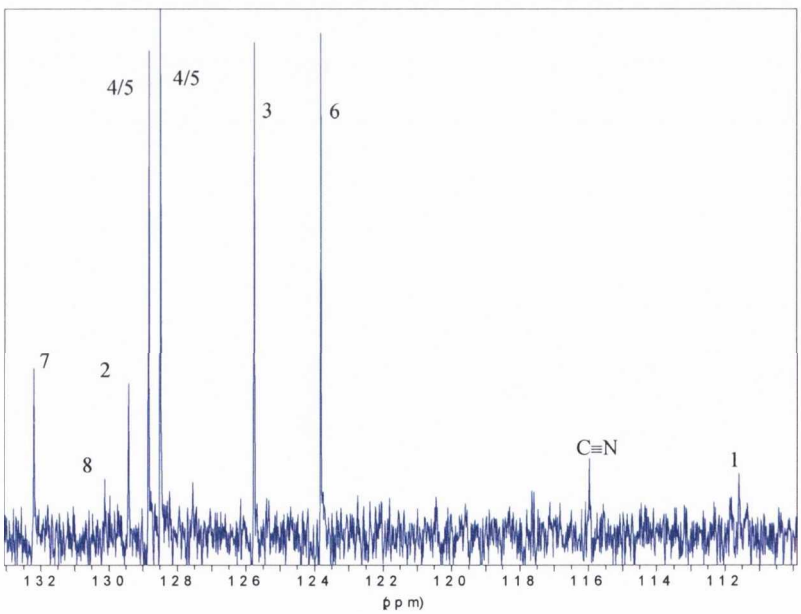
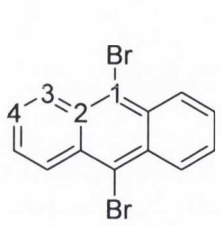
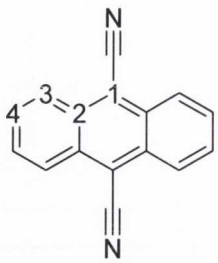


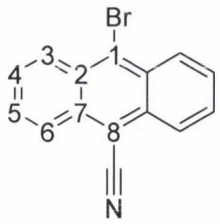
Figure 136: The aromatic region of the ^{13}C-NMR spectrum of 49 in $CDCl_3$ (δ 110-132 ppm shown)



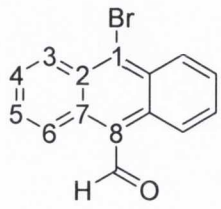
45



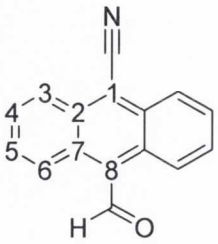
46



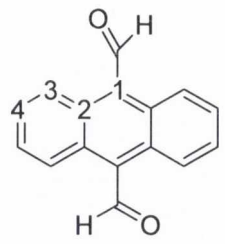
47



48



49



50

Compound	Chemical Shift (ppm)		
	H^3	H^4, H^5	H^6
45	8.61	7.66	-
46	8.56	7.88	-
47	8.61	7.75	8.45
48	8.60	8.82	7.63
49	8.53	7.78	8.81
50	8.77	7.73	-

Table 20: The ^{1}H-NMR chemical shifts associated with disubstituted anthracenes 45-50 in $CDCl_3$

Compound	Chemical Shift (ppm)							
	C^1	C^2	C^3	C^4	C^5	C^6	C^7	C^8
45	123.10	130.60	127.84	127.02	-	-	-	-
46	111.51	132.11	129.82	126.16	-	-	-	-
47	129.91	129.57	128.24	127.63	125.32	128.75	132.91	105.84
48	133.64	131.34	123.29	128.50	126.86	128.35	129.67	125.02
49	111.58	129.41	125.76	128.83	128.50	123.81	132.19	130.11
50	131.31	129.73	127.95	123.79	-	-	-	-

Table 21: The ^{13}C-NMR chemical shifts associated with these compounds in $CDCl_3$

The novel pyridyl- propenone substituted anthracene **52** was characterised by ^{1}H- and ^{13}C-NMR spectroscopy and with the help of two-dimensional spectra all the peaks could be assigned. The aromatic region of the ^{1}H-NMR spectrum is shown in Figure 137. The aldehyde peak, which appears at δ 11.57 ppm is not shown.

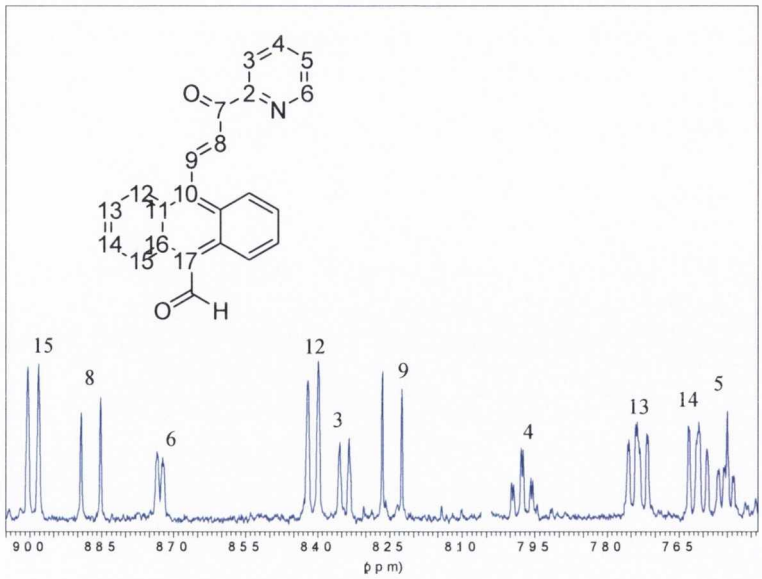


Figure 137: The ^{1}H-NMR spectrum of 52 in $CDCl_3$ (δ 7.5-9.0 ppm shown)

The aromatic peaks were identified by a combination of two-dimensional NMR experiments and their respective coupling constants. For example, both H^8 and H^9 have large coupling constants of 16 Hz which is typical of alkene protons but much larger than that of anthracene or 2-pyridyl derivatives. The anthracene peaks were identified by a combination of the integration of these peaks and the larger coupling constants (≅10 Hz) associated with anthracene protons. Finally, the 2-pyridyl protons could be assigned on the basis of their characteristic coupling constants as well as data from the ^{1}H-^{1}H COSY experiments. Similar two-dimensional data helped in assigning the ^{13}C-NMR spectrum of this compound.

3.7 Conclusion

The attempted synthesis of a novel fused di-terpyridine ligand resulted in the preparation of a number of interesting phenyl-centred compounds. An important factor in these syntheses was the reactivity of the phenyl ring adjacent to the functional group of the central ring. This reactivity often lead to the formation of novel fluorene and fluorenone type compounds which were unexpected. In addition, a number of small novel ligands have been prepared which are currently being used in the preparation of supramolecular frameworks.

Due to the lack of success with the preparation of suitably substituted phenyl-centred terpyridine precursors a different approach was taken using anthracene-centred compounds in an attempt to prevent the *ortho* phenyl groups reacting with the aldehyde

functionality. However despite numerous attempts employing both coupling methodologies and aldehyde preparation, no terpyridine compounds were isolated.

3.8 References

[1] C. Olagnier, Trinity College, (Dublin) **2005**.
[2] F. Murphy, Trinity College, (Dublin), **2008**.
[3] S. Ito, M. Wehmeier, J. D. Brand, C. Kübel, R. Epsch, J. P. Rabe, K. Müllen, *Chem. Eur. J.* **2000**, *6*, 4327.
[4] S. M. Draper, D. J. Gregg, R. J. Madathil, *J. Am. Chem. Soc.* **2002**, *124*, 3486.
[5] K. Harada, H. Hart, C.-J. F. Du, *J. Org. Chem.* **1985**, *50*, 5524.
[6] U. S. Schubert, H. Hofmeier, G. R. Newkome, *Modern Terpyridine Chemistry*, Wiley-vch, **2006**.
[7] O. Kohle, S. Ruile, M. Grätzel, *Inorg. Chem.* **1996**, *35*, 4779.
[8] E. C. Constable, A. J. Edwards, R. Martínez-Mañez, P. R. Raithby, A. M. W. C. Thompson, *J. Chem. Soc., Dalton Trans.* **1994**, 645.
[9] G. Chelucci, M. A. Cabras, A. Saba, *J. Mol. Catal.* **1995**, *95*, L7.
[10] G. Chelucci, A. Saba, F. Soccolini, D. Vignola, *J. Mol. Catal.* **2002**, *178*, 27.
[11] H.-Q. Liu, T.-C. Cheung, S.-M. Peng, C.-M. Che, *J. Mol. Catal.* **1995**, 1787.
[12] Y. Zhang, C. B. Murphy, J. Wayne E. Jones, *Macromolecules* **2002**, *35*, 630.
[13] A. K. Saha, K. Kross, E. D. Kloszewski, D. A. Upson, J. L. Toner, R. A. Snow, C. D. V. Black, V. C. Desai, *J. Am. Chem. Soc.* **1993**, *115*, 11032.
[14] M. D. Ward, *Chem. Soc. Rev.* **1995**, *121-134*.
[15] J.-P. Sauvage, J.-P. Collin, J.-C. Chambron, S. Guillerez, C. Coudret, *Chem. Rev.* **1994**, *94*, 993.
[16] U. S. Schubert, C. Eschbaumer, *Angew. Chem. Int. Ed.* **2002**, *41*, 2892.
[17] G. T. Morgan, F. H. Burstall, *Coord. Chem. Rev.* **1932**, 20.
[18] F. H. Burstall, *J. Chem. Soc.* **1938**, *160*, 1662.
[19] T. Kauffmann, J. König, A. Woltermann, *Chem. Ber.* **1976**, *109*, 3864.
[20] J. Uenishi, T. Tanaka, S. Wakabayashi, S. Oae, H. Tsukube, *Tetrahedron Lett.* **1990**, *31*, 4625.
[21] E. Negishi, *Current Trends in Organich Synthesis*, Pergamon, New York, **1983**.
[22] J. K. Stille, *Angew. Chem. Int. Ed.* **1986**, *25*, 508.
[23] U. Lehmann, O. Henze, A. D. Schlüter, *Chem. Eur. J.* **1999**, *5*, 854.
[24] A. M. W. C. Thompson, *Coord. Chem. Rev.* **1997**, *160*, 1.
[25] A. E. Tschitschibabin, *Journal fuer Praktische Chemie/Chemiker-Zeitung* **1924**, *2*, 107.
[26] F. Kröhnke, *Synthesis* **1976**, 1.
[27] K. T. Potts, D. A. Usifer, A. Guadalupe, H. D. Abruna, *J. Am. Chem. Soc.* **1987**, *109*, 3961.
[28] G. W. V. Cave, C. L. Raston, *Chem. Commun.* **2000**, 2199.
[29] E. C. Constable, M. D. Ward, *J. Chem. Soc., Dalton Trans.* **1990**, 1405.
[30] U. S. Schubert, C. Eschbaumer, O. Hien, P. R. Andres, *Tetrahedron Lett.* **2001**, *42*, 4705.
[31] M. Borgstrom, S. Ott, R. Lomoth, J. Bergquist, L. Hammarström, O. Johansson, *Inorg. Chem.* **2006**, *45*, 4823.
[32] R. Ziessel, J. Suffert, M.-T. Youinou, *J. Org. Chem.* **1996**, *61*, 6535.
[33] K. T. Potts, D. Konwar, *J. Org. Chem.* **1991**, *56*, 4815.

[34] A. C. Benniston, G. Chapman, A. Harriman, M. Mehrabi, C. A. Sams, *Inorg. Chem.* **2004**, *43*, 4227.
[35] G. D. Storrier, S. B. Colbran, D. B. Hibbert, *Inorg. Chim. Acta* **1995**, *239*, 1.
[36] E. C. Constable, P. Harverson, D. R. Smith, L. A. Whall, *Polyhedron* **1997**, *16*, 3615.
[37] E. C. Constable, P. Harveston, D. R. Smith, L.A.Whall, *Tetrahedron* **1994**, *50*, 7799.
[38] R. L. Frank, E. F. Riener, *J. Am. Chem. Soc.* **1950**, *72*, 4182.
[39] J. Uenishi, T. Tanaka, K. Nishiwaki, S. Wakabayashi, S. Oae, H. Tsukube, *J. Org. Chem.* **1993**, *58*, 4382.
[40] E. C. Constable, R. Chotalia, *J. Chem. Soc., Chem. Commun.* **1992**, 64.
[41] E. C. Constable, *Chem. Soc. Rev.* **2007**, *36*, 246.
[42] R. Ruminski, J. Kiplinger, T. Cockcroft, C. Chase, *Inorg. Chem.* **1989**, *28*, 370.
[43] F. Barigelletti, L. Flamigni, V. Balzani, J.-P. Collin, J.-P. Sauvage, A. Sour, E. C. Constable, A. M. W. C. Thompson, *J. Am. Chem. Soc.* **1994**, *116*, 7692.
[44] F. Loiseau, R. Passalacqua, S. Campagna, M. I. J. Polson, Y.-Q. Fang, G. S. Hanan, *Photochem. Photobiol.* **2002**, *1*, 982.
[45] S. Sankararaman, *Pericyclic Reactions - A Textbook*, Wiley -VCH, **2005**.
[46] C. F. H. Allen, *Chem. Rev.* **1945**, *37*, 209.
[47] M. A. Ogliaruso, M. G. Romanelli, E. I. Becker, *Chem. Rev.* **1965**, *65*, 261.
[48] D. M. White, *J. Org. Chem.* **1974**, *39*, 1951.
[49] L. N. Ferguson, *Chem. Rev.* **1946**, *38*, 227.
[50] R. C. Larock, *Comprehensive Organic Transformations*, Wiley-VCH, **1999**.
[51] M. P. Gore, S. J. Gould, D. D. Weller, *J. Org. Chem.* **1992**, *52*, 2774.
[52] T. J. Hagen, K. Narayanan, J. Names, J. M. Cook, *J. Org. Chem.* **1989**, *54*, 2170.
[53] G. Zweifel, G. R. Hahn, T. M. Shoup, *J. Org. Chem.* **1987**, *52*, 5487.
[54] V. Sharma, B. Bachand, M. Stimard, J. D. Wuest, *J. Org. Chem.* **1994**, *59*, 7785.
[55] V. C. E. Burnop, G. H. Elliott, R. P. Linstead, *J. Chem. Soc.* **1940**, 727.
[56] B. S. Joshi, Q. Jiang, T. Rho, S. W. Pelletier, *J. Org. Chem.* **1994**, *59*, 8220.
[57] Y. Ishii, K. Nakayama, M. Takeno, S. Sakaguchi, T. Iwahama, Y. Nishiyama, *J. Org. Chem.* **1995**, *60*, 3934.
[58] S.-I. Murahashi, Y. Oda, T. Naota, T. Kuwabara, *Tetrahedron Lett.* **1993**, *34*, 1299.
[59] A. W. Burgstahler, L. R. Worden, T. B. Lewis, *J. Org. Chem.* **1963**, *28*, 2918.
[60] A. O. Bedenbaugh, J. H. Bedenbaugh, W. A. Bergin, J. D. Adkins, *J. Am. Chem. Soc.* **1970**, *92*, 5774.
[61] H. C. Brown, B. C. S. Rao, *J. Am. Chem. Soc.* **1958**, *80*, 5377.
[62] T. H. Regan, J. B. Miller, *J. Am. Chem. Soc.* **1967**, *32*, 592.
[63] K. E. Maly, E. Gagnon, T. Maris, J. D. Wuest, *J. Am. Chem. Soc.* **2007**, *129*, 4306.
[64] C. Graebe, *Berichte der Deutschen Gesellschaft* **1874**, *7*, 48.
[65] G. J. Bodwell, J. N. Bridson, M. K. Cyranski, J. W. J. Kennedy, T. M. Krygowski, M. R. Mannion, D. O. Miller, *J. Org. Chem.* **2003**, *68*, 2089.
[66] X. Xue, L. T. Scott, *Org. Lett.* **2007**, *9*, 3937.
[67] S. Merlet, M. Birau, Z. Y. Wang, *Org. Lett.* **2002**, *4*, 2157.
[68] A. Padwa, U. Chiacchio, D. J. Fairfax, J. M. Kassir, A. Litrico, M. A. Semones, S. L. Xu, *J. Org. Chem.* **1993**, *58*, 5429.
[69] J. MLochowski, M. Brzaszcz, M. Giurg, J. Palus, H. Wojtowicz, *Eur. J. Org. Chem.* **2003**, 4329.

[70] D. H. R. Barton, R. A. H. F. Hui, S. V. Ley, *J. Chem. Soc., Perkin Trans. 1* **1982**, 2179.
[71] M. D. Clayton, Z. Marcinow, P. W. Rabideau, *Tetrahedron Lett.* **1998**, *39*, 9127.
[72] S. Narasimhan, K. G. Prasad, S. Madhavan, *Synth. Commun.* **1995**, *25*, 1689.
[73] J. S. Cha, J. E. Kim, M. S. Yoon, Y. S. Kim, *Tetrahedron Lett.* **1987**, *28*, 6231.
[74] R. d. Nimmagadda, C. McRae, *Tetrahedron Lett.* **2006**, *47*, 3505.
[75] P. Kovacic, F. W. Koch, *J. Org. Chem.* **1965**, *30*, 3176.
[76] L. Tong, H. Lau, D. M. Ho, J. Robert A. Pascal, *J. Am. Chem. Soc.* **1998**, *120*, 6000.
[77] K. Miyawaki, T. Kawano, I. Ueda, *Tetrahedron Lett.* **1998**, *39*, 6923.
[78] J. R. Heldt, J. Heldt, M. Jozefowicz, J. Kaminski, *Journal of Fluorescence* **2001**, *11*, 65.
[79] L. Biczok, T. Berces, *J. Phys. Chem.* **1988**, *92*, 3842.
[80] L. Biczok, T. Berces, H. Inoue, *J. Phys. Chem. A* **1999**, *103*, 3837.
[81] S. A. Rani, J. Sobhanadri, T. A. P. Rao, *J. Photochem. Photobiol., A* **1996**, *94*, 1.
[82] Y. Matsushita, T. Ichimura, T. Hikida, *Chem. Phys. Lett.* **2002**, *360*, 65.
[83] T. Nakagawa, D. Kumaki, J.-i. Nishida, S. Tokito, Y. Yamashita, *Chem. Mater.* **2008**, *20*, 2615.
[84] K. Yoshihara, D. R. Kearns, *J. Chem. Phys.* **1966**, *45*, 1991.
[85] D. Bailey, V. E. Williams, *Tetrahedron Lett.* **2004**, *45*, 2511.
[86] D. Bailey, V. E. Williams, *J. Chem. Soc., Chem. Commun.* **2005**, 2569.
[87] H. S. Kim, S. Kyung, D. O. Jang, *Supramol. Chem.* **2006**, *18*, 97.
[88] Y. i. Lin, S. A. L. Jr., C. M. Seifert, R. G. Child, G. O. Morton, P. F. Fabio, *J. Org. Chem.* **1979**, *44*, 4701.
[89] O. Cakmak, R. Erenler, A. Tutar, N. Celik, *J. Org. Chem.* **2006**, *71*, 1795.
[90] D. D. M. Wayner, D. R. Arnold, *Can. J. Chem.* **1985**, *63*, 871.
[91] G. Albano, V. Balzani, E. C. Constable, M. Maestri, D. R. Smith, *Inorg. Chim. Acta* **1998**, *277*, 225.
[92] S. Tu, T. Li, F. Shi, F. Fang, S. Zhu, X. Wei, Z. Zong, *Chem. Lett.* **2005**, *34*, 732.
[93] B. Whittle, S. R. Batten, J. C. Jeffrey, L. H. Rees, M. D. Ward, *J. Chem. Soc., Dalton Trans.* **1996**, 4249.
[94] S. G. Dimagno, V. S.-Y. Lin, M. J. Therien, *J. Org. Chem.* **1993**, *58*, 5983.
[95] J. Hovinen, H. Hakala, *Org. Lett.* **2001**, *3*, 2473.
[96] F. d. Montigny, G. Argouarch, C. Lapinte, *Synthesis* **2006**, 293.

Chapter 4

Experimental

4.0 Experimental

General Methods

Unless otherwise stated all reactions were carried out in air. Solvents were dried as required according to standard techniques. Flash chromatography was performed using silica gel or activated alumina (Aldrich Chemicals) as the stationary phase. Separations were undertaken in air. All chemicals were purchased from Aldrich Chemical Co. Ltd. and were used withou further purification unless otherwise stated. Deuterated ruthenium(II) *bis* bipyridine dichloride was obtained from the research group of Prof. Han Vos in Dublin City University.

Electrospray mass spectra were referenced against Leucine Enkephalin (555.6 g mol^{-1}) and reported within 5 ppm. MALDI-TOF mass spectra were recorded on a Waters MALDI-QTOF Premier spectrometer using an α-cyano-4-hydroxy cinnamic acid matrix. Accurate mass spectra were referenced against [Glu^1]-Fibrinopeptide B (1570.6 g mol^{-1}) and reported within 5 ppm.

Nuclear magnetic resonance spectra were recorded in deuterated acetonitrile or chloroform with (i) a Bruker Avance DPX-400 MHz spectrometer at the following frequencies: 400.13 MHz for ^{1} and 100.6 MHz for ^{13}C, (ii) an AV-400 MHz spectrometer at 400.23 MHz for ^1H and 100.6 MHz for ^{13}C or (iii) an AV-600 MHz MHz spectrometer at 600.13 MHz for ^1H and 150.6 MHz for ^{13}C. The signals for ^1H and ^{13}C spectra were referenced to TMS at δ 0.0 ppm and coupling constants were recorded in Hz. ^{13}C signals were assigned with the aid of DEPT 145 and DEPT 90 experiments. 2-D correlation spectra were recorded on the AV-400 MHz spectrometer or the AV-600 MHz spectrometer and were employed to assign the ^1H and ^{13}C peaks. Homonuclear correlation spectroscopy was performed using TOCSY or ^1H-^1H COSY experiments, heteronuclear correlation spectroscopy was performed using HSQC, HMQC or HMBC (long range) experiments. All coupling constants were cross-referenced with all the other coupling constants on each ring system, but are only reported once.

UV-Vis absorption spectra were recorded on a Shimadzu UV-2401PC UV-Vis recording spectrometer. The emission spectra were nit corrected and were recorded at room temperature on Varain Fluorescence Cary Eclipse spectrophotometer. IR spectra were obtained using a Perkin Elmer Diffuse Reflectence spectrometer in solid form in a KBr mixture. Elemental analyses were carried out at University College Dublin using a Carlo

Erba 1006 automatic analyser. Melting points are given uncorrected and were measured in capillary tubes using a Griffin melting points apparatus.

Crystal data and stuctural experimental details are summarised in Tables 1 and 2 in the Annex. Selected bond lengths and angles are given in the discussion. the remaining angles, distances and coordiantes as well as anisotropic diplacement parameters and hydrogen atom coordinates are available on the attached CD. The single-crystal analyses were performed by Dr. Christopher Fitchett, Dr. Tom McCabe and Dr. Sunil Varughese in Trinity College with a Brüker SMART APEX CCD diffractometer using graphite monochromised Mo-K_α (λ = 0.71073Å) radiation at the temperatures given in the tables. Data reduction was performed using SAINT. Intensities were corrected for Lorentz and polarization effects and for absorption by SADABS. Space groups were determined from systematic absences and checked for higher symmetry. The structures were solved by direct methods using SHELXS and refined on F^2 using all data by full-matrix least-squares procedures with SHELX-97. All non-hydrogen atoms were refined with anisotropic displacement parameters 1.3 times the isotropic equivalent of their carrier carbons. Absolute structure determinations were based on the Flack parameter. The functions minimised were $\Sigma w(F_o^2 - F_c^2)$, with $w = [\sigma^2(F_o^2) + (aP)^2 + bP]^{-1}$, where $P = [\max(F_o)^2 + 2F_c^2]/3$. In all cases, final Fourier synthesis showed no significant residual electron density in chemically sensible positions.

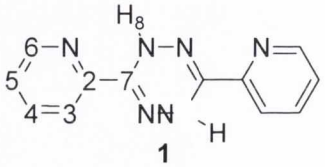
Synthesis of ligands

3,6-di(2-pyridyl)-1,2,4,5-tetrazine (2)

3,6-di(2-pyridyl)-1,2-dihydro-1,2,4,5-tetrazine (1).

2-cyanopyridine (5.29g, 51.0 mmol) was added to hydrazine hydrate (5 mL, 103 mmol) and stirred for 3 hours at 90°C. The resulting solid was filtered and recrystallised from ethanol to give 2.52g of product (41% yield).

^{1}H NMR ($CDCl_3$): δ 8.61 (s 2 H H^8), 8.59 (d 2 H H^6, $J_{5,6}$ = 5.3 Hz), 8.07 (d 2 H H^3, $J_{3,4}$ = 7.9 Hz), 7.77 (ddd 4 H H^4 $J_{4,5}$ = 7.8 $J_{4,6}$ = 1.46 Hz), 7.37 (dm 4 H H^5, $J_{3,5}$ = 1.5 Hz). ^{13}C NMR ($CDCl_3$): δ 148.34 (2 C C^6), 147.44 (2 C C^2), 146.59 (2 C C^7), 136.68 (2 C C^4), 124.83 (2 C C^5), 121.23 (2 C C^3).

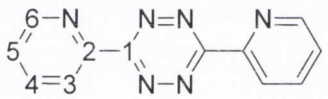


1

3,6 di(2-pyridyl)-1,2,4,5-tetrazine (2)

100 mL of a 6M solution of $NaNO_2$ was added dropwise to a solution of concentrated HCl (60 mL). The gas formed was then passed through a 60 mL dichloromethane solution containing 2.52 g (10.58 mmol) of **2**. The dichloromethane solution was kept at 0°C for the entire reaction. When all the sodium nitrite had been added, the dichloromethane solution was then allowed to return to room temperature. The solvent was then evaporated and the pink solid dissolved in water and neutralized with the addition of 10% ammonia solution. The mixture was then extracted into DCM, dried over $MgSO_4$ and 2.12g (85% yield) was recovered.

^{1}H NMR ($CDCl_3$): δ 9.01 (dm 2H H^6 $J_{5,6}$= 4.8 Hz), 8.77 (dm 2H H^3 $J_{3,4}$ =8.2 Hz), 8.03 (ddd 2H H^4 $J_{4,5}$ = 8.2 Hz, $J_{4,6}$ =2.0 Hz) 7.60 (ddd 2H H^5 $J_{3,5}$ = 2.0 Hz). ^{13}C NMR ($CDCl_3$): δ 163.40 (2 C, C^1=N), 150.59 (2 C C^6), 149.56 (2 C C^2), 137.09 (2 C C^3), 126.20 (2 C C^4), 124.09 (2 C C^5).



2

3,6-di-(2-pyridyl)-4-pyrimidyl pyridazine (3)

The reaction was carried out by refluxing **2** (0.102g, 0.433 mmol) and 5-ethynylpyrimidine (0.047g, 0.451 mmol) in 2.5 mL of toluene for 24 hours. The solvent was removed by evaporation, and purification was carried out by running the reaction mixture through a column of silica using ethyl acetate: methanol (5:1). 0.087g (0.279 mmol) of product was recovered (65% yield).

I.R. ν 3093m, 3065m, 3039m, 3022m, 1582s, 1571s, 1555s, 1477s, 1419s, 1393s, 991s, 793s, 773s, 724m, 656m, 629m, 620m, 588w, 531w cm^{-1}.

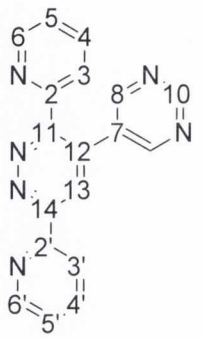
^{1}H NMR ($CDCl_3$): δ 9.21 (s 1H H^{10}), 8.81 (dm 1H $H^{3'}$ $J_{3',4'}$=8.0 Hz), 8.73 (dm 1 H $H^{6'}$ $J_{5',6'}$=4.0 Hz $J_{4',6'}$= 2.0 Hz), 8.68 (s 2H H^8), 8.67 (s 1 H H^{13}), 8.36 (dm 1 H H^6 $J_{5,6}$=4.5 Hz $J_{4',6}$=1.5 Hz) 8.32 (dm 1 H H^3 $J_{3',4}$=8.0 Hz), 7.94 (ddd 1 H $H^{4'}$ $J_{4',5'}$=7.4 Hz), 7.90 (ddd 1 H H^4 $J_{4,5}$=6.0 Hz), 7.45 (dm 1 H $H^{5'}$ $J_{3',5'}$=1.0 Hz), 7.31 (dm 1 H H^5 $J_{3,5}$=1.0 Hz).

^{13}C NMR ($CDCl_3$): δ 157.85 (1 C C^{10}), 157.74 (1C C^{14}), 157.09 (1C C^{11}), 155.95 (2 C C^8), 154.19 (1 C C^2), 152.49 (1 C $C^{2'}$), 149.53 (1 C $C^{6'}$), 148.68 (1 C C^6), 137.32 (1 C

$C^{4'}$), 137.17 (1 C C^{4}), 134.06 (1 C C^{12}), 131.95 (1 C C^{7}), 125.95 (1 C C^{13}), 125.16 (1C $C^{5'}$), 124.66 (1C C^{3}), 124.15 (1C C^{5}), 121.82 (1C $C^{3'}$).

ESI-MS (CH_3CN) m/z =335.0 (calculated for $C_{18}H_{12}N_6$ 335.4).

Anal. Calc. For $C_{18}H_{12}N_6$; C, 69.22; H, 3.87; N, 26.91. Found: C, 68.63; H, 3.85; N, 26.71. m.p. 170°-172°C.



3

3,4,6-tri (2-pyridyl) pyridazine (4)

1 mL of a 2.5% methanolic solution of KOH was added to a 5 mL solution of THF containing **2** (0.500g, 2.116 mmol) and 2-acetyl pyridine (400 µl, (3.567 mmol) at 40^0C. The mixture was stirred for 5 minutes, and then allowed to cool, washed with water, and extracted into dichloromethane. The solvent was then removed by vacuum, and the resultant mixture was run through a silica column (ethyl acetate:methanol 10:1) to give 0.530 g (1.702 mmol) of product (80% yield). This was further purified by recrystallisation in a mixture of ethyl acetate and petroleum ether.

IR (KBr): ν 3081m, 3066m, 3004m, 1587s, 1574s, 1560m, 1478m, 1468s, 1393s, 1095m, 993s, 788s, 769m, 748m, 619m, 584m, 537m cm^{-1}.

Note: TOCSY experiments were used to assign each proton to its neighbours on the same ring. However, it was not possible to say which ring was which. As a result rings a, b and c have been arbitrarily assigned.

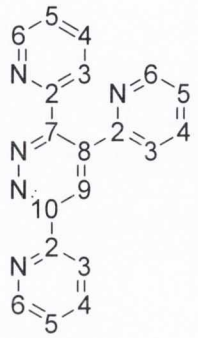
^{1}H NMR: ($CDCl_3$): δ 8.82 (s 1H H^{9}), 8.75 (dm 1H H^{3a} $J_{3,4}$=8.0 Hz), 8.69 (dm 1H H^{6a} $J_{5,6}$= 4.5 Hz $J_{4,6}$= 1.5 Hz), 8.51 (dm 1H H^{6b} $J_{5,6}$= 4.5 Hz $J_{4,6}$=1.5 Hz), 8.31 (dm 1 H H^{6c} $J_{5,6}$=4.5 Hz $J_{4,6}$= 1.5 Hz), 8.13 (dm 1H H^{3b} $J_{3,4}$=8.0 Hz), 7.88 (ddd 1H H^{4a} $J_{4,5}$=7.5 Hz, $J_{4,6}$=1.5 Hz), 7.82 (ddd 1H H^{4b} $J_{4,5}$=7.5 Hz $J_{4,6}$=1.5 Hz), 7.63 (ddd 1H H^{4c} $J_{4,5}$=7.5 Hz $J_{4,6}$=1.5 Hz), 7.36 (ddm 1H H^{5a} $J_{3,5}$=1.5 Hz), 7.34 (dm 1H H^{3c} $J_{3,4}$=8.0 Hz), 7.22 (dm 1H H^{5b}), 7.21 (dm 1H H^{5c}).

^{13}C NMR ($CDCl_3$): δ 157.67 (1C $C^{7/10}$), 157.50 (1C $C^{7/10}$), 155.33 (1C C^{2a}), 155.10 (1C C^{2b}), 152.75 (1C C^{2c}), 149.04 (2C $C^{6a,6b}$), 148.13 (1C C^{6c}), 138.94 (1C C^{8}), 136.76 (1C

C^{4a}), 136.38 (1C C^{4b}), 135.79 (1C C^{4c}), 125.32 (1C C^{9}), 124.42 (1C C^{3a}), 124.15 (1C C^{5a}), 123.60 (1C C^{3b}), 122.99 (1C C^{5b}), 122.41 (1C C^{5c}), 121.35 (1C C^{3c}).

ESI-MS (CH_3CN) m/z = 312.1252, calculated for $C_{19}H_{13}N_5$: 312.1249.

Anal. Calculated for $C_{19}H_{13}N_5$: C, 73.30; H 4.21; N, 22.49. Found; C, 72.27; H, 4.32; N 22.33. m.p. 165°-166°C.



4

3,6-di(2-pyridyl)-4,5-diphenyl pyridazine (6)

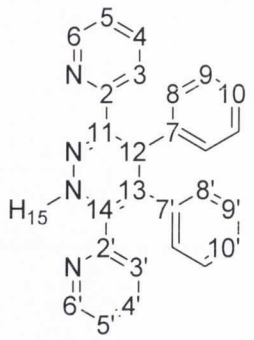
*3,6-di(2-pyridyl)-4,5-diphenyl hydropyridazine (**5**)*

0.600g (2.540mmol) of **2** and 0.469g (2.600 mmol) of trans-stilbene were refluxed in 20 mL of toluene for 24 hours. At this stage, the colour of the solution had changed from dark pink to bright yellow. The solvent was removed by vacuum, and the reaction mixture was purified by running it through a column of silica (dichloromethane: diethyl ether , 10:1). 0.906 g (2.337 mmol) of product was obtained. (Yield 92%)

^{1}H-NMR ($CDCl_3$): δ 9.43 (s 1H H^{15}), 8.67 (dm 1H H^6 $J_{5,6}$=3.8 Hz), 8.61 (dm 1H $H^{6'}$ $J_{5',6'}$=4.4 Hz), 8.10 (dm 1H $H^{3'}$ $J_{3',4'}$=7.9 Hz), 7.63 (ddd 1H $H^{4'}$ $J_{4',5'}$=7.8 Hz, $J_{4',6'}$=1.8 Hz), 7.57 (d 2H, $H^{8'}$, $J_{8',9'}$ = 7.0 Hz), 7.40 (ddd 1H H^4 $J_{4,5}$= 7.8 Hz, $J_{4,6}$= 1.5 Hz), 7.30-7.17 (m 11H, $H^{3,\ 5,\ 5',\ 9,10,8',\ 9',\ 10'}$), 5.82 (s 1H H^{12}).

^{13}C-NMR ($CDCl_3$): δ 154.18 (1C C^{11}), 151.56 (1C C^{14}), 149.02 (1C C^6), 148.30 (1C $C^{6'}$), 141.85 (1C C^Q), 138.85 (1C C^Q), 136.08 (1C $C^{4'}$), 135.86 (1C C^4), 135.11 (1C C^Q), 129.85 (2C), 128.54 (2C), 128.27 (4C), 128.25 (1C), 127.16 (1C), 126.70 (1C), 125.47 (1C), 123.02 (1C), 122.67 (1C), 121.48 (1C), 108.15 (1C C^{13}), 41.54 (1C C^{12}).

ESI-MS (CH_3CN) m/z = 389.1782, calculated for $C_{26}H_{21}N_4$: $[MH]^+$ m/z 389.1766.



5

*3,6 di(2-pyridyl) 4,5-diphenyl pyridazine (**6**)*

20 mL of a 6M solution of $NaNO_2$ was added dropwise to a solution of concentrated HCl (12 mL). The gas formed was then passed through a 40 mL dichloromethane solution containing 0.807g (2.093 mmol) of **5**. The dichloromethane solution was kept at 0°C for the entire reaction. When all the sodium nitrite had been added, the dichloromethane solution was then allowed to return to room temperature. The solvent was then evaporated and the reaction mixture dissolved in water and neutralized with the addition of 10% ammonia solution. The mixture was then extracted into DCM, dried over $MgSO_4$ and run through a column of silica (ethyl acetate:methanol, 10:1). 0.598 g (1.549 mmol) of product was recovered (74% yield).

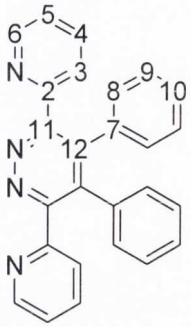
I.R. ν 3078m, 3054m, 3024m, 3003m, 1587s, 1569s, 1474s, 1377s, 1155s, 991s, 793s, 782s, 771s, 746s, 636s, 624s, 531m, 486m.

^{1}H-NMR (CH_3CN): δ 8.42 (dm 2H H^6 $J_{5,6}$=4.5 Hz), 7.68 (dm 2H H^4 $J_{4,5}$=6.5 Hz $J_{4,6}$=1.5 Hz), 7.63 (dm 2H H^3 $J_{3,4}$=7.5 Hz), 7.17 (dm 2H H^5 $J_{3,5}$=1.5 Hz), 7.05 (dm 3H H^8, H^{10} $J_{8,9}$=8.0 Hz, $J_{8,10}$=1.5 Hz), 6.87 (dm 2H H^9).

^{13}C NMR ($CDCl_3$): δ 158.50 (2C C^{11}), 155.55 (2C C^2), 148.42 (2C C^6), 138.72 (2C C^{12}), 135.72 (2C C^4), 134.20 (2C C^7), 129.67 (4C C^9), 127.11 (4C C^8), 126.86 (2C, C^{10}), 124.58 (2C, C^3), 122.48 (2C, C^5).

ESI-MS (CH_3CN) m/z = 387.1610, calculated. for $C_{26}H_{19}N_4$: $[MH]^+$ 387.1596.

Anal. Calculated for $C_{26}H_{18}N_4$: C, 80.81; H, 4.69; N, 14.50. Found: C, 79.92; H, 4.64; N, 14.26. m.p. 189°-191°C.



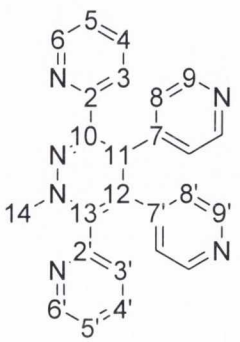
6

3,6- di(2-pyridyl)-4,5-di(4-pyridyl) pyridazine (8)

3,6-di(2-pyridyl) 4,5-di(4-pyridyl) hydropyridazine (7)

0.500 g (2.116 mmol) of **3** and 0.410 g (2.251 mmol) of 1,4 di(4-pyridyl) phenylene were added to 10 mL of toluene and heated in a sealed tube at 180°C for 24 hours. The solvent was then removed by vacuum and the reaction mixture was run through a column of silica (di-ethyl ether:methanol, 5:1). 0.618 g (1.587 mmol) of a bright yellow compound was isolated as the desired product (75% yield). ^{1}H-NMR ($CDCl_3$): δ 9.50 (s 1H H^{14}), 8.72 (dm 1H H^{6} $J_{5,6,}$=5.0 Hz), 8.61 (dm 1H $H^{6'}$ $J_{5',6'}$=6.0 Hz), 8.50 (d 2H, $H^{9/9'}$ $J_{8,9}$=6.5 Hz), 8.41 (d 2H $H^{9/9'}$ $J_{8,9}$=6.0 Hz), 8.13 (dm 1 H $H^{3'}$ $J_{3',4'}$=8.0 Hz), 7.66 (ddd 1 H $H^{4'}$ $J_{4',5'}$=7.8 Hz $J_{4',6'}$=1.5 Hz), 7.55 (ddd 1 H H^{4} $J_{4,5}$=7.5 Hz $J_{4,6}$=1.50 Hz), 7.46 (d 2 H $H^{8/8'}$), 7.36 (dm 1H H^{3} $J_{3,4}$=6.0 Hz), 7.32 (dm 1 H H^{5} $J_{3,5}$=2.0 Hz), 7.22 (dm 1H $H^{5'}$, $J_{3',5'}$=2.0 Hz), 7.06 (d 2 H $H^{8/8'}$), 5.86 (s 1H H^{11}).

^{13}C NMR ($CDCl_3$): δ 153.39 (1 C $C^{2'}$), 150.79 (1 C C^{2}), 150.09 (1 C $C^{9/9'}$), 150.02 (1C $C^{9/9'}$), 150.00 (1C C^{6}), 148.42 (1C $C^{6'}$), 146.30 (1C $C^{7'}$), 140.67 (1C C^{10}), 138.74 (2C C^{13}), 136.48 (2C C^{4}), 136.21 (1C $C^{4'}$), 125.64 (1C C^{3}), 124.14 (1C C^{5}), 123.90 (1C $C^{8/8'}$), 123.27 (1C $C^{5'}$), 123.09 (1C $C^{8/8'}$), 121.45 (1C $C^{3'}$), 102.52 (1C C^{11}), 39.48 (1C C^{7}). ESI-MS (CH_3CN) m/z =391.1667 calculated for $C_{24}H_{19}N_6$ $[MH]^+$:391.1671.



7

3,6-di(2-pyridyl)-4,5-di(4-pyridyl) pyridazine (**8**)

20 mL of a 6M solution of $NaNO_2$ was added dropwise to a solution of concentrated HCl (12 mL). The gas formed was then passed through a 40 mL dichloromethane solution containing 0.618g (1.587 mmol) of **7**. The dichloromethane solution was kept at 0°C for the entire reaction. When all the sodium nitrite had been added, the dichloromethane solution was then allowed to return to room temperature. The solvent was then evaporated and the reaction mixture dissolved in water and neutralized with the addition of 10% ammonia solution. The mixture was then extracted into DCM, dried over $MgSO_4$ and run through a column of silica (ether:methanol, 1:1). 0.308g (0.793 mmol) of product was recovered (50 % yield).

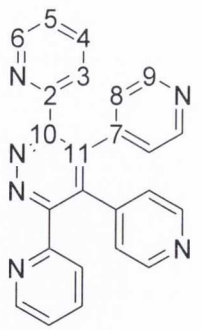
I.R. ν 3059m, 3039m, 3027m, 1596s, 1584s, 1568s, 1408s, 1382s, 1374s, 1218m, 991s, 813s, 808s, 796s, 786s, 750s, 648s, 624s, 538m, 489w cm^{-1}.

^{1}H-NMR ($CDCl_3$): δ 8.34 (d 2H H^9 $J_{8,9}$= 6.0 Hz), 8.30 (dm 2H H^6 $J_{5,6}$= 4.5 Hz), 8.01 (dm 2H H^3 $J_{3,4}$= 7.6 Hz), 7.81 (ddd 2H H^4 $J_{4,5}$= 7.0 Hz, $J_{4,6}$=1.5 Hz), 7.23 (ddm 2H H^5), 6.85(d 2H H^8).

^{13}C NMR ($CDCl_3$): δ 157.03 (2C C^{10}), 154.18 (2C C^2), 148.65 (2C C^9), 148.31 (2C C^6), 142.59 (2C C^7), 136.28 (2C C^4), 136.10 (2C C^{11}), 124.49 (2C C^3), 124.10 (2C C^8), 123.19 (2C C^5).

ESI-MS (CH_3CN) m/z = 388.1436, calculated. for $C_{24}H_{16}N_6$: $[M-H]^+$ 387.1504.

Anal. Calculated. for $C_{24}H_{16}N_6$; C, 74.21; H, 4.15; N, 21.64. Found: C, 75.83; H, 4.60; N, 20.88. m.p. 220°C.



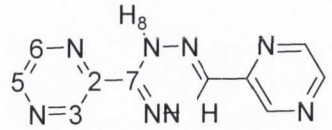
8

3,6-di(2-pyrazinyl)-1,2,4,5-tetrazine (10)

Dihydro-3,6-di(2-pyrazinyl)-1,2,4,5-tetrazine (***9***)

5.0 mL (55.05 mmol) of 2-cyano pyrazine and 9 mL of concentrated HCl were added to 90 mL THF and stirred for 20 mns. 10.3 mL (211.75mmol) hydrazine hydrate was then added and the mixture was refluxed for 300 mns. The mixture was cooled to room

temperature and filtered. The resulting solid was recrystallised from DMF to give 4.82 g (72%) yield. ^{1}H-NMR ($CDCl_3$) δ 9.90 (s 2H H^8), 8.92 (s 2H H^3), 8.87 (s 2H H^5), 8.77 (s 2H, H^6).



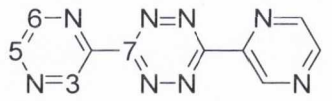
9

3,6-di(2-pyrazinyl)-1,2,4,5-tetrazine (10)

100 mL of a 6M solution of $NaNO_2$ was added dropwise to a solution of concentrated HCl (60 mL). The gas formed was then passed through a 20 mL dichloromethane suspension at room temperature containing 4.82 g (20.06 mmol) of **9** by blowing nitrogen through the acid and into the dichloromethane solution. The mixture was stirred for a further 30 mns. The solvent was then evaporated and the pink solid dissolved in water and neutralized with the addition of a sodium hydrogencarbonate solution. The mixture was extracted into dichloromethane, dried over $MgSO_4$ and 2.53g (38% yield) was recovered.

^{1}H-NMR ($CDCl_3$) δ 9.98 (d 2H H^3 $J_{3,5}$ = 1.4 Hz), 8.99 (dd 2H H^5 $J_{5,6}$ = 2.3 Hz), 8.93 (d 2H H^6).

^{13}C-NMR ($CDCl_3$) δ 162.89 (2C C^7), 147.28 (2C C^6), 145.28 (2C C^3), 145.22 (2C C^2), 144.99 (2C C^5).



10

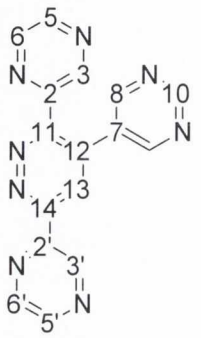
3,6-di-(2-pyrazinyl)-4-(pyrimidyl) pyridazine (11)

0.310 g (1.30 mmol) of **10** and 0.140 g (1.39 mmol) of 5-ethynyl pyrimidine were refluxed in 25 mL of toluene for 24 hours. The solvent was removed *in vacuo* and the reaction mixture washed with water. It was then extracted into dichloromethane and purified via column chromatography (10:1 ethyl acetate:methanol) to give 0.214 g (49% yield) of product.

I.R. ν 3130m, 3098m, 3033s, 1575s, 1556s, 1434s, 1380s, 1161s, 1101s, 1019s, 869s, 860s, 758m, 724s, 631s, 581m, 482m cm^{-1}.

^{1}H-NMR ($CDCl_3$): δ 10.05 (d 1H, $H^{3'}$, $J_{3',5'}$ = 1.4 Hz), 9.64 (d 1H, H^3, $J_{3,5}$ = 1.4 Hz), 9.28 (s 1H, H^{10}), 8.79 (d 1H, $H^{6'}$, $J_{5',6'}$ = 2.2 Hz), 8.73 (m 3H, H^8, $H^{5'}$), 8.66 (m 2H, H^6, H^{13}), 8.36 (dd 1H, H^5, $J_{5,6}$ = 2.0 Hz).

^{13}C-NMR ($CDCl_3$): δ 157.96 (1C, C^{10}), 156.38 (1C, C^{11}), 155.43 (2C, C^8), 154.93 (1C, C^{14}), 149.14 (1C, C^2), 147.16 (1C, $C^{2'}$), 145.83 (1C, $C^{6'}$), 145.46, (1C, C^3), 144.80, (1C, C^6), 143.67 (1C, $C^{5'}$), 143.43 (1C, $C^{3'}$), 142.49, (1C, C^5), 134.56, (1C, C^7), 130.73, (1C, C^{12}), 126.09, (1C, C^{13}). Anal. Calculated for $C_{16}H_{10}N_8$: C, 61.14, H, 3.21, N, 35.65. Found: C, 59.60; H, 3.17; N, 35.04. m.p. 226°-228°C.



11

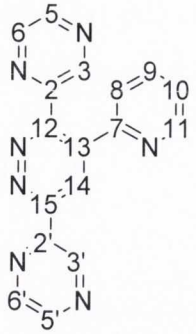
3,6-di-(2-pyrazinyl)-4-(2-pyridyl)-pyridazine (12)

0.310 g (1.30 mmol) of **10** and 147 µl (1.25 mmol) of 2-acetyl pyridine were added to 10 mL of THF and stirred at 40°C. 2 mL of a 2.5% methanol solution of KOH were added and the solution was further stirred for several minutes. The solvent was evaporated *in vacuo*. The mixture was then washed with water and extracted into dichloromethane. The product was purified by column chromatography (ethyl acetate: methanol, 10:1) to give 0.109 g (26% yield) of product.

I.R. ν 3062s, 3016s, 1698m, 1586s, 1571s, 1477s, 1469s, 1387s, 1154s, 1149s, 1020, 861s, 805s, 785s, 752s, 621m, 585m, 503m, 411s cm^{-1}.

^{1}H-NMR ($CDCl_3$): δ 10.02 (d 1H $H^{3'}$, $J_{3',5'}$ = 1.5 Hz), 9.42 (d 1H H^3 $J_{3,5}$ = 1.5 Hz), 8.81 (s 1H, H^{14}), 8.73 (d 1H $H^{6'}$, $J_{5',6'}$ = 2.5 Hz), 8.70 (dd 1H, $H^{5'}$, $J_{3',5'}$ = 1.5 Hz), 8.58 (d 1H, H^6, $J_{5,6}$ = 2.4 Hz), 8.53 (d 1H , H^{11}, $J_{11,12}$ = 4.7 Hz), 8.32 (dd 1H, H^5, $J_{3,5}$ = 1.5 Hz), 7.75 (ddd 1H H^9, $J_{9,10}$ = 8.0 Hz, $J_{9,11}$ = 1.5 Hz), 7.45 (d 1H, H^8, $H_{8,9}$ = 7.4 Hz), 7.29 (ddd 1H, H^{10}, $J_{8,10}$ = 0.9 Hz).

^{13}C-NMR ($CDCl_3$): δ 156.46 (1C, $C^{12/15}$), 155.92 (1C, $C^{12/15}$),154.30 (1C, C^7),150.65 (1C, C^2), 149.27 (1C, C^{11}), 147.78 (1C, $C^{2'}$), 145.42 (1C, $C^{6'}$), 145.25 (1C, C^3), 143.95 (1C, C^6), 143.57 (1C, $C^{5'}$), 143.37 (1C, $C^{3'}$), 142.54 (1C, C^5), 139.57 (1C, C^{13}), 136.27 (1C, C^9), 125.48 (1C, C^{14}), 123.51 (1C, C^8), 122.99 (1C, C^{10}). ESI-MS (CH_3CN) m/z = 313.1076, calculated for $C_{17}H_{12}N_7$ $[MH]^+$: 314.1158.



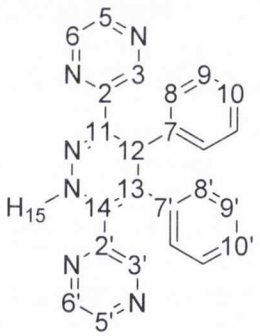
12

3,6-di-(2-pyrazinyl)-4,5-diphenylpyridazine (14)

*3,6-di-(2-pyrazinyl) -4,5-diphenyl hydro pyridazine (**13**)*

0.240 g (1.33 mmmol) of trans-stilbene and 0.310 g (1.30 mmol) of **10** were heated at 160°C in 10 mL toluene in a sealed tube for 24 hours. The solvent was evaporated, the mixture washed with water and extracted into dichloromethane. The mixture was purified by column chromatography (dichloromethane:ether, 10:1) to give 0.390 g (75% yield).

^{1}H-NMR ($CDCl_3$) δ 9.50 (s 1H, H^{15}), 9.43 (s 1H, $H^{3/3'}$), 8.57 (d 1H $H^{5/5'}$, $J_{5,6}$ = 2.2 Hz), 8.51 (d 1H, $H^{5/5'}$, $J_{5,6}$ = 2.2 Hz), 8.41 (m 3H, $H^{6,6'}$, $H^{3/3'}$), 7.55 (d 2H, $H^{9/9'}$, $J_{8,9}$ = 7.5 Hz), 7.27 (m 8H, $H^{8,8',9/9',10,10'}$), 5.67 (s 1H, H^{12}).



13

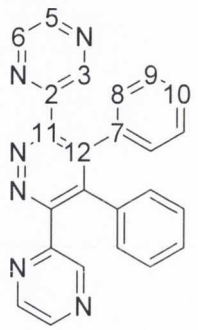
*3,6-di-(2-pyrazinyl)-4,5-diphenylpyridazine (**14**)*

40mL of a 6M solution of $NaNO_2$ was added dropwise to a solution of concentrated HCl (20 mL). The gas formed was then passed through a 20 mL dichloromethane suspension at room temperature containing 0.390 g (1.00 mmol) of **13**. The mixture was then stirred for a further 30 mns. The solvent was then evaporated and the brown solid dissolved in water and neutralized with the addition of a sodium hydrogencarbonate solution. The mixture was extracted into dichloromethane, dried over $MgSO_4$ and recrystallised from ethyl acetate/petroluem ether to give 0.327 g (84% yield).

I.R. ν 3075s, 3049s, 2963s, 2927s, 1963m, 1737m, 1493s, 1471s, 1444s, 1371s, 1262s, 1145s, 1070s, 1064s, 1036s, 863s, 772s, 756s, 701s, 659s, 639s, 628s, 536m, 527m cm^{-1}.

^{1}H-NMR: ($CDCl_3$): δ 8.98 (s 2H, H^3), 8.51 (d 2H, H^6, $J_{5,6}$ = 2.0 Hz), 8.43 (s 2H, H^5), 7.11 (m 6H, $H^{8,10}$), 6.89 (dd 4H, H^9, $J_{8,9}$ = 6.3 Hz, $J_{9,10}$ = 1.5 Hz).

^{13}C-NMR ($CDCl_3$): δ 156.33 (2C, C^{11}), 151.16 (2C, C^2), 145.38 (2C, C^3), 143.47 (2C, C^6), 143.02 (2C, C^5), 139.64 (2C, C^{12}), 133.17 (2C, C^7), 129.59 (4C, C^{11}), 127.48 (6C, $C^{10,12}$). ESI-MS (CH_3CN) m/z = 389.1515, calculated for $C_{24}H_{17}N_6$ $[MH]^+$: 389.1515. Anal. Calculated for C, 74.21; H, 4.15; N, 21.64. Found: C, 73.01; H, 4.35; N, 20.80. m.p. 161°-162°C.

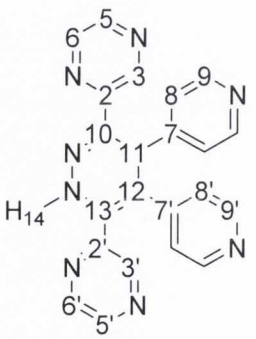


14

3,6-di(2-pyrazinyl)-4,5-di(4-pyridyl) pyridazine (16)

*3,6-di(2-pyrazinyl)-4,5,-di(4-pyridyl) hydropyridazine (**15**)*

0.300 g (1.26 mmol) of **10** and 0.238 g (1.30 mmol) of 1,2 di(4-pyridyl) ethene were added to 10 mL of toluene and heated in a sealed tube at 180°C for 72 hours. The solvent was then removed by vacuum and the reaction mixture was run through a column of silica (diethyl ether:methanol, 1:1). 0.437 g (0.76 mmol) of a bright yellow compound was isolated as the desired product (60% yield). ^{1}H-NMR ($CDCl_3$): δ 9.48 (s 1H, H^{14}), 9.41 (dd, 1H, $H^{3/3'}$, $J_{3/5}$ = 1.0 Hz), 8.70 (dd, 1H, $H^{3/3'}$, $J_{3/5}$ = 1.4 Hz), 8.51 (m 8H, $H^{5,5',6,6',9,9'}$), 7.44(dd, 2H, $H^{8/8'}$, $J_{8,9}$ = 5.9 Hz), 7.04 (dd, 2H, $H^{8/8'}$, $J_{8,9}$ = 5.9 Hz), 5.68 (s, 1H, H^{11}).



15

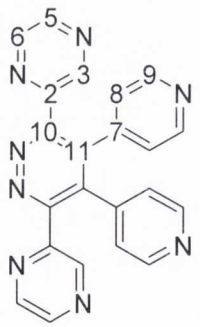
*3,6-di(2-pyridyl)-4,5-di(4-pyridyl) pyridazine (**16**)*

40 mL of a 6M solution of $NaNO_2$ was added dropwise to a solution of concentrated HCl (12 mL). The gas formed was then passed through a 40 mL dichloromethane solution containing 0.437g (0.76 mmol) of **15**. The solvent was then evaporated and the reaction mixture dissolved in water and neutralized with the addition of sodium hydrogencarbonate solution. The mixture was then extracted into DCM, dried over $MgSO_4$ and run through a column of silica (diethyl ether:methanol, 3:1). 0.175 g (0.30 mmol) of product was recovered (40 % yield).

I.R. ν 3069s, 3036s, 2987m, 1597s, 1409s, 1371s, 1154s, 1016s, 991m, 849s, 796s, 762m, 659s, 645s, 627s, 549m, 509m cm^{-1}.

^{1}H-NMR ($CDCl_3$): δ 9.37 (d 2H, H^3, $J_{3,5}$ = 1.0 Hz), 8.56 (d 2H, H^5, $J_{5,6}$ = 2.5 Hz), 8.40 (d 4H, H^9 $J_{8,9}$= 5.6 Hz), 8.29 (dd 2H, H^6), 6.88 (d 4H, H^8).

^{13}C-NMR ($CDCl_3$): 154.90 (2C, C^{10}), 149.62 (2C, C^2), 148.93 (4C, C^9), 145.36 (2C, C^3), 144.26 (2C, C^5), 142.65 (2C, C^6), 141.47 (2C, C^{11}), 137.02 (2C, C^7), 123.86 (4C, C^8). ESI-MS (CH_3CN m/z = 391.1515, calculated for $C_{22}H_{14}N_8$: $[MH]^+$ = 391.1515. Anal. Calculated for C, 67.68; H, 3.61; N, 28.70. Found: C, 66.86, H, 3.65, N, 28.41. m.p. 216°-218°C.



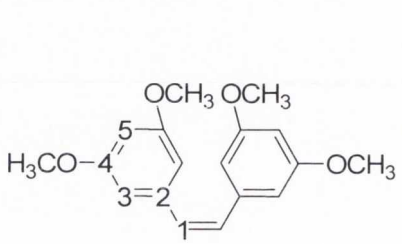
16

3,3'5,5'-tetramethoxystilbene (17)

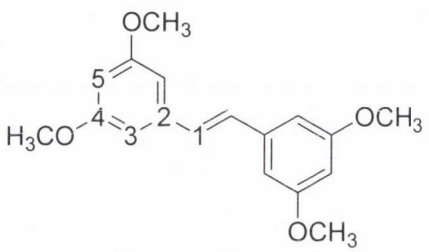
2.0 g (9.26 mmol) of 3,5-dimethoxybromobenzene and 2.27 g (8.65 mmol) of triphenylphosphine were added to 10 mL of dry degassed benzene and stirred overnight under argon. A white precipitate had formed after this time which was filtered and dried. 2.48 g (5.03 mmol) of this and 0.34 g (5.03 mmol) of sodium ethoxide were added to 20 mL of dry degassed THF and stirred under argon. The mixture immediately turned orange. 0.83 g (5.03 mmol) of 3,5-dimethoxybenzaldehyde was added to this and the mixture immediately turned white. The mixture was heated to reflux overnight. The product was isolated by column chromatography (dichloromethane:hexane, 5:2). 1.10 g

of a mixture of *trans* and *cis* tetramethoxystilbene was isolated (40% yield). The two isomers were separated by recrystallisation from toluene. Cis isomer: ^{1}H-NMR ($CDCl_3$): δ 6.57 (s 2H, H^5), 6.48 (d 4H, H^3, $J_{3,5}$ = 2.0 Hz), 6.35 (s 2H, H^1), 3.70 (s 12H, H^{OMe}). ^{13}C-NMR δ 160.05 (4C, C^4), 138.55 (2C, C^2), 130.13 (2C, C^5), 106.32 (4C, C^3), 99.67 (2C, C^1), 54.78 (12C, C^{OMe}). ES I-MS (CH_3CN) m/z = 301.1442 calculated for $C_{18}H_{21}O_4$ $[MH]^+$: 301.1440.

Trans isomer: ^{1}H-NMR ($CDCl_3$): δ 7.04 (s 2H, H^5), 6.69 (s 4H, H^3), 6.42 (s 2H, H^1), 3.86 (s 12 H, H^{OMe}). ^{13}C-NMR δ 160.53 (4C, C^4), 138.70 (2C, C^2), 128.73 (2C, C^5), 104.17 (4C, C^3), 99.47 (2C, C^1), 54.93 (12C, C^{OMe}). ESI-MS (CH_3CN) m/z = 301.1442 calculated for $C_{18}H_{21}O_4$ $[MH]^+$: 301.1438.



17 cis

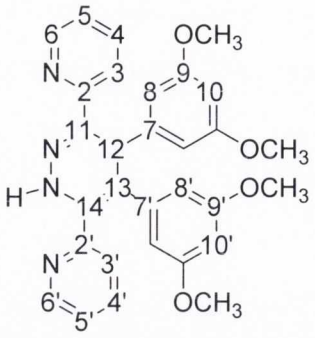


17 trans

3,6-di(2-pyridyl)-4,5-di-(3,5-dimethoxyphenyl) pyridazine (19)

*3,6-di(2-pyridyl)-4,5-di-(3,5-dimethoxyphenyl) hydropyridazine (**18**)*

0.78 g (3.29 mmol) of **2** and 0.99 g (3.29 mmol) of **17** were heated in a sealed tube in 10 mL of toluene at 180°C for 24 hours. The reaction mixture was dried in vacuo and purified using column chromatography in ether. 1.03 g of the bright yellow product was isolated (61% yield). ^{1}H-NMR ($CDCl_3$): δ 9.37 (s 1H, H^{N-H}), 8.64 (dm 1H, $H^{6/6'}$, $J_{5,6}$ = 4.9 Hz), 8.59 (dm 1H, $H^{6/6'}$, $J_{5,6}$= 4.6 Hz), 8.15 (dm 1H, $H^{3/3'}$, $J_{3,4}$ = 7.9 Hz) 7.64 (1H, $H^{4/4'}$, $J_{4,5}$ = 7.7 Hz), 7.47 (dm 1H, $H^{4/4'}$, $J_{4,5}$ =7.7 Hz), 7.36 (dm 1H, $H^{3/3'}$, $J_{3,4}$=8.0 Hz), 7.19 (m 1H, $H^{5/5'}$), 7.18 (m 1H, $H^{5/5'}$), 6.80 (d 2H, $H^{8/8'}$,$J_{8,10}$ = 2.0 Hz), 6.41 (d 2H, $H^{8/8'}$ $J_{8,10}$= 2.0 Hz), 6.35 (m, 1H, $H^{10/10'}$), 6.31 (m 1H, $H^{10/10'}$), 5.75 (s, 1H, H^{12}), 3.70 (s 6H, H^{OMe}), 3.61 (s 6H, H^{OMe}).



18

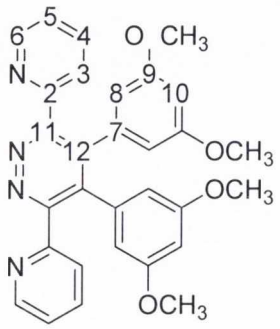
*3,6-di(2-pyridyl)-4,5-di-(3,5-dimethoxyphenyl) pyridazine (**19**)*

20 mL of a 6M solution of $NaNO_2$ was added dropwise to a solution of concentrated HCl (12 mL). The gas formed was then passed through a 40 mL dichloromethane solution containing 1.02 g (2.01 mmol) of **10**. The solution was kept at 0°C for the entire reaction. When all the sodium nitrite had been added, the dichloromethane solution was then allowed to return to room temperature. The solvent was then evaporated and the reaction mixture dissolved in water and neutralized with the addition of 10% ammonia solution. The mixture was then extracted into DCM, dried over $MgSO_4$ and run through a column of silica (dichloromethane:ethanol, 5:1). 0.855g (1.68 mmol) of product was recovered (75 % yield). I.R. (KBr) ν 3052s, 3005s, 2941s, 2839s, 1592s, 1494s, 1462s, 1425s, 1363s, 1343s, 1204s, 1145s, 1064s, 842s, 805s, 830s, 749s, 693s cm^{-1}.

^{1}H-NMR ($CDCl_3$): δ 8.55 (dm 2H, H^6, $J_{5,6}$ = 4.7 Hz), 7.72 (dm 2H, H^4, $J_{4,5}$ = 7.6 Hz, $J_{4,6}$ = 1.5 Hz), 7.61 (dm 2H, H^3, $J_{3,4}$ = 7.7 Hz), 7.25 (dm 2H, H^5, $J_{4,5}$ = 4.4 Hz, $J_{4,6}$ = 1.7 Hz), 6.22 (d 2H, H^{10}, $J_{8,10}$ = 2.1Hz), 6.10 (d 4H, H^8), 3.51 (s 12H, H^{OMe}).

^{13}C-NMR δ 160.03 (4C, C^9), 158.86 (2C, C^{11}), 156.11 (2C, C^2), 149.06 (2C, C^6), 138.65 (2C, C^{12}), 136.37 (2C, C^7), 136.19 (2C, C^4), 124.84 (2C, C^3), 123.01 (2C, C^5), 108.36 (4C, C^8), 100.42 (2C, C^{10}), 55.27 (4C, C^{OMe}).

ESI-MS (CH_3CN) m/z = 507.2032 calculated for $C_{30}H_{27}N_4O_4$ $[MH]^+$:507.2032. m.p. 148°C.



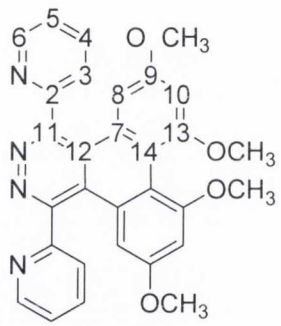
19

Attempted Cyclodehydrogenation of Ligands

0.100 g (0.197 mmol) of **19**, 1.205 g (9.04 mmol) of $AlCl_3$ and 1.215 g (9.04 mmol) of $CuCl_2$ were added to 25 mL of dry degassed CS_2 and stirred at room temperature for 4 days under argon. The reaction mixture was then washed with aqueous ammonia. The products were purified by column chromatography (dichloromethane:methanol, 10:1).

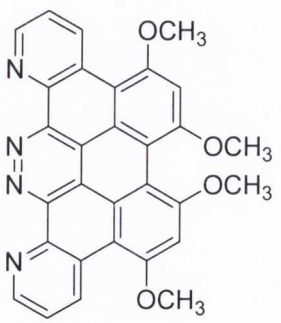
0.0045 g (0.009 mmol) of 1,4-di(2-pyridyl)-6,8,9,11-tetramethoxy-2,3-diazatriphenylene (**20**) was obtained (4.5% yield). ^{1}H-NMR ($CDCl_3$): δ 8.72 (dm 2H, H^6, $J_{5,6}$ = 5.3 Hz), 8.20 (2H, H^3, $J_{3,4}$ = 8.6 Hz), 8.01 (dm 2H, H^4, $J_{4,5}$ 7.5 Hz), 7.46 (dm 2H, H^5), 6.67 (d 2H, H^{10}, $J_{8,10}$ = 1.8 Hz), 6.44 (d 2H, H^8), 3.94 (s 6H, H^{OMe}), 3.39 (s 6H, $H^{OMe'}$).

^{13}C-NMR ($CDCl_3$): δ 158.69 (2C, C^Q), 158.17 (2C, C^Q), 157.96 (2C, C^Q), 155.52 (2C, C^Q), 149.81 (2C, C^6), 137.38 (2C, C^4),129.23 (2C, $C^{7/12}$), 128.43 (2C, $C^{7/12}$), 125.04 (2C, C^3), 123.73 (2C, C^5),116.11 (2C, C^{14}), 101.38 (2C, C^{10}), 101.13 (2C, C^8), 55.85 (2C, C^{OMe}), 54.80 (2C, $C^{OMe'}$). (MALDI–TOF) MS m/z = 503.1856, calculated for $C_{30}H_{23}N_4O_4$ $[M]^+$: 503.1845.



20

0.0082 g (0.016 mmol) of 1,14,15,16-tetraazo-5,7,8,10-tetramethoxy-phenanthro[f,g,h,i,j]picene was isolated (**21**). (8.3 % yield). ESI-MS (CH_3CN) m/z = 523.1373, calculated for $C_{30}H_{20}N_4O_4Na$: $[MNa]^+$:523.1382



21

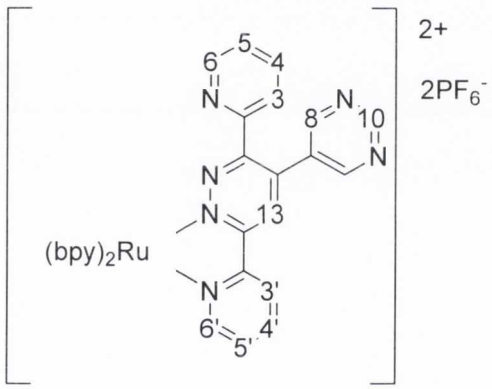
Synthesis of Ruthenium(II) bisbipyridine Complexes

$[Ru(bpy)_2(3)][PF_6]_2$ (22)

0.100g (0.320 mmol) of **3** and 0.156g (0.299 mmol) ruthenium(II) bisbipyridine dichloride were heated for 4 hours at 80°C in a mixture of 5 mL ethylene glycol and 5 mL water under argon. The reaction was then diluted with water and washed with dichloromethane. The aqueous layer was reduced by vacuum and a saturated solution of KPF_6 was added. The mixture was then filtered and the resulting filtrate was purified by chromatography on silica (MeCN: KNO_3:H_2O 10: ½:1 ½).

0.222g (0.218 mmol) of the product was obtained by anion exchange (65% yield).

^{1}H-NMR (CD_3CN): δ 9.18 (s 1H H^{10}), 8.71 (3H H^{13} H^8), 8.66-8.60 (m 2H), 8.51 (m 2H), 8.24 (m 1H), 8.20-8.05 (m 5H), 7.98 (m 3H), 7.89 (dm 1H 1H), 7.77-7.73 (m 2H), 7.58-7.46 (m 4H), 7.40-7.29 (1H 2H), 7.25 (dm 1H $H^3J_{3,4}$=7.9 Hz). ESI-MS (CH_3CN) m/z = 363.15 $[M-2PF_6]^{2+}$. Calculated for $C_{38}H_{28}N_{10}Ru$: 726.1542, found: 726.1550.



22

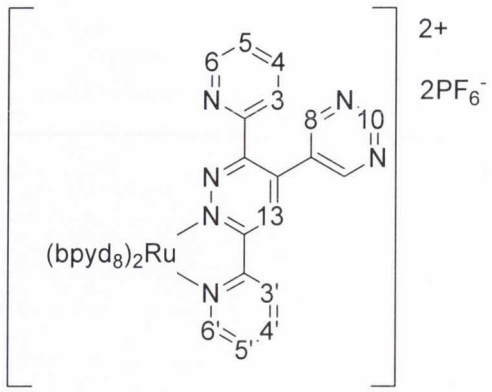
$[Ru(bpyd_8)_2(3)]PF_6]_2$ ($22d_8$)

0.015 g (0.049 mmol) of **3** and 0.0075g (0.014 mmol) of deuterated ruthenium bisbipyridine dichloride were heated for 6 hours at 80°C in a mixture of 5 mL ethylene glycol and 5 mL water under argon. The reaction was then diluted with water and washed with dichloromethane. The aqueous layer was reduced by vacuum and a saturated solution of KPF_6 was added. The mixture was then filtered and the resulting filtrate was purified by chromatography on silica (MeCN: KNO_3:H_2O 10: ½:1 ½).

0.0092g (0.009 mmol) of the product was obtained by anion exchange (64% yield).

^{1}H-NMR (CD_3CN): δ 9.20 (s 1H, H^{10}), 8.71 (s 1H, H^{13}), 8.69 (s 2H, H^8), 8.62 (dm 1H, $H^{3'}$, $J_{3',4'}$=7.9 Hz), 8.24 (dm 1H, H^6, $J_{5,6}$ = 4.6 Hz), 8.17 (dd 1H, $H^{4'}$, $J_{4',5'}$ = 7.9 Hz, $J_{4',6'}$ = 1.4 Hz), 7.95 (dm 1H, $H^{6'}$, $J_{5',6'}$ = 5.4 Hz), 7.77 (dd 1H, H^4, $J_{4,5}$ = 7.5 Hz, $J_{4,6}$ = 1.1 Hz),

7.58 (dd 1H, $H^{5'}$, $J_{3',5'}$ = 1.1 Hz), 7.38 (dd 1H, H^5, $J_{3,5}$ = 0.8 Hz), 7.23 (dm 1H, H^3, $J_{3,4}$ = 7.9 Hz).



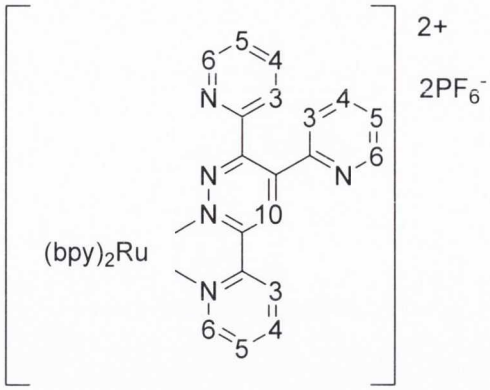
22d_8

[Ru(bpy)$_2$(4)][PF$_6$]$_2$(23)

0.105g (0.337 mmol) of **4** and 0.157g (0.301 mmol) ruthenium bisbipyridine dichloride were heated for 6 hours at 80°C in a mixture of 5 mL ethylene glycol and 5 mL water under argon. The reaction was then diluted with water and washed with dichloromethane. The aqueous layer was reduced by vacuum and a saturated solution of KPF_6 was added. The mixture was then filtered and the resulting filtrate was purified by chromatography on silica (MeCN: KNO_3:H_2O 10: ½:1 ½).

0.222g (0.218 mmol) of the product was obtained by anion exchange (73% yield).

^{1}H-NMR (CD_3CN): δ 8.99 (s 1H H^{10}), 8.71 (dm 1H H^3 $J_{3,4}$=7.8 Hz), 8.64 (dm 2H H^3 $J_{3,4}$=7.4 Hz), 8.60 (dm 1H H^6 $J_{3,4}$=3.9 Hz), 8.57-8.50 (m 3H), 8.23 (dm 1H H^6 $J_{5,6}$=4.0 Hz), 8.20 (ddd 1H H^4 $J_{4,5}$=8.0 Hz, $J_{4,6}$=1.0 Hz), 8.17-8.08 (m 5H), 7.99 (dm 1H, H^6 $J_{5,6}$=4.7), 7.98 (m 2H), 7.92 (dm 1H H^6 $J_{5,6}$=5.4), 7.82 (ddd 1H H^4 $J_{4,5}$=7.5 Hz, $J_{4,6}$=1.5 Hz), 7.80 (ddd 1H H^4 $J_{4,5}$=7.6 Hz, $J_{4,6}$=1.6 Hz),7.79 (m 1H), 7.63 (ddd 1H H^5 $J_{3,5}$=0.8 Hz), 7.61-7.46 (m 2H), 7.45 (ddd 1H H^5 $J_{3,5}$=0.9 Hz), 7.38 (m 1H H^5), 7.35 (dm 1H H^3 $J_{3,4}$=7.9 Hz), 7.32 (m 1H), 7.3 (dm 1H H^3 $J_{3,4}$=7.5 Hz). ESI-MS (CH_3CN) m/z = 362.57 $[M-2PF_6]^{2+}$. Calculated for $C_{39}H_{29}N_9Ru$: 725.1589, found: 725.1572.



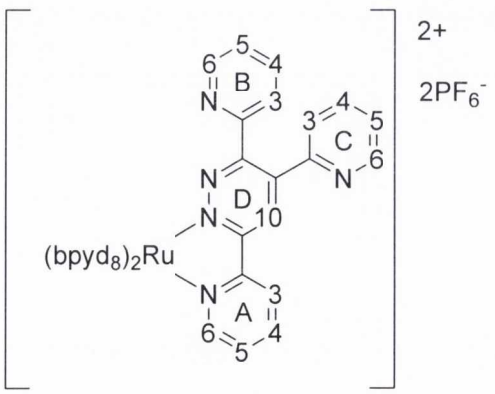
23

[Ru(bpyd$_8$)$_2$(4)][PF$_6$]$_2$(23d$_8$)

0.009g (0.028 mmol) of **4** and 0.015g (0.027 mmol) deuterated ruthenium bisbipyridine dichloride were heated for 6 hours at 80°C in a mixture of 5 mL ethylene glycol and 5 mL water under argon. The reaction was then diluted with water and washed with dichloromethane. The aqueous layer was reduced by vacuum and a saturated solution of KPF_6 was added. The mixture was then filtered and the resulting filtrate was purified by chromatography on silica (MeCN: KNO_3:H_2O 10: ½:1 ½).

0.222g (0.218 mmol) of the product was obtained by anion exchange (68% yield).

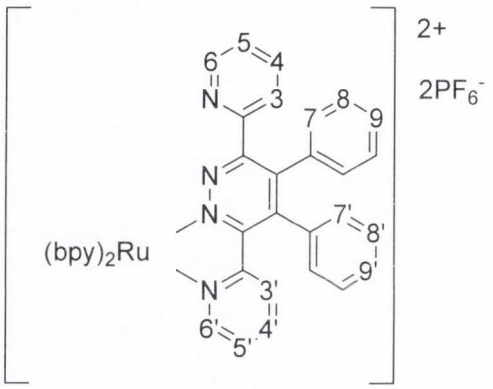
^{1}H-NMR (CD_3CN): δ 8.47 (s 1H, H^{D10}), 8.66 (dm 1H, H^{A3}, $J_{3,4}$ = 8.0 Hz), 8.57 (dm 1H, H^{B6}, $J_{5,6}$ = 4.3 Hz), 8.19 (dm 1H, H^{C6}, $J_{5,6}$ = 5.5 Hz), 8.15 (dm 1H, H^{A4}, $J_{4,5}$= 8.1 Hz), 7.94 (dm 1H, H^{A6}, $J_{5,6}$ = 5.7 Hz), 7.76 (2H, H^{C4}, H^{B4}), 7.56 (dm 1H, H^{A5}, $J_{4,5}$ = 6.8 Hz, $J_{3,5}$ = 1.1 Hz), 7.39 (dm 1H, H^{B5}, $J_{4,5}$ = 6.2 Hz, $J_{4,6}$ = 1.3 Hz), 7.30 (dm 1H, H^{C5}, $J_{4,5}$ = 7.6 Hz, $J_{4,6}$ = 1.1 Hz), 7.29 (dm 1H, H^{B3}, $J_{3,4}$ = 8.1 Hz), 7.22 (dm 1H, H^{C3}, $J_{3,4}$ = 7.6 Hz).



23*d*$_8$

[Ru(bpy)$_2$(6)][PF$_6$]$_2$ (24)

0.100 g (0.258 mmol) of **6** and 0.114g (0.222 mmol) ruthenium (II) bisbipyridine dichloride were heated for 6 hours at 80°C in a mixture of 5 mL ethylene glycol and 5 mL water under argon. The reaction was then diluted with water and washed with dichloromethane. The aqueous layer was reduced by vacuum and a saturated solution of KPF_6 was added. The precipitate was then filtered, and the solid collected and purified by column chromatography. (acetonitrile:water: sat. KNO_3 10:1.5:1) on silica and analysed after further anion exchange. (63% yield) ^{1}H-NMR (CD_3CN): δ 8.60-8.52 (m 3H), 8.44 (dm 1H H^3 $J_{3,4}$=8.2 Hz), 8.19-8.11 (m 5H), 7.95 (m 2H), 7.90 (m 2H), 7.69 (dd 1H H^3, $J_{3,4}$ =5.5 Hz, $J_{3,5}$ = 0.7 Hz), 7.68-7.56 (m 4H), 7.53-7.30 (m 7H), 7.20 (dm 1H, H^5 $J_{4,5}$ =6.1 Hz $J_{4,6}$ = 0.9 Hz), 7.11-7.05 (dm 5H) 6.92 (1H, H^3, $J_{3,4}$ =7.9 Hz). ESI-MS (CH_3CN) m/z = 399.47 $[M-2PF_6]^{2+}$. Calculated for $C_{46}H_{34}N_8Ru$: 800.1950, found: 800.1958.

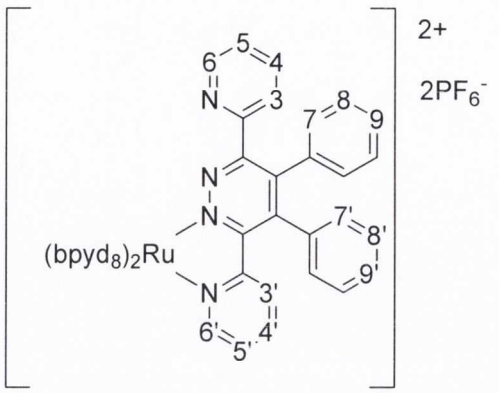


24

[Ru(bpyd$_8$)$_2$(6)][PF$_6$]$_2$ (24d$_8$)

0.005g (0.014 mmol) of **6** and 0.007g (0.014 mmol) ruthenium (II) bisbipyridine dichloride were heated for 4 hours at 100°C in a mixture of 5 mL ethylene glycol and 5 mL water under argon. The reaction was then diluted with water and washed with dichloromethane. The aqueous layer was reduced by vacuum and a saturated solution of KPF_6 was added. The precipitate was then filtered, and the solid collected .and analysed. 0.012 g of product (78% yield) was recovered. ^{1}H-NMR (CD_3CN): δ 8.16 (dm 1H, H^6, $J_{5,6}$ = 4.7 Hz,), 7.95 (dm 1H, H$^{6'}$, $J_{5',6'}$ = 5.8 Hz), 7.66 (dm 1H, H^4, $J_{4,5}$ = 7.8 Hz, $J_{4,6}$ = 0.8 Hz), 7.56 (dm 1H, H$^{4'}$, $J_{4',5'}$ = 7.5 Hz, $J_{4',6'}$ = 0.7 Hz), 7.47-7.33 (m 5H, H^{7,8}, H$^{5'}$), 7.20 (dm 1H, H^5, $J_{4,5}$ = 4.8 Hz, $J_{3,5}$ = 1.0 Hz), 7.13-7.06 (m 6H, H^{8,9}, H^3), 6.93 (dm 1H, H$^{3'}$, $J_{3,4}$ = 8.1 Hz).

ESI-MS (CH_3CN) m/z = 408.16 $[M-2PF_6]^{2+}$. Calculated for $C_{46}H_{18}D_{16}N_8Ru$: 816.3202, found: 816.3202.



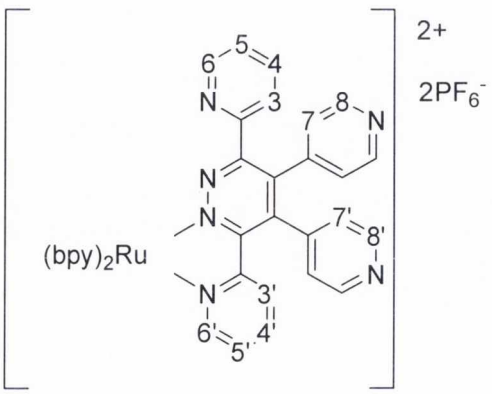
24d_8

[Ru(bpy)$_2$(8)][PF_6]$_2$ (25)

0.102g (0.264 mmol) of **8** and 0.130g (0.251 mmol) ruthenium(II) bisbipyridine dichloride were heated for 4 hours at 80°C in a mixture of 5 mL ethylene glycol and 5 mL water under argon. The reaction was then diluted with water and washed with dichloromethane. The aqueous layer was reduced by vacuum and a saturated solution of KPF_6 was added. The mixture was then filtered and the resulting filtrate was purified by chromatography on silica (acetone:ammonia:Sat. KNO_3 20:3:0.5)

0.144 g of the product was obtained after anion exchange with KPF_6 (54 % yield).

^{1}H-NMR (CD_3CN): δ 8.67-8.55 (m 4H, H^8, H^6), 8.49 (dd 1H, H^6, $J_{5,6}$ = 8.0 Hz), 8.41-8.08 (m 6H), 8.04-8.00 (m 2H), 7.92 (dd 1H, H^6,$J_{5,6}$ = 5.4 Hz), 7.88 (dd 1H, H^6, $J_{5,6}$ = 5.4 Hz), 7.71- 7.67 (m 3H), 7.59-7.52 (m 3H), 7.46 (dd 1H), 7.43-7.35 (m 2H), 7.25-7.14 (m 5H), 6.82 (s 1H). ESI-MS (CH_3CN) m/z = 401.20 $[M-2PF_6]^{2+}$. Calculated for $C_{44}H_{32}N_{10}Ru$: 802.1855, found: 802.1838.



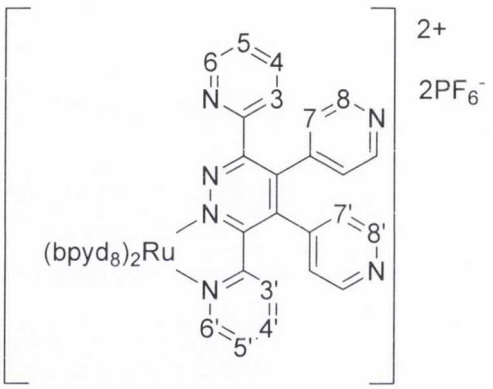
25

[Ru(bpyd$_8$)$_2$(8)][PF$_6$]$_2$ (25d$_8$)

0.006 g (0.015 mmol) of **8** and 0.008 g (0.015 mmol) ruthenium(II) bisbipyridine dichloride were heated for 4 hours at 80°C in a mixture of 5 mL ethylene glycol and 5 mL water under argon. The reaction was then diluted with water and washed with dichloromethane. The aqueous layer was reduced by vacuum and a saturated solution of KPF_6 was added. The mixture was then filtered and the resulting filtrate was purified by chromatography on silica (acetone:ammonia:sat. KNO_3 20:3:0.5)

0.012 g of the product was obtained after anion exchange with KPF_6 (75% yield).

^{1}H-NMR (CD_3CN): δ 8.67 (dd 1H, $H^{8'}$, $J_{7',8'}$ = 4.4 Hz), 8.62 (dd 1H, $H^{8'}$, $J_{7',8'}$ = 4.7 Hz), 8.29 (m 2H, H^8), 8.12 (dd 1H, H^6, $J_{5,6}$ = 3.9 Hz), 7.98 (dd 1H, $H^{6'}$, $J_{5',6'}$= 5.5 Hz), 7.67 (m 2H, H^4, $H^{4'}$), 7.40 (m 2H, H^3, H^5), 7.26 (dd 1H, $H^{5'}$, $J_{4',5'}$ = 5.0 Hz, $J_{3',5'}$ = 1.0 Hz), 7.13 (m 3H, $H^{3'}$, $H^{7'}$), 6.78 (m 1H, H^7). ESI-MS (CH_3CN) m/z = 409.17 $[M\text{-}2PF_6]^{2+}$. Calculated for $C_{44}H_{16}D_{16}N_{10}Ru$: 818.2068, found: 818.3107.



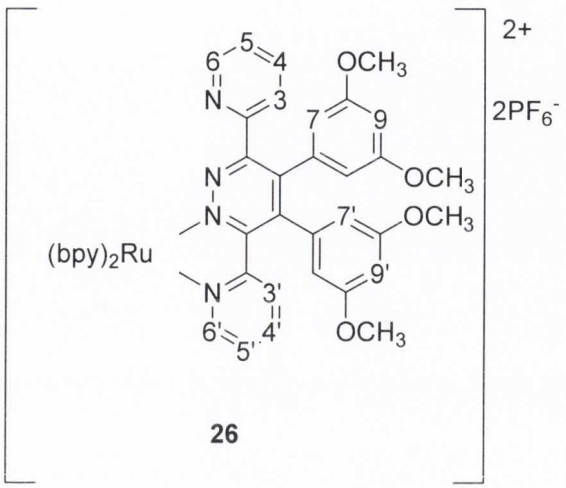
25*d*$_8$

[Ru(bpy)$_2$(19)][PF$_6$]$_2$ (26)

0.020 g (0.040 mmol) of **19** and 0.021 g (0.040 mmol) ruthenium(II) bisbipyridine dichloride were heated for 4 hours at 80°C in a mixture of 3 mL ethylene glycol and 3 mL water under argon. The reaction was then diluted with water and washed with dichloromethane. The aqueous layer was reduced by vacuum and a saturated solution of KPF_6 was added. The mixture was then filtered and the resulting filtrate was purified by chromatography on silica (acetone:ammonia:sat. KNO_3 20:2:2). 0.027 g of product was obtained after anion exchange with KPF_6. (56% yield).

^{1}H-NMR (CD_3CN): δ 8.60 (m 2H, H^6), 8.53 (dm 1H, H^6, $J_{5,6}$ = 7.9 Hz), 8.43 (dm 1H, H^6, $J_{5,6}$ = 8.1 Hz), 8.23 (dm 1H, H^6, $J_{5,6}$ = 4.7 Hz, $J_{4,6}$ = 1.0 Hz), 8.20 – 8.15 (m 3H), 8.08 (dm 1H, H^6, $J_{5,6}$ = 5.5 Hz, $J_{4,6}$ = 0.8 Hz), 7.97 (m 3H), 7.89 (dm 1H, H^3, $J_{3,4}$ = 5.0 Hz),

7.71 (m 3H), 7.61-7.49 (m 3H),7.37 (dm 1H, H^5, $J_{4,5}$ = 5.6 Hz, $J_{3,5}$ = 1.2 Hz), 7.22 (m 3H), 7.10 (dm 1H, H^3, $J_{3,4}$ = 7.8 Hz), 6.58 (dd 2H, H^7, $J_{7,9}$ = 1.5 Hz), 6.34 (dd 1H, H^9), 6.24 (d 1H, $H^{9'}$, $J_{7',9'}$ = 2.3 Hz), 3.73 (s 3H, $H^{OMe'}$), 3.71 (s 3H, $H^{OMe'}$), 3.56 (s 6H, H^{OMe}). ESI-MS (CH_3CN) m/z = 460.12 $[M-2PF_6]^{2+}$. Calculated for $C_{50}H_{42}N_8O_4Ru$: 920.2373, found: 920.2340.



26

Synthesis of Ruthenium (II) *tris* homoleptic Complexes

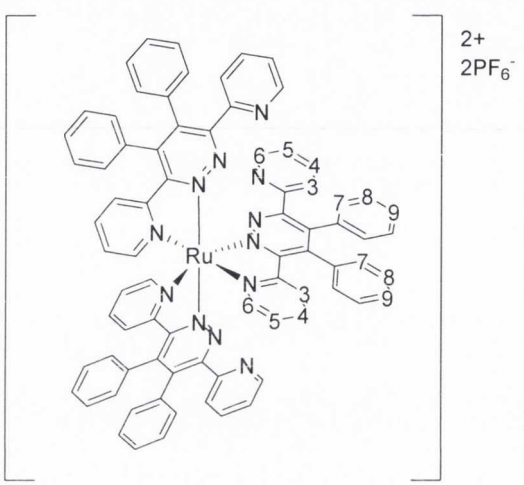
$[Ru(6)_3][PF_6]_2$ (27)

0.0209g (0.0542 mmol) of **6** was added to a small round bottomed flask containing 5 mL of ethylene glycol and 0.0029g (0.0142 mmol) of $RuCl_3$. 6 drops of ethyl morpholine were added to this and the mixture was degassed for 30 mns. The mixture was then heated at 170°C for 72 hours under argon. It was then allowed to cool and extracted into DCM. The facial isomer was separated using a TLC plate (acetone:water:sat.KNO_3, 120:12:0.5) (R_f = 0.35) followed by a second plate (acetonitrile:ammonia:sat.KNO_3, 20:2:4) from which the meridional isomer was isolated (R_f = 0.15)

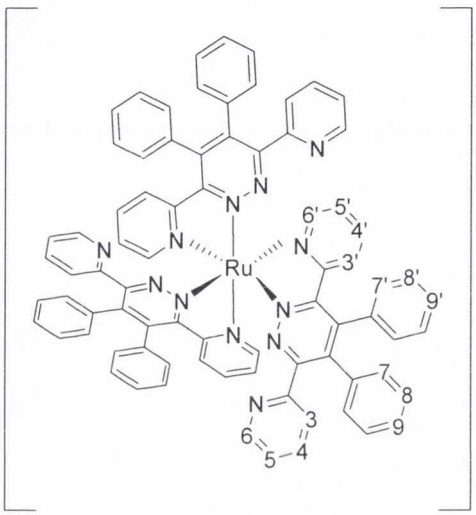
6.45 mgs of the *mer* isomer (29% yield) was isolated. ^{1}H-NMR (CD_3CN): δ 8.64 (dm 1H, H^6, $J_{5,6}$ = 5.0 Hz), 8.40 (dm 1H, H^6, $J_{5,6}$ = 4.6 Hz), 8.34 (dm, 1H, H^6, J = 5.1 Hz), 8.26 (dm, 2H, H^6, $J_{5,6}$ = 4.6 Hz), 8.18 (dm, 1H, H^6, $J_{5,6}$ = 4.2 Hz), 7.72 – 6.97 (m, 26 H), 6.98 (1H, H^3, $J_{3,4}$ = 7.4 Hz), 6.89 (1H, H^3, $J_{3,4}$ = 7.9 Hz), 6.86 (1H, H^3, $J_{3,4}$ = 7.9 Hz), 6.48 (1H, H^3, $J_{3,4}$ = 7.4 Hz). ESI-MS (CH_3CN) m/z = 630.18 $[M-2PF_6]^{2+}$. Calculated for $C_{78}H_{54}N_{12}Ru$: 1260.3638, found: 1260.3626.

2.70 mgs of the *fac* isomer (12% yield) was isolated. ^{1}H-NMR (CD_3CN): δ 8.46 (dm 3H, H^6, $J_{5,6}$ = 4.0 Hz), 8.43 (dm 3H, $H^{6'}$, $J_{5',6'}$ = 6.0 Hz), 7.72 (dd 3H, H^4, $H_{4,5}$ = 7.7 Hz), 7.71

(dm 3H, $H^{4'}$, $J_{4',5'}$ = 8.0 Hz), 7.57 (dm 3H, $H^{5'}$, $J_{5',6'}$ = 6.3 Hz), 7.42 (m 6H, $H^{7'/8'/9'}$), 7.31 (m 6H, H^{5}, $H^{7/8'/9'}$), 7.20 (dm 3H, H^{3}, $J_{3,4}$= 7.7 Hz), 7.09 (m 9H, $H^{7/8/9}$), 6.98 (3H, $H^{3'}$, $J_{3',4'}$ = 8.6 Hz), 6.68 (3H, $H^{7'/8'/9'}$), 6.1 (6H, $H^{7/8/9}$). ^{13}C-NMR (CD_3CN): δ 159.38 (3C, C^{Q}), 157.14 (3C, C^{Q}), 155.39 (3C, C^{Q}), 154.42 (3C, C^{Q}), 155.77 (3C, $C^{6'}$), 149.07 (3C, C^{6}), 143.11 (3C, C^{Q}), 139.34 (3C, C^{Q}), 137.44 (3C, $C^{4'}$), 136.56 (3C, C^{4}), 133.37 (3C, C^{Q}), 132.73 (3C, C^{Q}), 129.41 (3C, $C^{7'/8'/9'}$), 129.20 (3C, $C^{7'/8'/9'}$), 129.16 (3C, $C^{7'/8'/9'}$), 129.12 (3C, $C^{7'/8'/9'}$), 128.47 (3C, $C^{7'/8'/9'}$), 128.25 (3C, $C^{3'}$), 127.80 (3C, $C^{7/8/9}$), 127.59 (3C, $C^{5'}$), 127.18 (6C, $C^{7/8/9}$), 124.34 (3C, C^{3}), 123.70 (3C, C^{5}). ESI-MS (CH_3CN) m/z = 630.18 $[M-2PF_6]^{2+}$. Calculated for $C_{78}H_{54}N_{12}Ru$: 1260.3638, found: 1260.3618.



27 mer



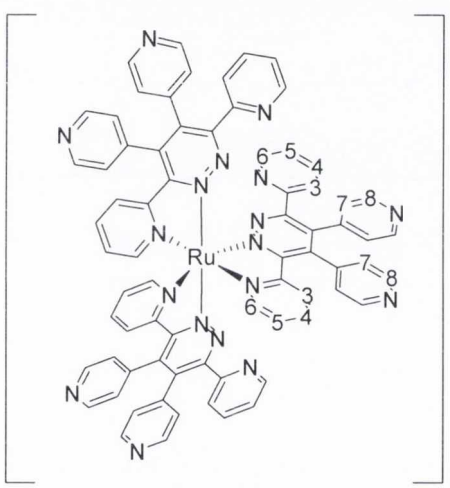
27 fac

$[Ru(8)_3][PF_6]_2$ (28)

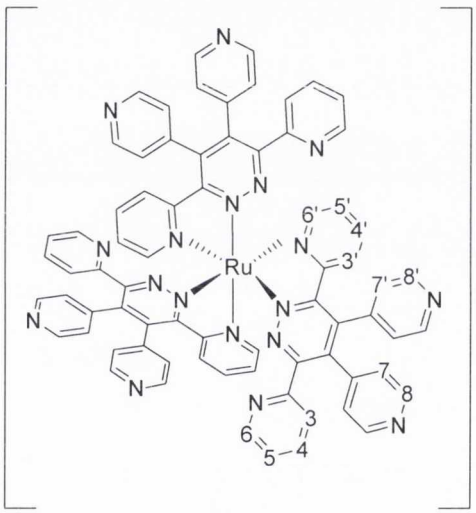
0.0212g (0.0546 mmol) of **8** was added to a small round bottomed flask containing 5 mL of ethylene glycol and 0.0032g (0.0156 mmol) of $RuCl_3$. 6 drops of ethyl morpholine were added to this and the mixture was degassed for 30 mns. The mixture was then heated at 170°C for 72 hours under argon. It was then allowed to cool and extracted into DCM. The facial isomer was separated using a TLC plate (acetone:water:sat. KNO_3, 20:5:1) (R_f = 0.33) followed by a second plate (acetonitrile:ammonia:sat. KNO_3, 20:3:1) on which the meridional isomer was isolated. (R_f = 0.70). 0.0034g (14.0% yield) of the meridional isomer. ^{1}H-NMR (CD_3CN): δ 8.73 (dm 1H, H^{6}, $J_{5,6}$ = 5.7 Hz), 8.68 (dm 1H, H^{6}, $J_{5,6}$ = 4.5 Hz), 8.67 (dm 1H, H^{6}, $J_{5,6}$ = 5.7 Hz), 8.60 (dm 1H, $H^{4\text{-pyr}}$, $J_{4\text{-pyr}}$ = 4.5 Hz), 8.56 (dm 1H, H^{6}, $H_{5,6}$ = 4.9 Hz), 8.52 (dm 1H, H^{6}, $J_{5,6}$ = 5.3 Hz), 8.41-8.26 (m 5H), 8.17 (dm 1H), 7.81 (m 2H, H^{4}), 7.68 (m 3H), 7.64 (m 1H), 7.43 (m 2H), 7.38 (m 1H), 7.30 (m 2H), 7.12 (m 2H), 7.07 (dm1H, H^{3}, $J_{3,4}$ = 8.0), 6.99 (m 2H), 6.83 (m 2H), 6.37 (dm 1H,

H^3, $J_{3,4}$ = 4.9 Hz). ESI-MS (CH_3CN) m/z = 633.17 $[M\text{-}2PF_6]^{2+}$. Calculated for $C_{72}H_{48}N_{18}Ru$: 1266.3353, found: 1266.3354.

0.0025g (10% yield) of the facial isomer ^{1}H-NMR (CD_3CN): δ 8.65 (dm 3H, $H^{8'}$, $J_{7',8'}$ = 4.7Hz), 8.53 (dm 3H, $H^{8'}$) 8.40 (m 6H, $H^{6'}$, H^6), 8.28 (m 6H, H^8), 7.81 (m 6H, $H^{4'}$ H^4), 7.64 (dm 3H, $H^{5'}$, $J_{4',5'}$ = 6.5 Hz), 7.38 (dm 3H, H^5, $J_{5,6}$ = 4.5 Hz, $J_{3,5}$ = 2.4Hz), 7.29 (m 6H, H^3, $H^{7'}$), 7.20 (dm 3H, $H^{3'}$, $J_{3',4'}$ = 8.5 Hz), 6.69 (dm 3H, $H^{7'}$), 6.61 (m 6H, H^7). ^{13}C-NMR (CD_3CN): δ 157.73 (3C, C^Q), 156.20 (3C, C^Q), 154.00(3C, C^Q), 152.65 (3C, C^Q), 152.42 (3C, $C^{6'}$), 150.81 (3C, $C^{8'}$), 150.71 (3C, $C^{8'}$), 149.12 (3C, C^6), 147.03 (6C, C^8), 140.53 (3C, C^Q), 139.83 (3C, C^Q), 138.33 (3C, $C^{4'}$), 137.15 (3C, C^4), 128.62 (3C, $C^{3'}$), 128.36 (3C, C^5), 124.62 (3C, $C^{7'}$), 124.38 (3C, $C^{7'}$), 123.87 (3C, C^Q), 123.03 (3C, C^Q). ESI-MS (CH_3CN) m/z = 633.17 $[M\text{-}2PF_6]^{2+}$. Calculated for $C_{72}H_{48}N_{18}Ru$: 1266.3353, found: 1266.3326.



28 *mer*



28 *fac*

[Ru(19)$_3$][PF$_6$]$_2$ (29)

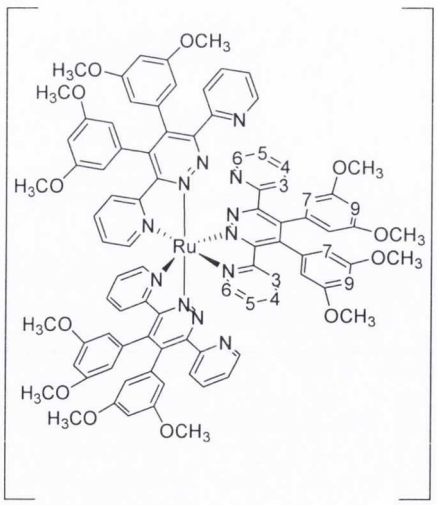
0.100g (0.197 mmol) of **19** was added to a small round bottomed flask containing 5 mL of ethylene glycol and 0.0146g (0.0706 mmol) of $RuCl_3$. 6 drops of ethyl morpholine were added to this and the mixture was degassed for 30 mns. The mixture was then heated at 170°C for 72 hours under argon. It was then allowed to cool and 10 mL of water were added. The mixture was extracted into dichloromethane after anion metathesis with PF_6. The facial isomer was isolated by column chromatography, (acetone:water:sat. KNO_3 12:1:0.2) (R_f =0.34). The meridional isomer needed further purification on a thick TLC plate (acetonitrile:ammonia:sat. KNO_3 20:1:1.5) (R_f = 0.12).

0.0207g (0.0108 mmol) of meridional isomer was isolated (5% yield).

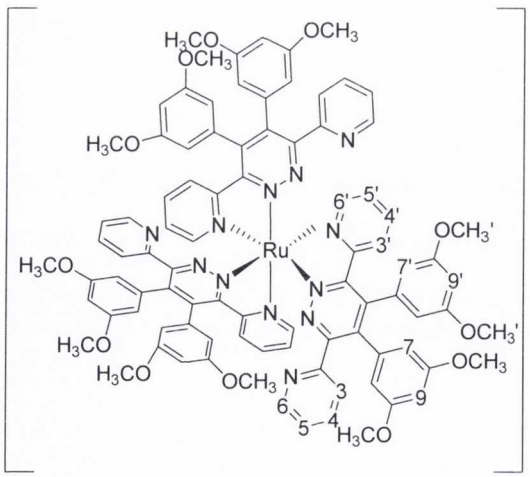
^{1}H-NMR (CD_3CN): δ 8.47 (dm 1H, H^6, $J_{5,6}$ = 4.9 Hz), 8.43 (dm 1H, H^6, $J_{5,6}$ = 3.7 Hz), 8.27 (dm 1H, H^6, $J_{5,6}$ = 4.3 Hz), 8.26 (dm 1H, H^6, $J_{5,6}$ = 4.6 Hz), 8.23 (dm 1H, H^6, $J_{5,6}$ = 6.1 Hz), 8.17 (dm 1H, H^6, $J_{5,6}$ 5.8 Hz), 7.81-7.62 (m 8H), 7.38-7.11 (m 11H), 6.60 (m 3H, $H^{7/9}$), 6.55 (m 1H, $H^{7/9}$), 6.52 (m 1H, $H^{7/9}$), 6.49 (m 1H, $H^{7/9}$), 6.40 (m 1H, $H^{7/9}$), 6.31 (m 1H, $H^{7/9}$), 6.27 (m 4H, $H^{7/9}$), 6.22 (m 2H, $H^{7/9}$), 3.75 (d 6H, H^{OMe}), 3.73 (d 3H, H^{OMe}), 3,70 (s 3H, H^{OMe}), 3.68 (s 6H, H^{OMe}), 3.55 (m 17H, H^{OMe}). ESI-MS (CH_3CN) m/z = 810.25 $[M-2PF_6]^{2+}$. Calculated for $C_{90}H_{78}N_{12}O_{12}Ru$: 1620.4906, found: 1620.4902.

0.012 g (0.0064 mmol) of facial isomer was isolated (3% yield.) ^{1}H-NMR (CD_3CN): δ 8.47 (dm 3H, $H^{6'}$, $J_{5',6'}$ = 4.7 Hz), 8.40 (dm 3H, H^6, $J_{5,6}$=5.5 Hz), 7.81 (dm 3H, H^4, $J_{4,5}$ = 7.6 Hz, $J_{4,6}$ = 1.5 Hz), 7.71 (dm 3H, $H^{4'}$, $J_{4',5'}$ = 7.8 Hz, $J_{4',6'}$ = 1.7 Hz), 7.60 (dm 3H, H^5, $J_{3,5}$ = 1.3 Hz), 7.30 (dm 3H, $H^{5'}$, $J_{3',5'}$ = 1.0 Hz), 7.27 (dm 3H, H^3, $J_{3,4}$ = 7.7 Hz), 7.15 (dm 3H, $H^{3'}$, $J_{3',4'}$ = 7.7 Hz), 6.56 (dm 4H, $H^{9'}$, $J_{7',9'}$ = 2.3 Hz), 6.43 (dm 3H, $H^{7'}$), 6.24 (dm 4 H, H^9), 5.94 (dm 3 H, $H^{7'}$), 3.70 (s 9 H, $H^{OMe'}$), 3.66 (s 9 H, $H^{OMe'}$), 3.55 (s 18H, H^{OMe}).

^{13}C-NMR (CD_3CN): δ 161.65 (3C, C^Q), 159.82 (3C, C^Q), 159.06 (3C, C^Q), 156.68 (3C, C^Q), 155.16 (3C, C^Q), 154 26 (3C, C^Q), 151.59 (3C, $C^{6'}$), 149.09 (3C, C^6), 142.50 (3C, C^Q), 138.60 (3C, C^Q), 137.65 (3C, C^4), 136.46 (3C, $C^{4'}$), 134.77 (3C, C^Q), 134.42 (3C, C^Q), 128.52 (3C, C^3), 127.66 (3C, C^5), 124.16 (3C, $C^{3'}$), 123.87 (3C, $C^{5'}$),117.26 (6C, C^7), 107.64 (3C, $C^{7'}$), 106.71 (3C, $C^{7'}$), 100.47 (3C, $C^{9'}$), 99.58 (3C, C^9), 55.39 (6C, C^{OMe}), 55.16 (6C, $C^{OMe'}$) ESI-MS (CH_3CN) m/z = 810.25 $[M-2PF_6]^{2+}$. Calculated for $C_{90}H_{78}N_{12}O_{12}Ru$: 1620.4906, found: 1620.4956.



29 *mer*



29 *fac*

Attempted Cyclodehydrogenation

$[Fe(6)]_3[PF_6]_2$ (30)

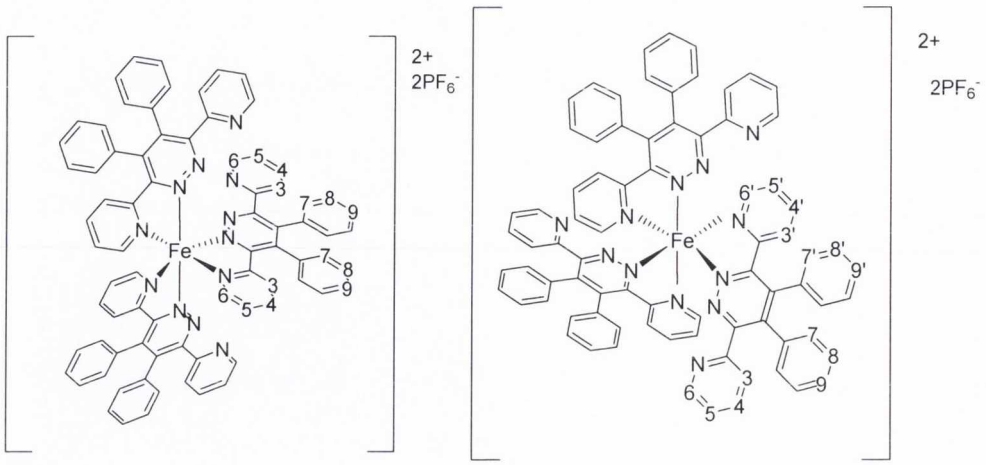
A solution of 0.080 g (0.21mmol) of **6** in 20 mL dichloromethane was prepared and argon was blown through it. 4 mL of a CH_3NO_2 solution of 1.1682 g (10.35 mmol) $FeCl_3$ were added to this dropwise and allowed to stir at 25°C for 45 mins. After this time, 25 mL of methanol were added to the reaction mixture and the solvents were then removed by vacuum. The mixture was washed with water and extracted into dichloromethane. The purple colour of the organic solvent indicated that the complexed ligand had extracted into the dichloromethane. This was then purified by chromatography (acetone:water:sat. KNO_3, 100:10:1). Following anion exchange, two purple products were isolated. 0.069g of *mer* isomer (24% Yield), $R_f = 0.74$.

^{1}H-NMR (CD_3CN): δ 8.58 (dm 1H H^6 $J_{5,6}$=4.4 Hz), 8.38 (dm 1H H^6 $J_{5,6}$=4.1 Hz), 8.26 (dm 1H H^6 $J_{5,6}$=4.1 Hz), 8.17 (dm 1H H^6 $J_{5,6}$=4.4 Hz), 8.10 (dm 1H H^6 $J_{5,6}$=3.8 Hz), 7.76 (m 4H), 7.63-6.94 (m 42H), 6.90 (dm 1H H^3 $J_{3,4}$=7.6 Hz), 6.81 (m 2H), 6.42 (dm 1H H^3 $J_{3,4}$=7.6 Hz). ESI-MS (CH_3CN) m/z = 607.20 $[M-2PF_6]^{2+}$. Calculated for $C_{78}H_{54}N_{12}Fe$: 1214.3944, found: 1214.3938.

Anal. Calculated for $C_{78}H_{54}F_{12}N_{12}P_2Fe$: C, 62.24; H, 3.62; N, 11.17. Found: C, 61.46, H, 4.61, N, 9.36.

Fac isomer:0.032g recovered. (11% Yield) $R_f = 0.26$. ^{1}H-NMR (CD_3CN): δ 8.45 (dm 3H H^6 $J_{5,6}$= 4.9 Hz), 8.16 (dm3H $H^{6'}$ $J_{5',6'}$=5.6 Hz), 7.74 (m, 6H, H^4, $H^{4'}$), 7.57 (m 3H, $H^{5'}$), 7.43 (m 6H $H^{7'/8'/9'}$), 7.33 (m 6H, $H^{7'/8'/9'}$, H^5), 7.21 (dm 3H, H^3, $J_{3,4}$ = 7.5 Hz), 7.01 (m 12H, $H^{7/8/9}$), 6.94 (dm 3H $H^{3'}$ $J_{3',4'}$=8.1 Hz), 6.65 (dm 3H $H^{7'/8'/9'}$), 6.08 (s, 3H, $H^{7/8/9}$).

ESI-MS (CH_3CN) m/z = 607.20 $[M-2PF_6]^{2+}$. Calculated for $C_{78}H_{54}N_{12}Fe$: 1214.3944, found: 1214.3938.Anal. Calculated for $C_{78}H_{54}P_2F_{12}N_{12}Fe$: C, 62.24; H, 3.62; N, 11.17. Found: C, 59.74, H, 3.55, N, 10.17.



30 ***mer*** **30** ***fac***

Formation of Iron Complexes using $Fe(BF_4)_2$

$[Fe(8)_3][PF_6]_2$ (31)

0.0201g (0.0515 mmol) of **8** was added to a 5 mL soln. containing 0.005g (14.8 mmol) of $Fe(BF_4)_2$ and heated at 60°C for 2 hours. Then solvent was then removed in vacuo and water added to the reaction mixture. A saturated soution of KPF_6 was added and the resulting precipitate extracted into dichloromethane and dried over $MgSO_4$.

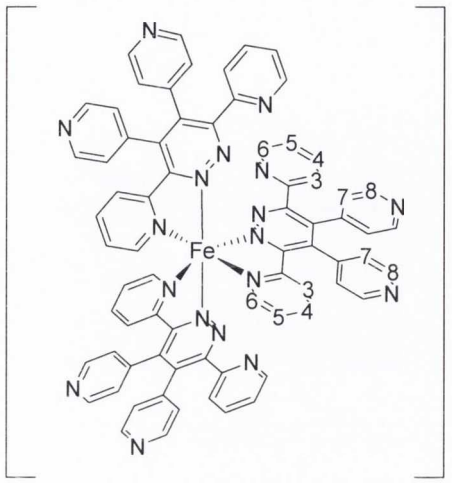
The mixture was separated on a TLC plate (acetone:ammonia:sat. KNO_3, 20:4:4).

The first product which was identified as the meridional isomer was obtained in 16% yield. $R_f = 0.77$. ^{1}H-NMR (CD_3CN): δ 8.75 (dm 1H, H^8, $J_{7,8}$ =5.3 Hz), 8.69 (dm 1H, H^8 $J_{7,8}$ = 4.5 Hz), 8.66 (dm 1H, H^8, $J_{7,8}$ = 5.0 Hz), 8.58 (dm 1H, H^8, $J_{7,8}$ = 5.0 Hz), 8.50 (dm 1H, H^6, $J_{5,6}$ = 5.0 Hz), 8.47 (1H, H^8, $J_{7,8}$ = 5.2Hz),8.43 (dm 1H, H^8, $J_{7,8}$ = 5.2 Hz), 8.33 (m 6H, H^6, H^8), 8.16 (dm 1H, H^6, $J_{5,6}$ = 4.8 Hz), 8.03 (1H, H^6, $J_{5,6}$ = 6Hz), 7.87 (dm 1H, H^4, $J_{4,5}$ = 7.6 Hz), 7.80 (dm 1H, H^4, $J_{4,5}$ = 7.9 Hz), 7.76 (dm 1H, H^3, $J_{3,4}$ = 5.9 Hz), 7.67 (m 4 H,) 7.63 (dm 1H, H^4, $J_{4,5}$ = 6.9 Hz), 7.46 (dm 1H, H^7), 7.39 (m 3H), 7.30 (m 2H), 7.26 (dm 1H, H^5, $H_{4,5}$ = 5.0 Hz), 7.19 (dm 1H, H^7), 7.12 (m 2H,) 7.06 (1H, H^3, $J_{3,4}$ = 7.6 Hz), 6.99 (m 3H), 6.88 (dm 1H, H^3, $J_{3,4}$ = 5.1 Hz), 6.35 (dm 1H, H^3, $J_{3,4}$ = 4.5 Hz). ESI-MS (CH_3CN) m/z = 610.18 $[M-2PF_6]^{2+}$. Calculated for $C_{72}H_{48}N_{18}Fe$: 1220.3659, found: 1220.3664.

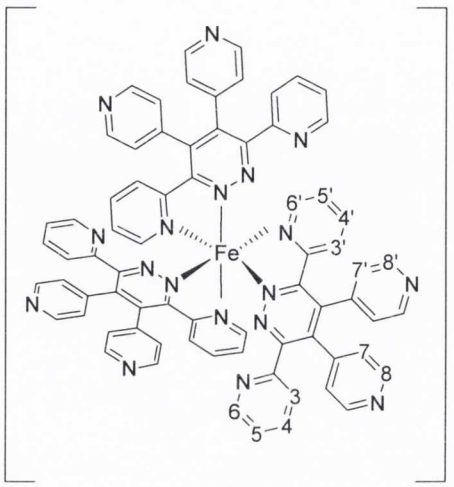
The second product, the facial isomer, was obtained in 42% yield. $R_f = 0.63$.

^{1}H-NMR (CD_3CN): δ 8.67 (dm 3H, $H^{8'}$, $J_{7',8'}$ = 5.2Hz), 8.55 (dm 3H, $H^{8'}$, $J_{7',8'}$ = 4.6Hz), 8.40 (dm 3H,H^6 $J_{5,6}$ = 4.3 Hz), 8.27 (s 6H, H^8), 8.12 (dm 3H, $H^{6'}$, $J_{5',6'}$ = 5.2 Hz), 7.88 (dd 3H, $H^{4'}$, $J_{4',5'}$ = 8.2 Hz, $J_{4',6'}$ = 1.2 Hz), 7.82 (dd 3H, H^4, $J_{4,5}$ = 7.4 Hz, $J_{4,6}$ = 1.3Hz), 7.63 (dd 3H, $H^{5'}$,$J_{3',5'}$ = 0.9 Hz), 7.38 (dd 3H, H^5, $J_{3,5}$ = 1.0 Hz), 7.31 (dd 3H, $H^{7'}$), 7.26 (dd 3H,

H^3, $J_{3,4}$ = 7.9 Hz), 7.21 (dd 3H, $H^{3'}$, $J_{3',4'}$ = 7.6 Hz), 6.67 (d 3H, $H^{7'}$), 6.15 (s 6H, H^7). ESI-MS (CH_3CN) m/z = 610.18 $[M\text{-}2PF_6]^{2+}$. Calculated for $C_{72}H_{48}N_{18}Fe$: 1220.3659, found: 1220.3640.



31 mer



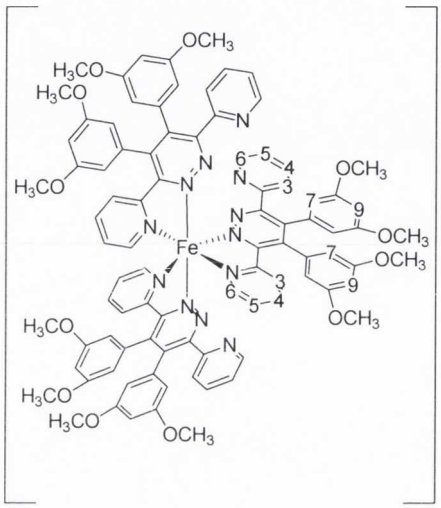
31 *fac*

$[Fe(19)_3][PF_6]_2$ (32)

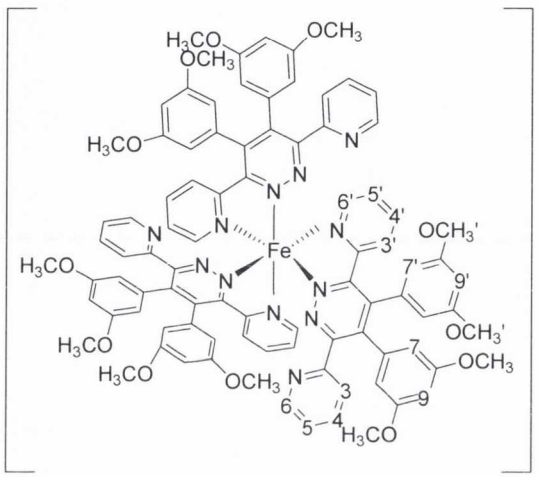
0.080g (0.181 mmol) of **19** was added to a 5 mL MeCN soln.containing 0.019g (56.6 mmol) of $Fe(BF_4)_2$ and heated at 60°C for 2 hours. The solvent was then removed in vacuo and water added to the reaction mixture. A saturated soution of KPF_6 was added and the resulting precipitate extracted into dichloromethane and dried over $MgSO_4$. The meridional and facial isomers were separated by column chromatography (1:1:0.1 of methanol:water:sat. KNO_3). 0.039g (0.021 mmol) of the meridional isomer was isolated (37% yield). R_f = 0.51. ^{1}H-NMR (CD_3CN): δ 8.42 (dm 1H, H^6, $J_{5,6}$ = 4.2 Hz), 8.37 (dm 1H, H^6, $J_{5,6}$ = 5.6 Hz), 8.30 (dm 1H, H^6, $J_{5,6}$ = 4.4 Hz), 8.26 (dm 1H, H^6, $J_{5,6}$ = 4.2 Hz), 7.89 (dm 1H, H^6, $J_{5,6}$ = 5.0 Hz), 7.86 (dm 1H, H^4, $H_{4,5}$ = 9.2 Hz, $J_{4,6}$ 1.5 Hz), 7.75 (m 2H), 7.65 (m 5H), 7.40 (dm 1H, H^3, $J_{3,4}$ = 8.3 Hz), 7.36 (dm 1H, H^3, $J_{3,4}$ = 8.0 Hz), 7.35 (m 3H), 7.31 (m 2H), 7.26 (dm 1H, H^3, $J_{3,4}$ = 8.3 Hz), 7.15 (dm 1H, H^3, $J_{3,4}$ = 7.9 Hz), 7.10 (dm 1H, H^3, $J_{3,4}$ = 7.8 Hz), 7.06 (dm 1H, H^3, $J_{3,4}$ = 8.4 Hz), 6.64 (m 3H), 6.55 (d 1H, H^9, $J_{7,9}$ = 1.2 Hz), 6.53 (d 1H, H^9, $J_{7,9}$ = 2.0 Hz), 6.50 (d 1H, $H_{7,9}$ = 1.2 Hz), 6.37 (d 1H, H^9, $J_{7,9}$ = 2.2 Hz), 6.29 (m 3H, H^7), 6.26 (m 2H, H^7), 6.23 (m 2H, H^7), 5.75 (m 1H, H^7), 3.76 (m 5H, H^{OMe}), 3.71 (s 3H, H^{OMe}), 3.67 (s 3H, H^{OMe}), 3.64 (m 4H, H^{OMe}), 3.57 (s 7H, H^{OMe}), 3.54 (s 7H, H^{OMe}). ESI-MS (CH_3CN) m/z = 787.26 $[M\text{-}2PF_6]^{2+}$. Calculated for $C_{90}H_{78}N_{12}O_{12}Fe$: 1574.5212, found: 1574.5142.

0.021 g (0.0113 mmol) of the facial isomer was isolated (20% yield).R_f = 0.14.

^{1}H-NMR (CD_3CN): δ 8.46 (dm 3H, H^6, $J_{5,6}$ = 4.2 Hz), 8.12 (dm 3H, $H^{6'}$, $J_{5',6'}$ = 5.6 Hz), 7.87 (dm 3H, $H^{4'}$, $J_{4',5'}$ = 7.01 Hz, $J_{4',6'}$ = 1.7 Hz), 7.73 (dm 3H, H^4, $J_{4,5}$ = 8.1 Hz, $J_{4,6}$ = 1.4 Hz), 7.60 (dm 3H, $H^{5'}$, $J_{3',5'}$ = 1.5 Hz), 7.31 (dm 3H, H^5, $J_{3,5}$ = 1.3 Hz), 7.25 (dm 3H, $H^{3'}$. $J_{3',4'}$ = 8.1 Hz), 7.17 (dm 3H, H^3, $J_{3,4}$ = 7.8 Hz), 6.58 (s 3H, H^7), 6.46 (s 3H, H^9), 6.24 (s 3H, $H^{7'}$), 5.90 (s 3H, $H^{9'}$), 3.72 (s 2H, $H^{OMe'}$), 3.66 (s 2H, $H^{OMe'}$), 3.55 (s 5H, H^{OMe}). ESI-MS (CH_3CN) m/z = 787.26 $[M-2PF_6]^{2+}$. Calculated for $C_{90}H_{78}N_{12}O_{12}Fe$: 1574.5212, found: 1574.5256.



32 mer



32 *fac*

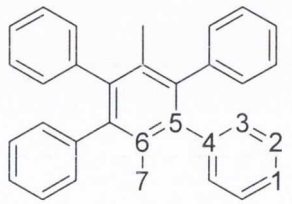
Synthesis of Phenyl-Centred Aromatically Substituted Compounds

3,6-dimethyl-1,2,4,5-tetraphenyl benzene (33)

1.0g (5.61 mmol) of diphenylacetylene and 0.5 g (0.96 mmol) of the 2,5-dimethyl-3,4-diphenylcyclopentadienone dimer were stirred in air at 250°C for 120 minutes. After cooling to room temperature, the mixture was washed with copious amounts of hexane. 0.8004 g of product were obtained (99% yield). I.R.(KBr) ν 3052s, 2961s, 2867m, 1950m, 1600s, 1444s, 1408s, 1379m, 1179m, 1025s, 772s, 538s, 516s cm^{-1}.

^{1}H-NMR ($CDCl_3$) δ 7.16 (dd 8H, H^2 $J_{2,3}$ = 8.05 Hz), 7.08 (dd 12 H, $H^{1,3}$), 1.83 (s 6H H^7).

^{13}C-NMR ($CDCl_3$) δ 140.99 (4H H^5), 140.40 (4H H^4), 130.85 (2H H^6), 129.78 (8H, $H^{2/3}$), 126.95 (8H, $H^{2/3}$), 125.37 (4H H^1), 19.13 (s 6H, H^7). m.p. 351°C.



33

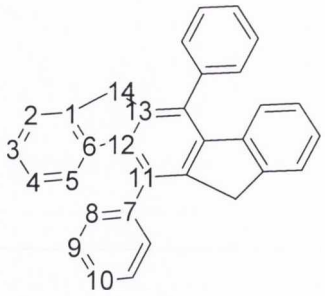
5,11–diphenyl-6,12-dihydroindeno-(1,2)-fluorene (34)

1.00 g (5.61 mmol) of diphenylacetylene and 0.500 g (0.96 mmol) of the 2,5-dimethyl-3,4-diphenylcyclopentadienone dimer were stirred in air at 610°C for 120 minutes. After cooling to room temperature, the mixture was recrystallised from toluene to give 0.105g of product (26 % yield). I.R.(KBr) ν 3055s, 2896s, 1602s, 1441s, 1297s, 1263s, 1071s, 1026s, 910m, 764s, 725s, 702s, 543m, 423m cm^{-1}. ^{1}H-NMR ($CDCl_3$) δ 7.63-7.44 (m 10H, $H^{8,9,10}$), 7.44 (dm 2H, H^2, $J_{2,3}$ = 7.7 Hz), 7.19 (dm 2H, H^3, $J_{3,4}$ = 6.9 Hz), 7.06 (dm 2H, H^4, $J_{4,5}$ = 7.7 Hz), 6.70 (dm 2H, H^5), 3.76 (s 4H, H^{14}).

^{13}C-NMR ($CDCl_3$) δ 143.85 (2C, C^1), 141.98 (2C, C^6), 141.32 (2C, C^{13}), 139.15 (2C, C^{11}), 136.92 (2C, C^{12}), 132.91 (2C, C^7), 128.65 (4C, C^8), 128.58 (4C, C^9), 127.23 (2C, C^{10}), 125.89 (2C, C^2), 125.61 (2C, C^3), 124.26 (2C, C^4), 122.22 (2C, C^5), 35.81 (4C, C^{14}).

ESI-MS (CH_3CN); m/z = 406.1738, calculated for $C_{32}H_{23}$ $[MH]^+$:406.1722

m.p. 244°C-246°C.



34

Attempted Cyclodehydrogenation of 33

0.250 g (0.61 mmol) of **33** was added to 20 mL of dry deaerated DCM and stirred at room temperature. Nitrogen was continuously bubbled through the mixture. 0.593 g (3.65 mmol) of $FeCl_3$ in 5 mL CH_3NO were added dropwise over 5 minutes. The reaction was stirred for several hours and 10 mL of CH_3OH was then added. Only starting material was retrieved.

Attempted Oxidation of 33

Method 1

0.200 g (0.487 mmol) of **33** was added to 10 mL of dry de-aerated DMF. 462 μl (2.240 mmol) of Bredereck reagent (tertbutoxy bis(dimethylamino) methane) were added to this and heated at 140°C for 36 hours in air. The reaction was then cooled and the solvent removed *in vacuo*. However only starting material was retrieved.

Method 2

0.100 g (0.243 mmol) of **33** was added to 25 mL of dioxane and 1mL of water. 0.131 g (1.18 mmol) of SeO_2 were added to this and the mixture was refluxed overnight in air. Subsequent TLC and ^{1}H-NMR analysis resulted in only the retrieval of starting material.

Method 3

0.500 g (1.218 mmol) of **33** and 0.974 g (9.744 mmol) of CrO_3 were added to 25 mL of dry acetic acid and the mixture was refluxed for eight hours. The reaction turned from dark brown to green and the mixture was filtered. Only starting material was retrieved.

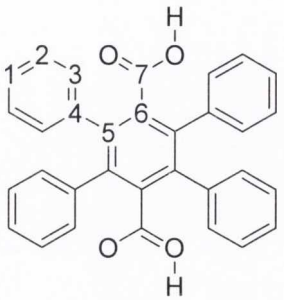
Method 4

3,6-dicarboxylate-1,2,4,5-tetraphenyl benzene (35)

0.500 g (1.22 mmol) of **33** were added to 1.80 g (113.8 mmols) of $KMnO_4$ and refluxed in a 9:1 mixture of pyridine and water. 1.00 g of $KMnO_4$ in 3 mL of water was added every half hour for two hours. After five hours, 20 mL of water were added and refluxed for 24 hours. The mixture was then filtered while hot and washed through with boiling

water. The solvent was reduced *in vacuo* and the addition of conc. HCl led to the precipitation of 0.254 g of product (44% yield). I.R. (KBr) ν 3057m, 1707s, 1602m, 1497m, 1443m, 1318m, 1225s, 1075m, 822m, 749m, 698s, 584m cm^{-1}.

^{1}H-NMR: ($CDCl_3$): δ 7.21-7.07 (m 20H, $H^{1,2,3}$) ^{13}C-NMR ($CDCl_3$): δ 129.70 (8C, C^2), 127.24 (8C, C^3), 126.76 (4C, C^1). m.p. >360°C.



35

Attempted Reduction of 35

0.200 g (0.425 mmol) of **35** was added to 20 mL of dry degassed DCM and cooled to 0°C. 118.47 μl (0.856 mmol) of triethyl amine and 107.88 μl of trimethyl silyl chloride were added to the solution and the temperature was then lowered to -78°C and 0.856 mL of a 1M solution of 4-dimethyl amino pyridine (DMAP) was added. This was then allowed to return to room temperature and stirred for 6 hours. Only starting material was retrieved.

1,2,4-triphenyl-3-methyl flouren-9-one (36) and 5,11-diphenyl indeno[1,2b] fluoren-6,12-dione (37)

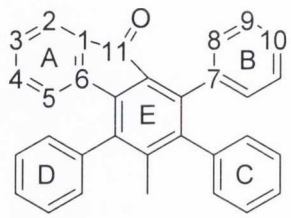
0.500 g (1.218 mmol) of tetraphenyl di-methyl benzene and 1.750 g (4.86 mmol) diselenic anhydride were refluxed in chlorobenzene for 5 days. The reaction was then allowed to cool and the excess selenenic anhydride removed by filtration. The solvent was removed *in vacuo* and the products isolated by column chromatography. (dichloromethane:hexane 10:1) to give 0.190 g of **36** (37% yield).

I.R. (KBr) ν 3066s, 3052s, 2333m, 1948m, 1865m, 1571s, 1473s, 1435s, 1068s, 1019s, 996s, 733s, 687s, 664s, 455s cm^{-1}.

^{1}H-NMR ($CDCl_3$): δ 7.58 (m 3H, $H^{9,10}$), 7.50 (dd 1H, H^2, $J_{2,3}$ = 6.7 Hz, $J_{2,4}$ = 1.1 Hz), 7.43 (dd 2H, H^8, $J_{8,9}$ = 6.6 Hz, $J_{8,10}$ = 1.8 Hz), 7.21 (m 5H, $H^{C/D}$), 7.15 (m 3H, $H^{C/D,4}$), 7.08 (m 2H, $H^{C/D,3}$), 7.04 (m 2H, $H^{C/D}$), 6.05 (dm 1H, H^5, $J_{4,5}$ = 7.0 Hz), 1.90 (s 3H, H^{Me}).

^{13}C-NMR ($CDCl_3$) δ 192.98 (1C, C^{11}), 143.71 (1C, C^Q), 143.11 (1C, C^Q), 142.24 (1C, C^Q), 141.41 (1C, C^Q),140.25 (1C, C^Q), 139.35 (1C, C^Q), 139.31 (1C, C^Q), 137.29 (1C, C^Q), 136.97 (1C, C^Q), 135.17 (1C, C^Q),133.92 (1C, C^3), 130.16 (2C, $C^{C/D}$), 129.56 (2C,

$C^{C/D}$), 129.38 (2C, C^9), 129.00 (2C, C^8), 128.41 (1C, C^4), 128.00 (1C, C^{10}), 127.77 (2C, $C^{C/D}$), 127.19 (2C, $C^{C/D}$), 126.76 (1C, $C^{C/Dpara}$), 126.54 (1C, $C^{C/Dpara}$), 123.65 (1C, C^2), 122.94 (1C, C^5), 19.59 (1C, C^{Me}). ESI-MS (CH_3CN) m/z $[MH]^+$ 423.17 ; (calculated 423.17); ESI-MS (CH_3CN); m/z = 423.1733, calculated for $C_{32}H_{23}O_1$: $[MH]^+$: 423.1749 . m.p. 231°C.

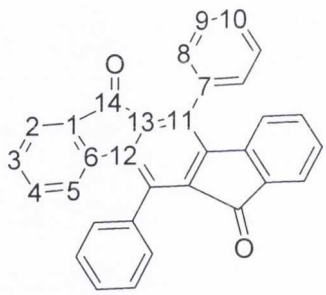


36

0.113 g of **37** was isolated (21% yield). I.R. (KBr) ν 2925s, 1713s, 1602s, 1466s, 1442s, 1261s, 1185s, 1091s, 1018s, 927s, 802s, 699s cm^{-1}.

^{1}H-NMR ($CDCl_3$): δ 7.63 (m 6H, $H^{8,10}$), 7.55 (dm 2H, H^2, $J_{2,3}$ =), 7.48 (m 4H, H^9), 7.19 (m 4H, $H^{3,4}$), 6.30 (m 2H, H^5).

^{13}C-NMR ($CDCl_3$) 192.30 (2C, C^{14}), 144.30 (2C, C^{13}), 142.81 (2C, C^6), 135.87 (2C, C^{12}), 135.56 (2C, C^{11}), 135.47 (2C, C^7), 134.70 (2C, C^4), 134.37 (2C, C^1), 128.97 (2C, C^{10}), 128.93 (4C, C^8), 128.55 (2C, C^3), 128.28 (4C, C^9), 123.94 (2C, C^2), 123.45 (2C, C^5). m.p.310°



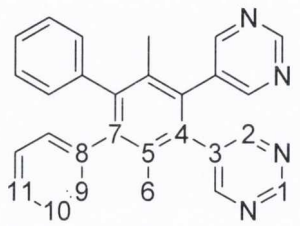
37

3,6-dimethyl-1,2-di-(5-pyrimidyl)-4,5-diphenyl benzene (38)

0.400 g (2.18 mmol) 1,2-bis-(5-pyrimidyl)ethyne and 0.546 g (2.10 mmol) of the 2,5-dimethyl-3,4-diphenylcyclopentadienone dimer were added to 2.00g of benzophenone and refluxed at 305^{0}C for 300 mns. The benzophenone was then removed by columning through a plug of silica using dichloromethane. The remainder of the reaction mixture was removed from the plug using a 1:1 mixture of methanol and dichloromethane. This was then washed several times with ethyl acetate to give 0.625 g (72%) yield.

I.R. (KBr) ν 3056m, 3023m, 1549s, 1419s, 1340s, 1187m, 773s, 702s, 665m cm^{-1}.

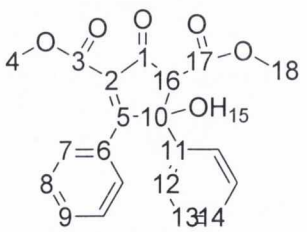
^{1}H-NMR: ($CDCl_3$): δ 9.06 (s 2 H H^1), 8.52 (s 4H H^2), 7.20 (dd 4H H^9 $J_{9,10}$ = 7.02 Hz), 7.14 (dd 2H H^{11} $J_{9,11}$=1.40 Hz), 7.04 (dd 4H H^{10} $J_{10,11}$=7.49 Hz), 1.85 (s 6 H, H^6).
^{13}C NMR ($CDCl_3$): δ 157.02 (2C C^1), 156.67 (4C C^2), 142.80 (2C C^7), 139.58 (2C C^8), 133.92 (2C C^4) 133.26 (2C C^3), 132.35 (2C C^5), 129.25 (4C C^9), 127.32 (4C C^{10}), 126.07 (2C C^{11}). ESI-MS (CH_3CN) m/z = 415.193, calculated for $C_{28}H_{23}N_4$: $[MH]^+$: 415.1923. m.p. 356°C.



38

2,5-dicarbomethoxy-4-hydroxy-3,4-diphenyl cyclopenten -2-one (39)

5.80 g (37.61 mmol) of dimethyl-1,3-acetonedicarboxylate and 7.00 g (33.29 mmol) benzil were added to 85 mL of ethanol. 0.333 g of KOH was added to this and the mixture was stirred at room temperature for 24 hours. The reaction mixture was added to 150 mL of cold water and stirred for 30 mns. It was then filtered and dried overnight to give 10.38 g (28.36 mmol) (85% yield). IR (KBr): ν 3467s, 2955m, 1742s, 1450m, 1436s, 1344s, 1175s, 992s, 699s, 643s cm^{-1}.
^{1}H-NMR: ($CDCl_3$): δ 8.00 (dd 2H, H^7, $J_{7,8}$ = 7.0 Hz,), 7.69 (dd 1H, H^9, $J_{7,9}$ = 1.5 Hz), 7.54 (dd 2H, H^8, $J_{8,9}$ = 8.1Hz), 7.47 (dm 1H, H^{14}, $J_{13,14}$ = 8.1 Hz), 7.37 (m 2H, H^{13}), 7.32 (m 2H, H^{12}), 5.07 (s 1H, H^{15}), 3.85 (s 3H, H^4), 3.83 (s 3H, H^{18}). ESI-MS (CH_3CN) m/z (%) $[MNa]^+$ 390.90 (100); (calculated 389.11); ESI-MS (CH_3CN) m/z =389.0988, calculated for $C_{21}H_{18}O_6$: $[MH]^+$:389.1001. m.p. 98°C-100°C.



39

2,5-dicarboxymethyl-3,4-diphenylcyclopentadienone (40)

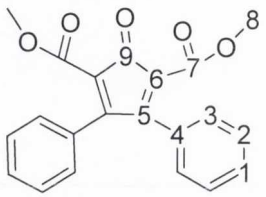
10.38 g (17.9 mmol) of **39** was added to 12 mL of acetic anhydride containing 1 drop of concentrated sulphuric acid. The mixture was heated while stirring ensuring all the material had dissolved and stirred whilst heating for a further 30 mns. The mixture was then allowed to cool to room temperature, after which time the precipitate was

filtered.and recrystallised from acetic acid. IR (KBr): ν 3060s, 2947s, 1824m, 1701s, 1600s, 1434s, 1249s, 1113s, 986s, 702s, 584s, 415s cm^{-1}.

^{1}H-NMR ($CDCl_3$) δ 7.39 (dd 2H H^1, $J_{1,2}$ = 7.0 Hz), 7.28 (dd 4H H^2, $J_{2,3}$ = 8.1 Hz), 7.04 (dd 4H, H^3, $J_{1,3}$ = 1.0 Hz), 3.76 (s 6H, H^8).

^{13}C-NMR ($CDCl_3$) δ 190.42 (1C, C^9), 162.32 (2C, C^5), 162.11 (2C, C^7), 130.32 (1C, C^4), 129.90 (2C, C^1), 128.50 (4C, C^3), 127.33 (4C, C^2), 118.97 (2C, C^6), 51.77 (2C, C^8).

ESI-MS (CH_3CN) m/z = 371.0900, calculated for $C_{21}H_{16}O_5$: $[MNa]^+$: 371.0895. m.p. 164°-166°C.



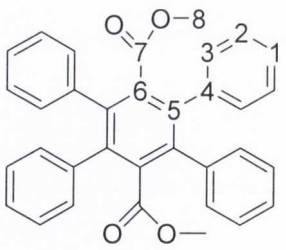
40

Synthesis of 1,2,4,5-tetraphenyl-3,6-dicarbomethoxy-benzene (41)

0.700g (3.92 mmol) of diphenylacetylene and 0.250g (0.57 mmol) of **40** were heated at 250°C for 120 mins and allowed to cool to room temperature. The reaction mixture was washed with hexane to give 0.302g (88% yield). I.R. (KBr) ν 3083m, 3058m, 3026m, 2950m, 1735s, 1601m, 1497m, 1442s, 1435s, 1329s, 1204s, 1174s, 1058s, 762s, 703s, 583m, 536m cm^{-1}.

^{1}H-NMR ($CDCl_3$): δ 7.16 (m 20 H, $H^{1,2,3}$), 3.19 (s 6H H^8).

^{13}C-NMR ($CDCl_3$): δ 168.40 (6H, H^7), 137.68 (4H $H^{4/5}$), 137.42 (4$H^{4/5}$), 136.05 (2H H^6), 129.49 (8H, H^3), 127.05 (8H, H^2), 126.64 (4H, H^1), 51.21 (6H, H^8). ESI-MS (CH_3CN) m/z = 499.1889, calculated for $C_{34}H_{27}O_4$: $[MH]^+$: 499.1909. m.p. 262°-264°C.



41

Attempted Reduction of 41

Method 1

2.2 g (0.0198 mmol) of $CaCl_2$, 1.52 g (0.040 mmol) of $NaBH_4$ and 20 mL of THF were added to a three-necked flask and stirred at reflux overnight. The reaction was then

cooled and directly injected into a refluxing THF solution containing 87.2 μls (0.008 mmol) of COD and 0.100 g (0.21 mmol) of **41**. Only starting material was retrieved.

Method 2

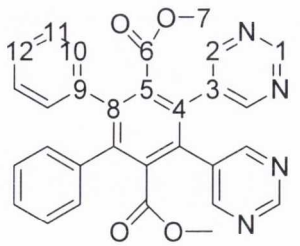
0.288 mL (28.85 mmol) of n-methyl piperazine in 0.8 mL toluene was added to 0.66 mL of a 65% solution of RedAl kept at 0°C and stirred for 30 mns. A solution of **41** in 15 mL of toluene was cooled to -20°C and the RedAl solution was added slowly to this and stirred at -20°C for 1 hour. 10 mL of water was then added and the solution was washed with 2mL of 1 M HCl and extracted into dichloromethane. Only the starting material was retrieved.

1,4-dicarbomethoxy-2,3-di(5-pyrimidyl)-5,6-diphenyl benzene (42)

0.300g (2.19 mmol) of 1,2-bis-(5-pyrimidyl)ethyne and 0.550g (1.58 mmol) were added to 2.00g of benzophenone and refluxed at 305°C for 300 mns. The benzophenone was then removed by columning through a plug of silica using dichloromethane. The remainder of the reaction mixture was removed from the plug using a 1:1 mixture of methanol and dichloromethane. This was then further purified in an ethyl acetate/pet ether column (10:1) to give 0.183 g (23% yield). I.R. (KBr) ν 3030s, 2953s, 1730s, 1578s, 1548s, 1449s, 1400s, 1334s, 1208s, 1177s, 1061s, 958s, 733s, 702s, 631s, 592s, 536m cm^{-1}.

^{1}H-NMR ($CDCl_3$): δ 9.10 (s 2H H^1), 8.58 (s 4H H^2), 7.21 (m 6H, $H^{10,12}$), 7.11 (m 4H, H^{11}), 3.26 (s 6H, H^7).

^{13}C-NMR ($CDCl_3$) δ 167.04 (2C, C^6), 157.54 (2C, C^1), 156.67 (4C, C^2), 140.22 (2C, C^9), 136.87 (2C, C^8), 136.21 (2C, C^5), 130.85 (2C, C^3), 130.64 (2C, C^4), 129.15 (4C, C^{11}), 127.37 (4C C^{10}), 127.33 (2C C^{12}). ESI-MS (CH_3CN) m/z = 503.1702 calculated for $C_{30}H_{23}N_4O_4$ $[MH]^+$: 503.1719. m.p. 280°C.



42

2,3,5-tri phenyl-4-methyl fluorenol (43)

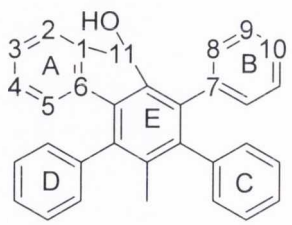
0.200 g (0.425 mmol) of **35** and 0.103 g (0.425 mmol) of 9-BBN (9-borabicyclo(3.3.1)nonane) dimer were added to a schlenk flask with 10 mL of dry

degassed THF. The mixture was cooled to -20°C, and 0.5 mL (0.85 mmol) of 1.6 M t-Butyl lithium was added dropwise and stirred for 10 mns at this temperature. 1.8 mL (0.9 mmol) of a 0.5 M BBN (9-borabicyclo(3.3.1)nonane) solution in THF was added to the mixture and it was allowed to return to room temperature and stirred overnight. The mixture was purified by column chromatography (dichloromethane) and 0.115 g (0.221 mmol) of the product was isolated (52% yield).

I.R. (KBr) ν 3553s, 3050s, 3031s, 1957m, 1716m, 1600s, 1442s, 1368s, 1023s, 762s, 747s, 700s, 579m cm^{-1}.

^{1}H-NMR ($CDCl_3$): δ 7.50-7.45 (m 3H, $H^{9,10}$), 7.40 (dm 1H, H^2, $J_{2,3}$ = 6.2 Hz), 7.35-7.28 (m 4H, H^8, $H^{C/D}$), 7.20 – 7.01 (m 10H, $H^{3/4}$, $H^{C,D}$), 6.93 (dm 1H, $H^{3/4}$), 6.85 (dm 1H, $H^{C/D}$), 6.10 (dm 1H, H^5, $J_{4,5}$ = 7.6 Hz), 5.63 (s 1H, H^{11}), 1.80 (s 3H, H^{Me}), 1.50 (sb 1H, H^{OH}).

^{13}C-NMR ($CDCl_3$) 145.02 (1C, C^Q), 140.86 (1C, C^Q), 140.33 (1C, C^Q), 139.83 (1C, C^Q), 139.80 (1C, C^Q), 138.44 (1C, C^Q), 137.66 (1C, C^Q), 136.64 (1C, C^Q),136.34 (1C, C^Q), 135.35 (1C, C^Q), 130.15 (1C, $C^{C/D}$), 129.54 (1C, $C^{C/D}$), 128.73 (1C, C^8), 128.69 (1C, C^9), 128.65 (1C, C^{10}), 128.09 (1C, $C^{3/4}$), 127.34 (1C, $C^{C/D}$)127.09 (1C, $C^{C/D}$), 126.75 (1C, $C^{C/D}$), 126.41 (1C, $C^{3/4}$), 125.81 (1C, $C^{C/D}$), 124.36 (1C, C^2), 122.40 (1C, C^5), 73.46 (1C, C^{11}), 18.40 (1C, C^{Me}). ESI-MS (CH_3CN) m/z = 447.1706, calculated for $C_{32}H_{24}ONa$: $[MNa]^+$: 447.1725. m.p. 262°C.



43

Attempted Cyclodehydrogenation of Phenyl-Centred Compounds

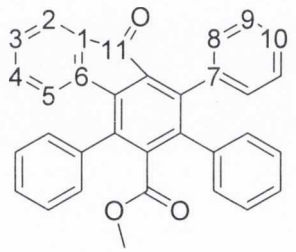
The following is an exampled of the procedure used in the attempted cyclodehydrogenation of some of the phenyl-centred compounds discussed above. This was the method used in the synthesis of **44** but in all other cases only insoluble material or starting material was retrieved.

1,2,4-triphenyl-3-carbomethoxy-flouren-9-one (44)

0.400g (0.843 mmol) of **41** was added to 60 mL of dry degassed dichloromethane. Nitrogen gas was bubbled constantly through the solution. A 5 mL nitromethane solution containing 2.8 g (17.3 mmol) of $FeCl_3$ was added dropwise and the mixture was allowed

to stir overnight. The reaction was quenched with methanol and the excess iron salts removed by washing with water. The mixture was purified by column chromatography to give 0.047 g (0.101 mmol) of 1,2,4-triphenyl-3-carbomethoxy-flouren-9-one (12% yield). I.R. (KBr) ν 2921s, 2852m, 1733s, 1712, 1600m, 1466m, 1443m, 1429m, 1317s, 1260m, 1222s, 1172m, 1092s, 1073s, 1059s, 1028s, 966m, 948m, 909m, 870m, 799s, 762s, 752s, 694s cm^{-1}. ^{1}H-NMR ($CDCl_3$): δ 7.53 (m 6H, $H^{8\text{-}10}$ H^2), 7.25 (m 3H, $H^{C/D}$, $H^{3/4}$), 7.15 (m 9H, $H^{C/D}$, $H^{3/4}$), 6.30 (d 1H, H^5, $J_{4,5}$ = 7.9 Hz), 3.20 (s, 3H, H^{OMe}).

^{13}C-NMR ($CDCl_3$) δ 191.93 (1C, C^{11}), 167.72 (1C, C^{COOMe}), 142.40 (1C, C^Q), 141.14 (1C, C^Q), 140.45 (1C, C^Q), 139.95 (1C, C^Q), 139.86 (1C, C^Q), 136.58 (1C, C^Q), 136.13 (1C, C^Q), 135 05 (1C, C^Q), 134.21 (1C, C^Q), 133.97 (1C, $C^{3/4}$), 133.47 (1C, C^Q), 130.69 (1C, C^Q), 129.53 (2C, $C^{C/D}$), 129.27 (2C, $C^{8/9}$), 128.76 (2C, $C^{C/D}$), 128.56 (1C, $C^{C/Dpara}$), 128.35 (2C, $C^{8/9}$), 128.17 (1C, C^{10}), 127.04 (2C, $C^{C/D}$), 126.93 (2C,$C^{C/D}$), 126.83 ($2C^{C/Dpara}$), 123 55 (1C, C^2), 122.78 (1C, C^5), 51.23 (1C, C^{OMe}). ESI-MS (CH_3CN) m/z = 489.1469, calculated for $C_{33}H_{22}O_3Na$: $[MNa]^+$: 489.1467. m.p = 268°C.

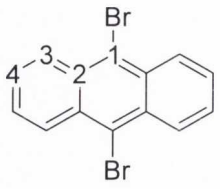


44

9,10-dibromo-anthracene (45)

1.78 g (10.0 mmol) of anthracene was added to 110 mL solution of dichloromethane and protected from the sunlight with aluminium foil. The mixture was cooled to 0°C and nitrogen was allowed to bubble through the system. This was allowed to bubble into a 1 M NaOH solution. 3.45 g (22 mmol) of Br_2 was added through a dropping funnel over 5 minutes. The mixture was then stirred for 1 hour . The solvent was removed in vacuo and the mixture was recrystallised from chloroform. 3.35 g (9.95 mmol) of product were obtained (99% yield). I.R. (KBr) ν 3077m, 3035m, 1952m, 1819m, 1622s, 1524s, 1438s, 1305s, 1257s, 1163m, 1028s, 927s, 844m, 747s, 676m, 747s, 605m, 579s, 393m cm^{-1}. ^{1}H-NMR ($CDCl_3$) δ 8.61 (dd 4H, H^3), 7.66 (4H, H^4).

^{13}C-NMR ($CDCl_3$) 130.60 (4C, C^2), 127.84 (4C, C^3), 127.02 (4C, C^4), 123.10 (2C, C^1). m.p 212°-214°C.

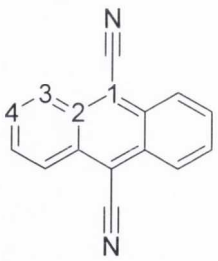


45

9,10-dicyano-anthracene (46)

3.51 g (10.4 mmol) of **45** and 2.14 g (23.9 mmol) of copper cyanide were added to 150 mL of degassed DMF and refluxed overnight. 250 cm^3 of a 1:1 mixture of ammonia and ice was added to the reaction while still hot and after cooling the mixture was extracted into dichloromethane. The extract was washed with 10% HCl and then water. The solvent was removed by vacuum and the resulting solid washed with hexane. The product was recrystallised from DMF after which 2.07 g (9.07 mmol) were obtained (87% yield). I.R. (KBr) ν 3063m, 2222s, 1976m, 1625s, 1526s, 1450s, 1439s, 1380s, 1284s, 1174s, 1157s, 958m, 886m, 852m, 765s, 740m, 642s, 613m, 497m, 432s cm^{-1}. ^{1}H-NMR ($CDCl_3$) δ 8.55 (dd 4H, H^3), 7.88 (dd 4H, H^4).

^{13}C-NMR ($CDCl_3$) 132.11 (4C, C^2), 129.82 (4C, C^3), 126.16 (4C, C^4), 115.91 (2C, $C^{C\equiv N}$), 111.51 (2C, C^1). m.p 328°-330°C.



46

Attempted Reduction of 46

9-bromo-10-cyanoanthracene ***(47)***

9-bromo-10-anthracenecarboxaldehyde ***(48)***

9- cyano-10-anthracenecarboxaldehyde ***(49)***

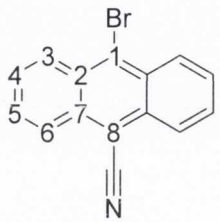
9,10-dianthracenecarboxaldehyde ***(50)***

1.21 g (5.30 mmol) of **46** was added to 60 mL of dry degassed toluene. 31.8 mL (31.8 mmol) of a 1 M solution of DibAl was added via syringe. The mixture was stirred for 20 hours and then cooled in an ice-bath. 30 mL of methanol was added, followed by 50mL of a 1:1 mixture of methanol and water. A 1:2 mixture of concentrated HCl and water was then added until the mixture was slightly acidic. It was then extracted into dichloromethane and washed with a sodium hydrogencarbonate solution. The mixture

was purified by column chromatography (dichloromethane :hexane 1:1) and two products were isolated. Further chromatography using toluene yielded two more products, including the desired product.

The first product isolated from the hexane:dichloromethane column was recrystallised from toluene and identified as 0.164 g (0.583 mmol) of 9-bromo-10-cyanoanthracene (**47**) (11% yield).

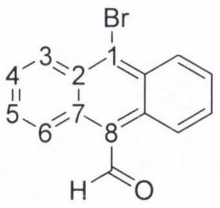
^{1}H-NMR ($CDCl_3$) δ 8.62 (d 2H, H^3, $J_{3,4}$ = 8.8 Hz), 8.45 (d 2H, H^6, $J_{5,6}$ = 8.6 Hz), 7.75 (m 4H, $H^{4,5}$). ^{13}C-NMR ($CDCl_3$) 132.91 (2C, C^7), 129.91 (1C, C^1), 129.57 (2C, C^2), 128.75 (2C, C^6), 128.24 (2C, C^3), 127.63 (2C, $C^{4/5}$), 125.32 (2C, $C^{4/5}$), 116.53 (1C, $C^{C\equiv N}$), 105.84 (1C, C^8).



47

The second product isolated from the hexane:dichloromethane column was identified as 9-bromo-10-anthracenecarboxaldehyde (**48**). 0.264 g (0.926 mmol) of product was obtained (17% yield). I.R. (KBr) ν 3081m, 3033m, 2963s, 2926s, 2856s, 1950m, 1677s, 1544s, 1439s, 1393s, 1261s, 1095s, 1024s, 800s, 743s, 398s, 384s cm^{-1}. ^{1}H-NMR ($CDCl_3$) δ 11.42 (s 1H, H^{CHO}), 8.82 (dd 2H, H^3, $J_{3,4}$ = 8.8 Hz), 8.60 (dd 2H, H^6, $J_{5,6}$ = 8.1 Hz), 7.65 (m 4H, $H^{4,5}$).

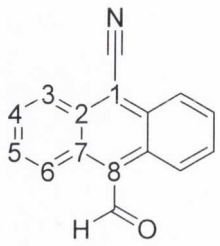
^{13}C-NMR ($CDCl_3$) 192.78 (1C, C^{CHO}), 133.64 (1C, C^8), 131.34 (2C, $C^{2/7}$), 129.67 (2C, $C^{2/7}$), 128.50 (2C, $C^{4/5}$), 128.35 (2C, C^3), 126.86 (2C, $C^{4/5}$), 125.02 (1C, C^1) 123.29 (2C, C^6). m.p 208°C.



48

The third product isolated from the toluene column was identified as 9-cyano-10-anthracenecarboxaldehyde (**49**). 0.168 g (0.726 mmol) was obtained (14% yield). I.R. (KBr) ν 3074m, 3053m, 2962s, 2925s, 2854s, 2219s, 1683s, 1526m, 1444s, 1263s, 1176s, 1054s, 1018s, 889s, 801s, 752s, 623s, 455s cm^{-1}.

^{1}H-NMR ($CDCl_3$) δ 11.50 (s 1H, H^{CHO}), 8.80 (m 2H, H^3, $J_{3,4}$ = 7.6 Hz, $J_{3,5}$ = 1.0 Hz), 8.53 (m 2H, H^6 $J_{5,6}$ = 7.4 Hz, $J_{4,6}$ = 2.1 Hz), 7.77 (m 4H, $H^{4,5}$). ^{13}C-NMR ($CDCl_3$) 192.97 (1C, C^{CHO}), 132.19 (2C, C^7), 130.11 (1C, C^8), 129.41 (2C, C^2), 128.83 (2C, $C^{4/5}$), 128.50 (2C, $C^{4/5}$), 125.76 (2C, C^3), 123.81 (2C, C^6), 115.97 (1C, $C^{C\equiv N}$), 111.58 (1C, C^1). m.p 272°-273°C.

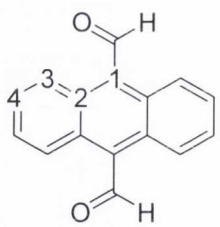


49

A fourth product was recrystallised from toluene to give 0.058 g (0.248 mmol) of the desired product, 9,10-anthracene dicarboxaldehyde (**50**) (5% yield). I.R. (KBr) ν 3074m, 3053m, 296s, 292s, 2854s, 2218m, 1683s, 1525s, 1444s, 1263s, 1176s, 1094s, 1054s, 1018m,889m, 801s, 752s, 623s, 455s cm^{-1}.

^{1}H-NMR ($CDCl_3$) δ 11.51 (s 2H, H^{CHO}), 8.77 (dd 4H, H^3), (dd 4H, H^4).

^{13}C-NMR ($CDCl_3$) 193.88 (2C, C^{CHO}), 131.31 (2C, C^1), 129.73 (4C, C^2), 127.95 (4C, C^3), 123.79 (4C, C^4).

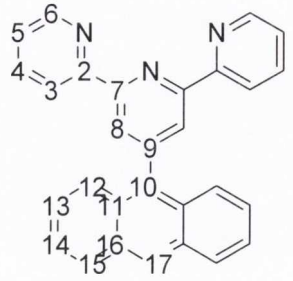


50

4'-(anthracen-9-yl)-2,2':6',2''-terpyridine (51)

5.2 g (25 mmol) 9-anthraldehyde, 6.1 g (50 mmol) of 2-acetyl pyridine, 3.9 g (69 mmol) of KOH, and 20 mL of ammonia were added to a flask containing 250 mL of ethanol. The mixture was refluxed overnight and the resulting precipitate filtered and recrystallised from ethanol. 3.27 g (8 mmol) were recovered (31% yield). I.R. (KBr) ν 3067s, 3050s, 3016s, 1956m, 1811m, 1623s, 1583s, 1567s, 1548s, 1466s, 1392s, 1264s, 1116s, 1071m, 998m, 893m, 886s, 854s, 794s, 739s, 654s, 627s, 638s, 531m, 421m, 404m cm^{-1}. ^{1}H-NMR ($CDCl_3$) δ 8.82 (dm 2H, H^3, $J_{3,4}$ = 7.9 Hz), 8.66 (dm 2H, H^6, $J_{5,6}$ = 4.5 Hz), 8.64 (s 2H, H^8), 8.58 (s 1H, H^{17}), 8.09 (dm 2H, H^{12}, $J_{12,13}$ = 8.4 Hz), 7.95 (dm 2H, H^4, $J_{4,6}$ = 1.9 Hz), 7.74 (dm 2H, H^{15}, $J_{14,15}$ = 9.0 Hz), 7.50 (m 2H, $H^{13/14}$), 7.37 (m 4H,

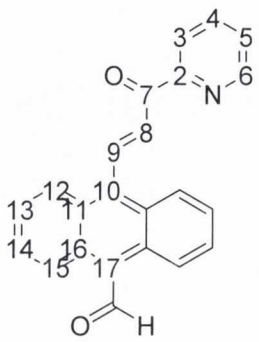
$H^{13/14,5}$). ^{13}C-NMR ($CDCl_3$) 156.12 (1C, $C^{2/7}$), 155.67 (1C, $C^{2/7}$), 149.59 (1C, C^{9}), 149.22 (2C, C^{6}), 136.99 (2C, C^{4}), 134.31 (1C, C^{10}), 131.24 (2C, $C^{11/16}$), 129.55 (2C, $C^{11/16}$), 128.43 (2C, C^{12}), 127.40 (1C, C^{17}), 126.41 (2C, C^{15}), 125.87 (2C, $C^{13/14/5}$), 125.23 (2C, $C^{13/14}$), 123.95 (2C, $C^{13/14/5}$), 123.86 (2C, C^{8}), 121.47 (2C, C^{3}). ESI-MS (CH_3CN) m/z = 410.1656 calculated for $C_{29}H_{20}N_3$ $[MH]^+$:410.1657. m.p 260°-262°C.



51

9-anthracenyl(10-al)-1-(2-pyridyl) propen-2-one (52)

0.020 g (0.085 mmol) of **50**, 80 µl (0.66 mmol) of 2-acetyl pyridine and 0.040 g (0.519 mmol) of ammonium acetate were added to a pressure tube and heated at 300 W in a microwave for 2 minutes, whilst stopping every 30 seconds to allow cooling. The mixture was purified by column chromatography (dichloromethane) and the product isolated. 0.0026 g (0.0078 mmol) (9% yield) .I.R. (KBr) ν 3429w, 1606m, 1584s., 1567s, 1542, 1490s, 1468s, 1444m, 1409s, 1380s, 1265m, 1104w, 1074, 1037s, 1008s, 903w, 889m, 821s, 782s, 733s, 703m, 660m cm^{-1}. ^{1}H-NMR ($CDCl_3$) δ 11.6 (s 1H, H^{CHO}), 8.98 (dm 2H, H^{15}, $J_{14,15}$ = 9.6 Hz), 8.86 (d 1H, H^{8}, $J_{8,9}$ = 16.4 Hz), 8.72 (dm 1H, H^{6}, $J_{5,6}$ = 5.1 Hz), 8.40 (dm 2H, H^{12}, $J_{12,13}$ = 9.6 Hz), 8.33 (dm 1H, H^{3}, $J_{3,4}$ = 8.1 Hz), 8.23 (d 1H, H^{9}), 7.97 (dd 1H, H^{4}, $J_{4,5}$ = 7.8 Hz, $J_{4,6}$ = 2.0 Hz), 7.73 (dm 2H, H^{13}, $J_{13,14}$ = 8.8 Hz, $J_{13,15}$ = 1.0 Hz), 7.61 (dm 2H, H^{14}), 7.54 (1H, H^{5}, $J_{3,5}$ = 1.0 Hz). ^{13}C-NMR ($CDCl_3$) 200.63 (1C, C^{CHO}), 149.11 (1C, C^{6}), 141.23 (1C, C^{8}), 137.14 (1C, C^{4}), 131.81 (1C, C^{9}), 128.74 (2C, C^{13}), 127.23 (1C, C^{5}), 126.59 (2C, C^{12}), 126.24 (2C, C^{14}), 123.92 (2C, C^{15}), 123.25 (1C, C^{3}).



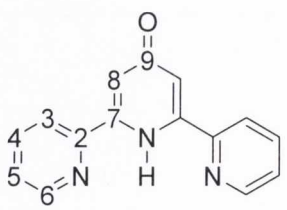
52

2,6-bis-(2-pyridyl)-4-terpyridone (53)

3.12 g (104.2 mmol) of sodium hydride was added to a 250 mL flask containing 50 mL of dry degassed 1,2-dimethoxyethane. 10.12 mL (75 mmol) of ethyl 2-pyridine and 1.84 mL (25 mmol) of acetone were added to a 100mL flask containing 50mL of dry 1,2-dimethoxyethane. This mixture was stirred for 5 minutes and then added to the sodium hydride suspension via canula. The mixture was then stirred at room temperature under a reflux condenser. The flask was heated gently with a hair dryer until the mixture began to bubble, upon which the flask was placed IMMEDIATELY into an ice-bath. After the reaction has ceased refluxing and cooled significantly, the mixture was heated to 88°C and refluxed overnight. The solvent was then removed in vacuo and the remaining solvent dissolved in 300 mL of water. A 10 % solution of HCl was then added slowly until the mixture had returned to a neutral pH. The yellow precipitate which formed was filtered, dried, and added to a 175 mL solution of ethanol. 14.5 g (188 mmol) of ammonium acetate was added to this and the mixture was refluxed overnight. 150 mL of ethanol was removed from the solution and the remaining mixture was left in an ice bath for one hour. The solid was then filtered, washed with ethanol and recrystallised from ethanol. 1.1 g (4.4 mmol) of product were obtained (18% yield). I.R. (KBr) ν 3293s, 3070m, 2410m, 1670s, 1572s, 1585s, 1513s, 1302s, 1084s, 1063s, 1007s, 997s, 884s, 784s, 699m, 549s, 453scm^{-1}.

^{1}H-NMR ($CDCl_3$) δ 12.03 (s 1H, H^{N-H}), 8.81 (dd 2H, H^6, $J_{5,6}$ = 4.5 Hz), 7.96 (dd 2H, H^3, $J_{3,4}$ = 8.1 Hz), 7.91 (dd 2H, H^4, $J_{4,5}$ = 7.5 Hz, $J_{4,6}$ = 1.5 Hz), 7.45 (dd 2H, H^5, $J_{3,5}$ = 1.0 Hz), 7.15 (s 2H, H^8). ^{13}C-NMR ($CDCl_3$) 174.94 (1C, C^9), 149.53 (2C, C^6), 148.42 (2C, $C^{2/7}$), 144.60 (2C, $C^{2/7}$), 137.76 (2C, C^4), 125.30 (2C, C^5), 120.61 (2C, C^3), 113.49 (2C, C^8).

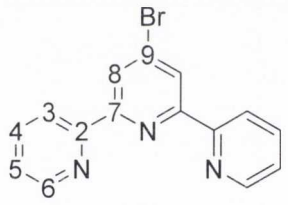
ESI-MS (CH_3CN) m/z = 250.0985, calculated for $C_{15}H_{12}N_3O$: $[MH]^+$: 250.0980. m.p 130°-132°C.



53

4-bromo-2,2',6',2''-terpyridine (54)

0.500 g (2.01 mmol) of **53**, 2.8 g (10.0 mmol) of phosphorous oxybromide and 4.3 g (10.0 mmol) of phosphorous pentabromide were added to a small flask and heated at 120°C overnight. The flask was allowed to cool and 10 mL of water was added cautiously. A 10% solution of KOH was added dropwise until the mixture was neutralized. It was then extracted into chloroform, washed with activated carbon and magnesium sulphate before removing the solvent in vacuo. 0.472 g (1.5 mmol) of product was obtained (75% yield). I.R. (KBr) ν 3087m, 3063m, 3012m, 1590m, 1549s, 1467s, 1391s, 1321m, 1264m, 1091m, 1065s, 994m, 880s, 787s, 781s, 740s, 731s, 673s, 658s, 623s, 560s, 400s cm^{-1}. ^{1}H-NMR ($CDCl_3$) δ 8.73 (dd 2H, H^6, $J_{5,6}$ = 4.0 Hz, $J_{4,6}$ = 1.1 Hz), 8.68 (s 2H, H^8), 8.62 (dm 2H, H^3, $J_{3,4}$ = 8.1 Hz), 7.90 (dm 2H, H^4, $J_{4,5}$ = 8.0 Hz), 7.39 (dm 2H, H^5, $J_{3,5}$ = 1.1 Hz). ^{13}C-NMR ($CDCl_3$) 156.45 (2C, $C^{2/7}$), 154.91 (2C, $C^{2/7}$), 149.24 (2C, C^6), 137.04 (2C, C^4), 135.13 (1C, C^9), 124.34 (2C, C^5), 124.21 (2C, C^8), 121.45 (2C, C^3). ESI-MS (CH_3CN) m/z = 312.0122 calculated for $C_{15}H_{11}N_3Br$: $[MH]^+$: 312.0136. m.p 122°-124°C.



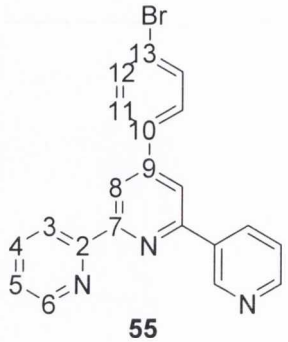
54

4-bromo-4-phenyl-2,2',6',2''-terpyridine (55)

5 mL (44.6 (mmol) of 2-acetyl pyridine and 10 mL of an aqueous solution of KOH were added to a three-necked flask containing 3.7 g (20 mmol) of 4-bromobenzaldehyde in 50 mL of ethanol. 20 mL of water followed by 20 mL of ammonia were added to this. The mixture was stirred for several minutes at room temperature and refluxed for 48 hours at 105°C. The resulting precipitate was filtered and recrystallised from ethanol to give 4.81 g (12.36 mmol) of product (62% yield). I.R. (KBr) ν 3365m, 3270m, 1606s, 1585s, 1568s, 1491s, 1469s, 1410s, 1381s, 1266s, 1075s, 1008s, 890m, 829s, 821s, 787s, 743s, 735s, 499 cm^{-1}.

^{1}H-NMR ($CDCl_3$) δ 8.75 (dm 2H, H^6, $J_{5,6}$ = 3.9 Hz), 8.73 (s 2H, H^8), 8.70 (dm 2H, H^3, $J_{3,4}$ = 8.0 Hz), 7.91 (dm 2H, H^4, $J_{4,5}$ = 7.5 Hz, $J_{4,6}$ = 1.5), 7.81 (dm 2H, H^{12}, $J_{11,12}$ = 8.5 Hz), 7.66 (dm 2H, H^{11}), 7.37 (dm 2H, H^5, $J_{3,5}$ = 1.0 Hz).

^{13}C-NMR ($CDCl_3$) 156.09 (2C, $C^{2/7}$), 156.03 (2C, $C^{2/7}$), 149.16 (2C, C^{6}), 149.08 (1C, C^{9}), 137.41 (1C, C^{13}), 136.97 (2C, C^{4}), 132.12 (2C, C^{12}), 128.92 (2C, C^{11}), 123.99 (2C, C^{5}), 123.50 (1C, C^{10}), 121.42 (2C, C^{3}), 118.57 (2C, C^{8}). ESI-MS (CH_3CN) m/z = 388.0447, calculated for $C_{21}H_{115}N_3Br$: $[MH]^+$: 388.0449. m.p 156°C.



55

Annex

Table 1: Crystal data and X-ray experimental details for compounds **3**, **4**, **6**, **36** and **43**.

Compound	**3**	**4**	**6**	**36**	**43**
Empirical formula	$C_{18}H_{12}N_6$	$C_{19}H_{13}N_5$	$C_{26}H_{18}N_4$	$C_{32}H_{22}O$	$C_{32}H_{24}O$
Formula weight	312.34	311.34	386.44	422.50	424.51
Temperature (K)	153(2)	153(2)	153(2)	153(2)	298(2)
Crystal system	Orthorhombic	Monoclinic	Triclinic	Triclinic	Monoclinic
Space group	$Pca2_{(1)}$	$P2_{(1)}/n$	P-1	*Pī*	*C2/c*
Unit cell dimensions: a (Å)	11.0611(6)	9.4836(4)	10.4655(5)	9.587(7)	22.987(5)
b (Å)	18.2383(10)	11.1365(5)	12.1742(6)	10.607(8)	11.135(2)
c (Å)	7.3490(4)	14.4323(6)	15.8820(8)	12.568(9)	18.164(4)
α (°)	90	90	93.6740(10)	112.889(1)	90
β (°)	90	90.8690(10)	91.2560(10)	94.178(1)	102.646(5)
γ (°)	90	90	101.7500(10)	100.065(1)	90
Volume(Å^3)	1482.56(14)	1524.08(11)	1975.77(17)	1145.22(15)	4536.5(17)
Z	4	4	4	2	8
Density (calculated) (Mg/m^3)	1.399	1.357	1.299	1.225	1.243
Absorption coefficient (mm^{-1})	0.090	0.085	0.079	0.072	0.073
F(000)	648	648	808	-	-
Crystal size (mm)	0.50 x 0.27 x 0.24	0.54 x 0.52 x 0.46	0.51 x 0.46 x 0.34	-	-
Theta range for data collection (°)	2.15 to 28.00	2.31 to 29.00	1.71 to 27.50	1.93-26.00	2.12-25.15
Reflections collected	16980	21231	25705	12861	23752
Independent reflections [R(int)]	3577 [0.0208]	4039 [0.0192]	9068 [0.0330]	4493	4042
Data / restraints / parameters	3577 / 1 / 217	4039 / 0 / 217	9068 / 0 / 543	4493/0/298	4042/0/378
Goodness-of-fit on F^2	1.035	1.025	1.008	1.071	1.062
R_1 [I>2sigma(I)]	0.0346	0.0440	0.0459	0.0532	0.0573
wR_2 (all data)	0.0984	0.1239	0.1189	0.1206	0.1564

Table 2: Crystal data and X-ray experimental details for compounds **22**, **23** and **27** *fac*.

Compound	**22**	**23**	**27** ***fac***
Empirical formula	$C_{41}H_{34}F_{12}N_{10}OP_2Ru$	$C_{42}H_{35}F_{12}N_9OP_2Ru$	$C_{78}H_{54}F_{12}N_{12}P_2Ru$
Formula weight	1073.79	1072.80	1550.34
Temperature (K)	153(2)	153(2)	293(2)
Crystal system	Monoclinic	Monoclinic	Trigonal
Space group	$P2_{(1)}/c$	$P2_{(1)}/c$	P-3
Unit cell dimensions: a (Å)	10.9856(10)	11.5464(10)	18.443(4)
b (Å)	20.2230(18)	19.7510(18)	18.443(4)
c (Å)	20.3436(18)	19.7135(17)	12.820(3)
α (°)	90	90	90
β (°)	104.637(2)	101.996(2)	90
γ (°)	90	90	120
Volume(Å^3)	4372.9(7)	4397.5(7)	3776.4(15)
Z	4	4	1
Density (calculated) (Mg/m^3)	1.631	1.620	1.208
Absorption coefficient (mm^{-1})	0.530	0.527	0.318
F(000)	2160	2160	-
Crystal size (mm)	0.45 x 0.35 x 0.04	0.38 x 0.32 x 0.02	-
Theta range for data collection (°)	1.44 to 27.00	1.80 to 26.00	1.60 to 28.36
Reflections collected	39906	37252	13260
Independent reflections [R(int)]	9528 [0.0475]	8657 [0.0843]	6253
Data / restraints / parameters	9528 / 0 / 604	8657 / 0 / 604	6253/0/330
Goodness-of-fit on F^2	1.023	1.008	0.909
R_1 [I>2sigma(I)]	0.0959	0.0538	0.0869
wR_2 (all data)	0.1062	0.1343	0.2388